Issue:
The modelled gasifier voids provided in 'Arrow Energy - Additional Information to support Hopeland Stage 2' (v1.0 dated 23/06/2026) shows a significant difference between the burn cavities reported by AECOM (2018) and total volume generated by multiplying seam thickness and area calculated by Perkins (2018), with the latter being significantly higher than the former.

Action required:
1. Provide the sensitivity analysis on gasifier volume and altered rock volume to justify this.

Arrow response:

The AECOM (2018) values represent estimates of the physical burn cavities created during UCG operations. In contrast, the groundwater model does not explicitly simulate cavity voids alone. Rather, it represents the broader volume of hydraulically altered rock associated with historical UCG operations, including the effects of thermal alteration, fracturing, geomechanical disturbance, collapse, and dewatering surrounding the gasifiers. Consequently, the altered-rock volumes (Figure 2-1 of the attached "***PL253 Groundwater Impact Assessment - Clynes Road FDP"*** report) incorporated within the model are expected to be larger than the physical burn cavity volumes reported by AECOM (2018).

The purpose of the modelling presented in the attached "***PL253 Groundwater Impact Assessment - Clynes Road FDP***" report was not to assess uncertainty associated with gasifier dimensions or altered-rock volumes within Lot 40 DY85. Rather, the assessment was specifically designed to evaluate the potential influence of the 55 proposed Clynes Road production wells located over 2km away from the gasifiers on contaminant migration from Lot 40.

To achieve this objective, a differential modelling approach was adopted, whereby simulations including the proposed production wells were compared directly against simulations without the production wells. The impact of the proposed development was therefore quantified as the difference between the two model scenarios.

Importantly, the gasifier conceptualisation and associated altered-rock volumes were represented identically in both scenarios. Consequently, any changes to the assumed altered-rock volume would be expected to affect both simulations in a similar manner. As a result, the relative difference between the two scenarios, which is the basis for assessing the impact of the proposed production wells, would be expected to remain unchanged.

Accordingly, sensitivity testing of gasifier or altered-rock volumes is unlikely to materially affect the conclusions of the assessment. While alternative assumptions regarding the extent of the altered-rock zone may influence absolute model responses, they would be expected to influence both model scenarios consistently and therefore have limited effect on the predicted incremental impact of the proposed 55 Clynes Road production wells on contaminant migration from Lot 40.

For these reasons, a sensitivity analysis on gasifier volume or altered-rock volume was not considered necessary for the purpose of assessing the development-related impacts addressed by the modelling study.

T +61 7 3012 4000
F +61 7 3012 4001
ARROW ENERGY PTY LTD
ABN 73 078 521 936
LEVEL 39, 111 EAGLE STREET
BRISBANE QLD 4000
GPO BOX 5262
BRISBANE QLD 4001
info@arrowenergy.com.au
arrowenergy.com.au

Issue:
Additional cross-sections (Figure 2 and Figure 3) were provided in 'Arrow Energy - Additional Information to support Hopeland Stage 2' (v1.0 dated 23/06/2026) to expand on the conceptual site model. Further clarifications are required on these cross-sections and conceptual site model.

Action required:
2. The horizontal scale is missing in these cross-sections. Provide updated Figure 2 and Figure 3 cross-sections including the horizontal scale. Writing/ labelling groundwater elevation (in mAHD) next to the observed water level in the bores as well as key hydro-stratigraphic units (e.g. base of the Macalister coal seam) would also be helpful.

Arrow response:

Figure 2 and Figure 3 cross-sections have been revised to include a horizontal scale. In addition, groundwater elevations (mAHD) corresponding to the observed water levels in the bores have been annotated, and key hydrostratigraphic units, including the base of the Macalister coal seam, have been labelled to improve clarity and interpretation. The updated figures are included in the updated model report (refer to Figure 2-1 of the attached "***PL253 Groundwater Impact Assessment - Clynes Road FDP***" report).

3. Clarify if the extrapolated hydraulic heads presented in these figures are based on modelling.

Arrow response:

Yes, the extrapolated hydraulic heads presented in these figures are derived from model results corresponding to the end of 2025.

4. Initial contamination migration has been attributed to high gas pressure conditions, which suggests dual phase flow conditions at the site. Clarify if the dual phase flow condition was considered during numerical modelling or during conceptualisation.

Arrow response:

Dual-phase (water-gas) flow processes were considered in the conceptualisation of the historical contaminant-emplacement mechanism. They were not, however, explicitly simulated as a transient gas-water flow and transport process in the numerical model because the assessment commenced from the observed post-UCG contaminant distribution rather than attempting to reproduce the period of active gasification. The initial dissolved-phase concentration distribution used in the transport model was developed from the available groundwater-monitoring data and is intended to represent the cumulative outcome of historical contaminant emplacement, including emplacement that may originally have occurred through the gas phase.

The historical emplacement of contaminants within and around the border of Lot 40 DY 85, due to historical UCG operations, is considered to have occurred, at least in part, through gas-phase migration under the elevated gas pressures that existed during gasification. As gas migrated away from the gasifiers, contaminants are understood to have condensed and dissolved into groundwater as pressure and temperature conditions decreased away from the gasifiers. This mechanism is considered a historical source emplacement process associated with UCG operations rather than an ongoing contaminant transport process.

T +61 7 3012 4000
F +61 7 3012 4001
ARROW ENERGY PTY LTD
ABN 73 078 521 936
LEVEL 39, 111 EAGLE STREET
BRISBANE QLD 4000
GPO BOX 5262
BRISBANE QLD 4001
info@arrowenergy.com.au
arrowenergy.com.au

Current site monitoring data, as presented in Figures 2-3, 2-4, 2-5, and 2-6 of the attached "***PL253 Groundwater Impact Assessment - Clynes Road FDP***" report, indicate that contamination is present in the dissolved phase within groundwater, with no evidence of ongoing gas-phase contaminant migration that could contribute to concentration of the contaminants in the groundwater monitoring bores (or a new breakthrough arrival of the contaminants). Accordingly, the assessment focused on evaluating the current and future migration of dissolved contaminants within the groundwater system.

The purpose of the modelling was to evaluate the potential influence of the proposed 55 Clynes Road production wells on the migration of dissolved contaminants from Lot 40. For this purpose, a single-phase groundwater flow model was considered appropriate because contaminant migration is controlled by groundwater flow and associated hydraulic gradients, and solute transport processes (i.e, advection, dispersion, diffusion).

Published studies investigating coal seam depressurisation indicate that single-phase groundwater flow models generally predict greater drawdown and a more extensive cone of depressurisation than equivalent dual-phase reservoir simulations (Moore et al., 2013; Moore et al., 2015; Herckenrath et al., 2015). This occurs because gas desorption during depressurisation reduces the relative permeability of the water phase, slowing pressure propagation through the coal seam. In addition, gas generation and expansion can release water from the coal system, further attenuating drawdown propagation.

Consequently, the use of a single-phase groundwater flow model is expected to overpredict the magnitude and spatial extent of drawdown relative to true dual-phase flow conditions. As contaminant migration from Lot 40 is driven by hydraulic gradients associated with CSG-induced depressurisation, the single-phase modelling approach provides a conservative assessment of potential contaminant migration. Therefore, while dual-phase flow processes were considered during conceptualisation, explicit simulation of dual-phase flow was not necessary for the purpose of assessing the potential impact of the proposed 55 Clynes Road production wells on dissolved-phase contaminant migration.

Issue:

Comparison of the calibrated (posterior) hydraulic property ranges from ensemble P5, P50 and P95, against parameter bounds from OGIA (2019) was provided in 'Arrow Energy - Additional Information to support Hopeland Stage 2' (v1.0 dated 23/06/2026) in Tables 4-5-6.

Action required:

5. If the values for P5, P50 and P95 are not available from OGIA's model, are there measured/tested values with P5, P50 and P95?

Arrow response:

Available hydraulic conductivity test data from bores screened within the Springbok Sandstone and Macalister coal seam package were compiled and analysed to derive measured P5, P50 and P95 statistics for comparison with the calibrated model parameters. The measured datasets comprise hydraulic conductivity estimates derived from field hydraulic testing undertaken within PL253 and adjacent ATP676 areas. The resulting statistics provide an independent line of evidence for evaluating the reasonableness of the calibrated groundwater model parameterisation.

The Springbok Sandstone and Macalister coal seam hydraulic conductivity test data are presented in *Table* 1 and Table *3*, respectively, with the corresponding hydraulic conductivity

T +61 7 3012 4000
F +61 7 3012 4001
ARROW ENERGY PTY LTD
ABN 73 078 521 936
LEVEL 39, 111 EAGLE STREET
BRISBANE QLD 4000
GPO BOX 5262
BRISBANE QLD 4001
info@arrowenergy.com.au
arrowenergy.com.au

statistics presented in Table *2* and Table *4*. A comparison of the measured hydraulic conductivity statistics with the calibrated model parameters is provided in *Table* 5.

Table 1: Springbok Sandstone Hydraulic Conductivity Test Data

Bore Name	Formation	Hydraulic Conductivity (m/day)
RN107857	Springbok Sandstone	0.030
RN87897	Springbok Sandstone	0.030
Hopeland 21	Springbok Sandstone	0.023
RN33553	Springbok Sandstone	0.014

Table 2: Measured Springbok Sandstone hydraulic conductivity statistics

Statistic	Hydraulic Conductivity (m/day)
Minimum	0.014
P5	0.015
P50 (Median)	0.027
P95	0.030
Maximum	0.030
Mean	0.024

Table 3: Macalister Coal Seam Package Hydraulic Conductivity Test Data

Bore Name	Formation	Hydraulic Conductivity (m/day)
RN24504	Macalister Seam	0.0100
RN24479	Upper Juandah Coal Measures (Macalister Seam)	0.1700
RN10790	Macalister Seam	0.0200
RN15868	Macalister Seam	0.1401
Hopeland 21	Macalister Seam	0.0012
Hopeland-6	Macalister Seam	0.1690
Hopeland-7	Macalister Seam	0.1000
Jammat-2	Macalister Seam	0.0172

Table 4: Measured Macalister coal seam hydraulic conductivity statistics

Statistic	Hydraulic Conductivity (m/day)
Minimum	0.0012
P5	0.0043
P50 (Median)	0.0601
P95	0.1697
Maximum	0.1700
Mean	0.0784

Table 5: Comparison with Calibrated Model Parameters

Hydrostratigraphic Unit	Measured P5 (m/day)	Measured P50 (m/day)	Measured P95 (m/day)	Calibrated Model P50 (m/day)
Springbok Sandstone	0.0150	0.0270	0.0300	0.0010 – 0.0211

T +61 7 3012 4000
F +61 7 3012 4001
ARROW ENERGY PTY LTD
ABN 73 078 521 936
LEVEL 39, 111 EAGLE STREET
BRISBANE QLD 4000
GPO BOX 5262
BRISBANE QLD 4001
info@arrowenergy.com.au
arrowenergy.com.au

Macalister Coal Seam	0.0043	0.0601	0.1697	0.0192 – 0.1384

** Note: The model P50 range is calculated from the median calibrated hydraulic conductivity of each HSU across the ensemble of calibrated realisations.*

The comparison (*Table* 5) indicates that the calibrated model hydraulic conductivities are generally consistent with the available measured hydraulic property data.

For the Macalister coal seam, the measured hydraulic conductivity values compare closely with the calibrated model posterior median hydraulic conductivity, with model values falling within the P5 to P95 range of the measured dataset. This indicates that the calibrated model parameters are generally consistent with the available field data.

For the Springbok Sandstone, the calibrated hydraulic conductivity range (0.0010 to 0.0211 m/day) is broadly consistent with the lower end of the measured hydraulic conductivity distribution (P5 = 0.015 m/day, P50 = 0.027 m/day). The overlap between the calibrated and measured ranges indicates that the model calibration remains aligned with available field observations while accounting for the spatial heterogeneity of the hydrostratigraphic unit and scale differences between field measurements and model parameterisation. The adoption of lower hydraulic conductivity values during calibration is also consistent with regional groundwater modelling undertaken by OGIA (2019), which incorporated hydraulic conductivity values ranging from 1.15×10^{-4} to 4.48×10^{-3} m/day.

It is noted that the hydraulic conductivity datasets available for the Springbok Sandstone and Macalister coal seam package are relatively limited in size, particularly for the Springbok Sandstone where only four test results were available. Consequently, the reported P5, P50 and P95 statistics should be regarded as indicative measures of the observed distribution rather than robust population percentiles. The calculated percentiles are based on empirical interpolation of the available data and are therefore subject to uncertainty associated with the limited sample size.

In addition, the available hydraulic conductivity test data are derived largely from bores constructed for groundwater supply, resource assessment or production-related purposes. Such bores are commonly screened within intervals exhibiting sufficient permeability to yield usable groundwater supplies, resulting in a potential bias toward higher measured hydraulic conductivity values relative to the broader hydrostratigraphic unit. Consequently, the measured hydraulic conductivity distribution may not fully represent lower-permeability portions of the Springbok Sandstone and Macalister coal seam package.

This effect is particularly relevant for the Springbok Sandstone, where the calibrated model hydraulic conductivity range is lower than the median of the measured dataset. The discrepancy is considered reasonable because groundwater model parameters represent effective hydraulic conductivity values at a much larger spatial scale than individual bore tests and therefore incorporate lower-permeability zones, spatial heterogeneity and anisotropy that are not captured by local-scale hydraulic testing. The tendency for hydraulic testing to preferentially sample more transmissive intervals may therefore contribute to the observed difference between measured and calibrated hydraulic conductivity values for the Springbok Sandstone.

Notwithstanding these limitations, the comparison demonstrates that the calibrated model hydraulic conductivity values remain broadly consistent with the range of available site-specific measurements and provide a reasonable representation of the hydraulic properties of the modelled hydrostratigraphic units.

T +61 7 3012 4000
F +61 7 3012 4001
ARROW ENERGY PTY LTD
ABN 73 078 521 936
LEVEL 39, 111 EAGLE STREET
BRISBANE QLD 4000
GPO BOX 5262
BRISBANE QLD 4001
info@arrowenergy.com.au
arrowenergy.com.au

Overall, the measured hydraulic conductivity statistics provide independent support for the reasonableness of the calibrated model parameterisation and indicate that the adopted hydraulic conductivity values are broadly consistent with the available site-specific hydrogeological data.

Issue:
The prior and posterior distributions of horizontal hydraulic conductivity (kh), vertical hydraulic conductivity (kv), specific storage (ss), and specific yield (sy) parameters were provided in '*Arrow Energy - Additional Information to support Hopeland Stage 2*' (v1.0 dated 23/06/2026) in Appendix A. The following were noted in relation to the posterior P50 parameters:

For Gasifier G1:
$Sy\_g1s = 5.55 \times 10^{-1}$
$Sy\_g1ki = 5.62 \times 10^{-2}$
$Sy\_g1m = 5.42 \times 10^{-1}$

Sy_g1s is very high, which is unlikely to be representative of the site conditions and requires further explanation.

For Gasifier G2:
$Sy\_g2s = 7.5 \times 10^{-1}$ (Sy is very high)
$Sy\_g2ki = 1.39 \times 10^{-1}$
$Sy\_g2m = 1.0 \times 100$
Sy_g2s is very high.

Sy_g2m value represents void, meaning the rock above the Macalister seam has not collapsed.

For Gasifier G3:
$Sy\_g3s = 2.94 \times 10^{-1}$
$Sy\_g3ki = 7.69 \times 10^{-2}$
$Sy\_g3m = 1.0 \times 100$

Sy_g3m value represents void, meaning the rock above the Macalister seam has not collapsed.

For Gasifier G4:
$Sy\_g4s = 7.5 \times 10^{-1}$
$Sy\_g4ki = 1.24 \times 10^{-1}$
$Sy\_g4m = 1.0 \times 100$

Sy_g4s is very high.

Sy_g4m value represents void, meaning the rock above the Macalister seam has not collapsed.
For Gasifier G5:
$Sy\_g5s = 2.66 \times 10^{-1}$
$Sy\_g5ki = 6.28 \times 10^{-1}$
$Sy\_g5m = 2.22 \times 10^{-1}$

Sy_g5ki is very high.

T +61 7 3012 4000
F +61 7 3012 4001
ARROW ENERGY PTY LTD
ABN 73 078 521 936
LEVEL 39, 111 EAGLE STREET
BRISBANE QLD 4000
GPO BOX 5262
BRISBANE QLD 4001
info@arrowenergy.com.au
arrowenergy.com.au

Specific yield (Sy) value used for the units impacted by the gasifiers are questionable. There is key concern about the Sy values being very high for most of the units and used in the model. Because of the high Sy values used in the model, it has taken longer for the water level to recover at the gasifier sites. This has may have resulted in inwards hydraulic gradient for a long period of time, meaning potential offsite impacts in terms of migration of contamination may have been underestimated by the model.

In addition, only a part of the Springbok Sst appears to be affected by the gasifier (according to CSM diagram) activities, and applying altered model parameters to the entire model layer (which is relatively thick (96 m)) may not be accurate. This model layer 3 (Springbok Sst) may need to be split into two or more layers so that the altered model parameters can be assigned properly in the relevant part of the model domain.

Action required:
6. To ensure that the rest of the modelling results are valid, provide further clarifications for those posterior P50 parameters as detailed above.

Arrow response:

To directly addresses the concern that high storage values may delay recovery and prolong inward gradients, Arrow has constrained the specific yield, and rerun the model, and updated the model report accordingly (see the attached "***PL253 Groundwater Impact Assessment - Clynes Road FDP***" report). The calibration thresholds, objective functions, parameter bounds other than Sy for the Springbok Sandstone and Kogan layer, observation weights and rejection criteria remained unchanged for the rerun of the model.

Specific Yield Parameters

Consistent with DETSI's comments, the groundwater model was revised to constrain specific yield values. The prior parameter distributions were updated and the maximum allowable specific yield assigned to UCG-affected portions of the Springbok Sandstone and Kogan was reduced to 10%. This upper bound was selected based on previous studies (OGIA, 2016; AGE, 2020, 2022; Intera, 2024, 2025), taking account of the lithology, estimated drainable porosity and potential effects of UCG-related fracturing and disturbance.

The groundwater flow model, contaminant transport model, and uncertainty analysis were subsequently re-run using the revised parameter ranges. A new ensemble of calibrated model realisations was generated (216 realisations relative to 364 realisations in the previous version of the report) and used as the basis for all updated predictions presented in the revised report (see the attached "***PL253 Groundwater Impact Assessment - Clynes Road FDP***" report). The resulting prior and posterior parameter distributions are provided in Appendix B of the attached "***PL253 Groundwater Impact Assessment - Clynes Road FDP***" report. Note that specific yield values were presented as decimals in the previously submitted **Gasifiers_hyd_prop_dist.pdf** file; however, they have been converted to percentages (Appendix B of the attached "***PL253 Groundwater Impact Assessment - Clynes Road FDP***" report).

Table 6 presents the prior and posterior P50 specific yield values within the gasifier-affected areas (i.e., zones of hydraulic property change) for both the revised and previous models. The upper bound of the specific yield (prior range in the uncertainty analysis) for the gasifier-affected areas in the Springbok Sandstone and Kogan layer has been reduced to 10% in the revised model (0 to 10%), whereas the prior range for the Macalister coal seam remains unchanged from the previous model (0 to 100%).

T +61 7 3012 4000
F +61 7 3012 4001
ARROW ENERGY PTY LTD
ABN 73 078 521 936
LEVEL 39, 111 EAGLE STREET
BRISBANE QLD 4000
GPO BOX 5262
BRISBANE QLD 4001
info@arrowenergy.com.au
arrowenergy.com.au

Table 6: Prior and posterior P50 specific yield values in the gasifier affected areas (zone of hydraulic property change) – previous model versus revised model

Gasifier	Parameter	Previous model (April 2026 ensemble)		Revised model (August 2026 ensemble)	
		Prior P50	Posterior P50	Prior P50	Posterior P50
1	Sy_g1s (%)	46.50	55.50	2.42	2.08
	Sy_g1ki (%)	52.20	56.20	1.85	1.74
	Sy_g1m (%)	89.00	54.20	9.92	5.64
2	Sy_g2s (%)	45.70	75.00	2.20	2.73
	Sy_g2ki (%)	50.10	13.90	2.32	1.88
	Sy_g2m (%)	71.80	100.00	9.78	8.65
3	Sy_g3s (%)	56.40	29.40	2.36	1.68
	Sy_g3ki (%)	43.50	7.69	1.89	2.76
	Sy_g3m (%)	66.30	100.00	7.52	5.99
4	Sy_g4s (%)	40.80	75.00	2.24	2.17
	Sy_g4ki (%)	48.20	12.40	1.90	1.81
	Sy_g4m (%)	99.10	100.00	8.81	0.10
5	Sy_g5s (%)	60.40	26.60	1.88	4.12
	Sy_g5ki (%)	51.00	62.80	2.24	2.10
	Sy_g5m (%)	96.00	22.20	11.20	6.64

Consistent with the original model, the updated calibration achieved acceptable history-matching performance for groundwater levels, hydraulic gradients, and contaminant concentrations, indicating that elevated specific yield values were not required to reproduce observed system behaviour. The revised ensemble therefore provides a more conservative and physically plausible representation of storage properties while maintaining consistency with available monitoring data.

Influence on Groundwater Recovery and Contaminant Migration

A comparison was undertaken between predictions generated using the April 2026 ensemble and the revised ensemble developed using the constrained specific yield distributions.

The comparison (see below tables) demonstrates that the reduction in specific yield values resulted in only minor changes to model predictions, including:

- **negligible changes in the proportion of boundary cells exhibiting inward hydraulic gradients toward Lot 40 DY85;**

  Table 5-2 of the report is updated (see the attached "***PL253 Groundwater Impact Assessment - Clynes Road FDP***" report) and the difference between the two ensembles (April 2026 ensemble and updated ensemble) is presented in the Table 7 below.

- **minor changes to particle travel distances within the Springbok Sandstone and Macalister coal seam;**

T +61 7 3012 4000
F +61 7 3012 4001
ARROW ENERGY PTY LTD
ABN 73 078 521 936
LEVEL 39, 111 EAGLE STREET
BRISBANE QLD 4000
GPO BOX 5262
BRISBANE QLD 4001
info@arrowenergy.com.au
arrowenergy.com.au

Table 5-3 of the report is updated (see the attached "***PL253 Groundwater Impact Assessment - Clynes Road FDP***" report) and the difference between the two ensembles (April 2026 ensemble and updated ensemble) is presented in the Table 8 below.

- **no change in the predicted year that benzene concentrations reach below the laboratory limit of reporting (LOR) in either hydrostratigraphic unit; and**
- **a maximum change of approximately one year in predicted naphthalene depletion timing within the Macalister coal seam.**

  Table 5-4 of the report is updated (see the attached "***PL253 Groundwater Impact Assessment - Clynes Road FDP***" report) and the difference between the two ensembles (April 2026 ensemble and updated ensemble) is presented in the Table 9 below.

Table 7: Difference between the April 2026 ensemble and the updated August 2026 ensemble in the summary statistics for the predicted percentage of cells with horizontal hydraulic gradients toward Lot 40 DY85 along 1,500 m sections of the southern and western boundaries

Modelling scenario	Percentile	Springbok sandstone			Macalister coal		
		2025	2040	2061	2025	2040	2061
Scenario 2 (approved)	P5	2%	3%	3%	-2%	0%	1%
	P50	2%	1%	-2%	-3%	0%	1%
	P95	0%	-2%	-3%	-3%	-1%	0%
Scenario 3 (Clynes Rd)	P5	2%	3%	4%	-2%	0%	0%
	P50	2%	0%	-1%	-3%	0%	1%
	P95	0%	-1%	-3%	-3%	0%	1%

Table 8: Difference between the April 2026 ensemble and the updated August 2026 ensemble in the statistics of the particle travel distances (from 2019 to 2225) for particles released within Springbok sandstone and Macalister coal seam

Modelling scenario	Layer	Particle location	P5 (m)			P50 (m)			P95 (m)		
			Min	Mean	Max	Min	Mean	Max	Min	Mean	Max
Scenario 2 (approved)	Springbok	Bores	<1	4	22	<1	2	12	-3	4	92
		Gasifiers	-4	<1	5	-7	-1	-8	-15	5	37
		Boundaries	<1	<1	-1	<1	-2	-15	-3	-14	91
	Macalister	Bores	2	1	8	-1	29	22	3	31	82
		Gasifiers	30	10	38	13	34	28	32	42	25

T +61 7 3012 4000
F +61 7 3012 4001
ARROW ENERGY PTY LTD
ABN 73 078 521 936
LEVEL 39, 111 EAGLE STREET
BRISBANE QLD 4000
GPO BOX 5262
BRISBANE QLD 4001
info@arrowenergy.com.au
arrowenergy.com.au

		Boundaries	-2	3	80	<1	18	45	6	33	73
Scenario 3 (Clynes Rd)	Springbok	Bores	<1	4	19	<1	2	12	-3	3	70
		Gasifiers	-4	<1	6	-7	-1	-8	-13	4	37
		Boundaries	<1	<1	-1	<1	-2	-14	-3	-14	93
	Macalister	Bores	2	-1	10	-1	25	20	3	32	-21
		Gasifiers	6	9	36	17	33	58	14	36	55
		Boundaries	-2	2	56	<1	17	38	-8	32	74

Table 9: Difference between the April 2026 ensemble and the updated August 2026 ensemble in the predicted year of contaminant concentration reaching below the LOR

Modelling scenario	**Compound**	**Springbok sandstone**			**Macalister coal**		
		P5	**P50**	**P95**	**P5**	**P50**	**P95**
Scenario 2 (approved)	Benzene	No change	No change	No change	No change	No change	1 year
	Naphthalene	No change	No change	No change	No change	No change	1 year
Scenario 3 (Clynes Rd)	Benzene	No change	No change	No change	No change	No change	1 year
	Naphthalene	No change	No change	No change	No change	No change	1 year

The updated results, therefore, indicate that constraining specific yield values does not materially alter the predicted groundwater flow regime, contaminant migration pathways, contaminant attenuation trends, or the overall impact assessment conclusions.

Importantly, the revised ensemble continues to predict inward hydraulic gradients toward Lot 40 DY85 within the Springbok Sandstone and a persistent downward vertical hydraulic gradient from the Springbok Sandstone to the Macalister coal seam. Consequently, the concern that high specific yield values may have caused off-site contaminant migration risks to be underestimated is not supported by the updated modelling results.

Springbok Sandstone Layer Representation

The current representation of the Springbok Sandstone as a single model layer is considered appropriate for the objectives and scale of the assessment.

While the conceptual site model indicates that gasifier-related impacts affect only part of the Springbok Sandstone, altered hydraulic properties are not assigned uniformly across the entire hydrostratigraphic unit. UCG-related hydraulic property changes are represented locally through gasifier-specific time-varying hydraulic conductivity and storage parameterisation during calibration and uncertainty analysis. This approach allows localised hydraulic impacts

T +61 7 3012 4000
F +61 7 3012 4001
ARROW ENERGY PTY LTD
ABN 73 078 521 936
LEVEL 39, 111 EAGLE STREET
BRISBANE QLD 4000
GPO BOX 5262
BRISBANE QLD 4001
info@arrowenergy.com.au
arrowenergy.com.au

associated with historical UCG activities to be represented without requiring subdivision of the regional-scale model layer.

The is no CSG production proposed from the Springbok Sandstone, and the proposed CSG wells therefore impose no direct pumping stress on that unit. Further subdivision of the Springbok Sandstone could provide additional local-scale resolution; however, given the regional assessment objectives of the model and the focus on groundwater flow behaviour, contaminant migration, and long-term recovery at and around Lot 40 DY85, such refinement is unlikely to materially alter the predictive outcomes. In addition, uncertainty associated with storage properties has been explicitly evaluated through the updated uncertainty analysis, which is considered a more appropriate assessment of prediction uncertainty than introducing additional layer subdivision solely for sensitivity-testing purposes.

Based on the revised calibration and uncertainty analysis, the modelling results continue to indicate that the proposed development does not materially alter groundwater flow directions, contaminant migration pathways, contaminant depletion timing, or long-term groundwater recovery associated with the former Hopeland UCG site.

Issue:
The response provided in 'Arrow Energy - Additional Information to support Hopeland Stage 2' (v1.0 dated 23/06/2026) for inward flow toward Lot 40 DY85, in the Springbok Sandstone (Figure 4), through to the end of the recovery period (2225) is not satisfactory. Inappropriate model parameters used at the gasifier and gasifier affected areas may be impacting the flow pattern and time of recovery.

Action required:
7. Clarify and provide further justification for the model parameters used.

Arrow response:

The updated ensemble predictions (discussed in the previous comment) indicate no material change in the predicted groundwater flow directions at the end of the recovery period. Please refer to response to Action 6.

Issue:
A contaminant transport model was developed to simulate the fate and transport of dissolved benzene and naphthalene within the Springbok sandstone and the Macalister coal seam. Section 2.4.2 of Report PL253 Groundwater Impact Assessment – Clines Road FDP provides information justifying the selection of benzene and naphthalene as representative contaminants in the contaminant transport model.

Previous groundwater investigations have identified elevated concentrations of other chemicals of potential concern (COPC) including total dissolved solids, metals, ammonia and cyanide which have not been considered by the groundwater model. These COPC have different characteristics (i.e. solubility, degradation rates) which may not correlate with the characteristics of benzene and naphthalene.

Action required:
8. Clarify how does the current contaminant transport model assess the risks associated with the fate and transport of other COPC identified at the site.
Arrow response:

T +61 7 3012 4000
F +61 7 3012 4001
ARROW ENERGY PTY LTD
ABN 73 078 521 936
LEVEL 39, 111 EAGLE STREET
BRISBANE QLD 4000
GPO BOX 5262
BRISBANE QLD 4001
info@arrowenergy.com.au
arrowenergy.com.au

The contaminant transport model was developed to assess the fate and transport of dissolved contaminants within the Springbok Sandstone and Macalister Coal Seam using benzene and naphthalene as representative chemicals of potential concern (COPCs). The selection of these compounds is consistent with **Environmental Authority (EA) 0001401 Water Conditions, Table 3 - Investigation Limits** (see Table 10 below), and with previous groundwater assessments completed for the site and documented in Appendix E (Section 126A.pdf).

Table 10: Investigation Limits (EA0001401, Water Conditions, Table 3)

Chemical Group	**Investigation Limits (mg/L)**
Phenolic compounds	> Limit of Reporting (LOR)
Polynuclear aromatic hydrocarbons (PAHs) including Naphthalene	> LOR
Total recoverable hydrocarbons (TRH) (Silica Gel cleanup)	> LOR
Cyanide	0.08
Benzene	0.001
Toluene	0.8
Ethylbenzene	0.3
Xylene	0.6

The purpose of the transport modelling was not to explicitly simulate every identified COPC, but rather to evaluate contaminant migration using representative compounds that bound the range of mobility and attenuation behaviour expected for contaminants present at the site. Benzene and naphthalene were selected because they represent relatively mobile and less-mobile hydrocarbon end-members, respectively.

Previous investigations have identified additional COPCs including cyanide, toluene, ethylbenzene, xylenes (BTEX compounds), phenolic compounds, polycyclic aromatic hydrocarbons (PAHs) and total recoverable hydrocarbons (TRH). While these compounds exhibit differing physicochemical properties, their relative dissolved-phase mobility can be broadly assessed relative to benzene and naphthalene.

The expected relative mobility of the identified COPCs is:

Cyanide ≈ Benzene > Toluene > Ethylbenzene > Xylenes > Phenolic Compounds > Naphthalene (PAHs) > TRH

This ranking is based principally on aqueous solubility, sorption potential and attenuation processes.

- Benzene is expected to be the most mobile hydrocarbon constituent and is therefore likely to generate one of the longest dissolved hydrocarbon plumes under equivalent hydrogeological conditions.
- Toluene, ethylbenzene and xylenes exhibit lower mobility than benzene due to greater retardation and attenuation and would therefore be expected to migrate shorter distances.

T +61 7 3012 4000
F +61 7 3012 4001
ARROW ENERGY PTY LTD
ABN 73 078 521 936
LEVEL 39, 111 EAGLE STREET
BRISBANE QLD 4000
GPO BOX 5262
BRISBANE QLD 4001
info@arrowenergy.com.au
arrowenergy.com.au

- Phenolic compounds exhibit moderate mobility due to relatively high solubility but are generally subject to greater sorption and attenuation than BTEX compounds.
- PAHs, including naphthalene, are more strongly retarded by sorption to organic matter and coal and therefore represent less-mobile hydrocarbon contaminants.
- TRH constituents generally exhibit the lowest dissolved-phase mobility owing to strong sorption and limited aqueous solubility.

Accordingly, the transport behaviour of the majority of hydrocarbon-related COPCs is expected to fall within, or be more attenuated than, the range represented by benzene and naphthalene. The benzene and naphthalene transport simulations therefore provide a reasonable and scientifically defensible assessment of potential migration behaviour for the broader suite of hydrocarbon contaminants identified at the site.

Cyanide-Specific Considerations

Cyanide differs from the hydrocarbon COPCs because its environmental behaviour is strongly influenced by pH-dependent speciation. Cyanide exists in equilibrium between hydrogen cyanide (HCN) and the cyanide ion (CN^-):

$$HCN \rightleftharpoons H^+ + CN^- \qquad (1)$$

Under acidic to neutral pH conditions, cyanide occurs predominantly as HCN, which may volatilise, oxidise and biodegrade, resulting in attenuation rates that can exceed those of benzene. Under alkaline conditions, cyanide exists predominantly as CN^-, which is less volatile and generally more persistent in groundwater.

Groundwater monitoring data from Lot 40 DY85 indicate pH values ranging from approximately 5.7 to 12.3, demonstrating that cyanide speciation, mobility and attenuation mechanisms may vary significantly across the site. However, the available groundwater monitoring dataset reports Total Cyanide concentrations only and does not distinguish between HCN and CN^- species. Consequently, reliable species-specific transport parameters cannot be developed from the available data without introducing substantial uncertainty.

Although cyanide is expected to be highly mobile because of its high aqueous solubility and low sorption potential, the elevated groundwater pH observed at portions of the site suggests cyanide persistence may be greater than would be expected under neutral or acidic conditions. For screening purposes, cyanide attenuation could therefore be considered broadly comparable to, or potentially more conservative than, benzene under alkaline groundwater conditions.

Given the uncertainty regarding cyanide speciation and the absence of species-specific concentration data, explicit cyanide transport modelling was not considered sufficiently robust to support predictive assessment.

Assessment of Other COPCs

The contaminant transport model therefore assesses the risks associated with other COPCs through the use of representative bounding contaminants:

- Benzene represents the mobile hydrocarbon end-member.
- Naphthalene represents a less-mobile, more strongly retarded hydrocarbon end-member.
- Other hydrocarbon COPCs are expected to exhibit transport behaviour within the range defined by benzene and naphthalene.

T +61 7 3012 4000
F +61 7 3012 4001
ARROW ENERGY PTY LTD
ABN 73 078 521 936
LEVEL 39, 111 EAGLE STREET
BRISBANE QLD 4000
GPO BOX 5262
BRISBANE QLD 4001
info@arrowenergy.com.au
arrowenergy.com.au

- Cyanide was evaluated qualitatively because transport behaviour is controlled by pH-dependent speciation that cannot be reliably characterised with the available monitoring dataset.

In addition, particle tracking analyses were undertaken to provide a conservative assessment of potential groundwater flow paths and migration extents from Lot 40 DY85. These analyses provide insight into the maximum potential migration pathways (conservative scenario) for dissolved contaminants irrespective of contaminant-specific attenuation assumptions.

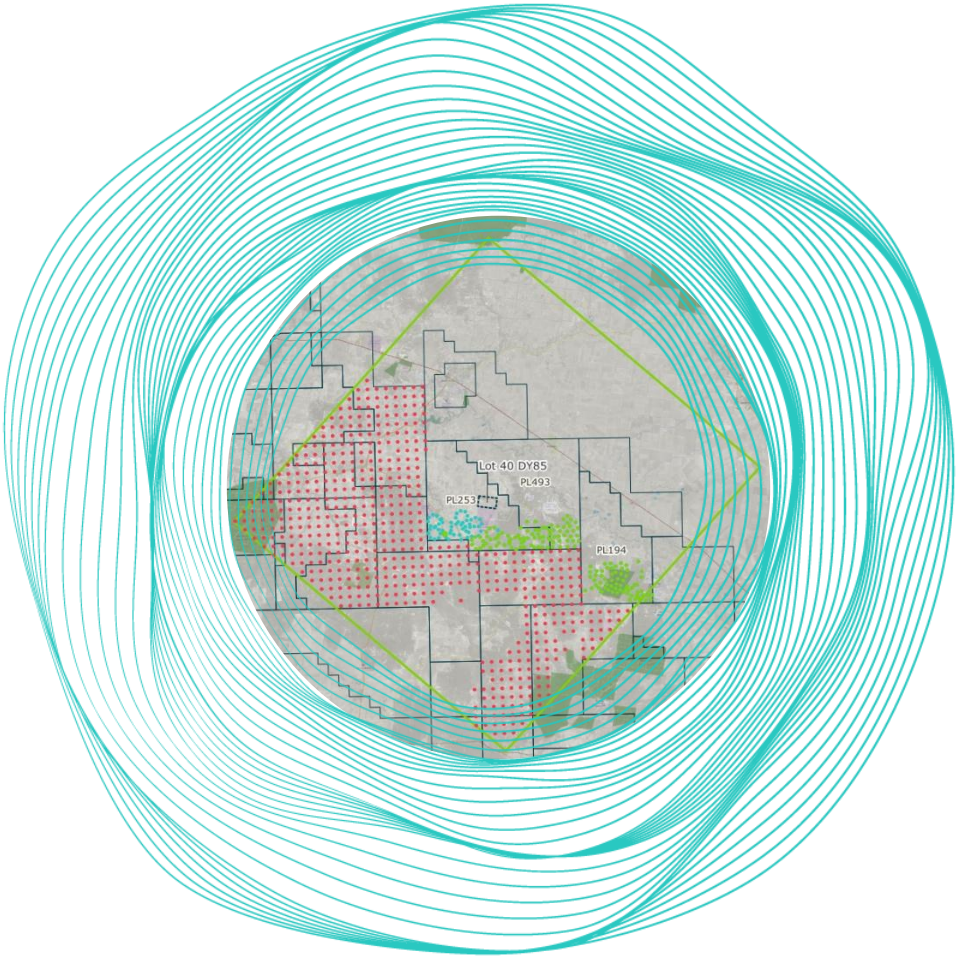
Accordingly, the contaminant transport modelling, together with particle tracking results, provides a reasonable and scientifically defensible assessment of the potential fate and transport of the broader suite of COPCs identified at the site, while recognising the limitations associated with cyanide speciation data.

T +61 7 3012 4000
F +61 7 3012 4001
ARROW ENERGY PTY LTD
ABN 73 078 521 936
LEVEL 39, 111 EAGLE STREET
BRISBANE QLD 4000
GPO BOX 5262
BRISBANE QLD 4001
info@arrowenergy.com.au
arrowenergy.com.au

ARROW ENERGY PTY LTD

PL253 Groundwater Impact Assessment - Clynes Road FDP

Document no. Rev 1: 411001-00917-REP-HG-002



20 August 2026

Level 23, 123 Albert Street
Brisbane QLD 4000
PO Box 15081, City East QLD 4002
Australia
T: +61 7 3377 7000
Worley Consulting Pty Ltd
ABN 50 098 008 818

© Copyright 2026 Worley ACN 096 090 158. No part of this document or the information it contains may be reproduced or transmitted in any form or by any means electronic or mechanical, including photocopying, recording, or by any information storage and retrieval system, without permission in writing from Worley.

worley.com

Disclaimer

This report has been prepared on behalf of and for the exclusive use of Arrow Energy Pty Ltd, and is subject to and issued in accordance with the agreement between Arrow Energy Pty Ltd and Worley Consulting Pty Ltd. Worley Consulting Pty Ltd accepts no liability or responsibility whatsoever for it in respect of any use of or reliance upon this report by any third party. Copying this report without the permission of Arrow Energy Pty Ltd or Worley Consulting Pty Ltd is not permitted.

The information contained in these documents is protected by the Global Data Protection Regulation (GDPR). Worley complies with the provisions of the Regulation and the information is disclosed on the condition that the Recipient also complies with the provisions of the (GDPR). In particular, all of the resumes and the information contained therein, must be kept securely, must be used only for the purposes of assessing the suitability of the individuals to perform the tasks proposed and/or assessing the overall capabilities of Worley to undertake the Work proposed and must be destroyed upon completion of those purposes.

Details on how personal information provided to Worley is processed can be found at https://www.worley.com/site-services/privacy.

PROJECT - 411001-00917-REP-HG-002: PL253 Groundwater Impact Assessment - Clynes Road FDP

Rev	Description	Originator	Reviewer	Worley Approver	Revision Date	Customer Approver	Approval Date
Rev B	Draft report	M. Azadi	G. Jacobs	M. Azadi	17 April 2026		
Rev 0	Final report	M. Azadi	G. Jacobs	M. Azadi	29 April 2026		
Rev 1	Updated to address DETSI comments	M. Azadi	G. Jacobs	M. Azadi	20 August 2026		

-

20 August 2026

Level 23, 123 Albert Street
Brisbane QLD 4000
PO Box 15081, City East QLD 4002
Australia
T: +61 7 3377 7000
Worley Consulting Pty Ltd
ABN 50 098 008 818

© Copyright 2026 Worley ACN 096 090 158. No part of this document or the information it contains may be reproduced or transmitted in any form or by any means electronic or mechanical, including photocopying, recording, or by any information storage and retrieval system, without permission in writing from Worley.

worley.com

Table of contents

Acronyms and abbreviations **1**

1. Introduction **2**

1.1 Scope of work 4

1.2 Study objectives 5

2. Site conceptualisation model **6**

2.1 Previous studies 6

2.2 Site setting and geology 8

2.3 Groundwater flow regime 8

2.4 Groundwater Monitoring 9

2.4.1 Groundwater level 9

2.4.2 Groundwater quality and contaminants of concern 12

3. Groundwater modelling **20**

3.1 Groundwater flow model 20

3.1.1 Model layers 22

3.1.2 Hydraulic properties 24

3.1.3 Boundary conditions 25

3.1.4 Temporal discretisation 30

3.1.5 Metric systems 30

3.2 Particle tracking 31

3.3 Contaminant transport model 33

3.3.1 Transport model coupling 33

3.3.2 Initial condition 33

3.3.3 Boundary condition 34

4. History matching **38**

4.1 Calibration approach 38

4.2 Parameterisation 38

4.3 Observation data assimilation 42

4.4 Groundwater flow model 44

4.4.1 History matching metrics 44

4.4.2 Groundwater levels and flow directions 47

4.4.3 Calibrated hydraulic parameters 49

4.5 Contaminant transport model 51

4.5.1 History-matching metrics 51

4.5.2 Simulated benzene and naphthalene concentrations 54

5. Predictive groundwater flow modelling **57**

5.1 Predictive model setup 57

5.2 Groundwater level and flow directions 58

5.3 Vertical hydraulic gradient 64

5.4 Particle tracking 66

5.5 Contaminant transport and fate 71

5.6 Impact assessment 74

6. Conclusions and recommendations **77**

7. References **80**

Appendices

Appendix A. Modelled versus observed hydrographs

Appendix B. Median prior and posterior parameter distributions

Appendix C. Modelled versus observed concentration time series plots - Benzene

Appendix D. Modelled versus observed concentration time series plots - Naphthalene

Appendix E. Predictive uncertainty - groundwater levels

Appendix F. Predictive uncertainty – Benzene concentrations

Appendix G. Predictive uncertainty – Naphthalene concentrations

List of tables

Table 3-1 Model layers 22
Table 3-2 Summary of initial hydraulic properties 24
Table 3-3 Initial annual recharge rate for each zone 25
Table 3-4 Contaminant transport parameters 35
Table 5-1 Probabilistic terminology used (from Peeters & Middlemis, 2023) 57
Table 5-2 Summary statistics of predicted percentage of cells along 1,500 m sections of the southern and western boundaries with horizontal hydraulic gradients toward Lot 40 DY85 63
Table 5-3 Summary statistics of particle travel distances (from 2019 and 2225) for particles released within Springbok sandstone and Macalister coal seam 71
Table 5-4 Predicted year of contaminant concentration reaching below the LOR 72

List of figures

Figure 1-1 Project location and distribution of Arrow and non-Arrow wells 3
Figure 2-1 Conceptual Site Model of former Hopeland UCG 7
Figure 2-2 Groundwater level contours in Springbok sandstone and Macalister coal seam (Q3 2025) 11
Figure 2-3 Time series benzene concentration for a) on-site and b) off-site bores completed in the Springbok sandstone (provided by Arrow) 13
Figure 2-4 Time series benzene concentration for a) on-site and b) off-site bores completed in the Macalister coal seam (provided by Arrow) 14
Figure 2-5 Time series naphthalene concentration for a) on-site and b) off-site bores completed in the Springbok sandstone (provided by Arrow) 15
Figure 2-6 Time series naphthalene concentration for a) on-site and b) off-site bores completed in the Macalister coal seam (provided by Arrow) 16
Figure 2-7 Benzene concentration for all monitoring bores compared with exponential curve of source depletion term for a) Springbok sandstone and b) Macalister coal seam 18
Figure 2-8 Naphthalene concentration for all monitoring bores compared with exponential curve of source depletion term for a) Springbok sandstone and b) Macalister coal seam 19
Figure 3-1 3D groundwater model with 30x vertical exaggeration (from Intera, 2025) 21
Figure 3-2 PL253 3D groundwater model (with 30x vertical exaggeration of the 3D model and cross-sections) 23
Figure 3-3 Simulated recharge zones 26
Figure 3-4 Monthly total abstraction rates for FDP scenarios 2 and 3 28
Figure 3-5 Particle release locations 32
Figure 4-1 Pilot point locations 41

Figure 4-2 Bore locations with transient groundwater level data 43
Figure 4-3 Calculated RMS and SRMS for converged model realisations 44
Figure 4-4 Calibration fit of reference case 45
Figure 4-5 Observed vs modelled groundwater levels in monitoring bores 46
Figure 4-6 Simulated groundwater levels in Springbok sandstone and Macalister coal seam (end of December 2025) 48
Figure 4-7 Calibrated hydraulic property ranges 50
Figure 4-8 Calculated RMS and SRSM for benzene concentration across the posterior ensemble 51
Figure 4-9 Calculated RMS and SRSM for naphthalene concentration across the posterior ensemble 52
Figure 4-10 Benzene history matching fit for the reference case 53
Figure 4-11 Naphthalene history matching fit for the reference case 53
Figure 4-12 Simulated benzene and naphthalene concentration trends for representative monitoring bores screened in the Springbok sandstone and Macalister coal seam 54
Figure 4-13 Simulated benzene concentrations in Springbok sandstone and Macalister coal seam (end of December 2025) 56
Figure 5-1 Predicted median groundwater levels in Springbok sandstone and Macalister coal seam for scenario 3 (end of December 2061) 59
Figure 5-2 Predicted median groundwater levels in Springbok sandstone and Macalister coal seam for scenario 3 (end of December 2225) 60
Figure 5-3 Predicted median difference in groundwater levels between scenario 2 and 3 in Springbok sandstone and Macalister coal seam (end of December 2061) 61
Figure 5-4 Lot 40 DY85 boundary sections (red dashed lines, 1500 m each) and 100 m buffer lines within the boundary (green dashed lines) used for calculation of horizontal hydraulic gradient 63
Figure 5-5 Predicted vertical hydraulic gradient between the Springbok sandstone and Macalister coal seam at paired monitoring locations 65
Figure 5-6 Probability of particle tracking pathlines in Springbok sandstone and Macalister coal seam for scenario 3 (particles released at monitoring bores) 67
Figure 5-7 Probability of particle tracking pathlines in Springbok sandstone and Macalister coal seam for scenario 3 (particles released at gasifiers) 68
Figure 5-8 Probability of particle tracking pathlines in Springbok sandstone and Macalister coal seam for scenario 3 (particles released at Lot 40 DY85 boundaries) 69
Figure 5-9 Predicted median benzene concentrations in the Springbok sandstone (end of December 2040) and Macalister coal seam (end of December 2030) 73

Acronyms and abbreviations

Acronym/abbreviation	Definition
BGL	Below Ground Level
COC	Contaminants of Concern
CSG	Coal Seam Gas
FDP	Field Development Plan
GHB	General Head Boundary
HSU	Hydrostratigraphic Units
LOR	Limit of Reporting
OGIA	Office of Groundwater Impact Assessment
QOI	Quantities of Interest
SCM	Site Conceptual Model
UCG	Underground Coal Gasification
WCM	Walloon Coal Measures

1. Introduction

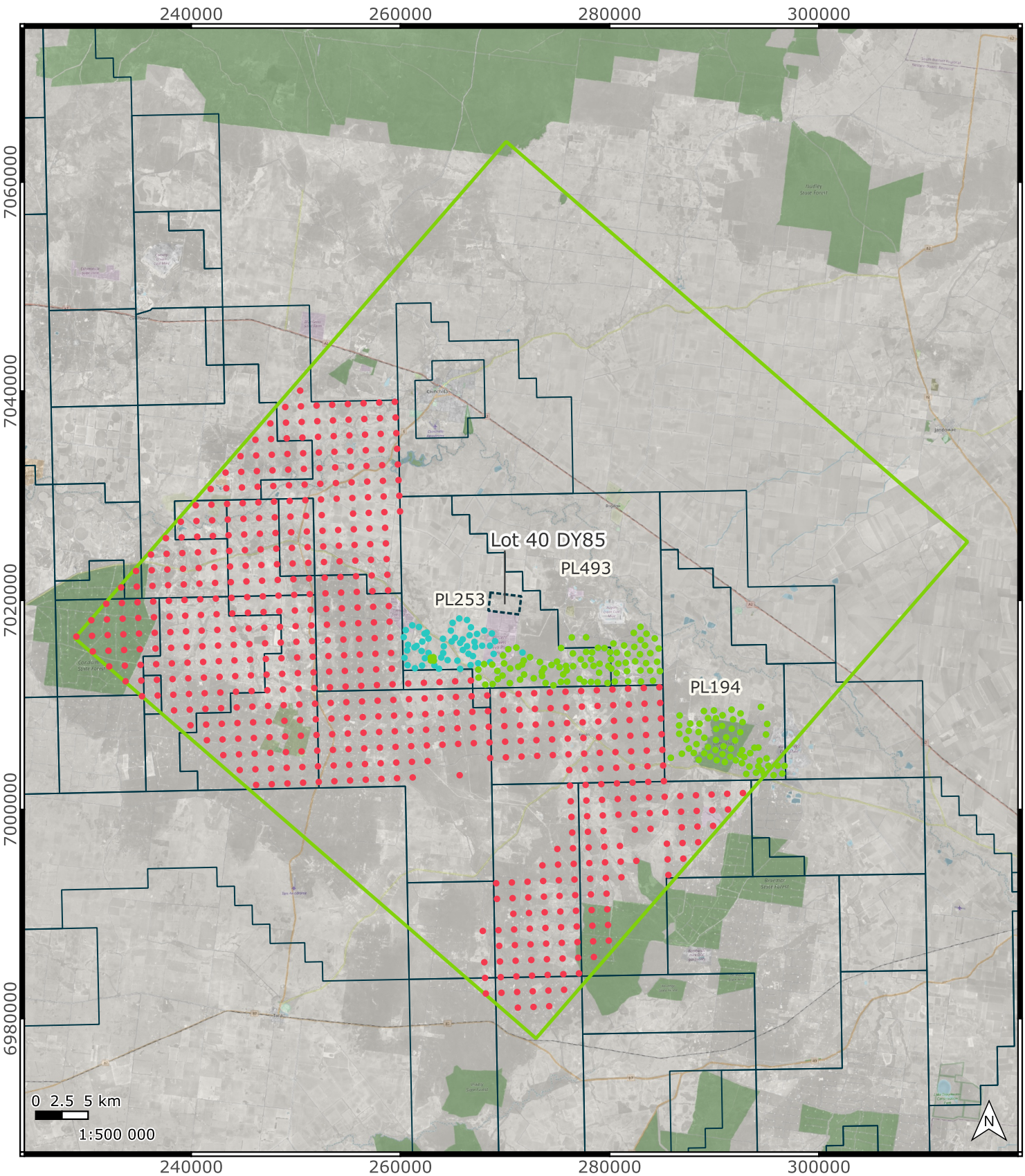
Arrow Energy Pty Ltd (Arrow) proposes to undertake coal seam gas (CSG) production activities within Production Licence 253 (PL253), Queensland. The PL253 area includes the former Hopeland Underground Coal Gasification (UCG) site located on Lot 40 DY85, where historical UCG operations undertaken by Linc Energy resulted in residual hydrocarbon contamination and other UCG by-products within the groundwater system.

Arrow has conducted groundwater monitoring, numerical modelling, and annual reporting in and around the former UCG site since 2018 to characterise groundwater conditions, contaminant behaviour, and potential risks to surrounding receptors. Environmental Authority EA0001401, in effect since November 2023, authorises Stage 1 development activities within PL253, including the drilling and operation of 55 CSG production wells (Kogan Creek development).

Arrow is proposing additional development under an expanded Field Development Plan (FDP) associated with the Jammat project and is seeking regulatory approval for further 55 CSG wells along Clynes Road.

The location of the PL253 project area, the former Hopeland UCG site, and the distribution of Arrow (approved wells and proposed Clynes Road wells) and non-Arrow abstraction wells relevant to this assessment are shown in Figure 1-1.

As part of the Environmental Authority application process, updated groundwater modelling is required to assess the potential impacts of Arrow's proposed activities on groundwater flow, contaminant migration, and long-term groundwater recovery associated with the former Hopeland UCG site. Based on Arrow's previous studies (GHD, 2019; AGE, 2021, 2023; Intera, 2024, 2025), this assessment has been prepared by Worley to support Arrow's application for approval of the proposed expansion.



Legend

- Groundwtaer model extent
- Lot 40 DY85
- Petroleum Leases

Well groups

- Approved Arrow wells
- Arrow Clynes Rd wells
- Non-Arrow abstraction points (from UWIR 2021)

Project location and distribution of Arrow and non-Arrow wells

Project No.	Client	Figure No.
411001-00917	Arrow	1-1

Notes:
Project CRS: GDA94 / MGA zone 56
Last Saved: 12:58 25/02/2026
Filename: Figure_1-1
Exported by User: Mohsen.Azadi
Project Exported: 13:15 25/02/2026

References:
N/A

File Path: C:\modelling\Arrow\deliverables\Figures_REP-HG-001\Figure_1-1.qgz

© Worley Pty Ltd While every care is taken to ensure the accuracy of this data, Worley makes no representations or warranties aboutits accuracy, reliability, completeness or suitability for any particular purpose and disclaims all responsibility and all liability (including without limitation liability in negligence) for all expenses, losses, damages (including indirect or consequential damage) and costs which might be incurred as a result of the data being inaccurate or incomplete in any way and for any reason.

worley consulting

1.1 Scope of work

The scope of work of this study is to assess the potential impacts of Arrow's proposed activities on groundwater flow, contaminant migration, and long-term groundwater recovery associated with the former Hopeland UCG site. The scope includes:

Site conceptual model development

Building on Arrow's previous investigations and modelling studies (GHD, 2019; AGE, 2021, 2023; Intera, 2024, 2025), the Site Conceptual Model (SCM) was updated to incorporate the latest hydrostratigraphic units (HSUs) defined in Arrow's geology model and to refine the understanding of groundwater flow and contaminant behaviour at Lot 40 DY85. The updated SCM integrates groundwater monitoring data from existing bores located both within and beyond Lot 40 DY85 and incorporates current interpretation of residual contaminant source zones associated with historical UCG activities.

The updated SCM was developed to identify potential contaminant mobilisation pathways and to characterise groundwater flow directions and concentration distributions in the vicinity of Lot 40 DY85. This refined conceptualisation provides a robust and informed basis for subsequent numerical model development, history matching, and impact assessment.

Groundwater flow and transport models development

Numerical groundwater flow and contaminant transport models were developed to represent aquifers on and in the vicinity of Lot 40 DY85, with particular focus on the Springbok sandstone and the Macalister coal seam including relevant Walloon Coal Measures (WCM) units. The models were configured to evaluate historical and future changes in groundwater flow directions, and contaminant migration associated with UCG and CSG abstraction. Building on Arrow's most recent PL253 numerical groundwater flow and transport models (Intera, 2025), the models were updated to incorporate the proposed FDP for the Jammat project, including the Clynes Road wells.

The numerical simulation period was extended to the end of 2225 (200 years predictive period), to enable assessment of long-term groundwater recovery and potential contaminant migration beyond the abstraction period.

History matching groundwater flow and contaminant transport models

History matching (i.e., calibration) of the groundwater flow and contaminant transport models was undertaken using all available groundwater level and contaminants' concentration data, including monitoring data from Arrow's newly installed Hopeland wells (HL34–HL37).

Particle tracking and contaminant transport modelling

Two approaches were considered to assess the impact of Arrow's proposed FDP on migration of contaminants within PL253, in particular around and within Lot 40 DY85. These include particle tracking and contaminant transport modelling.

First, the particle tracking model was developed based on the history-matched groundwater flow model and used to assess potential contaminant flow paths without including natural attenuation processes, effectively simulating the centre of a plume of a conservative tracer. The contaminant transport model was then developed based on the calibrated groundwater

flow model. Unlike particle tracking model, the contaminant transport model includes mechanical dispersion, molecular diffusion, as well as natural attenuation (sorption and biodegradation/decay) and dual domain mass transfer processes continuously occurring within subsurface.

Particle tracking fulfilled the following objectives:

- Assessed the effect of particle tracking starting in wells that have exhibited elevated UCG contaminants.
- Particles included the following locations:
  - All monitoring bores,
  - All model cells intercepting gasifier locations, and
  - All model cells intercepting Lot 40 DY85 boundaries.
- Assessed particle tracks (travel times, distances and trajectories) to evaluate the impact of Arrow's proposed FDP on migration of contaminants from Lot 40 DY85.

The contaminant transport model, developed based on the SCM and groundwater flow model, incorporates:

- the most recent groundwater quality data for model history matching, and
- dual porosity (or dual permeability) capability to better represent contaminant transport into and out of fractures and low permeability pore spaces that may contain residual contaminant sources.

Predictive uncertainty analysis

An uncertainty analysis was undertaken to evaluate the influence of hydrogeological variability on model predictions.

Impact assessment

Predictive impact assessment was undertaken to evaluate potential future contaminant migration from Lot 40 DY85 during the abstraction period and long-term groundwater recovery associated with the former Hopeland UCG site.

1.2 Study objectives

The overarching objective of this study is to provide a comprehensive understanding of the potential impacts of Arrow's proposed FDP on groundwater flow and contaminant migration associated with the former Hopeland UCG site on Lot 40 DY85.

The outcomes of this study are intended to:

- Support Arrow's Environmental Authority application, ongoing groundwater management, and
- Provide confidence that potential impacts to groundwater resources and receptors are appropriately understood and managed.

2. Site conceptualisation model

2.1 Previous studies

Hydrogeological understanding of the former Hopeland UCG site and surrounding PL253 area has evolved through a sequence of investigations, conceptual studies and modelling exercises completed since the start of (and informed by) UCG operations. UCG trial activities conducted on Lot 40 DY85 between 1999 and 2013 established the disturbance setting that subsequent studies sought to characterise, including local depressurisation, potential formation fracturing, and hydrocarbon byproducts in groundwater. Early conceptualisation work documented the site setting and identified the Springbok sandstone and the Macalister coal seams as the principal water-bearing horizons of interest, along with potential recharge mechanisms and the influence of historical operations on pressures and groundwater flow pathways. An SCM of contamination sources, groundwater flow pathways and monitoring bores is shown in Figure 2-1.

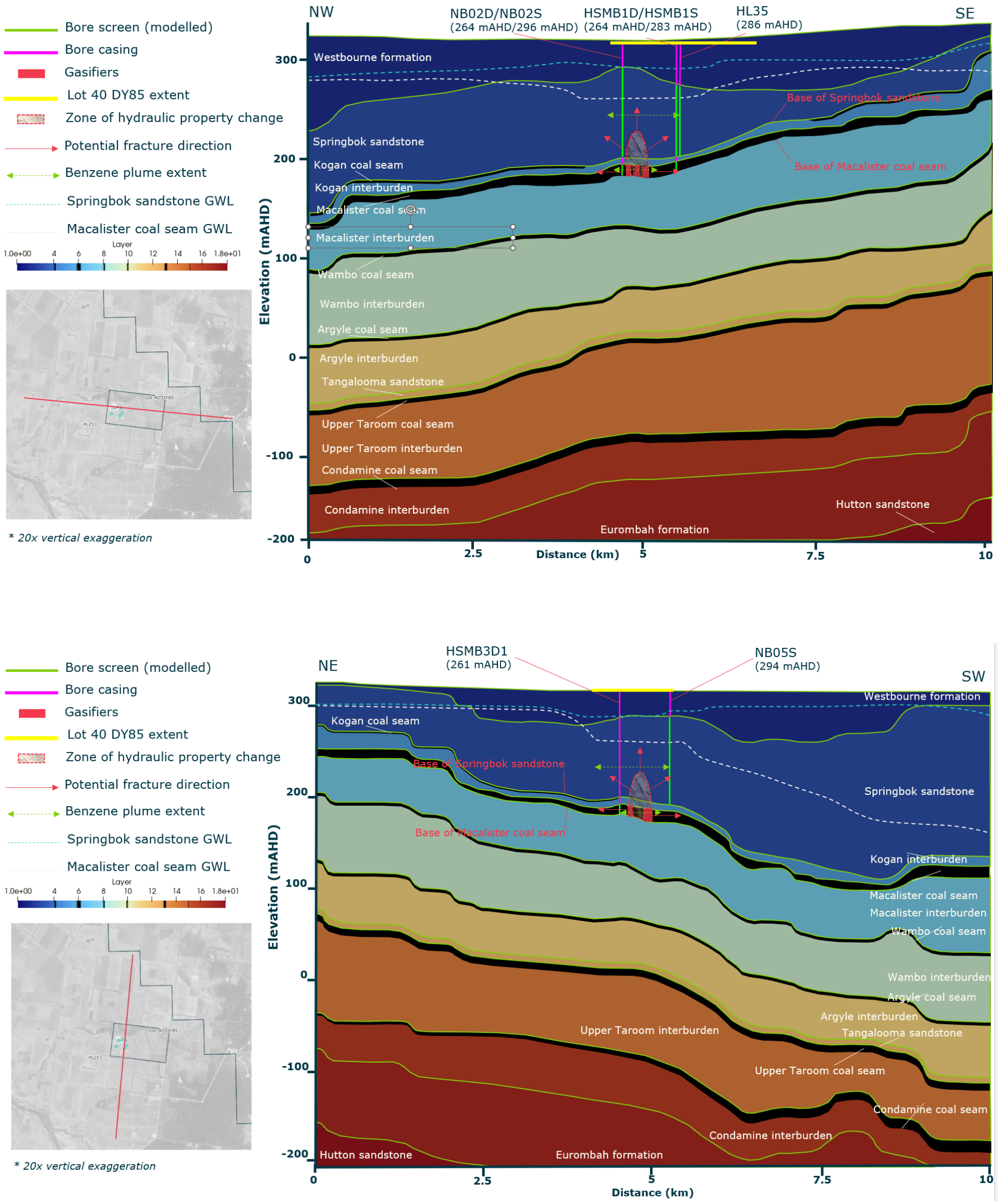


Figure 2-1 Conceptual Site Model of former Hopeland UCG

Previous hydrogeological studies (GHD, 2019; OGIA, 2021; AGE, 2021, 2023; Intera, 2024, 2025) have progressively integrated regional hydrogeological understanding and datasets, including basin-scale conceptualisation and parameter compilations widely used in the Surat Basin, and groundwater impact assessment studies that represent cumulative CSG influences. These earlier efforts informed the selection of HSUs, parameter ranges and boundary condition approaches used later in numerical groundwater modelling, particularly where regional depressurisation from CSG production governs vertical gradients and flow patterns.

Within PL253 and the immediate Hopeland area, prior groundwater modelling provided the basis for progressively refined representations of stratigraphy, hydraulic properties, and operational stresses. The groundwater modelling studies include earlier models developed by GHD (2019), AGE (2021 and 2023), and Intera (2024 and 2025). These site-focused modelling and assessments aimed to support groundwater monitoring network planning and the evaluation of contaminant mobility under CSG influences. These works collectively established the baseline model domain, local refinement requirements around Lot 40 DY85, and the need to represent UCG-related pressure changes and potential property alterations in and above the gasifier zone.

Detailed hydrogeological conceptualisation of the Surat Basin and PL253 has been reported previously (GHD, 2019; OGIA, 2021a, 2021b; Intera, 2025). The following sections provide a brief overview of the site hydrogeology and summarise relevant updates to date.

2.2 Site setting and geology

The PL253 area is located approximately 20 km south-east of Chinchilla within the Surat Basin. The geological setting comprises Jurassic to Early Cretaceous sedimentary sequences that host multiple aquifers and aquitards relevant to groundwater flow and contaminant transport.

Key HSUs include the Springbok sandstone and the WCM, which are separated by lower-permeability formations that limit vertical groundwater movement. The Macalister coal seam within the WCM was identified as a primary unit of interest due to its association with historical UCG operations and residual contamination. Previous studies (GHD, 2019; AGE, 2021, 2023; Intera, 2024, 2025) used this stratigraphic representation as the basis for numerical model development and conceptualisation.

In these studies, local geological complexity, including heterogeneity within coal seams and interburden units, was incorporated into the groundwater model using pilot point parameterisation. Structural features such as minor faults and fractures were recognised as potential sources of uncertainty but were not considered to form persistent preferential pathways at the site scale.

2.3 Groundwater flow regime

Regional groundwater flow within the Surat Basin is generally directed towards the south to southwest, consistent with basin-scale hydraulic gradients. The localised changes to this regional pattern are influences associated with historical UCG operations and regional CSG production.

Previous modelling works (GHD, 2019; AGE, 2021, 2023; Intera, 2024, 2025) have identified a localised hydraulic depression centred on Lot 40 DY85, reflecting residual effects at the end of UCG activities. Groundwater levels within this area have shown relative stability since the end of UCG activities, with evidence of gradual recovery in some monitoring bores.

Vertical hydraulic gradients are characterised by higher heads in overlying Springbok formation relative to the Macalister coal seam, indicating downward gradients that limit the potential for upward contaminant migration under current conditions.

2.4 Groundwater Monitoring

Groundwater monitoring within and surrounding Lot 40 DY85 has been undertaken over several years to characterise groundwater levels, assess groundwater quality, and track the behaviour of residual contaminants associated with historical UCG activities at Lot 40 DY85. The monitoring network includes bores installed in the Springbok sandstone and WCM, with a particular focus on the Macalister coal seam, reflecting the primary HSUs relevant to contaminant migration risk.

Monitoring data have been collected through a combination of Arrow's groundwater monitoring programs, Queensland Government (DETSI/DoR) monitoring, and targeted investigations implemented to satisfy Environmental Authority (EA0001401) requirements. The monitoring framework has been progressively expanded and refined, including installation of additional Springbok sandstone monitoring bores (Hopeland 34 to Hopeland 37), to improve spatial coverage and vertical resolution in the vicinity of the former UCG site and along inferred flow paths.

Groundwater monitoring data has been used to inform groundwater flow directions, assess water quality trends, and support the ongoing history matching of groundwater flow and contaminant transport models, consistent with EA Water Conditions.

2.4.1 Groundwater level

Groundwater level monitoring is undertaken across a network of monitoring bores (including nested bores) screened in the Springbok sandstone and multiple seams within the WCM, including the Macalister coal seam. Regional context indicates that groundwater flow in the Surat Basin is generally towards the south to south-west, with widespread depressurisation of the WCM associated with historical and ongoing CSG production (OGIA, 2021b).

Monitoring data show vertical hydraulic gradients are predominantly directed towards the WCM, indicating downward gradients from the Springbok sandstone and upward gradients from deeper units, consistent with OGIA conceptualisation and reducing the likelihood of vertical contaminant migration out of the coal measures.

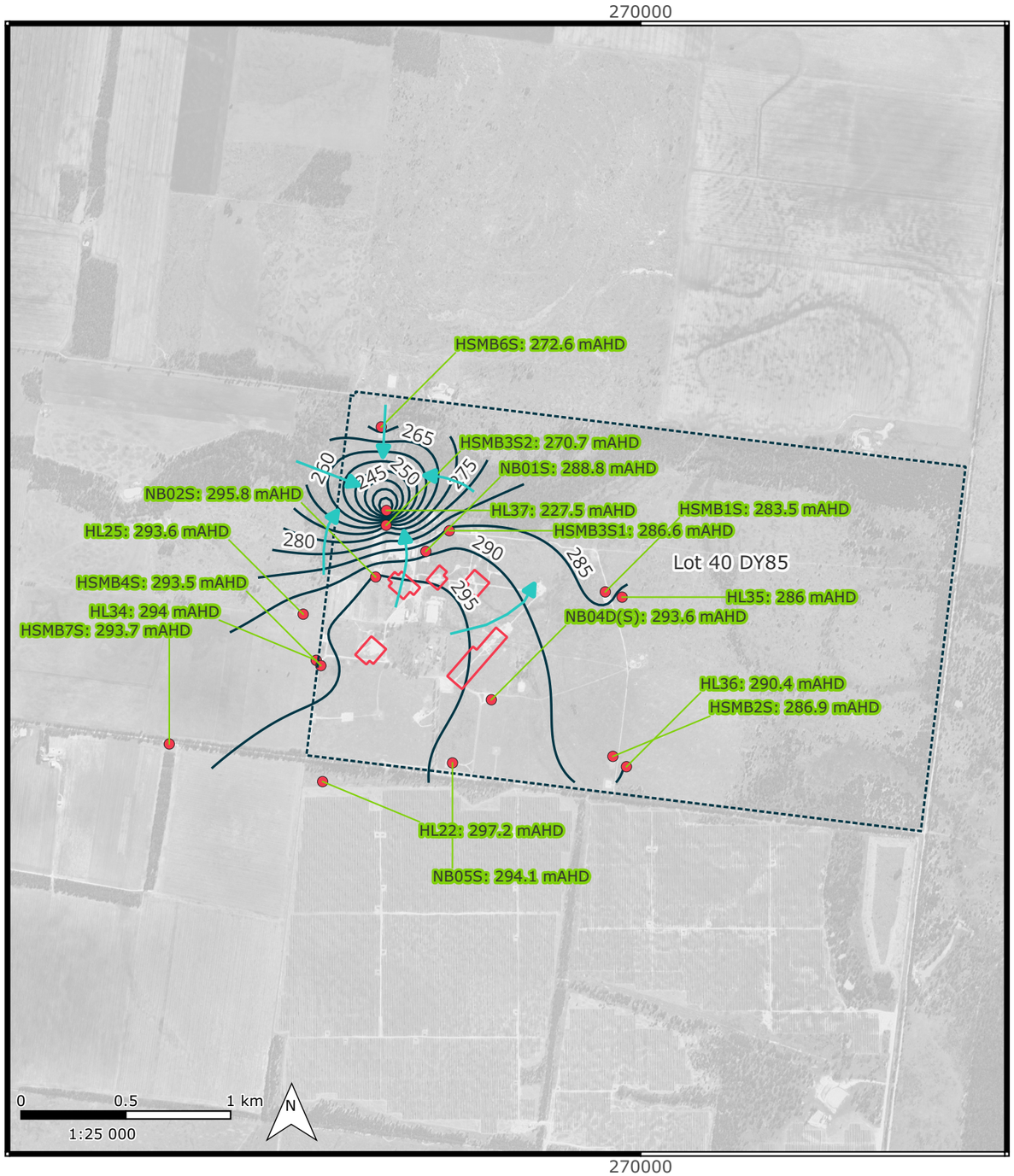
Site-specific groundwater level data indicate that, following the end of UCG activities, water levels within the Springbok sandstone and Macalister coal seam have shown partial recovery, with trends stabilising in recent years. Localised variability remains evident near former gasifier locations, reflecting heterogeneity in formation properties and the historical influence of gasifier voids.

Groundwater level observations collected from all monitoring bores up to Q4 2025 were reviewed to remove outlier or non-representative measurements (e.g., data affected by gas interference or incomplete recovery following sampling) prior to use in model history matching. The resulting dataset was used to inform model parameterisation with both absolute head targets and vertical head difference targets, consistent with OGIA (2021a) regional groundwater modelling methodology and Australian Groundwater Modelling Guidelines (Barnett et al., 2012).

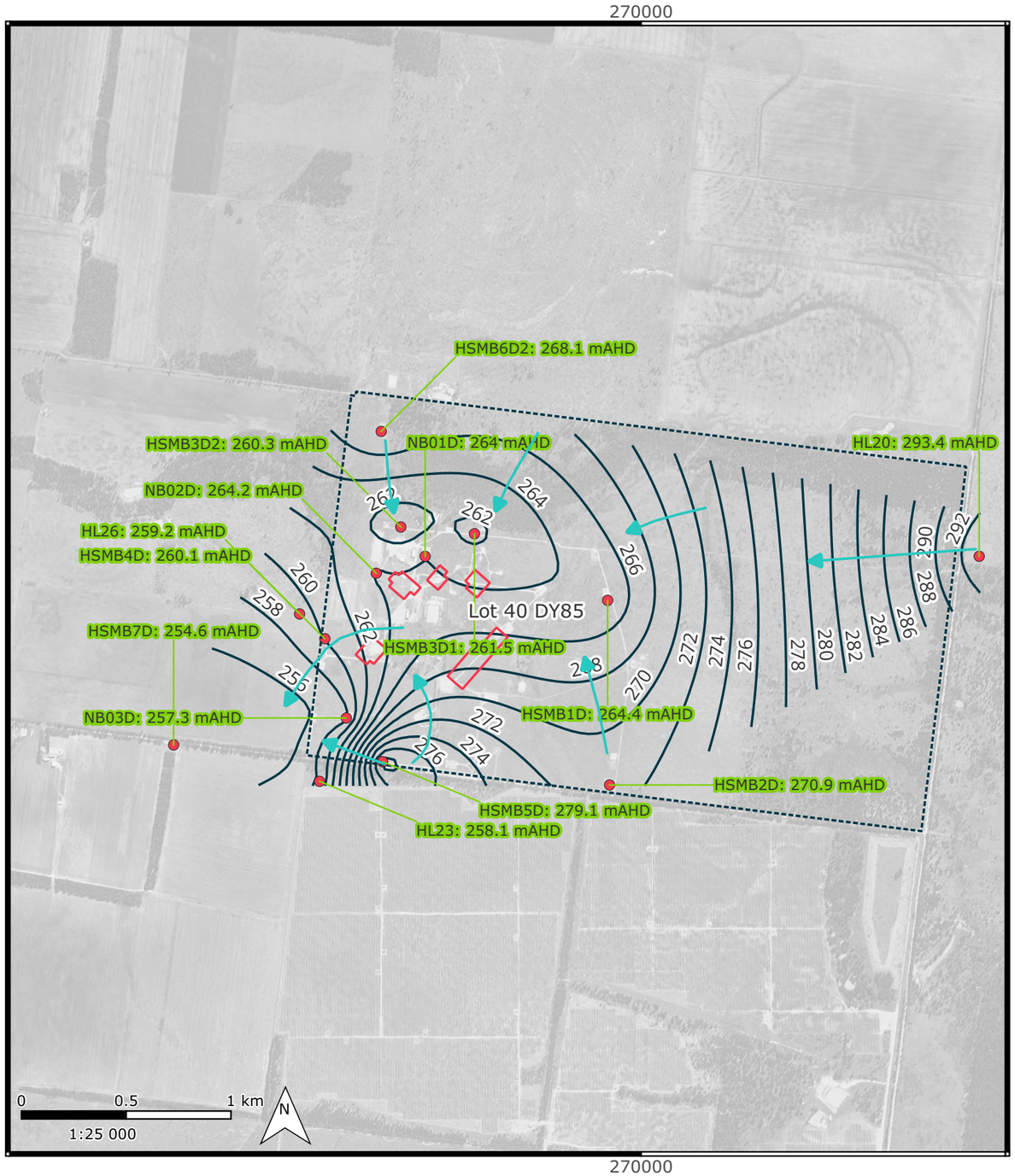
To better represent the most recent groundwater flow directions near Lot 40 DY85, groundwater level contours for the Springbok sandstone and Macalister coal seam were generated using Q3 2025 data. Q3 2025 was selected rather than Q4 2025 because it corresponds to the monitoring period with the greatest number of concurrent groundwater level observations across Lot 40 DY85. These contours (shown in Figure 2-2) provide the most recent estimate of potentiometric conditions and were used to inform interpretation of lateral flow directions and hydraulic gradients in the vicinity of the former UCG site.

The Q3 2025 groundwater level indicates that hydraulic gradients in the Springbok sandstone directed inward towards Lot 40 DY85, while for Macalister coal seam it is directed to the west and southwest corner of Lot 40 DY85. These variability of hydraulic gradients reflect the continued influence of historical depressurisation associated with UCG activities and regional WCM drawdown.

Springbok sandstone



Macalister coal seam



Legend

- Lot 40 DY85
- Gasifiers
- Monitoring bores
- Groundwater contours (mAHD)

Groundwater level contours in Springbok sandstone and Macalister coal seam (Q3 2025)

Project No.	Client	Figure No.
411001-00917	Arrow	2-2

Notes:
Project CRS: GDA94 / MGA zone 56
Last Saved: 02:20 05/06/2026
Filename: Figure_2-2_GWL_contours_2025

Exported by User: Mohsen.Azadi
Project Exported: 13:43 08/06/2026

References:
N/A

File Path: C:\modelling\Arrow\deliverables\Figures_REP-HG-002\Figure_2-2_GWL_contours_2025.qgz

© Worley Pty Ltd While every care is taken to ensure the accuracy of this data, Worley makes no representations or warranties aboutits accuracy, reliability, completeness or suitability for any particular purpose and disclaims all responsibility and all liability (including without limitation liability in negligence) for all expenses, losses, damages (including indirect or consequential damage) and costs which might be incurred as a result of the data being inaccurate or incomplete in any way and for any reason.

2.4.2 Groundwater quality and contaminants of concern

Similar to previous studies (AGE, 2021, 2023; Intera, 2024, 2025), benzene and naphthalene were selected as representative contaminants of concern (COCs) for the contaminant transport modelling. Benzene, a known carcinogen, is the most mobile of the BTEX (benzene, toluene, ethylbenzene, and xylene) compounds due to its high solubility in water and low adsorption potential (Odermatt, 1994), while naphthalene is the most water-soluble polycyclic aromatic hydrocarbon (PAH) (Bayard et al., 2020). Both compounds exhibited the highest concentrations among their respective groups in the site's chemical dataset. Furthermore, benzene has been shown to degrade more slowly than the other BTEXN compounds (Prommer et al., 2003), making it a reliable indicator of the spatial extent of groundwater contamination.

Elevated concentrations of benzene and naphthalene are generally confined to monitoring bores located on Lot 40 DY85 and in proximity to former gasifier locations. Monitoring data for Springbok sandstone and Macalister coal seam (shown in Figure 2-3 to Figure 2-6) indicate mostly declining concentration trends since 2018, consistent with natural attenuation processes.

Benzene concentrations are generally higher and more persistent than concentrations of other BTEX compounds. Elevated benzene concentrations have been observed onsite in proximity to Gasifiers 1 and 2 (NB01S). In this location, benzene concentrations have shown relative temporal stability or slow decline, consistent with proximity to residual contaminant sources. Offsite monitoring bores generally show low or non-detectable benzene concentrations.

Naphthalene concentrations are typically lower than benzene and are detected less frequently. Monitoring results indicate that naphthalene concentrations have declined over time across most bores, with many locations now recording concentrations below laboratory Limit of Reporting (LOR). This is due to naphthalene's stronger sorption and attenuation characteristics relative to benzene.

Overall, monitoring data demonstrate a general declining trend in benzene and naphthalene concentrations since approximately 2020, attributable to a combination of natural attenuation processes, limited advective transport due to low groundwater velocities, and the persistence of inward hydraulic gradients for Springbok sandstone towards Lot 40 DY85.

The groundwater quality dataset provides no evidence of progressive offsite migration of benzene or naphthalene under current conditions and supports the conclusion that residual contamination remains localised and effectively contained within the former UCG site area under existing and proposed CSG development scenarios.

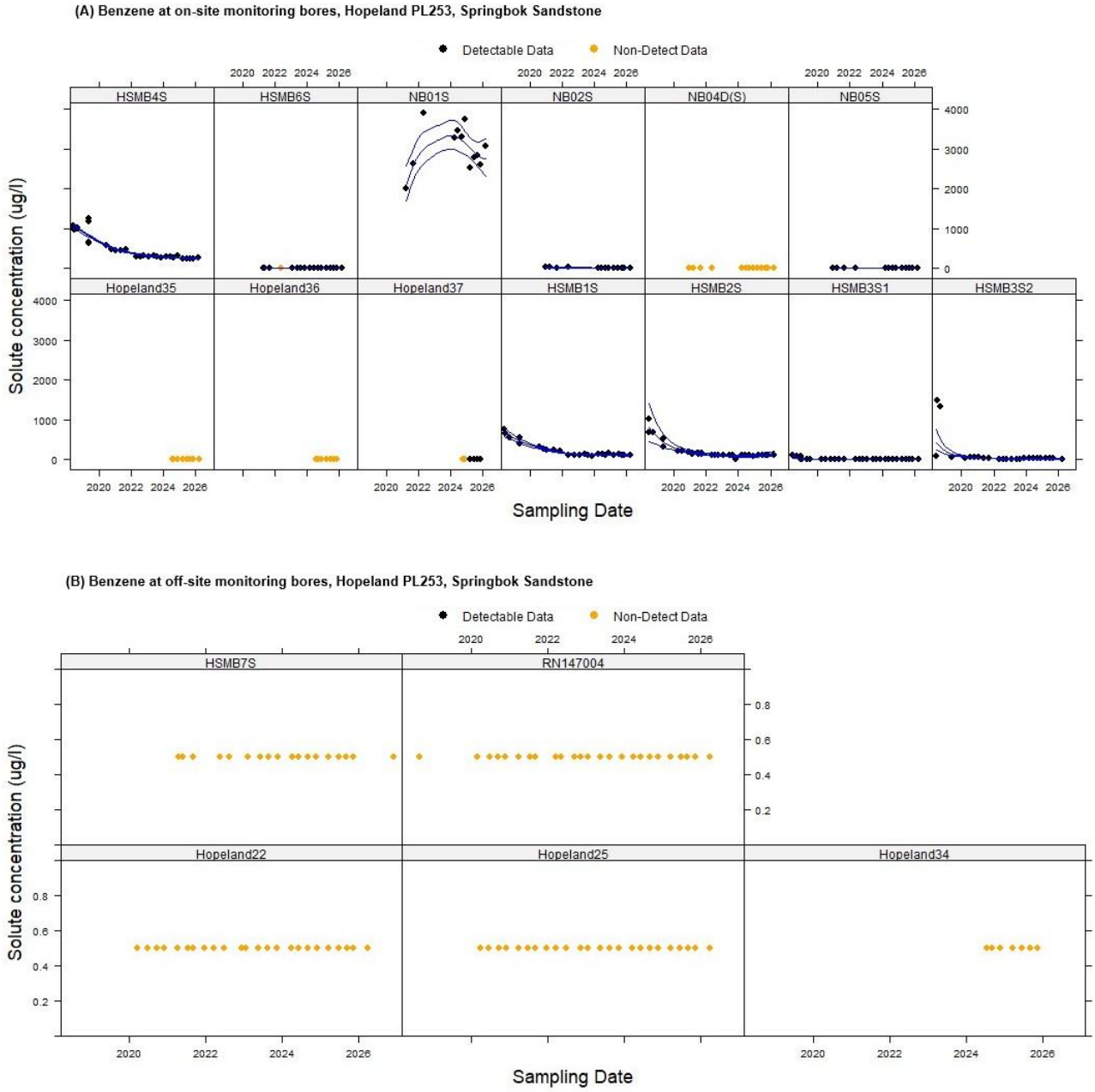


Figure 2-3 Time series benzene concentration for a) on-site and b) off-site bores completed in the Springbok sandstone (provided by Arrow)

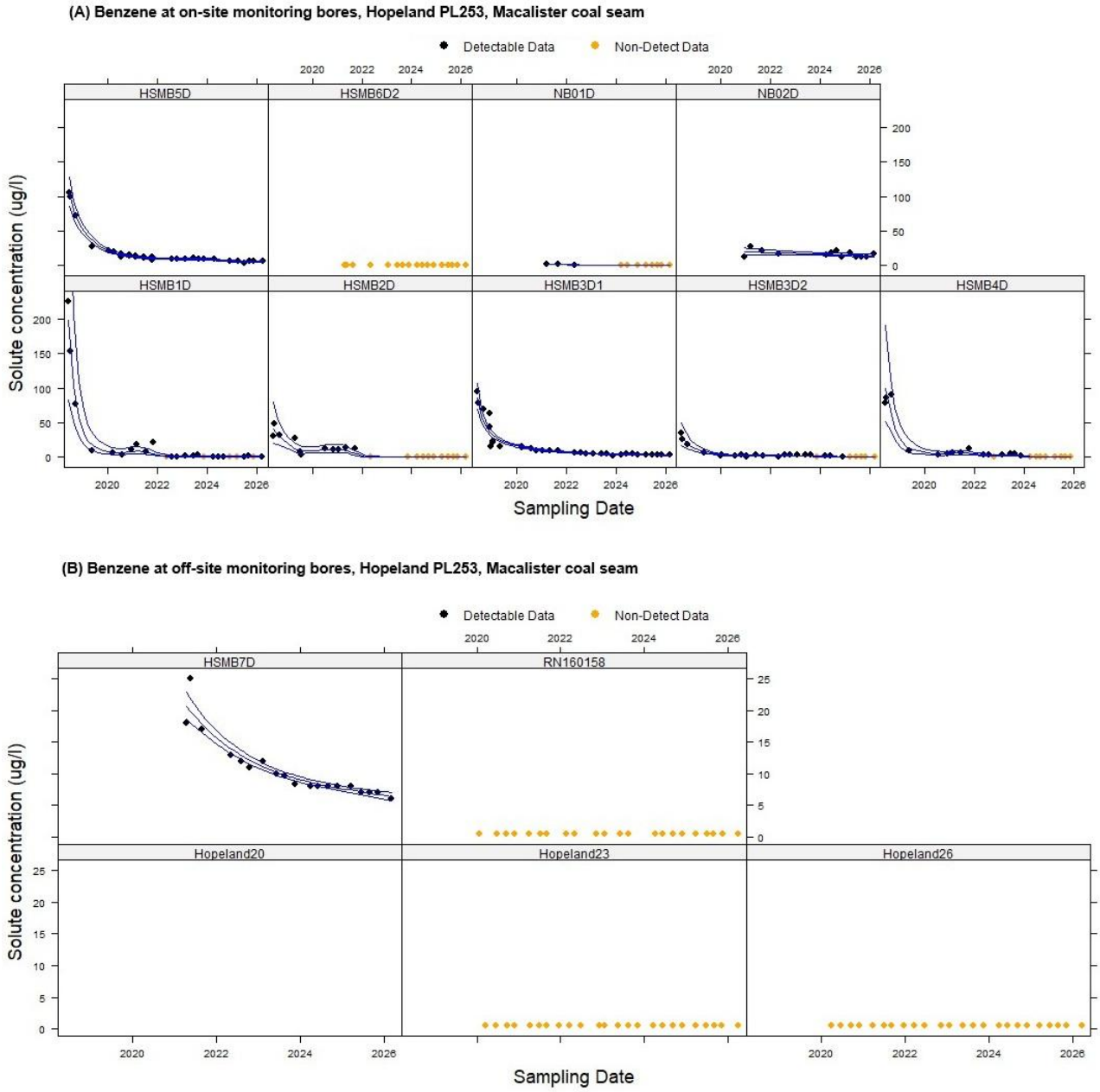


Figure 2-4 Time series benzene concentration for a) on-site and b) off-site bores completed in the Macalister coal seam (provided by Arrow)

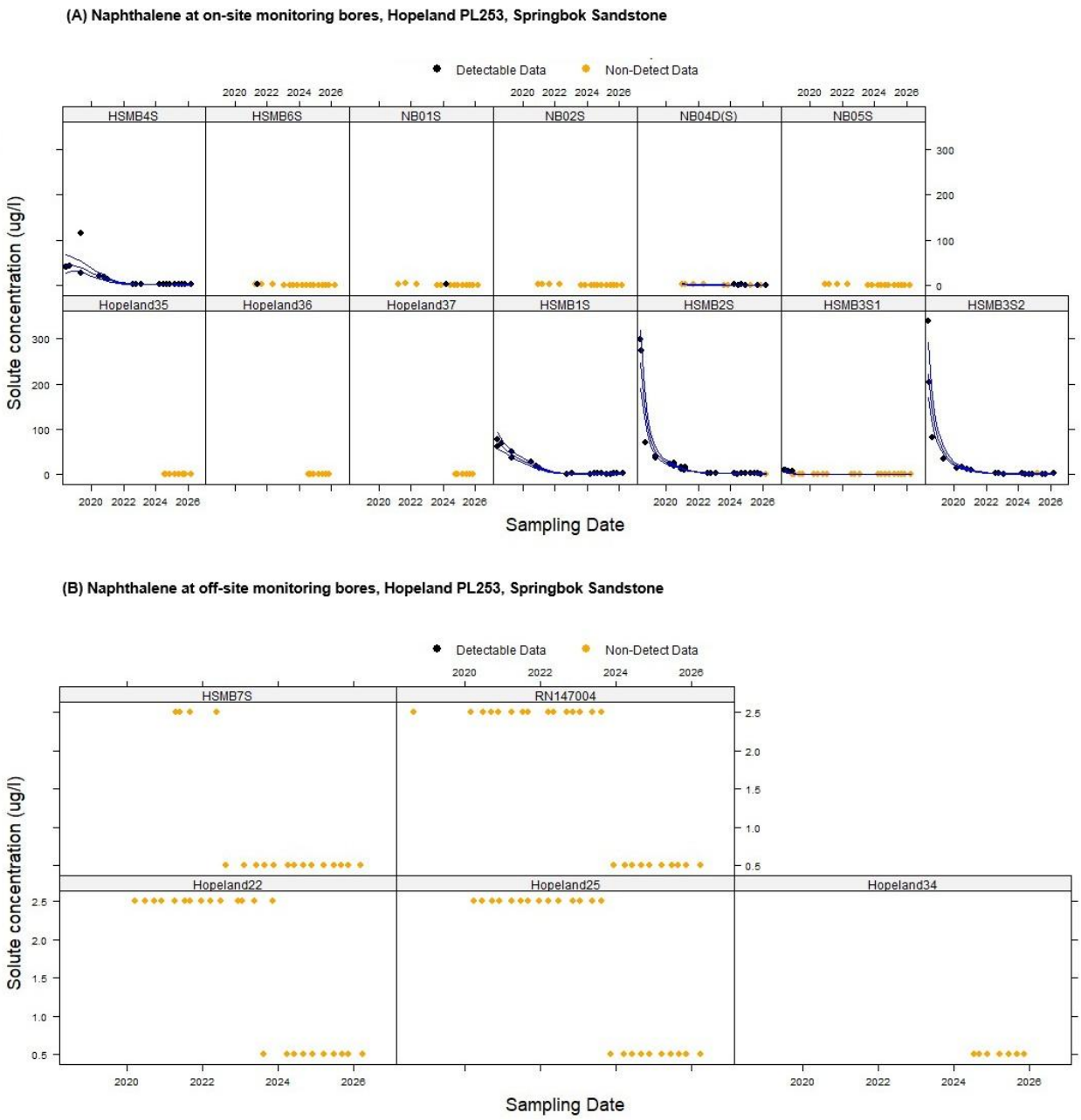


Figure 2-5 Time series naphthalene concentration for a) on-site and b) off-site bores completed in the Springbok sandstone (provided by Arrow)

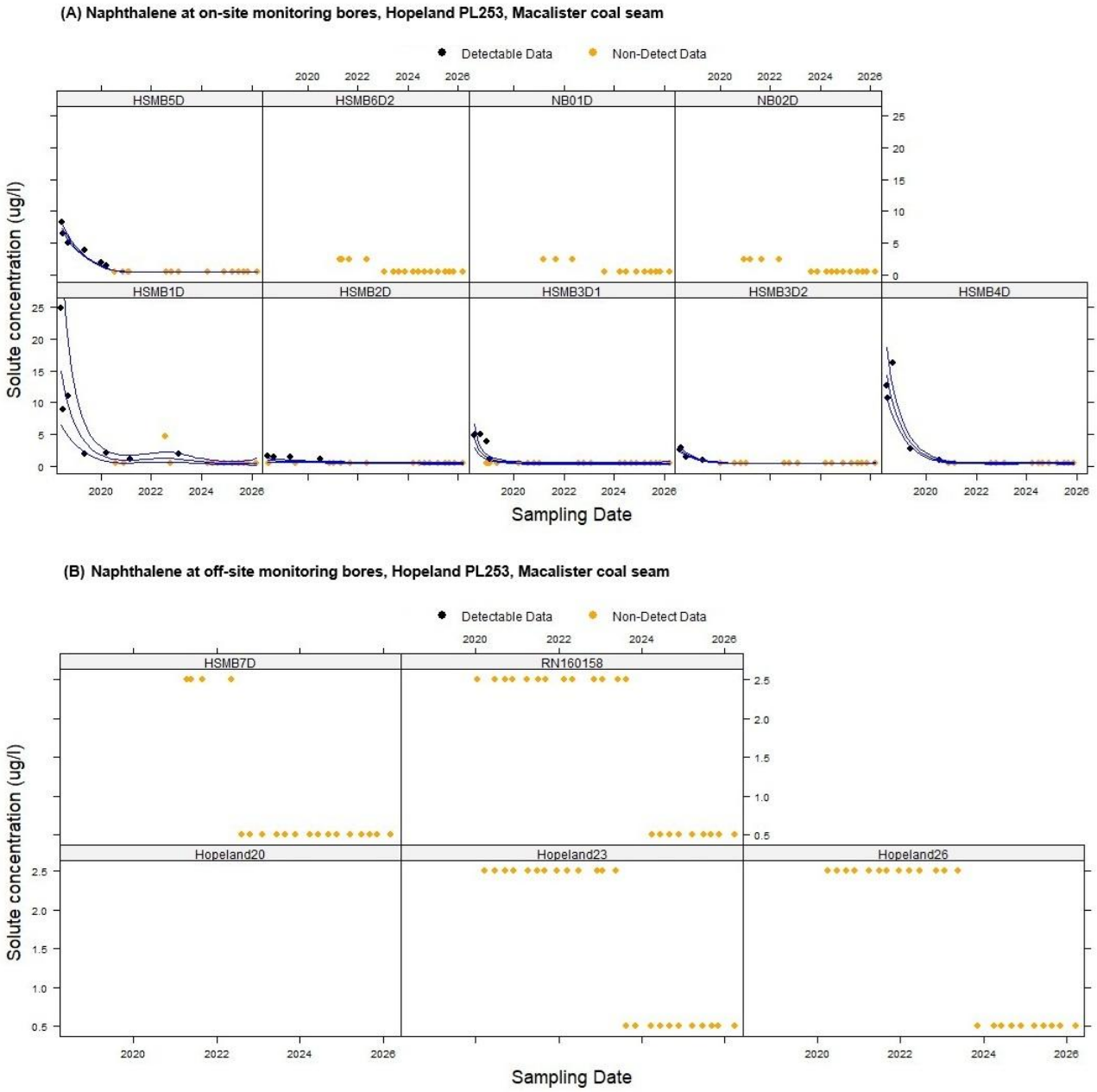


Figure 2-6 Time series naphthalene concentration for a) on-site and b) off-site bores completed in the Macalister coal seam (provided by Arrow)

2.4.2.1 Contaminant source depletion at gasifiers

The contaminant transport model incorporates a time-varying source depletion term to represent the gradual reduction in residual contaminant mass available for dissolution from the gasifiers. Source depletion was implemented to capture long-term declines in contaminant concentrations attributable to natural attenuation processes (i.e., sorption, and degradation). Rather than assuming a constant or infinite source, this approach provides a more realistic representation of contaminant behaviour, while allowing for the continued release of residual contaminants from dead-end pores.

The source depletion formulation was defined using the most comprehensive available groundwater quality dataset. For each compound and HSU (Springbok sandstone and Macalister coal seam), the highest observed concentration from all monitoring bores at each sampling event was extracted from the full time-series record as shown in Figure 2-7 and Figure 2-8 for benzene and naphthalene, respectively. This upper-envelope dataset was used conservatively to derive an exponential decay relationship describing the temporal reduction in source concentration. The fitted exponential functions were then used to define time-varying source boundary conditions in the contaminant transport model.

For benzene, the extracted maximum concentration time series shows a gradual but persistent decline over time across monitoring bores screened in the Springbok sandstone and Macalister coal seam. An exception is elevated concentrations observed in monitoring bore NB01S within the Springbok sandstone (blue points above the fitted exponential decay curve in Figure 2-7). The elevated benzene concentrations at NB01S, which is proximal to former gasifier areas, are interpreted to represent a localised and spatially confined source. This interpretation is supported by groundwater monitoring data from surrounding bores (HSMB3S1, HSMB3S2, and NB02S), which indicate substantially lower concentrations consistent with the broader monitoring network.

Given the localised nature of the elevated benzene concentrations at NB01S, an ongoing source term with a constant concentration was adopted within a 50 m radius of this bore and assessed separately within the contaminant transport model. This approach allows the broader, data-derived source depletion term to be applied across Lot 40 DY85, while explicitly accounting for localised residual contamination in the vicinity of NB01S.

An exponential decay function was fitted to the upper-envelope benzene dataset for all the remaining monitoring bores, representing the depletion of benzene source as shown in equations (1) and (2) for springbok sandstone and Macalister coal seam, respectively:

$$C(t) = 1750\, e^{-0.00065\, t} \quad (1)$$

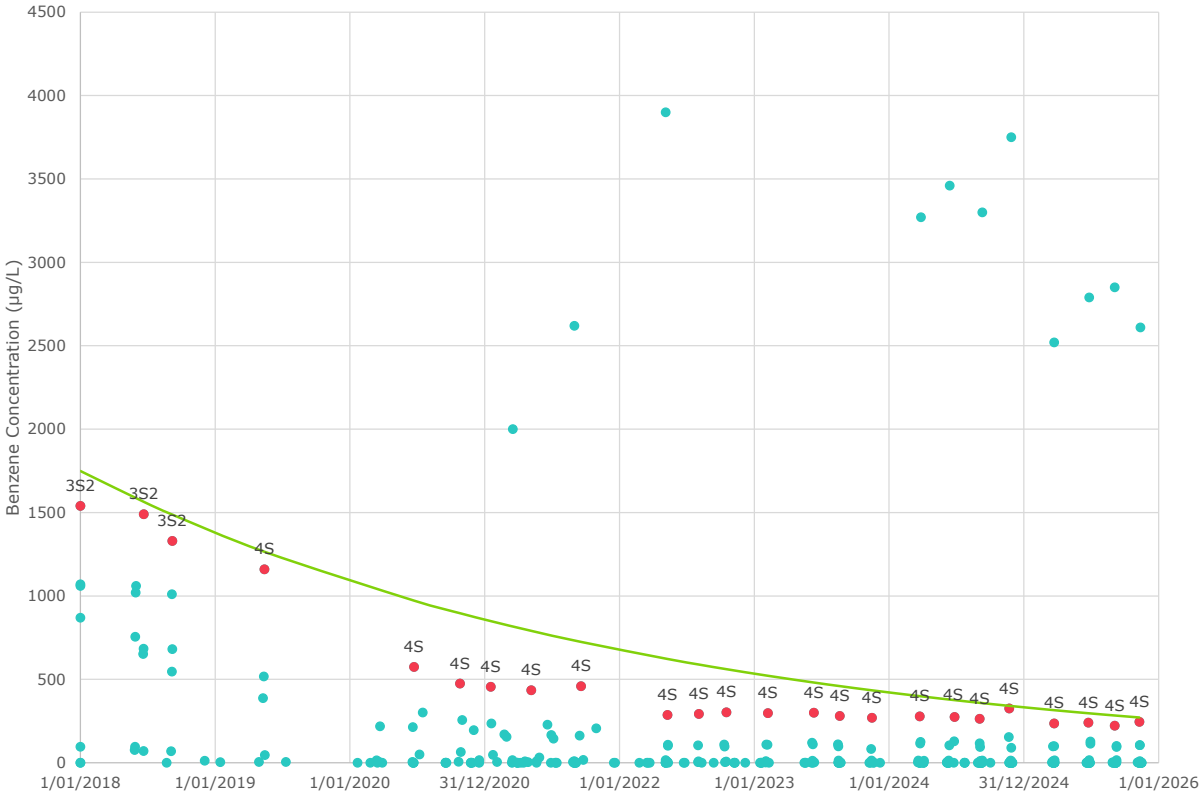
where C(t) is source concentration term in (µg/L), and t is the number of days from the first day of contaminant transport simulation on 1/1/2018.

Naphthalene monitoring data indicate lower maximum concentrations and a more rapid decline relative to benzene, consistent with stronger sorption and attenuation characteristics. The same upper-envelope methodology was applied, with maximum naphthalene concentrations extracted from all monitoring bore records and fitted with an exponential decay function. The resulting relationship was used to define the naphthalene source depletion term in the transport model as shown in equations (3) and (4) for springbok sandstone and Macalister coal seam, respectively:

$$C(t) = 500\, e^{-0.0019\, t} \quad (3)$$

$$C(t) = 75\, e^{-0.0019\, t} \quad (4)$$

Springbok sandstone



Macalister coal seam

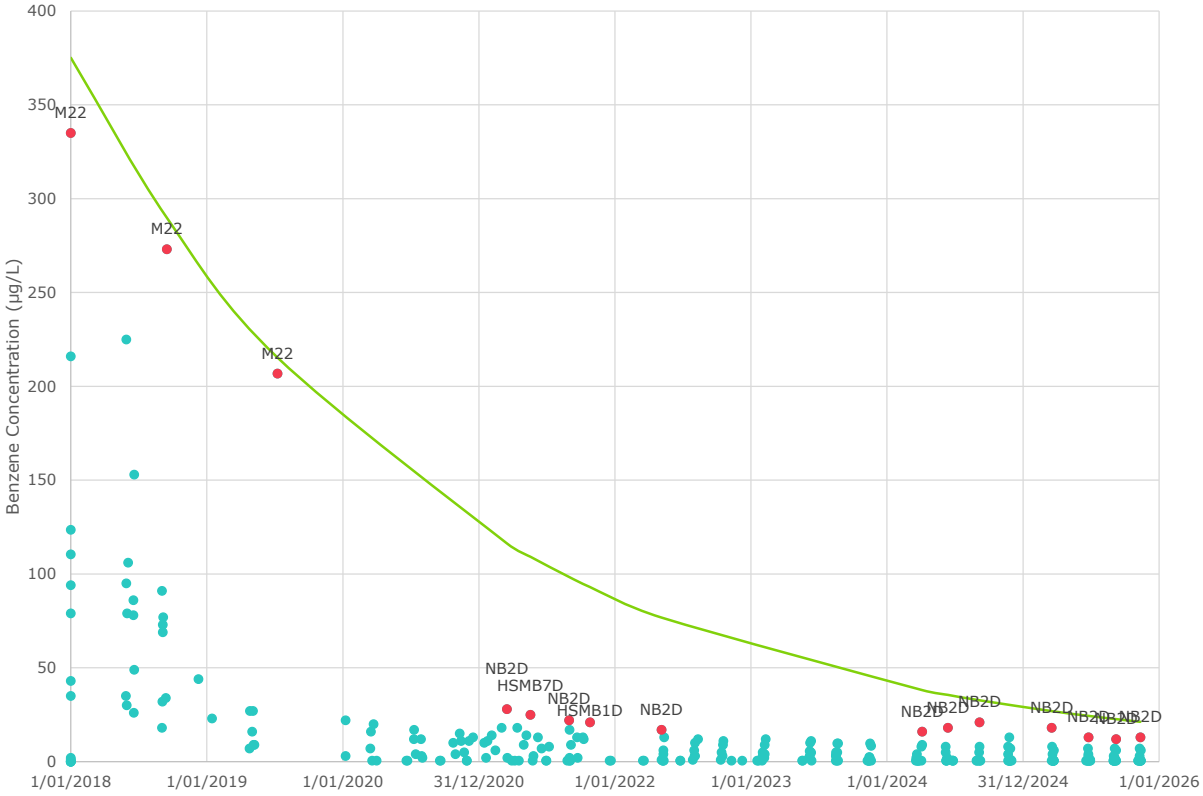
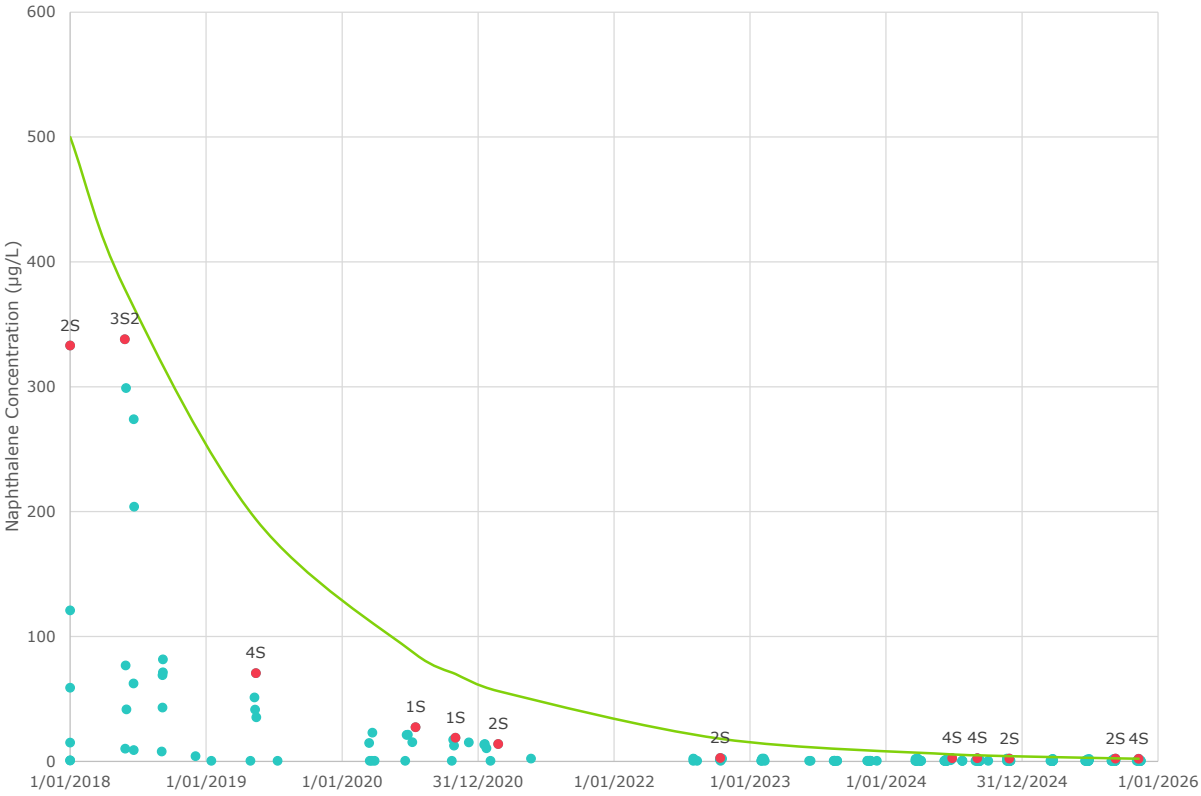


Figure 2-7 Benzene concentration for all monitoring bores compared with exponential curve of source depletion term for a) Springbok sandstone and b) Macalister coal seam

Springbok sandstone



Macalister coal seam

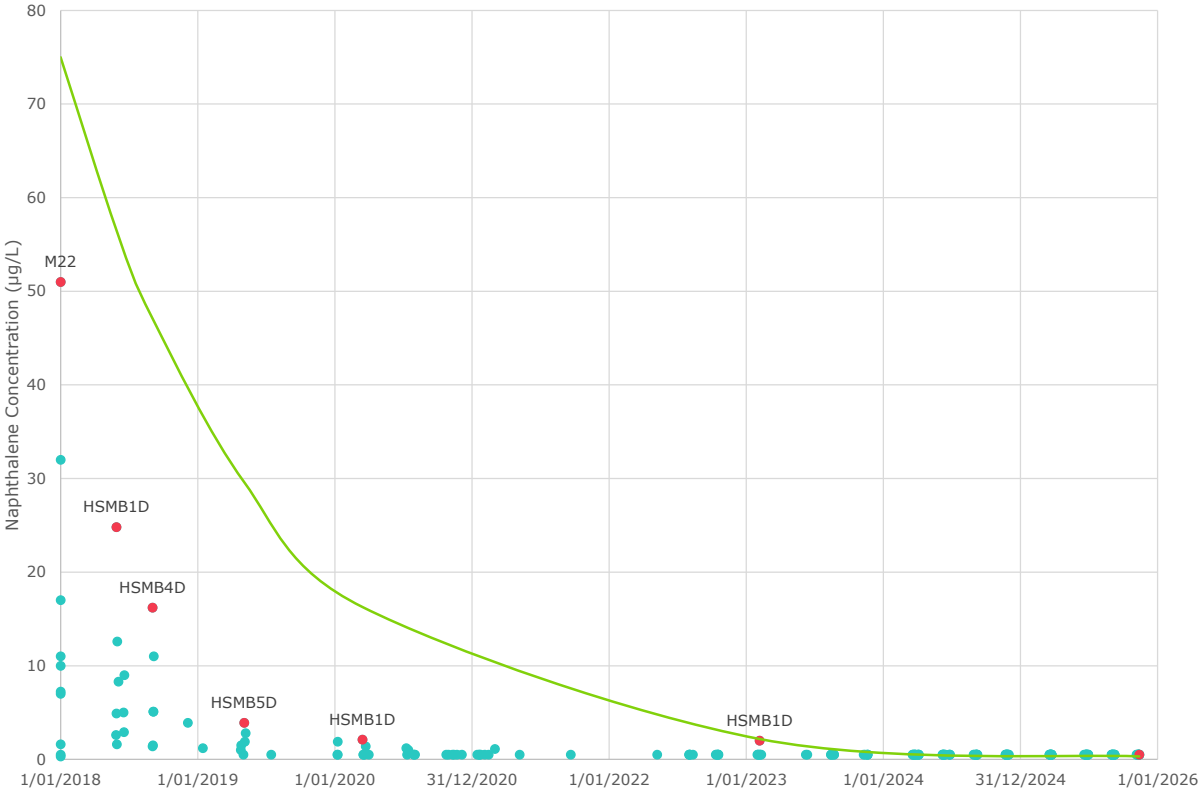


Figure 2-8 Naphthalene concentration for all monitoring bores compared with exponential curve of source depletion term for a) Springbok sandstone and b) Macalister coal seam

3. Groundwater modelling

3.1 Groundwater flow model

Building on Arrow's recent PL253 numerical groundwater model (INTERA, 2025), a numerical groundwater model was developed to assess the impacts of Arrow's proposed FDP for the Clynes Road wells. The model focuses on aquifers on and surrounding Lot 40 DY85, including the Springbok sandstone and the Macalister coal seam and associated aquifers within the WCM. The groundwater model is developed to evaluate and predict potential changes in contaminant transport, groundwater flow directions, and drawdown resulting from development of the Clynes Road wells.

The groundwater model extent (Figure 1-1), is consistent with the area adopted by previous studies (e.g., GHD, 2019, 2020; AGE, 2021, 2023; INTERA, 2024, 2025). It encompasses an approximately 20-km radius around Lot 40 DY85 and includes PLs 253, 493 and 185, as well as adjacent areas, ensuring the model captures key hydrogeological stresses and their zones of influence during past and future activities.

The rectangular model domain (Figure 1-1) was rotated so that the northeastern boundary aligns with the extent of WCM, while the northwest and southeastern boundaries are roughly parallel to the strata dip and regional groundwater flow direction. From a numerical modelling perspective, the boundaries were defined to minimise potential boundary effects and ensure that all relevant flow pathways can be fully simulated within the required timeframes.

Consistent with the most recent groundwater model (INTERA 2025, shown in Figure 3-1), the updated model is developed in MODFLOW 6 incorporating local grid refinement around Lot 40 DY85, with 18 layers representing the key HSUs in the area. The use of MODFLOW 6 introduced improvements in modelling assumptions and boundary condition representation (e.g. incorporation of dual-porosity processes). However, the predictive model remained subject to a wide range of uncertainty in some aspects of the predictions. Accordingly, while maintaining the MODFLOW 6 modelling platform, a comprehensive review of the previous modelling work was undertaken, and key boundary conditions and HSU representation were revised. This approach enabled incorporation of hydrogeological information to revise the model boundary conditions, while retaining the strengths of the MODFLOW 6 platform in the current groundwater model.

Boundary conditions (presented in this chapter) represent regional groundwater influences, historical UCG depressurisation, and CSG abstraction from Arrow and non-Arrow wells. Time-varying hydraulic properties are used to reflect changes associated with UCG operations.

The prediction period extends to the end of 2225 (200 years), well beyond the groundwater abstraction period, when off-site contaminant migration may become possible.

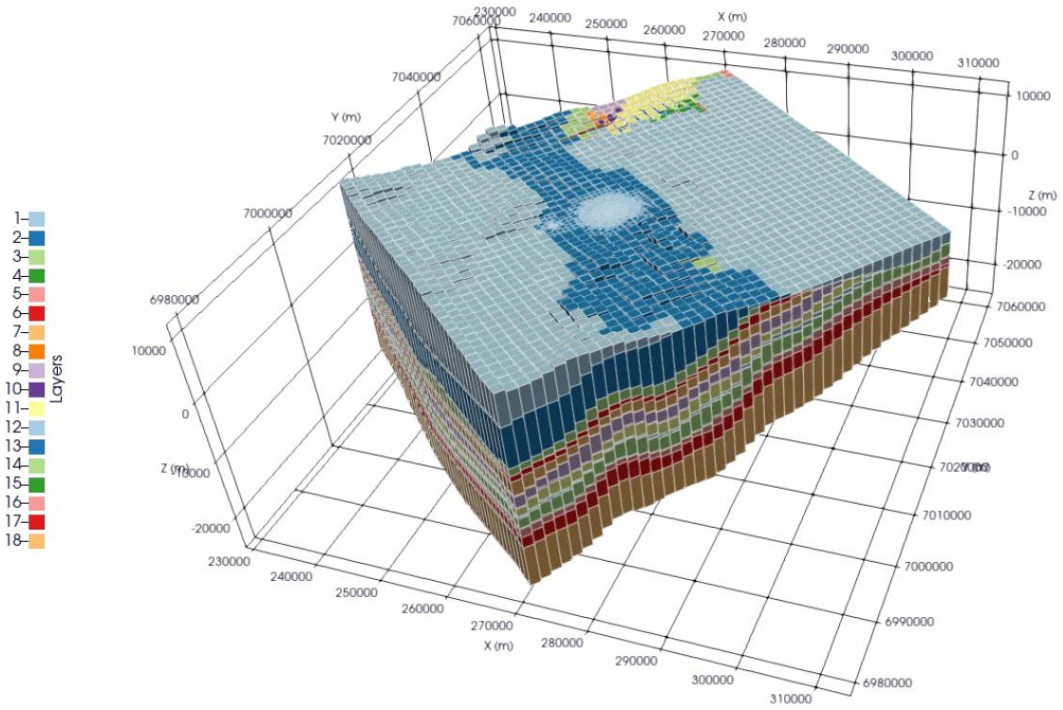


Figure 3-1 3D groundwater model with 30x vertical exaggeration (from Intera, 2025)

Key updates incorporated in the current numerical groundwater flow model include:

- Updated HSUs based on the latest geology model developed by Arrow.
- The General Head Boundary (GHB) conditions were extracted from the OGIA (2021) cumulative groundwater model and assigned to model boundary layers ensuring alignment between the two model layers. Additionally, excessively high conductance values used at the model boundaries in the previous model (INTERA, 2025) were updated based on the individual cells' hydraulic conductivity and thickness.
- The drain (DRN) package elevations were extracted from the OGIA (2021) cumulative groundwater model for simulation of CSG abstraction. The extracted elevation time series were assigned to the groundwater model layers ensuring alignment between the two model layers. Additionally, conductance values were calculated based on the individual cells' hydraulic conductivity, thickness and a multiplier factor informed during history matching.
- Simulation solver settings were updated to ensure the numerical model converges in all the model time steps aligned with Australian Groundwater Modelling Guidelines (Barnett et al 2012). If the model does not converge during a specific time step, the simulation stops and does not proceed further.
- Unlike the previous model (INTERA, 2025), which used the Drain Package to simulate groundwater abstraction under FDP scenarios (with and without the Clynes Road wells), the current model uses the WEL Package. This approach avoids estimation errors associated with converting well flow rates to drain elevations in the drain boundary condition. Model inputs include bore locations, screened intervals, and time-series pumping rates.
- Updated groundwater level datasets to inform both steady-state and transient history matching and incorporated current groundwater flow directions into the calibration targets.
- Refinement of pilot points location to capture spatial heterogeneity in hydraulic parameterisation of the aquifer system based on a conceptual understanding of groundwater flow directions and monitoring bore locations.

- A review and revision of the other modelled boundary conditions (e.g. recharge, and multi-aquifer well boundary conditions) in the previous model (INTERA, 2025) to improve the simulation of groundwater flow regimes consistent with the hydrogeological conceptualisation.
- Model calibration, predictive simulations and uncertainty analysis using the combined Ensemble Space Inversion[1] (PEST-ENSI) and Iterative Ensemble Smoother (PESTPP-IES, White, 2018) methods to replicate historical groundwater flow systems and understand the probability envelope associated with environmental impacts within PL253.

3.1.1 Model layers

Model layers are built based on HSU geometry from Arrow's geological model. The lithological contacts were discretised using Intera's model grid to construct the updated model layers and are aligned with the previous groundwater models as presented in Table 3-1 and shown in Figure 3-2.

Table 3-1 Model layers

Hydrogeological Domain	Average thickness (m)	Model Layer
Condamine alluvium/Gubberamunda sandstone	43.8	1
Westbourne formation	56.7	2
Springbok sandstone	96.3	3
WCM Kogan coal seam	1.2	4
WCM Kogan interburden	11.9	5
WCM Macalister coal seam	9.5	6
WCM Macalister interburden	54.9	7
WCM Wambo coal seam	3.7	8
WCM Wambo interburden	60.3	9
WCM Argyle coal seam	3.5	10
WCM Argyle interburden	50.8	11
WCM Tangalooma sandstone	8.7	12
WCM Upper Taroom coal seam	4.0	13
WCM Upper Taroom interburden	88.5	14
WCM Condamine coal seam	5.5	15
WCM Condamine interburden	43.3	16
Eurombah formation	81.0	17
Hutton sandstone	197.1	18

[1] https://gmdsi.org/blog/ensemble-space-inversion/

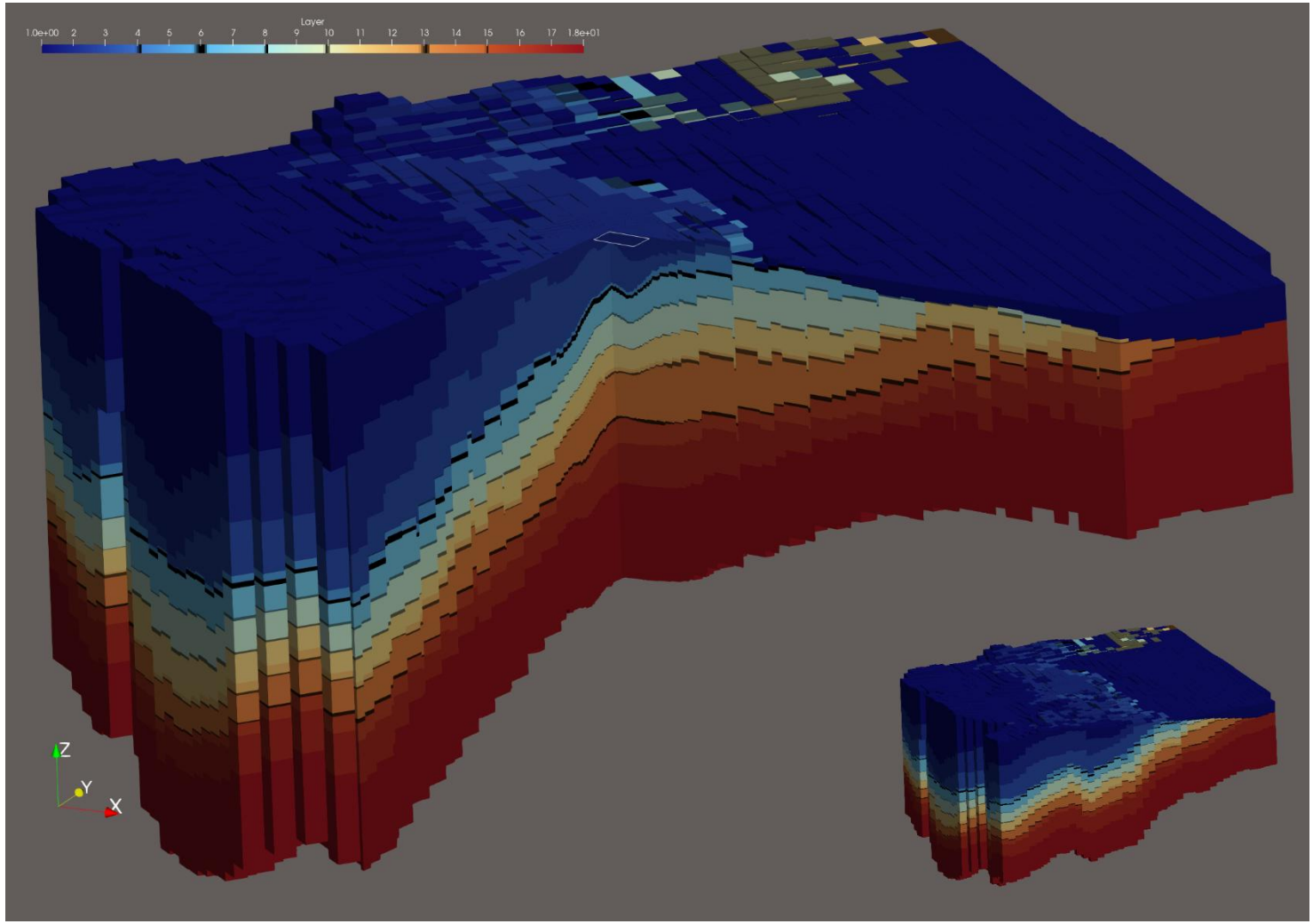


Figure 3-2 PL253 3D groundwater model (with 30x vertical exaggeration of the 3D model and cross-sections)

3.1.2 Hydraulic properties

Initial hydraulic properties were assigned as a single value across each model zone based on the learnings from the previous groundwater model history matching (AGE, 2023; Intera, 2025). The initial horizontal hydraulic conductivity (k_h), vertical to horizontal hydraulic conductivity ratio (k_v/k_h), specific storage (S_s), and specific yield (S_y) values assigned in each model layer is presented in Table 3-2.

Once the parameter zones were initialised with a hydraulic property value, a 2D distribution of hydraulic properties of each zone was generated using the pilot points with multipliers. This allows for improved data assimilation by extracting information from measured observations in scenarios where the use of a single value for hydraulic properties within a zone is not sufficient to interpret the groundwater level variability or trends in bores located close to each other.

Other details of the parameterisation approach will be discussed further in Section 4.2.

Table 3-2 Summary of initial hydraulic properties

Hydrogeological Domain	Layer	K_h (m/day)	K_v/K_h	S_s (m^{-1})	S_y (%)
Condamine alluvium	1	2.6E+01	1.0E-01	2.3E-05	10
Gubberamunda sandstone	1	1.3E-01	1.0E-02	5.0E-06	2.5
Westbourne formation	2	8.9E-04	1.0E-03	2.3E-05	2.5
Springbok sandstone	3	1.6E-02	5.0E-03	1.0E-05	5
WCM Kogan coal seam	4	6.9E-02	1.0E-01	1.0E-05	1
WCM Kogan interburden	5	2.8E-02	1.0E-03	5.0E-06	1
WCM Macalister coal seam	6	4.0E-02	1.0E-01	5.0E-06	1
WCM Macalister interburden	7	4.9E-03	1.0E-03	5.0E-06	1
WCM Wambo coal seam	8	1.3E-01	1.0E-01	2.3E-05	1
WCM Wambo interburden	9	4.2E-03	1.0E-03	5.0E-06	1
WCM Argyle coal seam	10	1.4E-01	1.0E-01	2.3E-05	1
WCM Argyle interburden	11	5.2E-03	1.0E-03	1.0E-05	1
WCM Tangalooma sandstone	12	9.6E-03	1.0E-03	1.0E-05	1
WCM Upper Taroom coal seam	13	1.7E-01	1.0E-01	5.0E-06	1
WCM Upper Taroom interburden	14	1.7E-02	1.0E-03	5.0E-06	1
WCM Condamine coal seam	15	1.5E-01	1.0E-01	5.0E-06	1
WCM Condamine interburden	16	3.1E-02	1.0E-03	2.3E-05	2.5
Eurombah formation	17	1.8E-04	1.0E-03	5.0E-06	2.5
Hutton sandstone	18	3.4E-02	1.0E-03	2.3E-05	2.5

3.1.3 Boundary conditions

The MODFLOW 6 boundary packages are used to assign the boundary conditions and simulate relevant flow exchange processes. The assigned boundary conditions for PL253 groundwater model are presented in sections 3.1.3.1 to 3.1.3.7.

3.1.3.1 Recharge

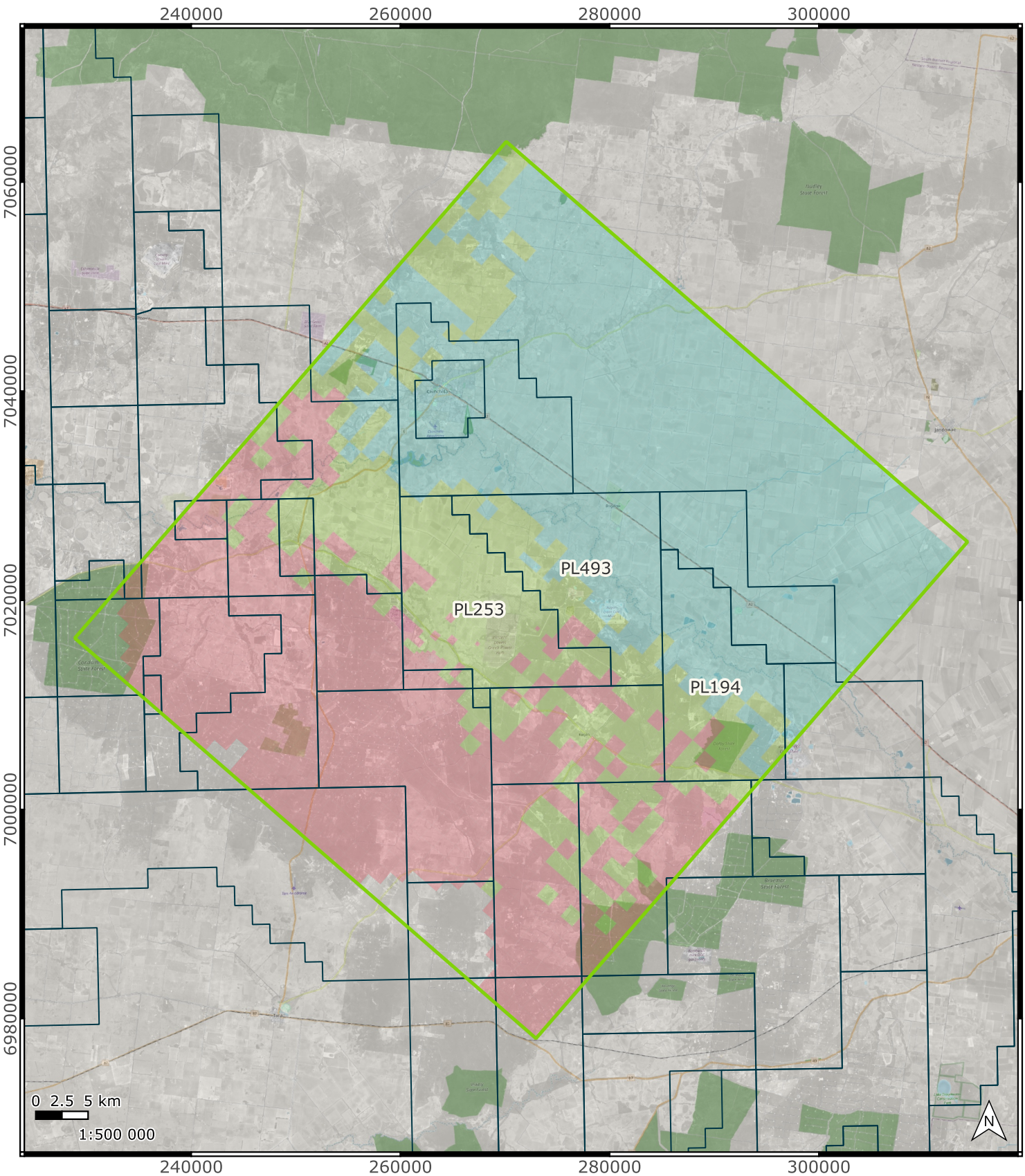
Recharge to the groundwater system is represented by setting up three distinct recharge zones (shown in Figure 3-3) including:

- Condamine alluvium,
- Gubberamunda sandstone, and
- Westbourne formation and outcropping layers.

The initial annual recharge rates for each zone, adapted from previous studies (AGE, 2023; INTERA, 2025), are presented in Table 3-3. A recharge factor for each zone was defined and allowed to be adjusted during the model calibration.

Table 3-3 Initial annual recharge rate for each zone

Recharge zone	Initial annual recharge, mm/year
Condamine alluvium	3.5
Gubberamunda sandstone	1.0
Westbourne formation and outcropping layers	0.2



Legend

- Groundwater model extent
- Petroleum Leases

Recharge zones

- Condamine alluvium
- Gubberamunda sandstone
- Westbourne formation and outcropping layers

Simulated recharge zones

Project No.	Client	Figure No.
411001-00917	Arrow	3-3

Notes:
Project CRS: GDA94 / MGA zone 56
Last Saved: 08:35 16/04/2026
Filename: Figure_3-3_recharge
Exported by User: Mohsen.Azadi
Project Exported: 15:17 16/04/2026

References:
N/A

File Path: C:\modelling\Arrow\deliverables\Figures_REP-HG-002\Figure_3-3_recharge.qgz

© Worley Pty Ltd While every care is taken to ensure the accuracy of this data, Worley makes no representations or warranties aboutits accuracy, reliability, completeness or suitability for any particular purpose and disclaims all responsibility and all liability (including without limitation liability in negligence) for all expenses, losses, damages (including indirect or consequential damage) and costs which might be incurred as a result of the data being inaccurate or incomplete in any way and for any reason.

worley consulting

3.1.3.2 Surface drainage

Surface drainage was simulated using drain (DRN) boundary conditions assigned to the uppermost active model cells, with drain elevations set to the model top (land-surface elevation). This allows groundwater discharge when simulated heads exceed land surface. This head-dependent approach representing surface drainage provides a numerically stable representation of topographically controlled groundwater discharge without imposing fixed hydraulic constraints.

3.1.3.3 General head boundaries

Time series of GHB elevations were extracted from the OGIA (2021) regional groundwater model and assigned to boundary cells in the updated HSUs, with careful alignment of layer elevations between the regional OGIA and PL253 models. Inferred hydraulic heads were obtained for the following units:

- Gubberamunda sandstone,
- Westbourne formation,
- Springbok formation,
- WCM Kogan interburden,
- WCM Macalister coal seam,
- WCM Wambo coal seam,
- WCM Argyle coal seam, and
- WCM Condamine coal seam.

During calibration, GHB head values were allowed to vary through vertical shifting of the prescribed head time series, while boundary conductance was adjusted using multiplier factors. This approach enabled adjustment of the quantitative influence of regional boundary conditions on simulated groundwater flow while preserving the temporal structure of the heads extracted from OGIA (2021) model. All remaining boundary cells, including the northeastern model boundary, were represented as no-flow boundaries.

3.1.3.4 Non-Arrow CSG wells

In the current model, non-Arrow CSG wells included in the OGIA (2021) regional groundwater model were simulated using drain (DRN) boundary conditions. Drain elevation time series were extracted directly from the corresponding OGIA (2021) model layers and assigned to the PL253 model to ensure consistency with the regional depressurisation conceptualisation. Drain conductance for each cell was calculated based on the product of horizontal hydraulic conductivity and individual cell thickness and scaled by a dimensionless multiplier. This multiplier was informed through history matching of observed regional groundwater responses and subsequently assessed during uncertainty analysis. This provides a simplified yet physically consistent representation of non-Arrow CSG extraction impacts while maintaining alignment with OGIA regional groundwater flow directions.

3.1.3.5 FDP abstraction scenarios

In order to quantify the impact of Arrow's proposed FDP (Clynes Road development) on groundwater flow and migration of contaminants, the following groundwater abstraction scenarios were initially considered in the current study:

- **Scenario 1:** this includes all non-Arrow production wells in proximity of PL253 (within the modelled domain).
- **Scenario 2:** this corresponds to the six existing Hopeland pilot wells and the soon to be installed 55 Kogan Creek CSG wells approved under the current EA for PL253 (green points in Figure 1-1), together with approved wells in Arrow's neighbouring tenure. This scenario reflects Arrow's currently authorised Field Development Plan (FDP).
- **Scenario 3:** this includes all wells from Scenario 2, plus the additional 55 Clynes Road wells for which Arrow is seeking approval.

Assessing incremental changes between scenario 2 and scenario 3 will provide insight into understanding impacts from Lot 40 DY85 attributable to Arrow's proposed Clynes Road FDP for the expansion project.

The abstraction rates for Arrow wells scenarios 2 and scenario 3 (simulated using the WEL package), are shown in Figure 3-4.

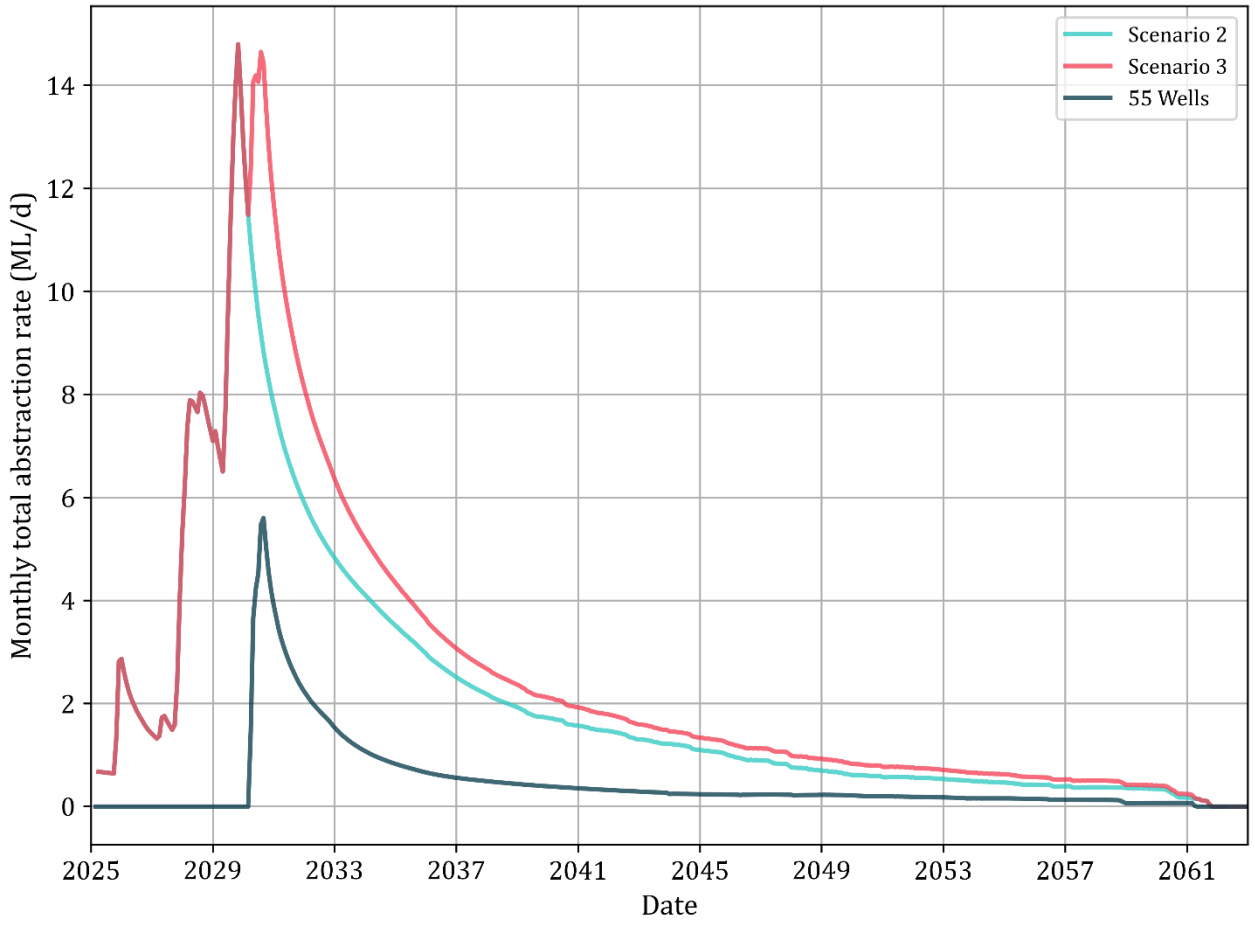


Figure 3-4 Monthly total abstraction rates for FDP scenarios 2 and 3

Extraction from existing and proposed Arrow CSG wells was distributed across multiple WCM layers using a transmissivity-weighted approach. Using this approach, the total abstraction rate from each well is apportioned based on the relative hydraulic conductivity and thickness of the intersected model layers. This ensures that groundwater extraction is preferentially assigned to more transmissive coal seams, consistent with the conceptual understanding of multi-seam CSG production in the Surat Basin.

3.1.3.6 Hopeland pilot wells

Hopeland pilot wells were explicitly simulated in the groundwater flow model to represent multi-seam extraction and to reproduce observed groundwater level responses associated with historical pilot testing at the Hopeland site. The pilot wells are located approximately 8 km southwest of Lot 40 DY85 and comprise six authorised CSG bores completed across several WCM coal seams. Given the vertical extent of well completions and the importance of simulating groundwater level responses to abstraction during pilot tests, these wells were represented using the MODFLOW 6 Multi-Aquifer Well (MAW) package.

Use of the MAW boundary condition allows abstraction to be distributed dynamically along the well as a function of layer transmissivity and simulated hydraulic heads, providing a physically realistic representation of vertical flow within multi-seam CSG wells. The MAW formulation enables interaction between the well and multiple WCM model layers providing improved simulation of observed drawdown behaviour recorded in pilot wells and monitoring bore HL17. Parameters controlling MAW behaviour, including well conductance and scaling height above the pump elevation, were subject to calibration and uncertainty analysis.

3.1.3.7 Historical UCG activities

Historical UCG activities were explicitly simulated over their respective operational periods using drain (DRN) boundary conditions. Combustion processes and subsequent collapse of gasifier voids may have induced broader-scale fracturing beyond the target coal seams, with fractures propagating upward into overlying formations. This secondary fracturing could locally enhance hydraulic connectivity and influence post-UCG groundwater flow and contaminant migration pathways.

The DRN package was used to represent depressurisation and enhanced groundwater discharge associated with gasifier operation. Drain elevations were assigned consistent with the affected HSUs and UCG activities at each gasifier, allowing groundwater discharge to occur. The drain elevation and conductance were allowed to be adjusted during history matching and uncertainty analysis.

To account for changes in hydraulic properties induced by gasification processes, time-varying hydraulic properties were applied to HSUs affected by UCG activities, including the Macalister coal seam, Kogan interburden, and the Springbok sandstone. UCG-related fracturing, material removal, and permeability enhancement were represented by modifying hydraulic conductivity and storage properties during defined gasification periods. Allowing hydraulic property changes in the layers overlying Macalister coal seam provides a conservative representation of the

potential for vertical migration of contaminants into or out of overlying units, including the Springbok sandstone.

Time-varying hydraulic conductivity (TVK) and time-varying storage (TVS) parameters were applied on a gasifier-specific basis, enabling localised impacts to be simulated independently for each gasifier footprint. Spatial variability in fracturing intensity and material alteration was allowed to be adjusted during history matching, uncertainty analysis, and predictive assessment under post-UCG recovery and CSG development scenarios.

3.1.4 Temporal discretisation

The groundwater model simulation starts with a steady state stress period to simulate the "steady-state" groundwater flow regime, reflecting the chosen parameterisation and boundary conditions, before progressing to a transient model.

The combined steady-state and transient model simulations are divided into 215 stress periods for historical matching (calibration) and prediction periods. The number and duration of transient stress periods are tailored based on the dates associated with the recorded groundwater levels, and former UCG activities as follows:

- History-matching period (159 stress periods):
  - 1 steady-state stress period,
  - 14 annual stress periods from 1/1/2000 to 1/1/2014, and
  - 144 quarterly stress periods from 1/1/2014 to 1/1/2026.
- Prediction period (56 stress periods):
  - 40 annual stress periods from 1/1/2026 to 1/1/2066, and
  - 16 10-year stress periods from 1/1/2066 to 1/1/2226.

3.1.5 Metric systems

The groundwater flow model uses units of meters and days. The geographic coordinate system used is the Geographic Datum of Australia 1994 (GDA94), and the projection used is the Map Grid of Australia (MGA) zone 56.

The following units are adopted throughout this groundwater modelling report:

- Groundwater level elevation: mAHD,
- Groundwater contaminant concentration: µg/L,
- Horizontal hydraulic conductivity (Kh): m/day,
- Vertical hydraulic conductivity (Kv): m/day,
- Specific storage (Ss): 1/m, and
- Specific yield: %.

3.2 Particle tracking

Particle tracking was undertaken to assess potential groundwater flow pathways and provide a conservative assessment of advective contaminant migration (compared with contaminant transport model) under approved and proposed coal seam gas (CSG) development scenarios. The particle tracking analysis was designed to evaluate groundwater flow directions, travel distances, and relative changes in migration behaviour, independent of chemical processes such as sorption, decay, or dispersion, thereby providing a conservative representation of potential solute movement.

Particles were released in 2019 at locations representative of residual contaminant source areas (gasifiers), Lot 40 DY85 boundaries, and key monitoring points (shown in Figure 3-5) within the Springbok sandstone and the Macalister coal seam. Release locations were selected to reflect both the former UCG footprint and bore locations where elevated benzene and naphthalene concentrations have been historically observed. Particle releases were distributed both laterally and vertically within the groundwater model to adequately capture local flow variability. The density and placement of particles were selected to ensure consistent coverage of potential transport pathways and to support interpretation of site-scale flow patterns.

Particle tracking simulations were carried out using groundwater flow fields generated by the calibrated numerical model for both FDP scenarios. The analysis focused on both relative differences between scenarios and absolute travel distance, while recognising uncertainty associated with effective porosity and residual multi-phase effects following UCG operations. Particle tracking simulations were treated as a conservative tool to inform risk assessment rather than a predictive representation of contaminant concentrations.

Porosity values adopted for the particle tracking simulations were derived from the calibrated specific yield values, obtained from the groundwater flow model, with the addition of a layer-wide specific retention component. This approach ensures consistency between the simulated groundwater flow field and particle velocities while accounting for spatially varying storage behaviour within coal seams and interburden lithologies. A range of specific retention between 1% and 10% was explored as part of history matching and uncertainty analysis to assess particle travel distances and trajectories with a plausible variability in porosity.



Legend

- Groundwater model extent
- Lot 40 DY85

Particles released at:

- Monitoring bores
- Gasifiers
- Lot 40 DY 85 boundaries

Particle release locations

Project No.	Client	Figure No.
411001-00917	Arrow	3-5

Notes:
Project CRS: GDA94 / MGA zone 56
Last Saved: 14:45 16/04/2026
Filename: Figure_3-5_prt_locs
Exported by User: Mohsen.Azadi
Project Exported: 15:15 16/04/2026

References:
N/A

File Path: C:\modelling\Arrow\deliverables\Figures_REP-HG-002\Figure_3-5_prt_locs.qgz

© Worley Pty Ltd While every care is taken to ensure the accuracy of this data, Worley makes no representations or warranties aboutits accuracy, reliability, completeness or suitability for any particular purpose and disclaims all responsibility and all liability (including without limitation liability in negligence) for all expenses, losses, damages (including indirect or consequential damage) and costs which might be incurred as a result of the data being inaccurate or incomplete in any way and for any reason.

worley consulting

3.3 Contaminant transport model

The contaminant transport model was developed to simulate the fate and transport of dissolved benzene and naphthalene within the Springbok sandstone and the Macalister coal seam. The model was configured to represent key processes controlling contaminant migration and attenuation following historic UCG activities, and to assess potential changes under the approved and proposed FDP scenarios.

The transport model focuses on reproducing observed concentration trends and predicting potential future behaviour rather than predicting exact concentrations at individual monitoring locations. Model setup and parameterisation were informed by available monitoring data, previous contaminant transport modelling for PL253, and the Australian Groundwater Modelling Guidelines (Barnett et al., 2012), providing a risk-based impact assessment.

3.3.1 Transport model coupling

In the present study, the contaminant transport model is coupled with the calibrated groundwater flow model, using the simulated transient flow field to represent advective transport processes. The spatial discretisation, layering, and groundwater flow boundary conditions are consistent between the flow and transport models, ensuring internal coherence between groundwater flows and contaminant migration.

Coupling the transport model to the flow model allows changes in hydraulic gradients and groundwater velocities arising from different development scenarios to be directly reflected in simulated contaminant behaviour. This provides a consistent and interconnected basis for assessing migration pathways in both the Springbok sandstone and the Macalister coal seam.

3.3.2 Initial condition

Initial conditions for benzene and naphthalene were defined using groundwater quality monitoring data from Arrow and DoR operated monitoring bores. Similar to the approach used in the previous groundwater modelling studies (AGE, 2023; Intera, 2025), concentrations were spatially assigned to represent residual dissolved contamination associated with former UCG activities, commencing on 1/1/2018.

The initial concentration distributions for benzene and naphthalene within the Springbok sandstone and Macalister coal seam reflect the best available estimate of groundwater quality conditions post-UCG activities and were adjusted to be conservative where uncertainty exists. This approach ensures that subsequent transport simulations evaluate conservative impacts over the assessment period.

Initial contaminant concentration distributions and transient source depletion release at gasifiers (discussed in section 2.4.2.1) were both implemented using the MODFLOW 6 Constant Concentration (CNC) package. Initial concentrations for benzene and naphthalene were defined to represent residual dissolved impacts within Lot 40 DY85 and in the vicinity of former gasifier locations within the Springbok sandstone and Macalister coal seam. Time-varying source boundary conditions at these locations were assigned through compound-specific exponential

depletion equations (1) to (4) derived from the upper-envelope groundwater monitoring datasets within the Springbok sandstone and Macalister coal seam.

3.3.3 Boundary condition

Contaminant transport model was coupled with the calibrated groundwater flow model to ensure that predicted concentrations and plume evolution appropriately reflect the simulated flow regime and contaminant transport parameters. The transport response is therefore governed partially by transport boundary conditions defined by formation physical properties (porosity and bulk density), source representation, and key transport processes such as dispersivity, dual-domain porosity, and natural attenuation (sorption and degradation).

A summary of the parameters used in the transport model with the initial value, lower bound and upper bounds considered in the transport model history matching is summarised in Table 3-4. The transport boundary conditions are described in the following sections.

Table 3-4 Contaminant transport parameters

Transport parameter	Unit	Compound	Layer	Initial	Min	Max	Reference
Effective molecular diffusion-coefficient	m^2/d	Benzene	All	1.1E-05	3.9E-06	1.9E-05	Gustafson & Dickhut (1994)
Effective molecular diffusion-coefficient	m^2/d	Naphthalene	All	8.4E-06	3.0E-06	1.4E-05	Gustafson & Dickhut (1994)
Longitudinal dispersivity	m	All	Non-coal	5.0E+00	1.0E+00	1.0E+01	Gelhar et al. (1992), Schulze-Makuch (2005), Bjerg et al. (2025)
Longitudinal dispersivity	m	All	Coal	1.0E+01	5.0E+00	3.0E+01	Gelhar et al. (1992), Schulze-Makuch (2005), Dong et al. (2018)
Transverse horizon-al dispersivity	m	All	Non-coal	5.0E-01	1.0E-01	1.0E+00	Gelhar et al. (1992), Schulze-Makuch (2005), Bjerg et al. (2025)
Transverse horizon-al dispersivity	m	All	Coal	1.0E+00	5.0E-01	3.0E+00	Gelhar et al. (1992), Schulze-Makuch (2005), Dong et al. (2018)
Transverse vertical dispersivity	m	All	Non-coal	5.0E-02	1.0E-02	1.0E-01	Gelhar et al. (1992), Schulze-Makuch (2005), Bjerg et al. (2025)
Transverse vertical dispersivity	m	All	Coal	1.0E-02	1.0E-03	5.0E-02	Gelhar et al. (1992), Grathwohl et al. (2000)
First-Order Decay Rate Coefficients	1/day	Benzene	Non-coal	1.0E-03	1.0E-04	1.0E-02	US EPA (1999), Newell et al. (2002), Zhang et al. (2005)
First-Order Decay Rate Coefficients	1/day	Naphthalene	Non-coal	7.5E-03	5.0E-05	5.0E-02	Anderson & Lovley (1998), Wiedemeier et al. (1999), ATSDR (2022)
First-Order Decay Rate Coefficients	1/day	Benzene	Coal	5.0E-04	1.0E-06	1.0E-03	API (1998), US EPA (1999); Anderson et al. (1998)
First-Order Decay Rate Coefficients	1/day	Naphthalene	Coal	5.0E-03	1.0E-06	1.0E-02	Wiedemeier et al. (1999), Bjerg et al. (1999), Musat et al. (2008)
Immobile First-Order Decay Rate Coefficients	1/day	Benzene	Non-coal	1.0E-04	3.0E-05	1.0E-03	US EPA (1999) Newell et al. (2002); Anderson & Lovley (1998)
Immobile First-Order Decay Rate Coefficients	1/day	Naphthalene	Non-coal	1.0E-03	2.5E-06	1.5E-02	Anderson & Lovley (1998), Wiedemeier et al. (1999), Bjerg et al. (1999), Musat et al. (2008)
Immobile First-Order Decay Rate Coefficients	1/day	Benzene	Coal	5.0E-04	3.0E-07	1.0E-03	US EPA (1999), Newell et al. (2002), Anderson & Lovley (1998)
Immobile First-Order Decay Rate Coefficients	1/day	Naphthalene	Coal	1.0E-04	5.0E-08	3.0E-03	Anderson & Lovley (1998), Wiedemeier et al. (1999), Bjerg et al. (1999), Musat et al. (2008)
Freundlich coefficient	m^3/kg	Benzene	Non-coal	1.0E-04	5.0E-05	3.0E-04	Shi et al. (2020), U.S. EPA (1996), ECETOC (2013)
Freundlich coefficient	m^3/kg	Naphthalene	Non-coal	7.5E-03	2.0E-04	1.0E-02	Osagie & Owabor (2015), Shi et al. (2020), ECETOC (2013)
Freundlich coefficient	m^3/kg	Benzene	Coal	1.0E-03	5.0E-04	3.0E-03	ECETOC (2013), U.S. EPA (1996)
Freundlich coefficient	m^3/kg	Naphthalene	Coal	5.0E-02	2.0E-03	1.0E-01	Ahangar (2010), Ukalska-Jaruga & Smreczak (2020), Osagie & Owabor (2015), ECETOC (2013)
Non-linearity exponent	-	Benzene	Non-coal	9.5E-01	9.0E-01	1.0E+00	Shi et al. (2020), U.S. EPA (1996), ECETOC (2013)
Non-linearity exponent	-	Naphthalene	Non-coal	9.5E-01	9.5E-01	1.0E+00	Osagie & Owabor (2015), Shi et al. (2020), ECETOC (2013)
Non-linearity exponent	-	Benzene	Coal	9.0E-01	8.5E-01	1.0E+00	ECETOC (2013), U.S. EPA (1996)
Non-linearity exponent	-	Naphthalene	Coal	9.5E-01	9.5E-01	1.0E+00	Ahangar (2010), Ukalska-Jaruga & Smreczak (2020), Osagie & Owabor (2015), ECETOC
Immobile non-linearity exponent	-	Benzene	Non-coal	9.0E-01	8.5E-01	9.5E-01	Shi et al. (2020), U.S. EPA (1996), ECETOC (2013)
Immobile non-linearity exponent	-	Naphthalene	Non-coal	8.5E-01	7.5E-01	9.0E-01	Osagie & Owabor (2015), Shi et al. (2020), ECETOC (2013)
Immobile non-linearity exponent	-	Benzene	Coal	8.0E-01	7.0E-01	8.5E-01	ECETOC (2013), U.S. EPA (1996)
Immobile non-linearity exponent	-	Naphthalene	Coal	7.0E-01	5.0E-01	8.5E-01	Ahangar (2010), Ukalska-Jaruga & Smreczak (2020), Osagie & Owabor (2015), ECETOC (2013)
Immobile domain fraction	-	All	Non-coal	2.0E-01	1.0E-02	3.0E-01	Warren & Root (1963), Aguilera (2004), Langevin et al. (2022)
Immobile domain fraction	-	All	Coal	7.0E-01	6.0E-01	8.5E-01	King & Ertekin (1988), Pruess & Narasimhan (1985)
Mass transfer rate coefficient	1/day	All	Non-coal	5.0E-04	1.0E-04	1.0E-03	Warren & Root (1963), Pruess & Narasimhan (1985), Langevin et al. (2022)
Mass transfer rate coefficient	1/day	All	Coal	1.0E-05	1.0E-06	1.0E-04	King & Ertekin (1988)

3.3.3.1 Dispersivity

Dispersivity describes the spreading of dissolved contaminants in groundwater arising from variations in groundwater velocity at different spatial scales and is a key process controlling solute transport behaviour. Contaminant plume dispersion occurs both along the direction of groundwater flow (longitudinal dispersivity) and perpendicular to flow in the horizontal and vertical directions (transverse horizontal and transverse vertical dispersivity), reflecting aquifer heterogeneity, pore-scale velocity differences, and preferential flow pathways. In addition to mechanical dispersion, solute spreading is influenced by molecular diffusion, which governs mass transfer driven by concentration gradients, particularly in low-velocity or low-permeability zones. Together, these processes control plume shape, extent, and dilution over time. MODFLOW 6 Dispersion (DSP) package was used in the contaminant transport model to simulate mechanical dispersion and molecular diffusion. The input parameters included longitudinal, transverse horizontal, and transverse vertical dispersivity (Table 3-4) defined on a layer-specific basis and effective molecular diffusion-coefficient defined on a compound-specific basis. All these input parameters were adjusted during history matching of the transport model.

3.3.3.2 Natural attenuation

Natural attenuation processes were incorporated in the contaminant transport model to represent the reduction in contaminant mobility and mass through physicochemical and biological mechanisms occurring within the subsurface. For benzene and naphthalene, natural attenuation was represented through equilibrium-controlled sorption and first-order degradation processes, which together influence plume migration, and long-term concentration trends.

MODFLOW 6 Mobile Storage and Transfer (MST) package was used in the contaminant transport model to simulate natural attenuation processes. This included both first-order degradation processes, as outlined above, and equilibrium-controlled sorption described using a Freundlich isotherm formulation. These processes were applied to simulate reduction in contaminant mass and mobility for benzene and naphthalene within the mobile groundwater domain. The input parameters included porosity, bulk density of the layer, first-order decay rate coefficient, Freundlich coefficient and mobile non-linearity exponent (Table 3-4) defined on a layer-specific basis and adjusted during history matching of the transport model.

3.3.3.3 Dual-Domain Porosity

Dual-porosity behaviour was simulated in the contaminant transport model to represent mass exchange between mobile groundwater flowing through fracture-dominated pathways and immobile pore water stored within low-permeability micropore domains. Solute mass can transfer from the fracture-scale flow system into the rock matrix and micro-porosity, and subsequently diffuse back into the mobile domain over time. This bidirectional mass transfer mechanism allows contaminant mass to be temporarily retained or released depending on concentration gradients, influencing plume persistence and long-term concentration trends.

Representation of immobile-mobile mass transfer is particularly relevant for coal seams and fine-grained sandstone units, where pore structure heterogeneity and sorptive surfaces can result in delayed contaminant breakthrough. MODFLOW 6 Immobile Storage and Transfer (IST) package was used in the transport model to simulate dual-domain porosity and associated mass exchange processes. This boundary condition allows for diffusion-controlled mass transfer between micro-pores and fracture-scale flow. The input parameters included porosity, bulk density of the layer, immobile domain fraction, mass transfer rate coefficient, first-order decay rate coefficient, Freundlich coefficient and immobile non-linearity exponent (Table 3-4) defined on a layer-specific basis and adjusted during history matching of the transport model.

4. History matching

4.1 Calibration approach

This section details the approach used for history matching the historical groundwater flow regime, UCG activities, and contaminant transport migration within Lot 40 DY85, PL253 and the model domain.

In this study, "history matching" refers to the process of assimilating observed transient groundwater data into the model, its calibration and its outputs. The purpose of history-matching in this context is to constrain model parameters and allowable ranges, based on what we know from field testing, conceptual ideas and observed system behaviour (ideally of direct relevance to the model predictions of interest), using a range of observation data.

This in turn constrains the suite of parameter fields that are used to make model predictions and to assess their uncertainty. This approach provides a sound basis for enhanced use and understanding of model outputs, including their limitations, in decision-making.

PEST, the tool providing the basis for calibration, represents a family of optimisation and uncertainty analysis tools. PEST also represents a suite of workflows for highly parameterised environmental model optimisation (inversion), uncertainty analysis and associated tasks.

ENSI (Ensemble Space Inversion) is a relatively new method for fast history-matching. It attains its speed through estimation of "super parameters" instead of parameters themselves. These super parameters are factors applied to random parameter vectors which, ideally, should be samples of the prior parameter probability distribution. The number of realisations required for achieving a high level of model-to-measurement fit can be far fewer than the number of parameters that are used by a model (Doherty, 2024).

In contrast to other calibration methods such as SVD-assist (which also estimates super parameters), it is not necessary to calculate a Jacobian matrix in order to formulate super parameters prior to implementing ENSI inversion. What it gets is an ensemble of random samples of the prior parameter probability distribution.

The combined steady-state and history-matching transient model is calibrated by adjusting aquifer parameters and other boundary condition parameters for the groundwater flow and transport models to develop a suitable match between the observed and simulated groundwater levels and concentrations across the model domain.

4.2 Parameterisation

This section discusses additional details with respect to the PESTPP-ENSI model parameterisation. Once a good model-to-measurement fit was achieved using PESTPP-ENSI, the model parameterisation was used to inform the PESTPP-IES workflow of uncertainty quantification.

Use of PEST-ENSI for history-matching suggests that its model run efficiency is greater than that of PEST_HP in highly parameterised cases, and its model-to-measurement fit is better than that of PESTPP-IES (Doherty, 2024). However, PEST-ENSI associates no uncertainty with the parameter field that it calculates, and with model predictions that are calculated using this field. The complementary PESTPP-IES methodology is therefore deployed for predictive uncertainty analysis.

Both PEST-ENSI and PESTPP-IES PPP-IES approaches allow for large numbers of pilot points as in practice they sample a subset of pilot points (ensemble) during each iteration. This does not charge parameterisation approach with any further computational penalties.

The parameterisation scheme uses pilot points in the proximity of monitoring sites, acknowledging the need for spatial interpolation and extraction of information from observed data. All pilot points are assigned spatial covariance structures to encourage the history matching process to honour the initial (prior) parameters and their spatial differences as closely as possible. Departures from this would occur where necessary to significantly improve the simulation of historical system behaviour as measured by PESTPP-ENSI against the strategically weighted observation data.

These covariances are computed using PEST utilities MKPPSTAT and PPCOV_SVA. Covariances are computed using a variogram with the range based on the mean distance from each pilot point and its ten nearest neighbours. No nugget is applied.

For parameters that are not spatially correlated, standard deviations are defined in the same way (one quarter of the allowable parameter range). These standard deviations and covariance matrices are provided to PESTPP-IES via a PEST parameter uncertainty file.

The parameterisation scheme was reviewed and revised during history matching with learnings from each iteration feeding to the next round. A total of seven rounds of history matching (each running for several iterations) were conducted.

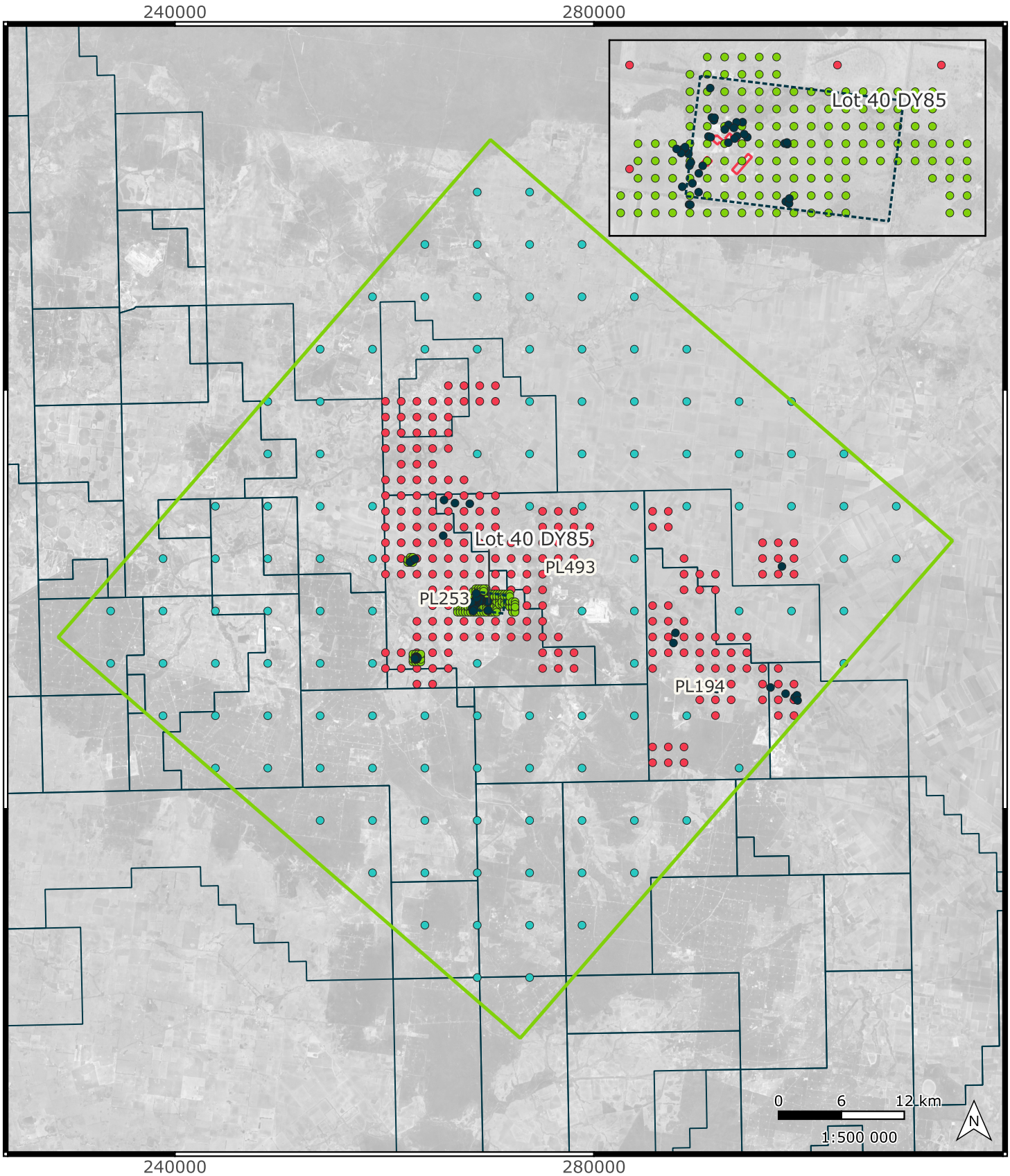
Pilot point interpolation across the model zones using the PLPROC kriging and Python scripting were applied to parameterise successive model runs and adjust model boundary conditions discussed in section 3.1.3.

Overall, the numerical groundwater model has 26,032 adjustable parameters. PEST-ENSI/PESTPP-IES randomly samples parameter fields based on prior parameter ranges where each parameter field is referred to as a "realisation". An initial ensemble size of 800 realisations was defined for PEST-ENSI/PESTPP-IES automated history matching which was reduced to 216 realisations after eight rounds of calibration iterations removing realisations that did not converge for all the time steps or did not satisfy history matching metrics for the groundwater flow and contaminant transport model. The prior and posterior ranges of parameters were compared ensuring that the posterior parameters fields are not over-constrained.

Pilot point application is described below:

- A total of 578 pilot points is used across the model domain as shown in Figure 4-1.
- Pilot points allow for perturbations in:
  - hydraulic conductivity (horizontal and vertical),
  - specific storage, and
  - specific yield.
- Pilot points are spread out based on their proximity to monitoring sites and potential parameterisation of structures and geological zones within each layer with the following spacings:
  - 250 m within Lot 40 DY85,
  - 1,500 m within areas with groundwater level records, and
  - 5,000 m in areas with no groundwater level data.

A pilot point is placed between each pair of monitoring sites to allow for capturing different groundwater trends in bores caused by heterogeneity in hydraulic properties of HSUs.



Legend

- Groundwater model extent
- Lot 40 DY85

Pilot points with:

- 250 m
- 1500 m
- 5000 m
- Additional PP near monitoring sites

Pilot point locations

Project No.	Client	Figure No.
411001-00917	Arrow	4-1

Notes:
Project CRS: GDA94 / MGA zone 56
Last Saved: 14:49 16/04/2026
Filename: Figure_4-1_pilot_points
Exported by User: Mohsen.Azadi
Project Exported: 15:11 16/04/2026

References:
N/A

File Path: C:\modelling\Arrow\deliverables\Figures_REP-HG-002\Figure_4-1_pilot_points.qgz

© Worley Pty Ltd While every care is taken to ensure the accuracy of this data, Worley makes no representations or warranties aboutits accuracy, reliability, completeness or suitability for any particular purpose and disclaims all responsibility and all liability (including without limitation liability in negligence) for all expenses, losses, damages (including indirect or consequential damage) and costs which might be incurred as a result of the data being inaccurate or incomplete in any way and for any reason.

worley consulting

4.3 Observation data assimilation

PEST is designed to progressively minimise its objective function (phi) by adjusting model parameters in an iterative fashion within prescribed bounds. Phi is calculated internally by PEST as the sum of squared weighted residuals between observations and their modelled counterparts.

PEST allows the user to group different observation data types and apply different weights (and individual observations within each group). This facilitates strategic weighing of different observation types and locations according to the objectives of the modelling and accuracy of various data sources.

For example, strategic weighting may be used to account for the fact that some bores can have far more data than others; those with fewer observation data may be less "visible" to PEST during inversion, unless their weighting is increased relative to those sites with more data.

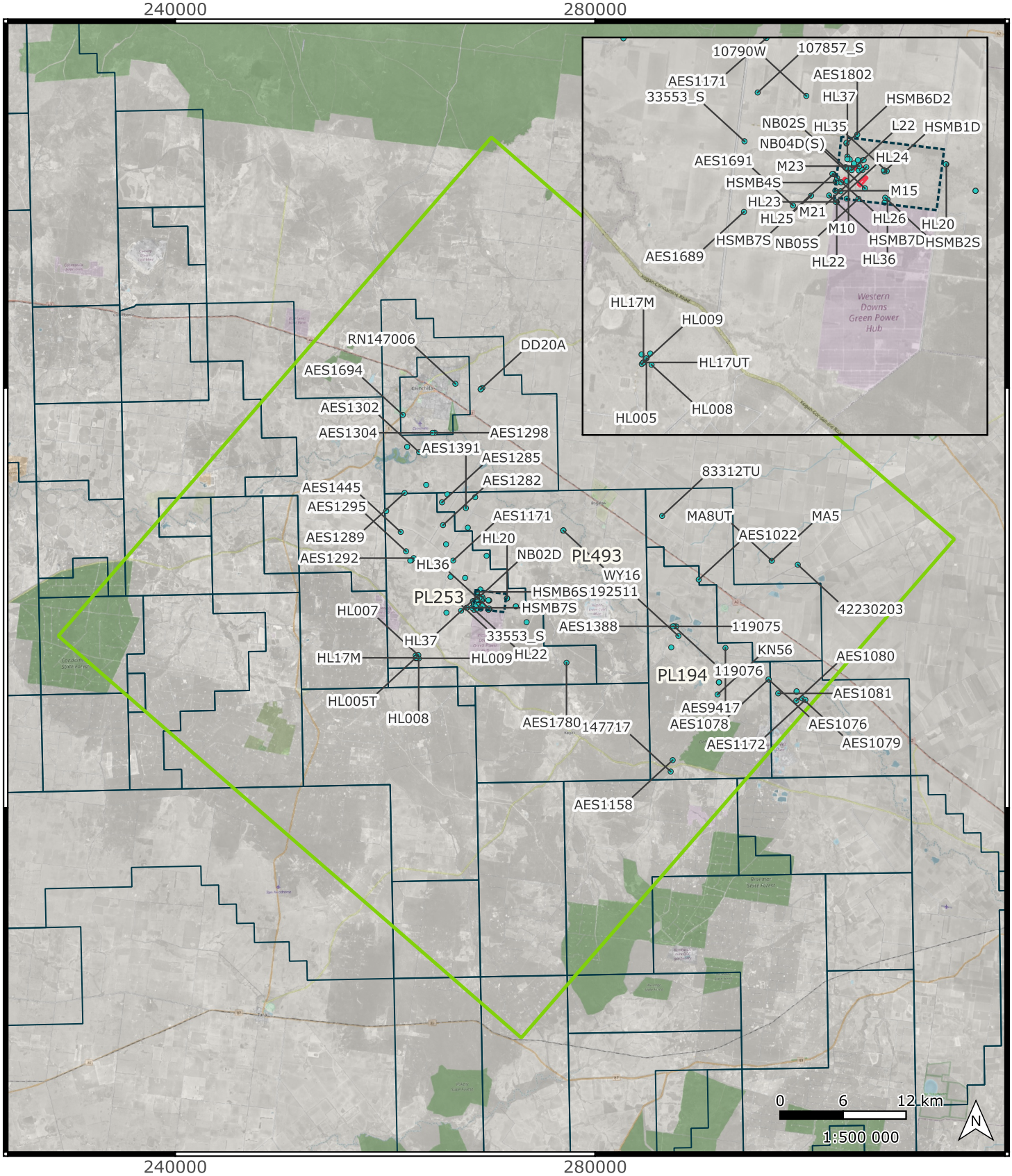
Other reasons for different weightings may include less reliable versus more reliable data. Or bores in a particular area are more important to the project objectives than those in other areas. In the current model, weight adjustment is focused on monitoring bores within PL253 and Lot 40 DY85.

The performance of the model is tested against the measured groundwater levels and concentrations (for benzene and naphthalene) as well as pumping data for Hopeland pilot wells. Observation data used for history matching of the groundwater flow model and the weights assigned to them are defined so that the total calculated phi is distributed among various calibration targets (shown in Figure 4-2):

- Starting water levels in 115 monitoring sites - representing background (pre-abstraction) groundwater level in each monitoring site (10%),
- Transient water levels recorded between 2008 and 2025 in 115 monitoring sites (30%),
- Temporal changes in the transient water levels for 115 monitoring sites (5%),
- Vertical head differences in 18 pairs of monitoring sites (10%),
- Inferred water levels based on Q3 2025 contours in Macalister coal seam shown in Figure 2-2 to replicate current hydraulic gradients within Lot 40 DY85 – water levels in 1,683 model cells across the contoured areas were sampled for a refined per cell history matching (15%),
- Monitoring bores within Springbok sandstone for Q3 2025 (5%), and
- Transient water levels, recorded in the Hopeland pilot wells and HL17 (25%).

For the contaminant transport model, the total calculated phi is distributed among various calibration targets:

- Benzene concentration in 18 monitoring sites located in the Springbok sandstone (50%),
- Benzene concentration in 12 monitoring sites located in the Macalister coal seam (30%),
- Naphthalene concentration in 19 monitoring sites located in the Springbok sandstone (15%), and
- Naphthalene concentration in 12 monitoring sites located in the Macalister coal seam (5%).



Legend

- Groundwater model extent
- Lot 40 DY85
- Monitoring bores

Bore locations with transient groundwater level data

Project No.	Client	Figure No.
411001-00917	Arrow	4-2

Notes:
Project CRS: GDA94 / MGA zone 56
Last Saved: 17:17 16/04/2026
Filename: Figure_4-3_bore_loc
Exported by User: Mohsen.Azadi
Project Exported: 17:22 16/04/2026

References:
N/A

File Path: C:\modelling\Arrow\deliverables\Figures_REP-HG-002\Figure_4-3_bore_loc.qgz

© Worley Pty Ltd While every care is taken to ensure the accuracy of this data, Worley makes no representations or warranties aboutits accuracy, reliability, completeness or suitability for any particular purpose and disclaims all responsibility and all liability (including without limitation liability in negligence) for all expenses, losses, damages (including indirect or consequential damage) and costs which might be incurred as a result of the data being inaccurate or incomplete in any way and for any reason.

4.4 Groundwater flow model

4.4.1 History matching metrics

Model performance acceptance is evaluated based on Australian Groundwater Modelling Guidelines (Barnett et al., 2012) using a number of measures that are not necessarily related to model history matching. The following aspects of the model performance are considered:

- Model convergence: the head change tolerance of 0.001 m between iterations is set in the solver setting,
- Water balance: A value of less than 1% should be achieved at any time step and cumulatively,
- Qualitative measures: robustness/plausibility of model parameters, groundwater flow directions, and temporal groundwater level trends must be consistent with the conceptual model, and
- Quantitative measures such as root mean square error (RMS) and scaled root mean square error (SRMS).

The performance of the 216 model realisations was analysed to ensure the models used during predictive uncertainty analysis are calibrated. A maximum SRMS of 10% was considered as the criterion to assess the model calibration with all 216 models deemed calibrated as shown in Figure 4-3.

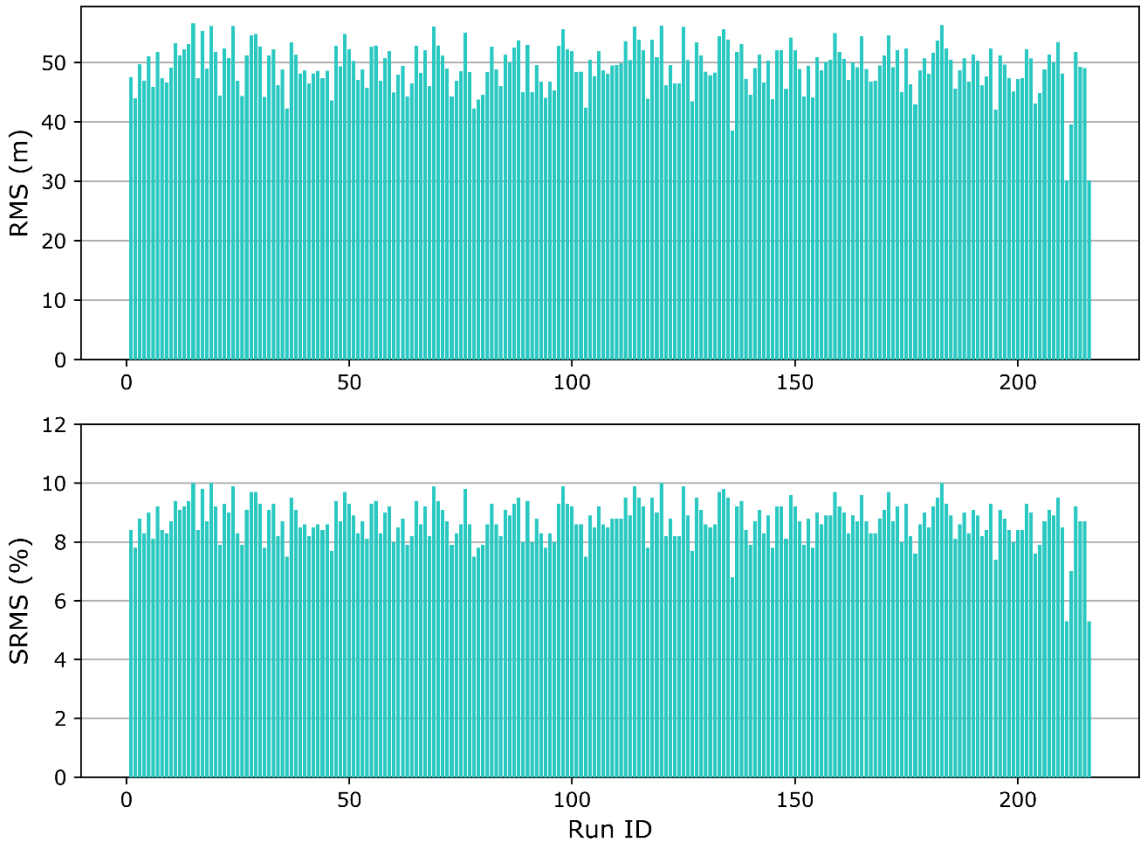


Figure 4-3 Calculated RMS and SRMS for converged model realisations

The results presented in the remainder of this section are extracted from the realisation that yields the best statistical fit with the observed groundwater levels, referred to as reference case.

The matches between individual water level measurements are presented as a scatter plot in Figure 4-4. The calibration statistics are expressed by RMS and the scaled RMS values of 30.2 m and 5.4%, respectively. Barnett et al. (2012) propose that groundwater models should aim to minimise the SRMS (RMS divided by the range of observed data) error to below 10%. Therefore, a value of 5.4% is deemed a satisfactory level of calibration.

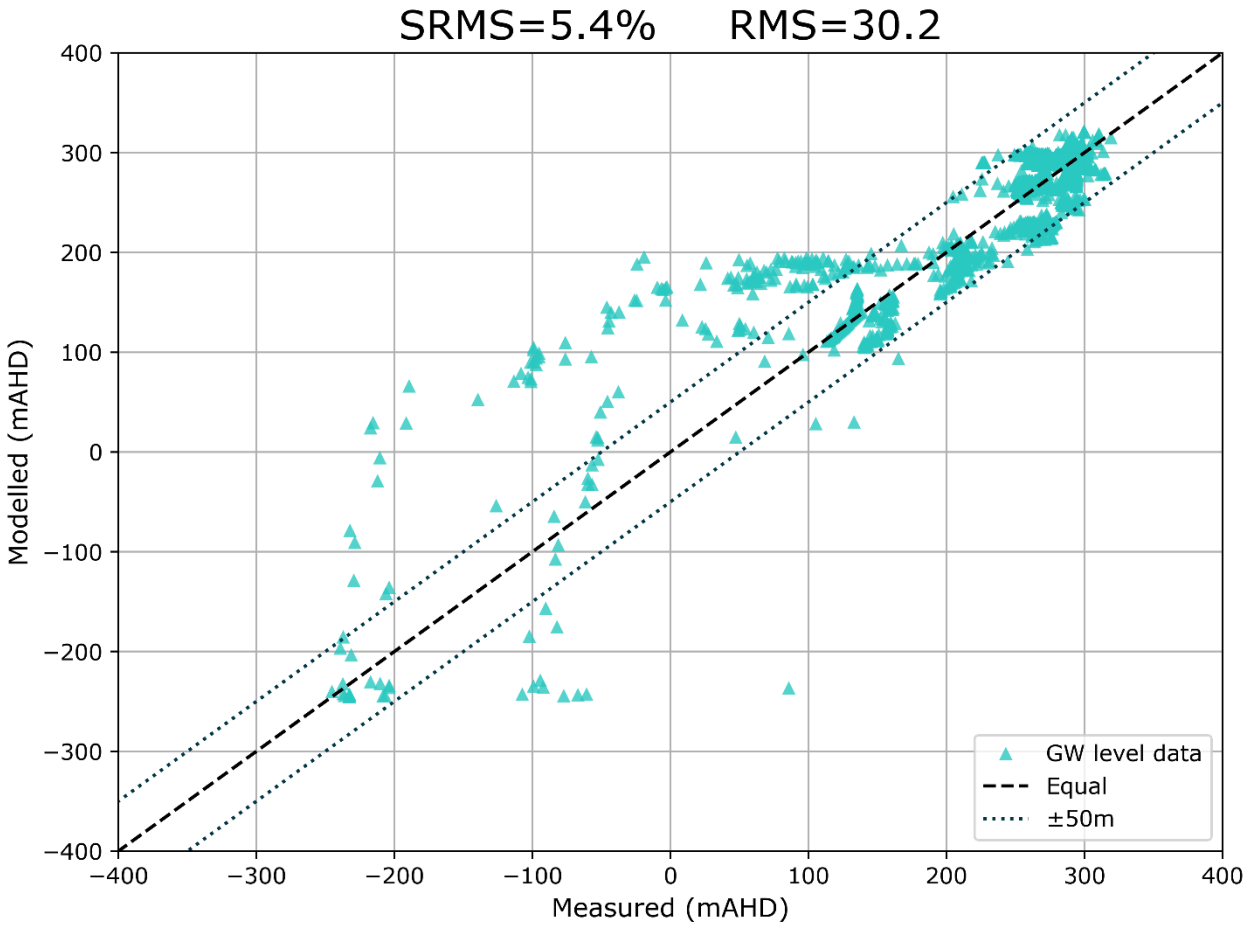
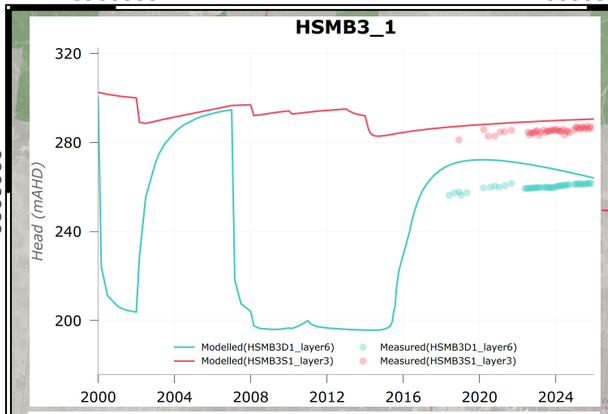


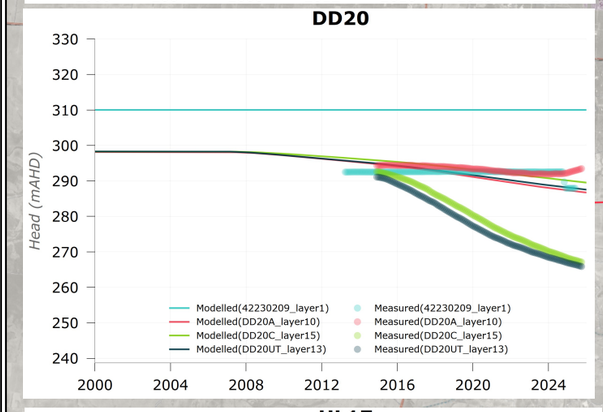
Figure 4-4 Calibration fit of reference case

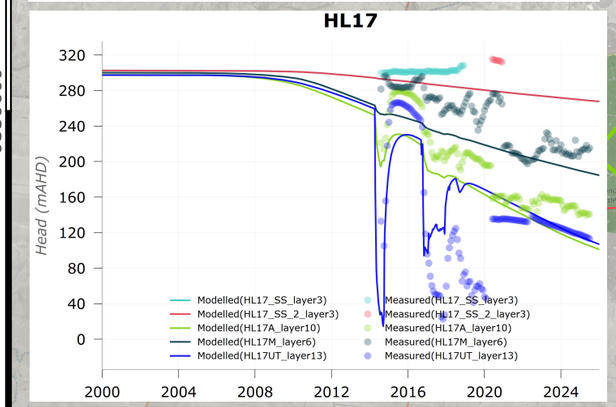
One of the metrics to evaluate groundwater model performance is by quantifying the match between the observed and modelled groundwater levels and by assessing the consistency of their trends.

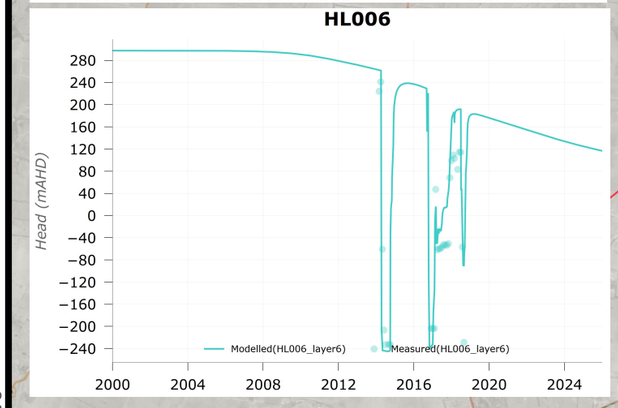
A reasonable match for groundwater level trends was achieved (shown in Figure 4-5) as noted in the observed groundwater levels showing recovering trends or declining trends due to groundwater abstraction.

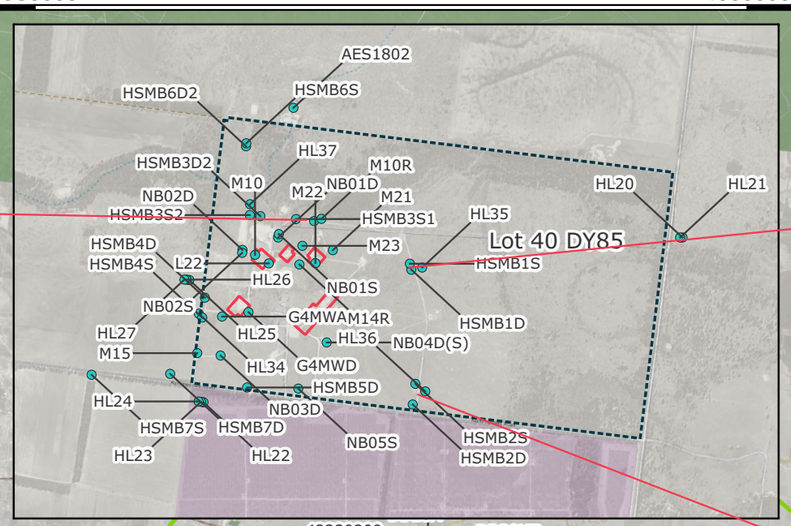
All hydrographs for simulated groundwater levels are presented in Appendix A.

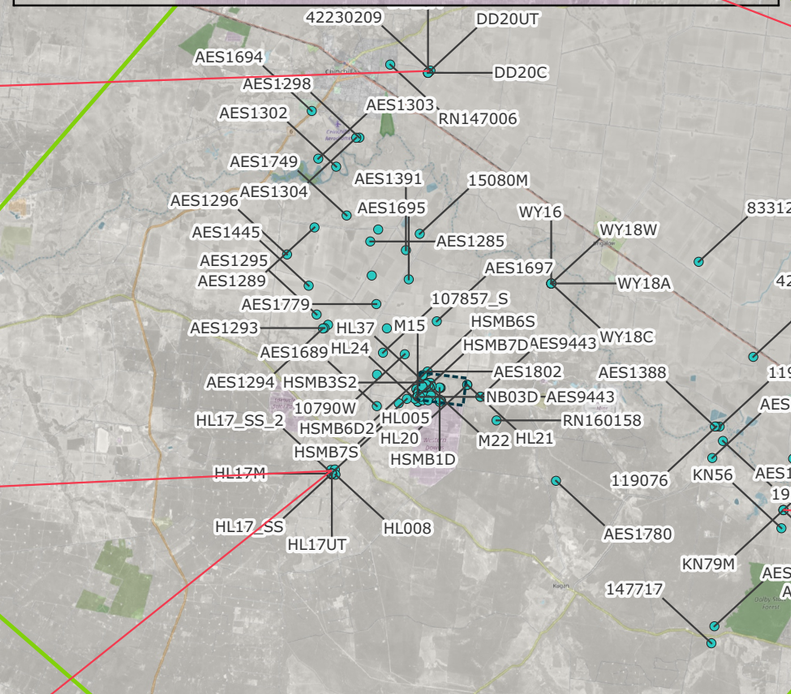


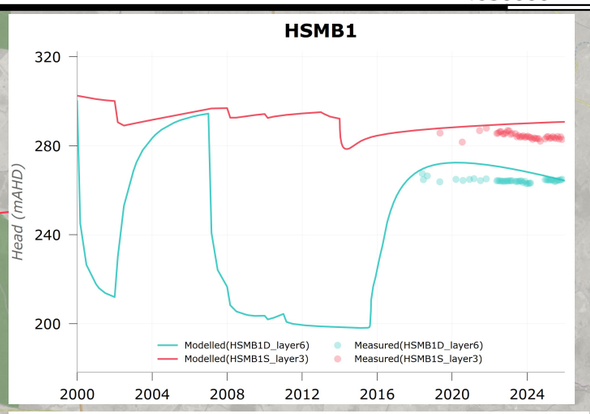


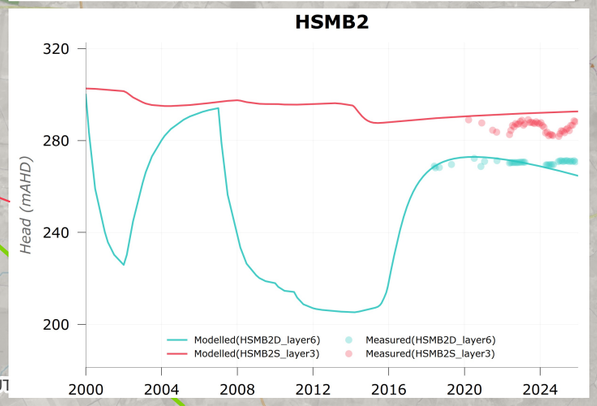


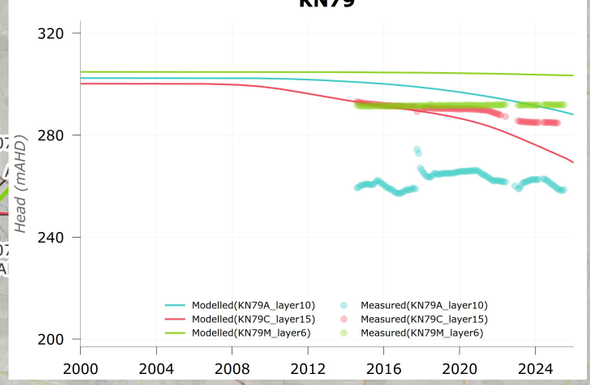












Legend

Groundwater model extent
Gasifiers
Monitoring bores
Lot 40 DY85

Observed vs modelled groundwater levels in monitoring bores

Project No.	Client	Figure No.
411001-00917	Arrow	4-5

Notes:
Project CRS: GDA94 / MGA zone 56
Last Saved: 22:28 03/08/2026
Exported by User: Mohsen.Azadi
Project Exported: 22:40 03/08/2026

References:
N/A

File Path: C:\modelling\Arrow\deliverables\Figures_REP-HG-002\Figure_4-5_GW_trends_v2.qgz

© Worley Pty Ltd While every care is taken to ensure the accuracy of this data, Worley makes no representations or warranties aboutits accuracy, reliability, completeness or suitability for any particular purpose and disclaims all responsibility and all liability (including without limitation liability in negligence) for all expenses, losses, damages (including indirect or consequential damage) and costs which might be incurred as a result of the data being inaccurate or incomplete in any way and for any reason.

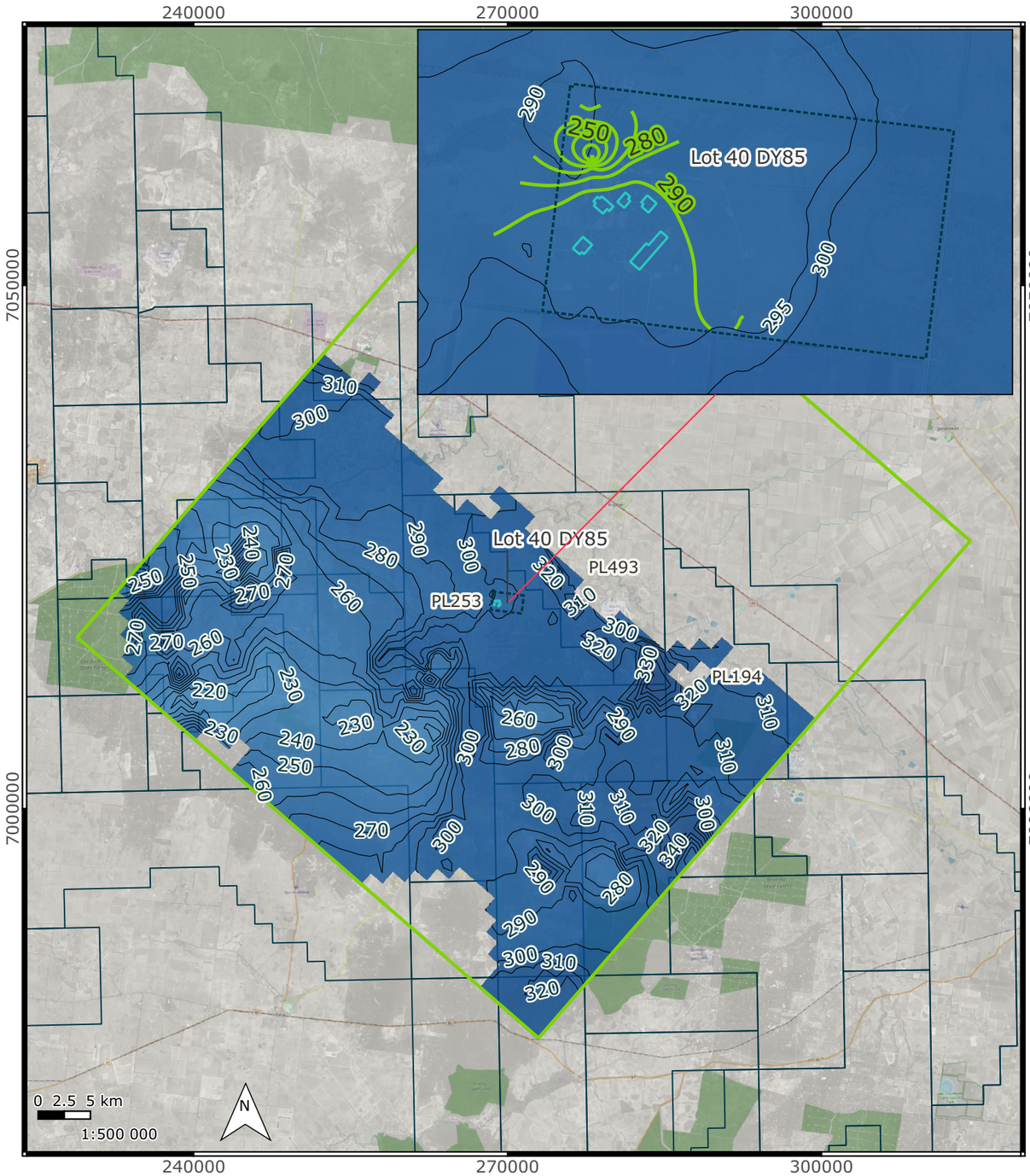
0 4 8 12 16 km
1:391,516
N

4.4.2 Groundwater levels and flow directions

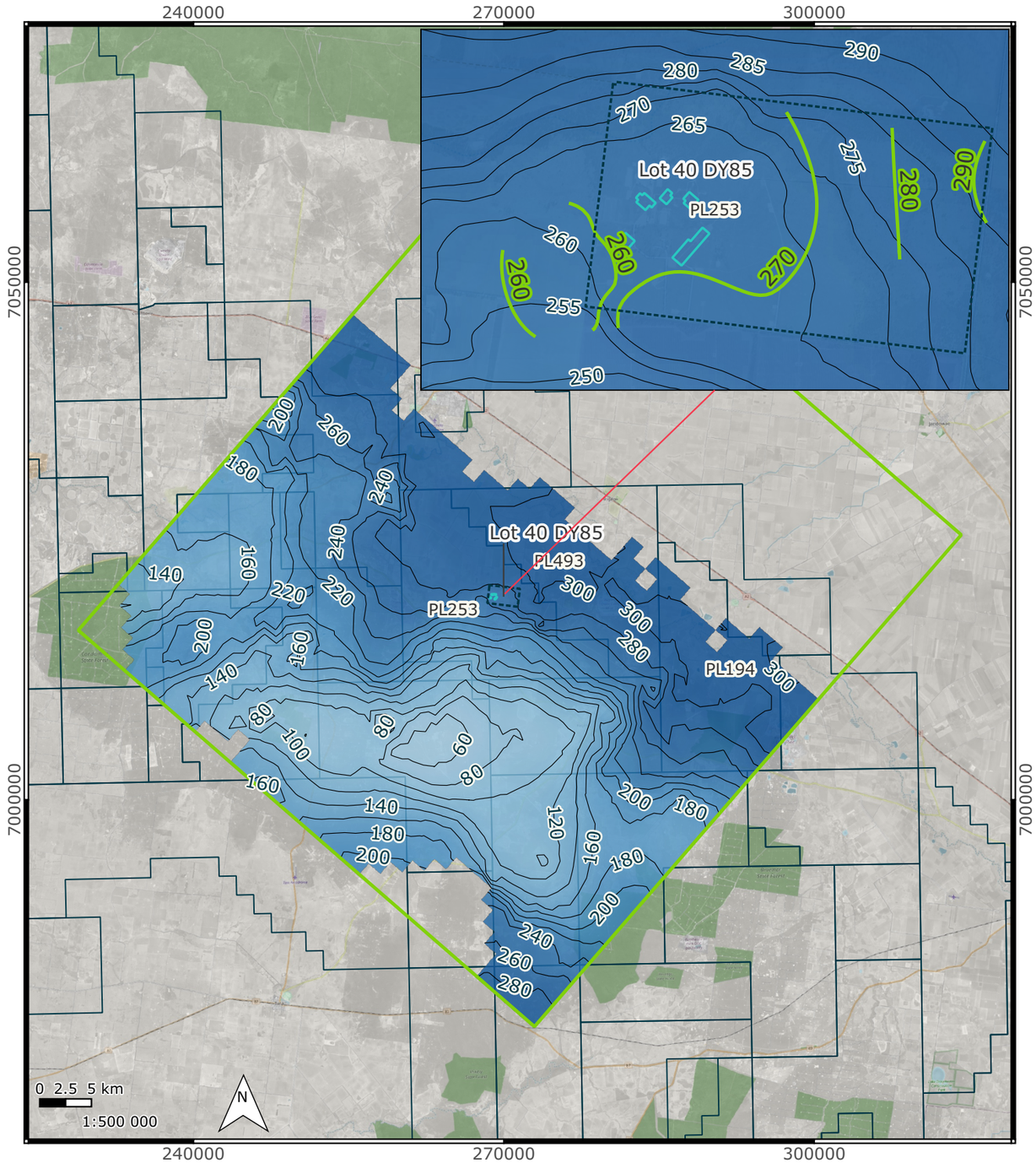
Figure 4-6 shows the simulated groundwater levels (reference case) at the end of the history matching period. As discussed in section 4.3, Q3 2025 groundwater levels were used as a calibration target to ensure the current simulated groundwater flow directions are largely aligned with the interpreted groundwater contours within Lot 40 DY85 (discussed in section 2.4.1). The calibration results indicate this approach achieves a reasonable spatial match between simulated and inferred (from bore measurements) groundwater levels and flow directions.

Modelled groundwater flow gradients within the Springbok sandstone indicate inward flow towards Lot 40 DY85. In the Macalister coal seam, hydraulic gradients are directed towards the gasifiers from the east, north, and parts of the west boundary, with groundwater continuing to flow towards the southwest corner of Lot 40 DY85. This flow direction potentially reflects partial groundwater recovery near the gasifiers and regional south to southwest groundwater flow associated with the current CSG abstraction beyond the PL253 area.

Springbok sandstone



Macalister coal seam



Legend

- Groundwater model extent
- Lot 40 DY85
- Petroleum leases
- Groundwater contours - Q3 2025

Groundwater level (mAHD)

- -200
- -100
- 0
- 100
- 200
- 300
- 400

Simulated groundwater levels in Springbok sandstone and Macalister coal seam (end of December 2025)

Project No.	Client	Figure No.
411001-00917	Arrow	4-6

Notes:
Project CRS: GDA94 / MGA zone 56
Last Saved: 22:44 03/08/2026
Filename: Figure_4-6_GW_cal_end_v2

Exported by User: Mohsen.Azadi
Project Exported: 22:48 03/08/2026

References:
N/A

File Path: C:\modelling\Arrow\deliverables\Figures_REP-HG-002\Figure_4-6_GW_cal_end_v2.qgz

© Worley Pty Ltd While every care is taken to ensure the accuracy of this data, Worley makes no representations or warranties aboutits accuracy, reliability, completeness or suitability for any particular purpose and disclaims all responsibility and all liability (including without limitation liability in negligence) for all expenses, losses, damages (including indirect or consequential damage) and costs which might be incurred as a result of the data being inaccurate or incomplete in any way and for any reason.

4.4.3 Calibrated hydraulic parameters

The ranges of calibrated hydraulic properties derived from the calibration ensemble (reference case realisation) are summarised by respective box and whiskers (BAW) plots shown in Figure 4-7. The BAW plot characterises:

- a median value with the line inside the box
- the range between the 25th and 75th percentiles - box extent
- the minimum and maximum values as whiskers
- an area-averaged value for the cells in each zone (the red line shows) which is discussed below for comparison of hydraulic properties across different zones.

The calibrated hydraulic property ranges indicate that:

- Condamine alluvium has the highest horizontal conductivity with a median value of 14.9 m/day.
- The remaining model layers are calibrated to a median range of horizontal conductivity between 0.001 m/day and 0.1 m/day with the following exceptions:
  - Kogan interburden, Macalister interburden, and Eurombah formation are calibrated to median values between 0.001 m/day to 0.00001 m/day, and
  - Kogan coal seam and Condamine coal seam is calibrated to median values slightly over 0.1 m/day.
- Vertical hydraulic conductivity is calibrated to lower values compared to horizontal hydraulic properties with similar trend among various layers with Condamine alluvium and Eurombah formation having the highest and lowest values, respectively.
- The specific storage and specific yield values[1] are calibrated within the plausible bounds, with a general trend of higher storage values for coal seams and lower values for interburden units and deeper HSUs as the storativity values reduce with depth.

Prior and posterior distribution of median value for each HSU across the full ensemble is presented in Appendix B.

[1] The specific yield values in this document are reported as percentages.



Figure 4-7 Calibrated hydraulic property ranges

4.5 Contaminant transport model

Contaminant transport history matching was undertaken to replicate observed groundwater quality trends for benzene and naphthalene and to provide confidence in subsequent predictive uncertainty analysis. The process focused on assessing whether the combined representation of groundwater flow fluxes, source term characterisation, transport parameters, and natural attenuation processes could reasonably replicate the magnitude, spatial extent, and temporal evolution of measured concentrations.

4.5.1 History-matching metrics

The performance of the 216 model realisations was analysed to ensure the transport models used during predictive uncertainty analysis are calibrated. A maximum SRMS of 10% was adopted as the criterion to assess history matching fit for benzene and naphthalene, with all 216 realisations meeting the history matching criterion, as shown in Figure 4-8 and Figure 4-9.



Figure 4-8 Calculated RMS and SRSM for benzene concentration across the posterior ensemble



Figure 4-9 Calculated RMS and SRSM for naphthalene concentration across the posterior ensemble

The results presented in the remainder of this section are extracted from the realisation that yields the best statistical fit with the observed groundwater concentrations, referred to as reference case.

The matches between individual water concentration measurements are presented as a scatter plot in Figure 4-10 and Figure 4-11. The history matching results indicate that a good calibration fit is achieved for the magnitude of benzene and naphthalene concentrations in the contaminant transport model.

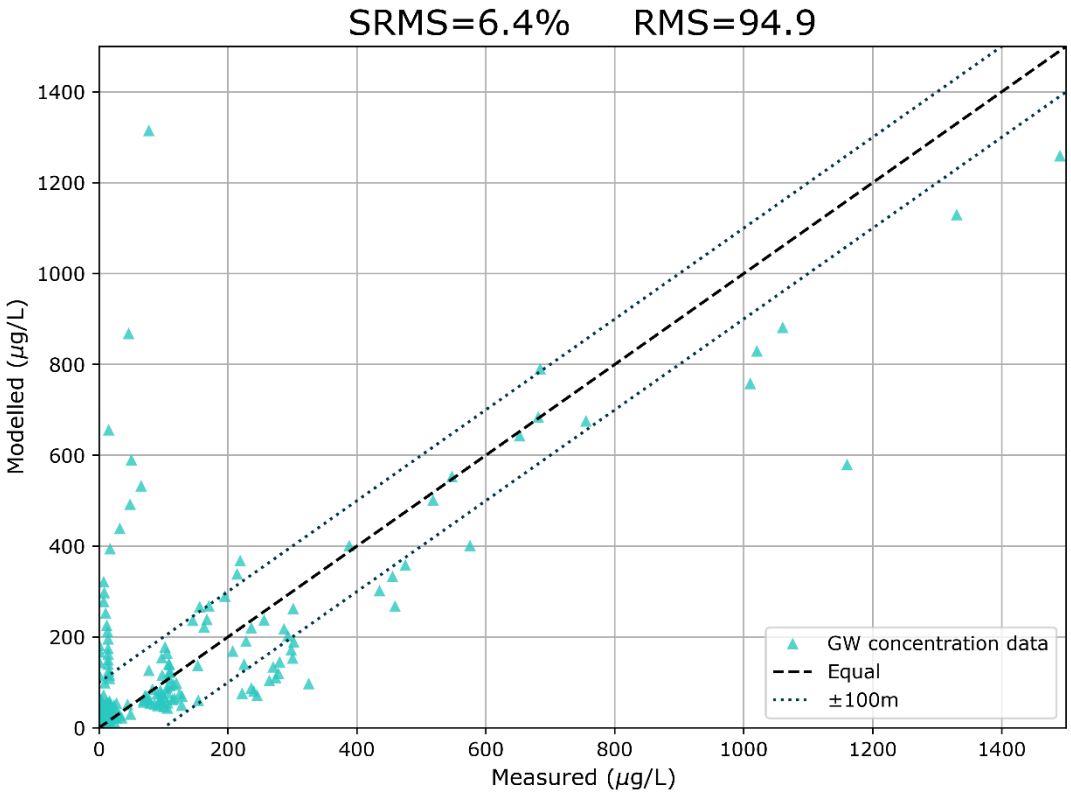


Figure 4-10 Benzene history matching fit for the reference case

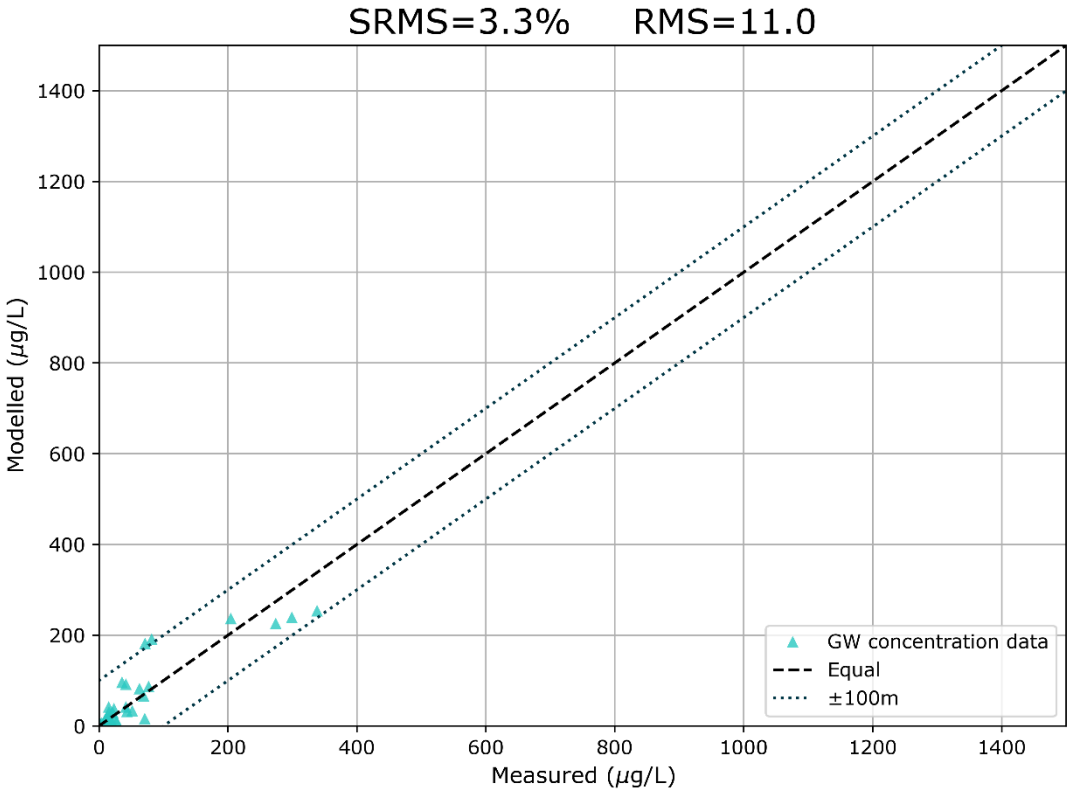


Figure 4-11 Naphthalene history matching fit for the reference case

One of the metrics used to evaluate the transport model performance is by quantifying the match between the observed and modelled groundwater concentrations and by assessing the consistency of their trends.

A reasonable match for groundwater concentration trends was achieved for both benzene and naphthalene (example shown in Figure 4-12) as noted in the observed groundwater concentrations showing below LOR values or declining trends due to groundwater dilution and natural attenuation.

The simulated benzene and naphthalene concentration trends for remaining monitoring bores are presented in Appendix C and D, respectively.

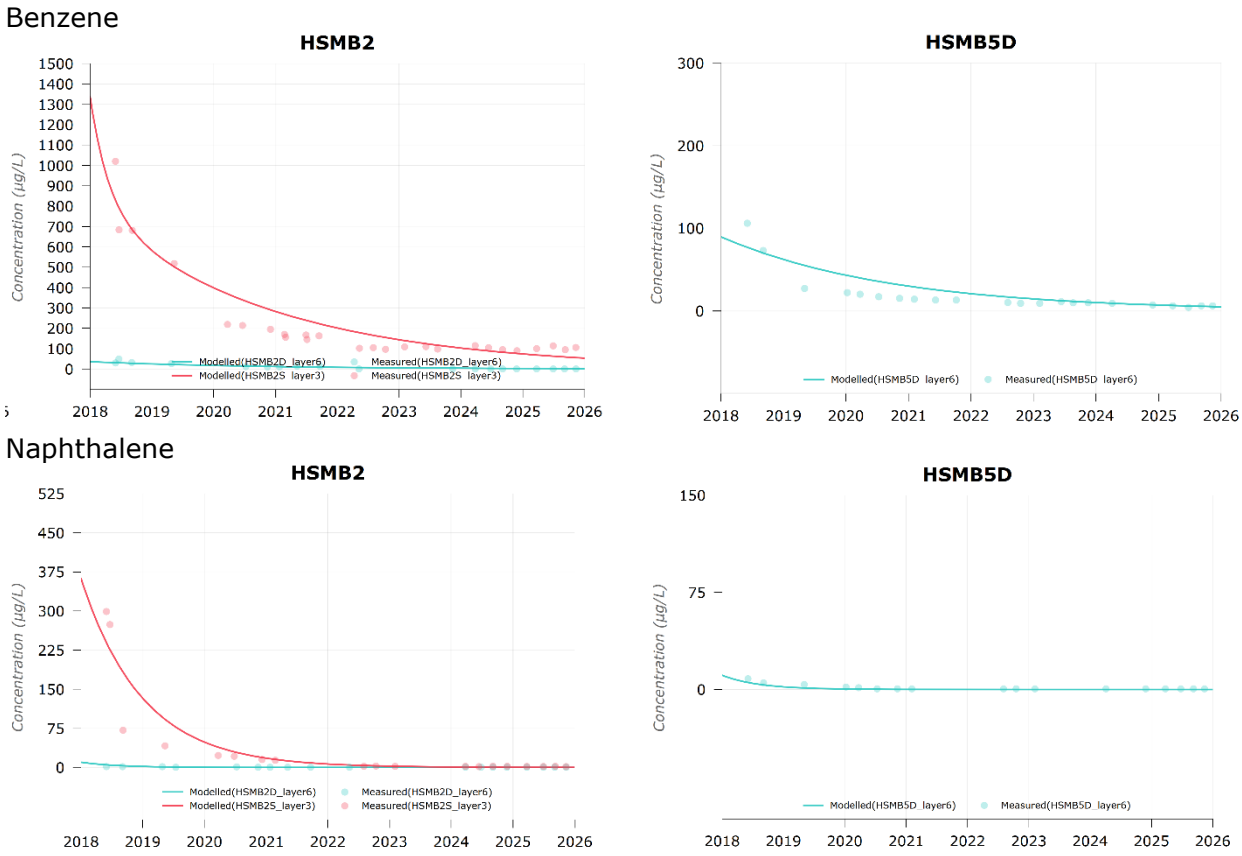


Figure 4-12 Simulated benzene and naphthalene concentration trends for representative monitoring bores screened in the Springbok sandstone and Macalister coal seam

4.5.2 Simulated benzene and naphthalene concentrations

Figure 4-13 shows the simulated benzene concentration (reference case) at the end of the history matching period in the Springbok sandstone and Macalister coal seam. The simulation results indicate that, for both formations, the benzene plume with concentrations exceeding 10 µg/L is largely contained within Lot 40 DY85. This is consistent with groundwater quality monitoring data from bores located outside the Lot 40 DY85 boundary (HL22, HL23, HL25, HL26, HSMB7D, and HL34), where benzene concentrations have remained below the LOR.

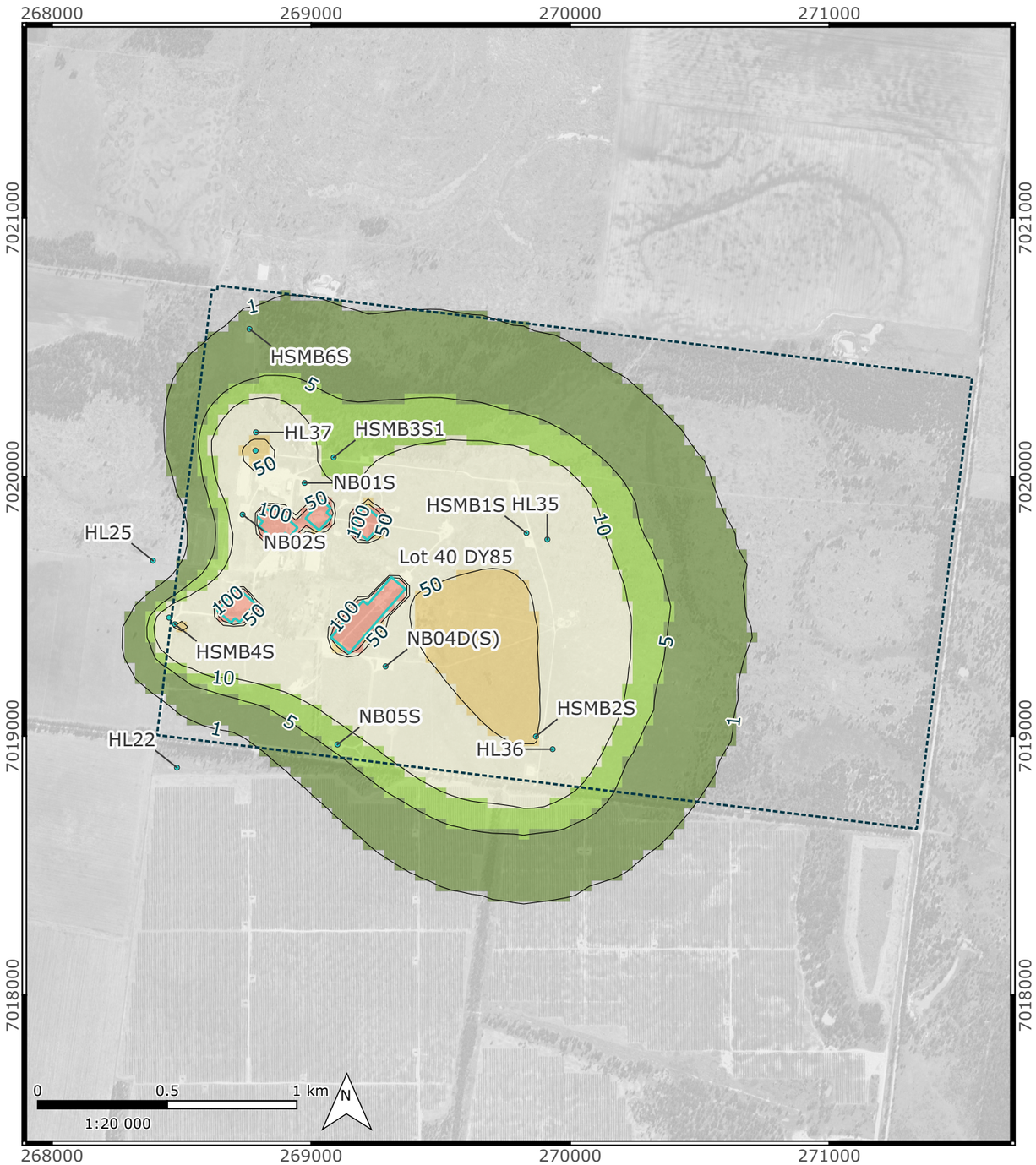
While monitoring bore HSMB4S is located within the Lot 40 DY85 boundary and indicates the potential for limited migration of benzene at concentrations above 10 µg/L beyond the boundary, monitoring results from downstream bores HSMB7S and HL22 have consistently reported below LOR concentrations for several years. This indicates that elevated benzene concentrations observed at HSMB4S are localised, with limited plume migration beyond the Lot 40 DY85 boundary.

The simulated benzene plume shows a zone of elevated concentrations (approximately 50–100 µg/L) within the central part of Lot 40 DY85, extending east of gasifier 5. This zone reflects history matching of the coupled groundwater flow and contaminant transport model to monitoring data that include both below LOR and elevated concentrations, spanning several orders of magnitude. Monitoring data from bores NB04D(S), HL36, HSMB1S, and HL35 (with concentrations below LOR), together with data from bore HSMB2S, define the extent, magnitude, and orientation of the simulated plume in this area.

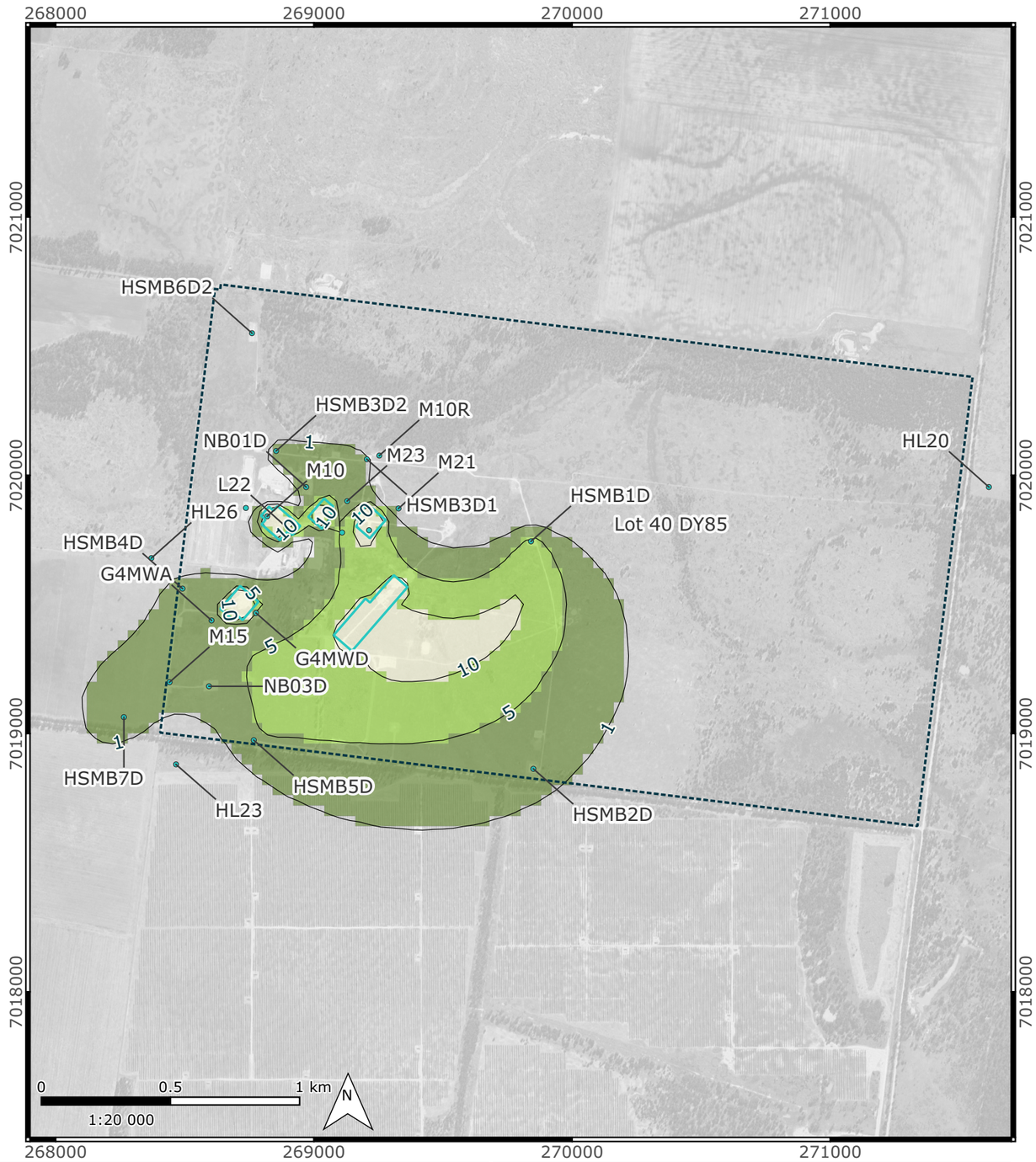
These monitoring data are reflected with spatial variations in calibrated hydraulic conductivity, which indicate the potential presence of a locally enhanced permeability zone near gasifier 5. This feature is interpreted to reflect hydrogeological alteration associated with historical UCG activities, including fracturing of the formation in this direction.

Simulation results at the end of history matching period for naphthalene indicate concentrations below the LOR within the Macalister coal seam across the model domain. In the Springbok sandstone, simulated naphthalene concentrations remain spatially confined within the former gasifier locations. These results reflect the conservative source depletion formulation adopted in the transport model, where the maximum source concentration was defined as 2.2 µg/L at the end of 2025. The results indicate limited migration potential for naphthalene beyond localised source zones, consistent with groundwater monitoring data.

Springbok sandstone



Macalister coal seam



Legend

- Lot 40 DY85
- Gasifier
- Monitoring bores

Concentration (ug/L)

- 1 - 5
- 5 - 10
- 10 - 50
- 50 - 100
- 100 - 500
- 500 - 1000
- 1000 - 5000

Simulated benzene concentrations in Springbok sandstone and Macalister coal seam (end of December 2025)

Project No.	Client	Figure No.
411001-00917	Arrow	4-13

Notes:
Project CRS: GDA94 / MGA zone 56
Last Saved: 23:03 03/08/2026
Filename: Figure_4-13_benzene_cal_end_v2

Exported by User: Mohsen.Azadi
Project Exported: 23:10 03/08/2026

References:
N/A

File Path: C:\modelling\Arrow\deliverables\Figures_REP-HG-002\Figure_4-13_benzene_cal_end_v2.qgz

© Worley Pty Ltd While every care is taken to ensure the accuracy of this data, Worley makes no representations or warranties aboutits accuracy, reliability, completeness or suitability for any particular purpose and disclaims all responsibility and all liability (including without limitation liability in negligence) for all expenses, losses, damages (including indirect or consequential damage) and costs which might be incurred as a result of the data being inaccurate or incomplete in any way and for any reason.

5. Predictive groundwater flow modelling

5.1 Predictive model setup

Predictive groundwater modelling was undertaken to assess the potential impacts of current and proposed CSG FDP scenarios on groundwater flow and contaminant transport and fate within the Springbok sandstone and the Macalister coal seam. The predictive assessment was based on an ensemble of 216 calibrated realisations, generated through history matching and uncertainty analysis, to quantify the range of potential future outcomes and provide a basis for risk-based impact assessment and decision-making. Model predictions are presented using the P5, P50, and P95 percentiles, representing different likelihoods of predictive outcomes.

Predictive simulations were completed for scenario 2 (existing approved development, including Hopeland pilot wells and authorised Arrow CSG wells) and scenario 3 (maximum proposed development incorporating additional Clynes Road wells). For each scenario, predicted impacts were evaluated separately for the Springbok sandstone and Macalister coal seam. Comparison of percentile-based outcomes between scenarios enabled assessment of incremental impacts attributable to proposed development while explicitly accounting for uncertainty in model parameters and boundary conditions.

All simulations incorporated the full simulation period starting from year 2000, with predictive model starting in 2026, groundwater abstraction ceasing in 2061, and followed by extended recovery simulations through to the end of year 2225. This long-term simulation period allowed assessment of post-abstraction recovery trajectories, potential long-term drawdown or concentration changes. The results of the uncertainty are presented using the risk-based terminology outlined in Peeters & Middlemis (2023) as presented in Table 5-1.

Table 5-1 Probabilistic terminology used (from Peeters & Middlemis, 2023)

Percentile	Probability	Description
<10%	>90%	It is **very likely** that the outcome is **larger** than this value
10–33%	67–90%	It is **likely** that the outcome is **larger** than this value
33–67%	33–67%	It is **as likely as not** that the outcome is **larger** than this value
67–90%	10–33%	It is **unlikely** that the outcome is **larger** than this value
>90%	<10%	It is **very unlikely** that the outcome is **larger** than this value

5.2 Groundwater level and flow directions

Cumulative groundwater abstraction progressively lowers groundwater levels. The extent of the zone affected by abstraction is dependent on the properties of the hydrogeologic units, pumping rates and locations, cumulative production rates, schedule and target aquifer(s) relative to the water table.

Predicted median groundwater levels in the Springbok sandstone and Macalister coal seam at the end of the abstraction period (December 2061), and at the end of the recovery period (December 2225), for non-Arrow wells and Arrow wells in scenario 3, are shown in Figure 5-1 to Figure 5-2.

Model results indicate the development of a cone of depression around abstraction wells because of cumulative groundwater extraction, with regional groundwater flow directed predominantly toward the south and southwest of the model domain.

Within Lot 40 DY85, simulated groundwater flow directions vary by formation. In the Springbok sandstone, predicted groundwater flow is directed toward the gasifiers, with inflow from the north, east, and south boundaries of Lot 40 DY85 and a relatively flat hydraulic gradient along the western boundary. Groundwater flow in the Macalister coal seam is directed toward the southwest. Comparison with groundwater level contours at the end of 2025 (Figure 4-6), indicates partial groundwater recovery in the Springbok sandstone, while groundwater levels in the Macalister coal seam is lowered due to ongoing CSG abstraction from the WCM.

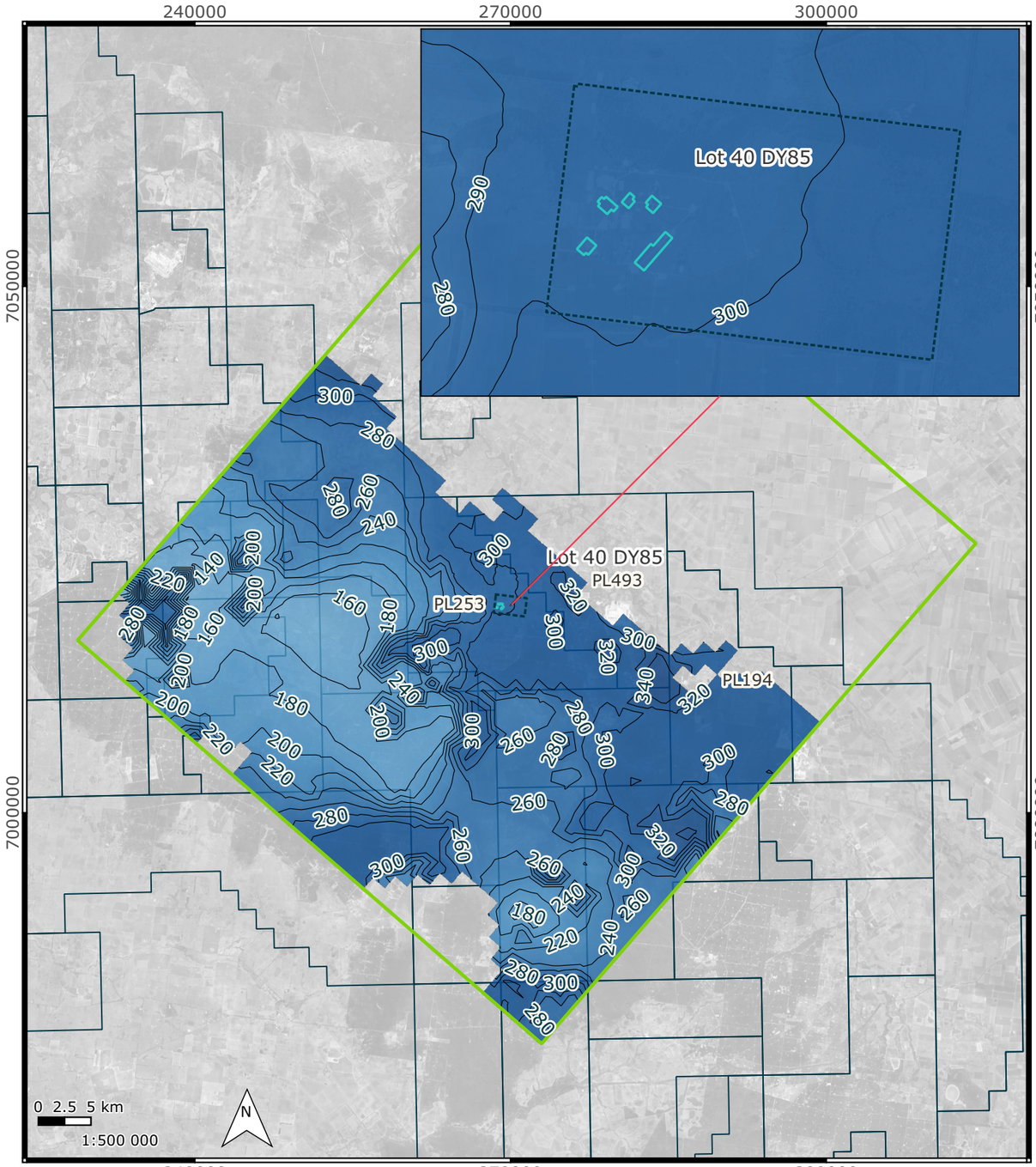
By the end of the recovery period, simulated regional groundwater levels increase relative to those at the end of abstraction period. However, groundwater levels are not predicted to fully return to pre-abstraction conditions. Long-term water balance recovery simulations indicate that total groundwater outflows, including evaporative losses and boundary fluxes, continue to exceed rainfall recharge, limiting full recovery to pre-development groundwater levels.

Differences between the predicted median groundwater levels at the end of abstraction period for scenarios 2 and 3 were evaluated across the ensemble for both the Springbok sandstone and the Macalister coal seam, as shown in Figure 5-3. The predictions indicate a limited area of difference, with up to 1 m change in median groundwater levels occurring at the southwest corner of PL253 within the Springbok sandstone. In the Macalister coal seam, a localised zone with predicted differences of approximately 1–2 m occurs in the vicinity of the proposed Clynes Road wells. These results indicate that the additional abstraction associated with the proposed Clynes Road development results in only minor incremental changes to groundwater levels when compared with the approved development scenario.

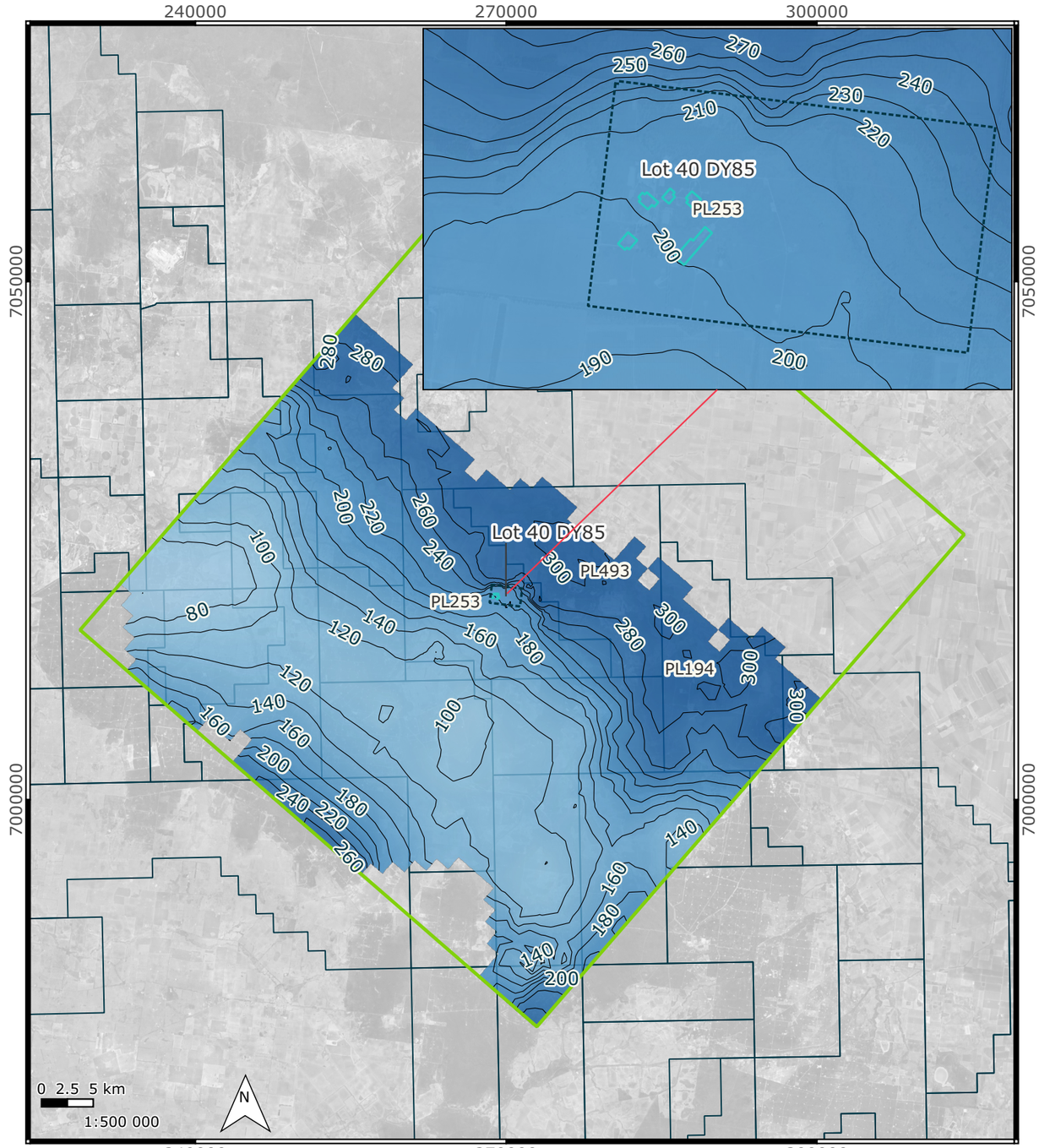
Predicted differences in median groundwater levels at the end of the recovery period between scenarios 2 and 3 are less than 1 m, indicating that inclusion of the proposed Clynes Road wells is not expected to result in a material change to groundwater level recovery relative to the currently approved development.

Predicted groundwater level trends at monitoring bores across the ensemble, showing declining trend during the abstraction period and subsequent recovery following the end of abstraction, are presented in Appendix E.

Springbok sandstone



Macalister coal seam



Legend

- Groundwater model extent
- Lot 40 DY85
- Petroleum leases
- Gasifiers

Groundwater level (mAHD)

- -200
- -100
- 0
- 100
- 200
- 300
- 400

Predicted median groundwater levels in Springbok sandstone and Macalister coal seam for scenario 3 (end of December 2061)

Project No.	Client	Figure No.
411001-00917	Arrow	5-1

Notes:
Project CRS: GDA94 / MGA zone 56
Last Saved: 20:09 04/08/2026
Filename: Figure_5-1_GW_abs_end_v2

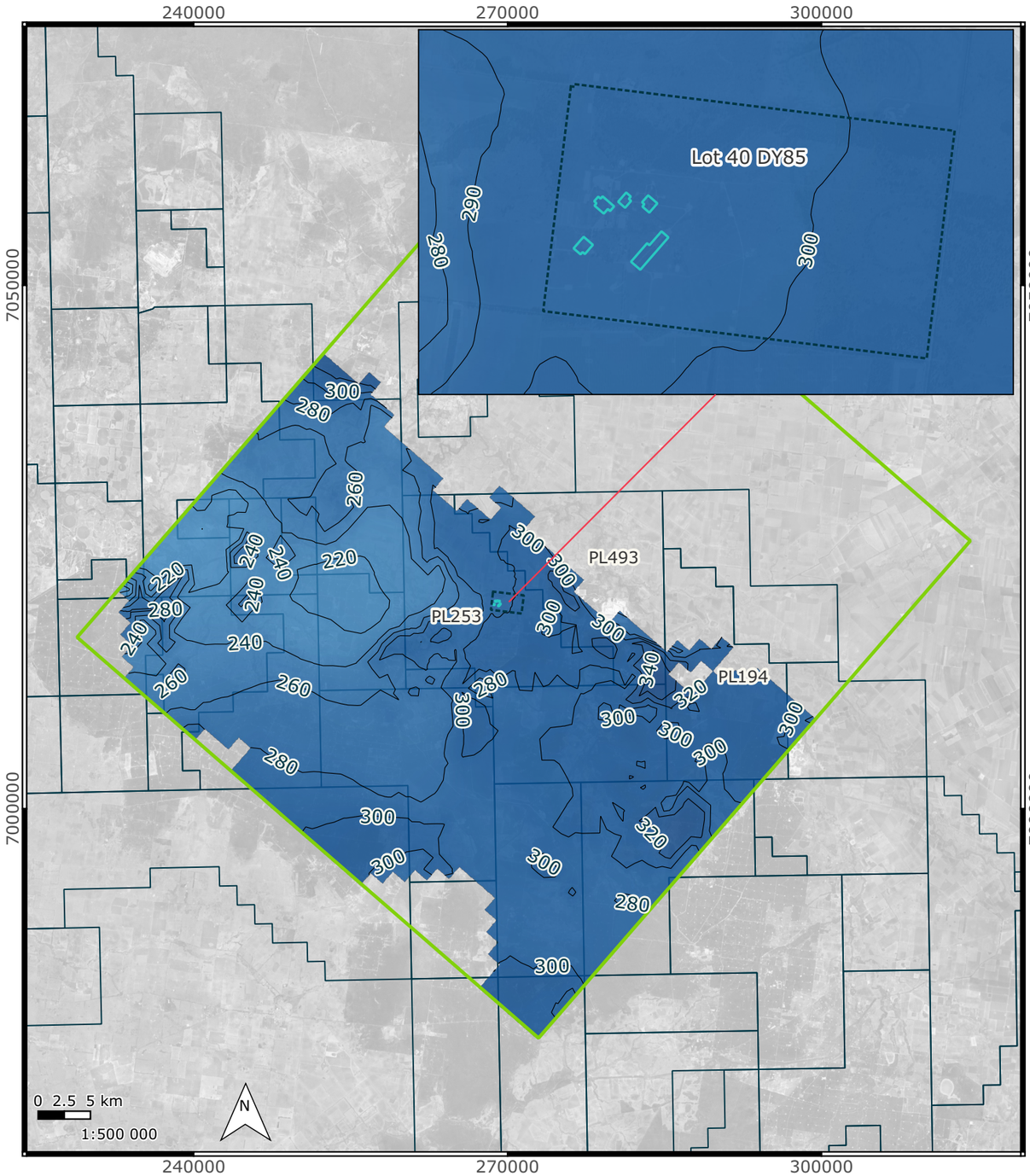
Exported by User: Mohsen.Azadi
Project Exported: 20:15 04/08/2026

References:
N/A

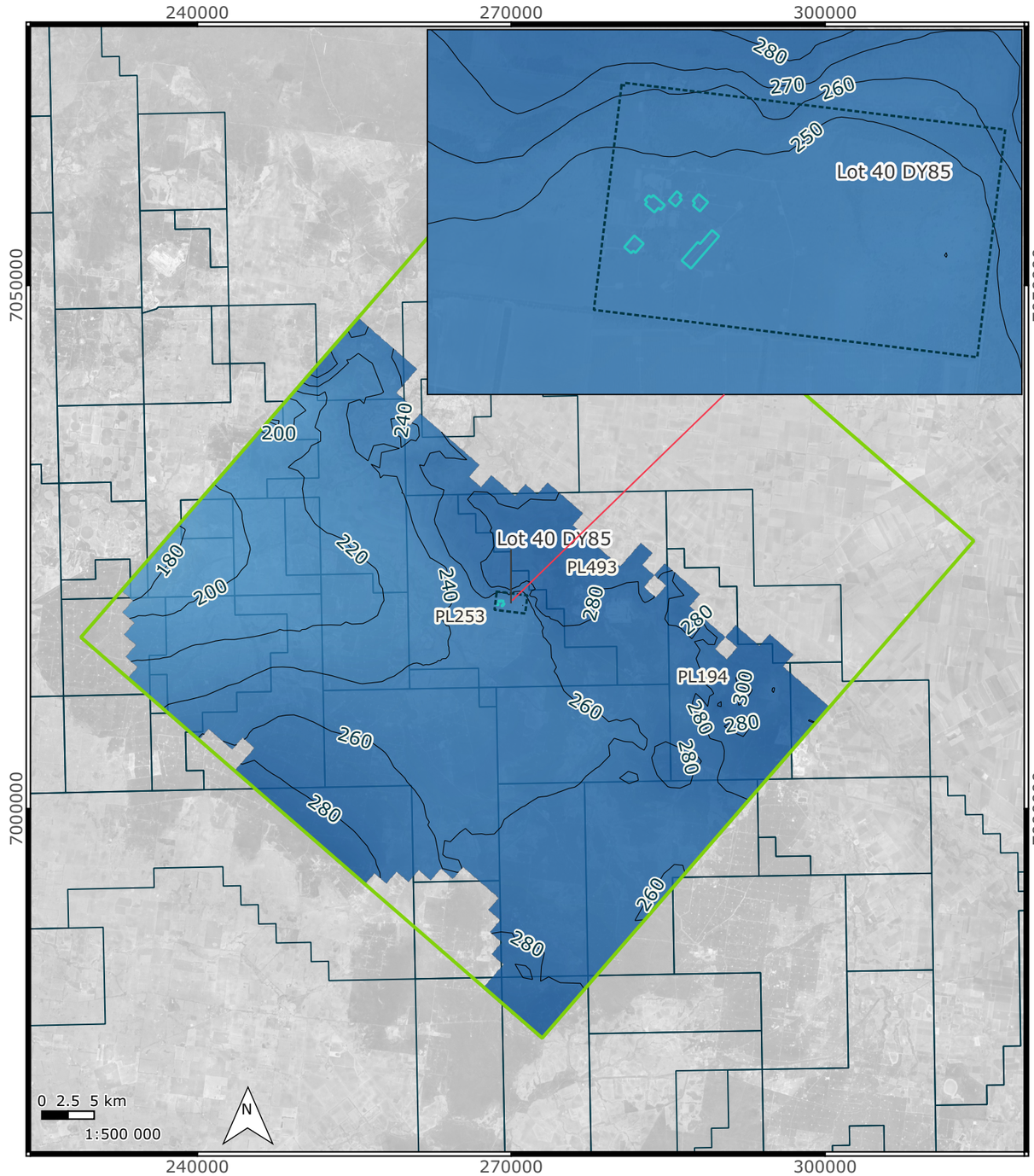
File Path: C:\modelling\Arrow\deliverables\Figures_REP-HG-002\Figure_5-1_GW_abs_end_v2.qgz

© Worley Pty Ltd While every care is taken to ensure the accuracy of this data, Worley makes no representations or warranties aboutits accuracy, reliability, completeness or suitability for any particular purpose and disclaims all responsibility and all liability (including without limitation liability in negligence) for all expenses, losses, damages (including indirect or consequential damage) and costs which might be incurred as a result of the data being inaccurate or incomplete in any way and for any reason.

Springbok sandstone



Macalister coal seam



Legend

- Groundwater model extent
- Lot 40 DY85
- Petroleum leases
- Gasifiers

Groundwater level (mAHD)

- -200
- -100
- 0
- 100
- 200
- 300
- 400

Predicted median groundwater levels in Springbok sandstone and Macalister coal seam for scenario 3 (end of December 2225)

Project No.	Client	Figure No.
411001-00917	Arrow	5-2

Notes:
Project CRS: GDA94 / MGA zone 56
Last Saved: 20:22 04/08/2026
Filename: Figure_5-2_GW_rec_end_v2

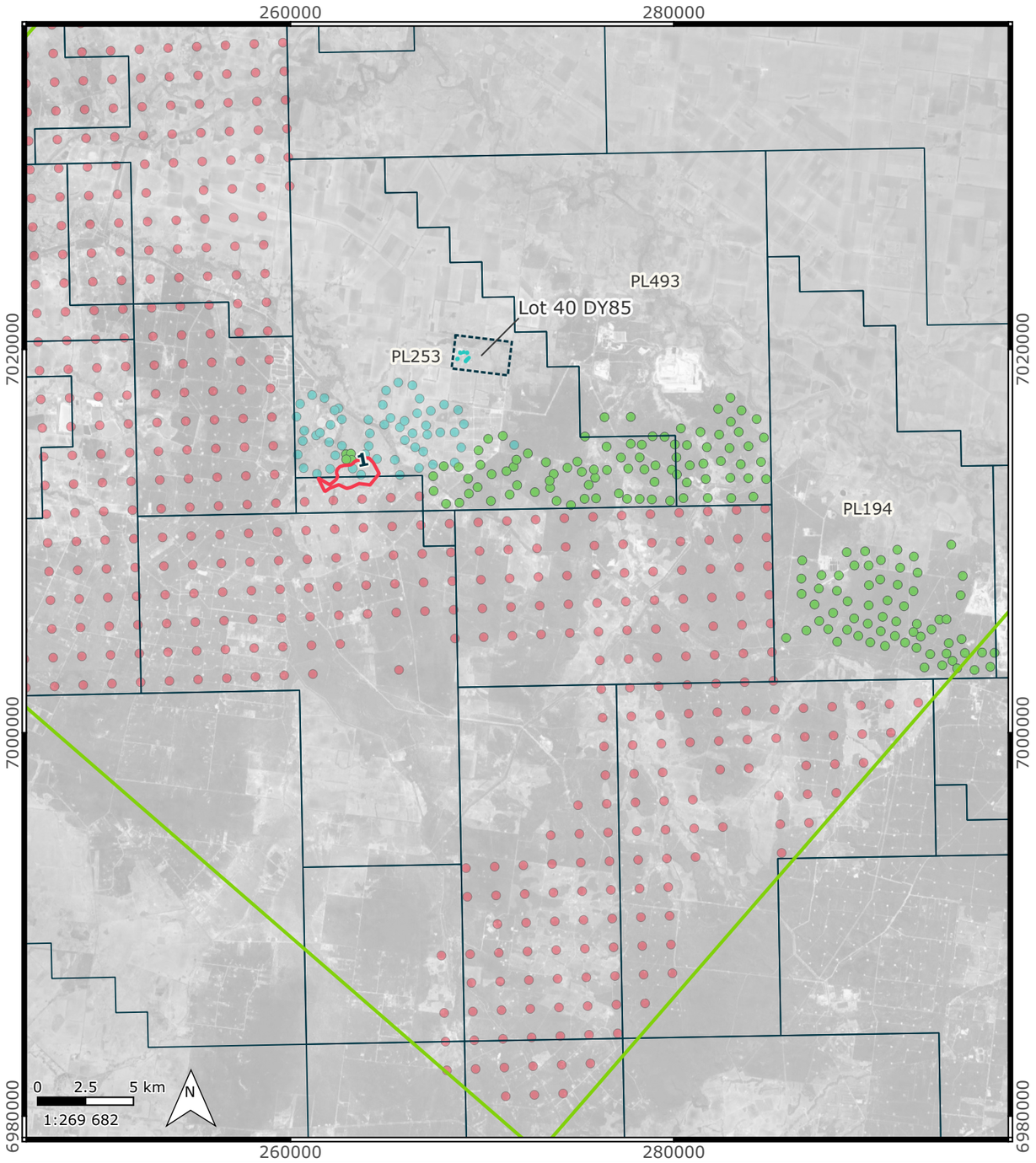
Exported by User: Mohsen.Azadi
Project Exported: 20:27 04/08/2026

References:
N/A

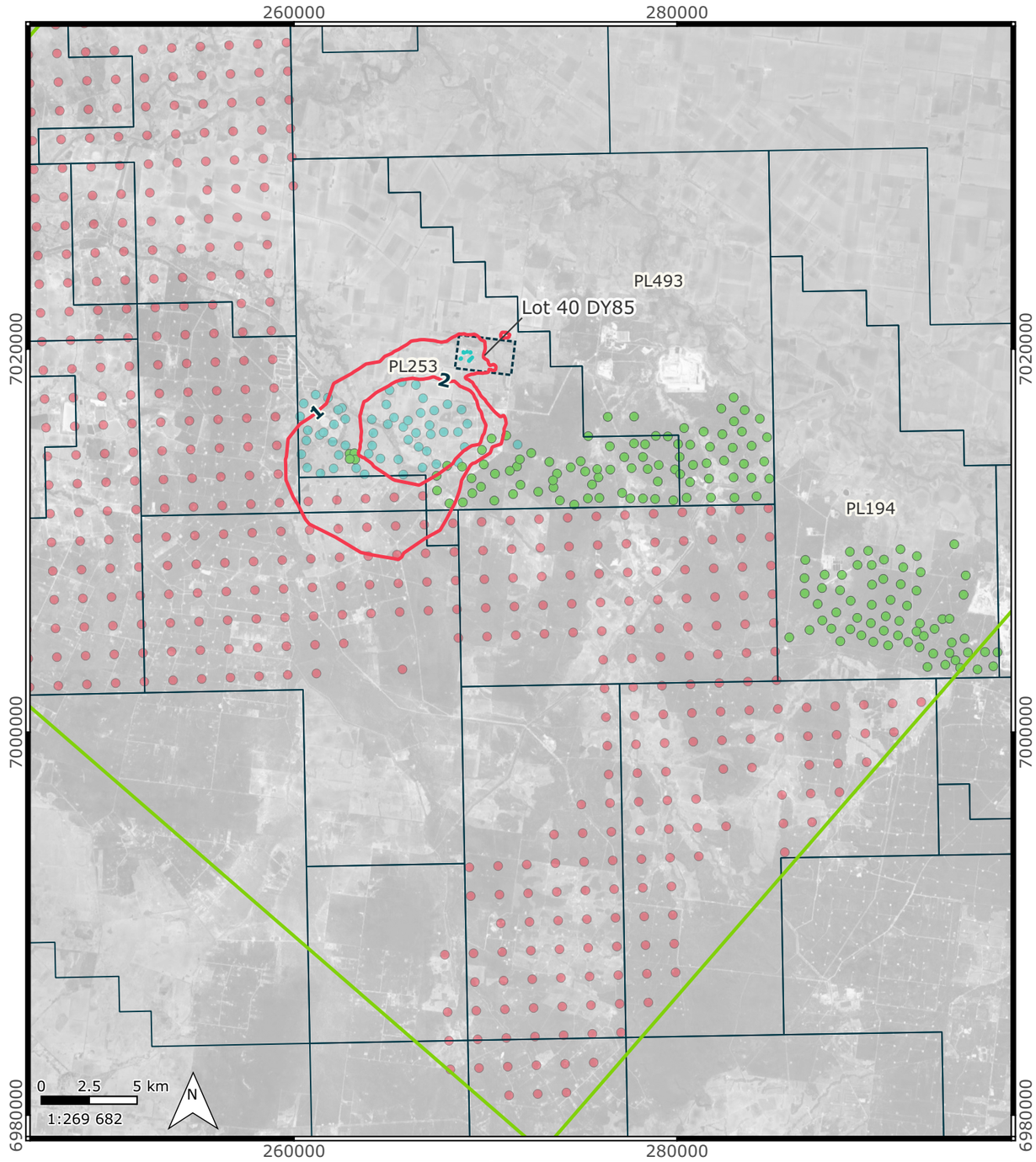
File Path: C:\modelling\Arrow\deliverables\Figures_REP-HG-002\Figure_5-2_GW_rec_end_v2.qgz

© Worley Pty Ltd While every care is taken to ensure the accuracy of this data, Worley makes no representations or warranties aboutits accuracy, reliability, completeness or suitability for any particular purpose and disclaims all responsibility and all liability (including without limitation liability in negligence) for all expenses, losses, damages (including indirect or consequential damage) and costs which might be incurred as a result of the data being inaccurate or incomplete in any way and for any reason.

Springbok sandstone



Macalister coal seam



Legend

- Groundwater model extent
- Lot 40 DY85
- Gasifiers
- Petroleum Leases

Well groups

- Approved Arrow wells
- Arrow Clynes Rd wells
- Non-Arrow abstraction points (from UWIR 2021)

Contours of groundwater level difference (m)

Predicted median difference in groundwater levels between scenario 2 and 3 in Springbok sandstone and Macalister coal seam (end of December 2061)

Project No.	Client	Figure No.
411001-00917	Arrow	5-3

Notes:
Project CRS: GDA94 / MGA zone 56
Last Saved: 20:31 04/08/2026
Filename: Figure_5-3_GW_Sc2m3_v2

Exported by User: Mohsen.Azadi
Project Exported: 20:32 04/08/2026

References:
N/A

File Path: C:\modelling\Arrow\deliverables\Figures_REP-HG-002\Figure_5-3_GW_Sc2m3_v2.qgz

© Worley Pty Ltd While every care is taken to ensure the accuracy of this data, Worley makes no representations or warranties aboutits accuracy, reliability, completeness or suitability for any particular purpose and disclaims all responsibility and all liability (including without limitation liability in negligence) for all expenses, losses, damages (including indirect or consequential damage) and costs which might be incurred as a result of the data being inaccurate or incomplete in any way and for any reason.

worley consulting

As discussed in section 2.4.1, historical UCG activities altered local hydraulic gradients within Lot 40 DY85. One of the key QOIs assessed in this study is the incremental change in horizontal hydraulic gradients across the site under the two FDP scenarios. Intera (2025), previously assessed hydraulic gradients using the full extent of Lot 40 DY85.

In the current impact assessment, and in consideration of gasifier locations, regional flow directions, and the need to evaluate the potential for contaminant migration beyond the site boundary, the analysis focused on 1,500 m sections along the southern and western boundaries of Lot 40 DY85 (shown in Figure 5-4). Groundwater level differences were calculated between model cells along these boundary sections and corresponding cells located within a 100 m buffer inside the site boundary. The proportion of boundary cells with higher groundwater levels than interior cells was used as an indicator of groundwater flow direction from locations beyond Lot 40 DY85 toward zones within Lot 40 DY85 (in the vicinity of gasifiers). Comparison of results between scenarios 2 and 3 provides a quantitative basis for assessing the extent to which the proposed Clynes Road wells may influence these hydraulic gradients and associated flow directions.

Summary statistics of predicted horizontal hydraulic gradients toward Lot 40 DY85 along 1,500 m sections of the southern and western boundaries are presented in Table 5-2. The simulation results indicate stronger inward hydraulic gradients in the Springbok sandstone compared to the Macalister coal seam, consistent with the groundwater contour patterns discussed previously. This is considered to reflect potential vertical hydraulic connectivity (near historical UCG activities) between the Springbok sandstone and the underlying Macalister coal seam, together with a downward vertical gradient driven by CSG abstraction within the WCM.

Comparison of summary statistics between the two FDP scenarios indicates that incremental changes in hydraulic gradients across these boundary sections are negligible, with differences generally within 1%. These results suggest that it is unlikely that the proposed Clynes Road wells materially alter regional groundwater flow directions or hydraulic gradients at the boundaries of Lot 40 DY85.

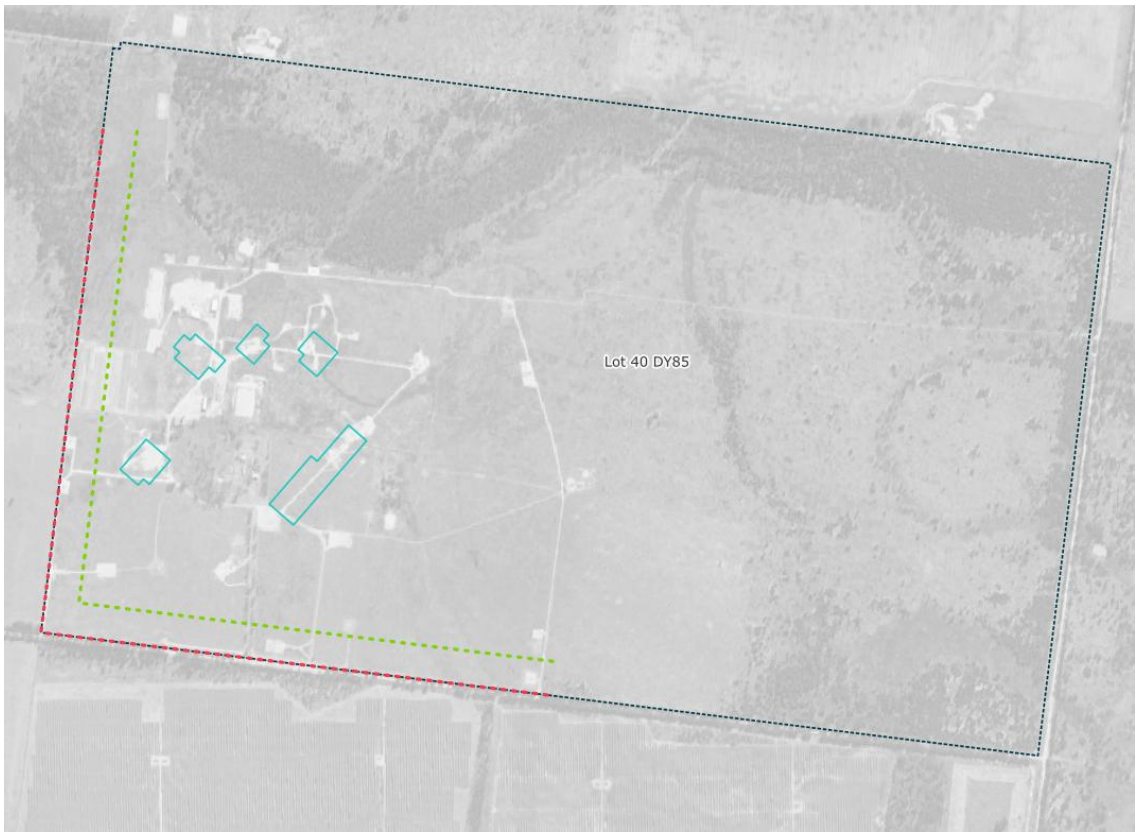


Figure 5-4 Lot 40 DY85 boundary sections (red dashed lines, 1500 m each) and 100 m buffer lines within the boundary (green dashed lines) used for calculation of horizontal hydraulic gradient

Table 5-2 Summary statistics of predicted percentage of cells along 1,500 m sections of the southern and western boundaries with horizontal hydraulic gradients toward Lot 40 DY85

Modelling scenario	Percentile	Springbok sandstone			Macalister coal		
		2025	2040	2061	2025	2040	2061
Scenario 2 (approved)	P5	48%	56%	57%	7%	6%	5%
	P50	76%	76%	76%	17%	13%	14%
	P95	92%	90%	89%	41%	22%	22%
Scenario 3 (Clynes Rd)	P5	48%	56%	57%	7%	5%	5%
	P50	76%	76%	77%	17%	13%	14%
	P95	92%	90%	89%	41%	22%	23%
Predicted impact	P5	0%	0%	0%	0%	1%	0%
	P50	0%	0%	-1%	0%	0%	0%
	P95	0%	0%	0%	0%	0%	-1%

5.3 Vertical hydraulic gradient

Assessment of the vertical hydraulic gradient between the Springbok sandstone and the underlying Macalister coal seam was undertaken to confirm the direction of vertical groundwater flow under scenario 3, representing the maximum proposed development. This assessment was intended to evaluate whether vertical gradients are upward or downward under abstraction and recovery conditions. Understanding the direction of vertical flow is important for interpreting potential vertical migration pathways under a conservative development scenario.

The assessment was carried out using 10 pairs of monitoring locations where groundwater level monitoring data was available in both the Springbok sandstone and the Macalister coal seam. For each pair, the groundwater level difference between the two formations was calculated across the ensemble of model realisations. Positive and negative values indicate the direction of the vertical hydraulic gradient, to evaluate whether groundwater flow is directed downward from the Springbok sandstone to the Macalister coal seam (for positive values), or upward in the opposite direction (for negative values).

As shown in Figure 5-5, the predicted groundwater level differences under scenario 3 are positive from 2026 through to 2226, indicating a continuous downward vertical hydraulic gradient from the Springbok sandstone to the Macalister coal seam. This is consistent across all realisations and through both the abstraction and recovery periods.

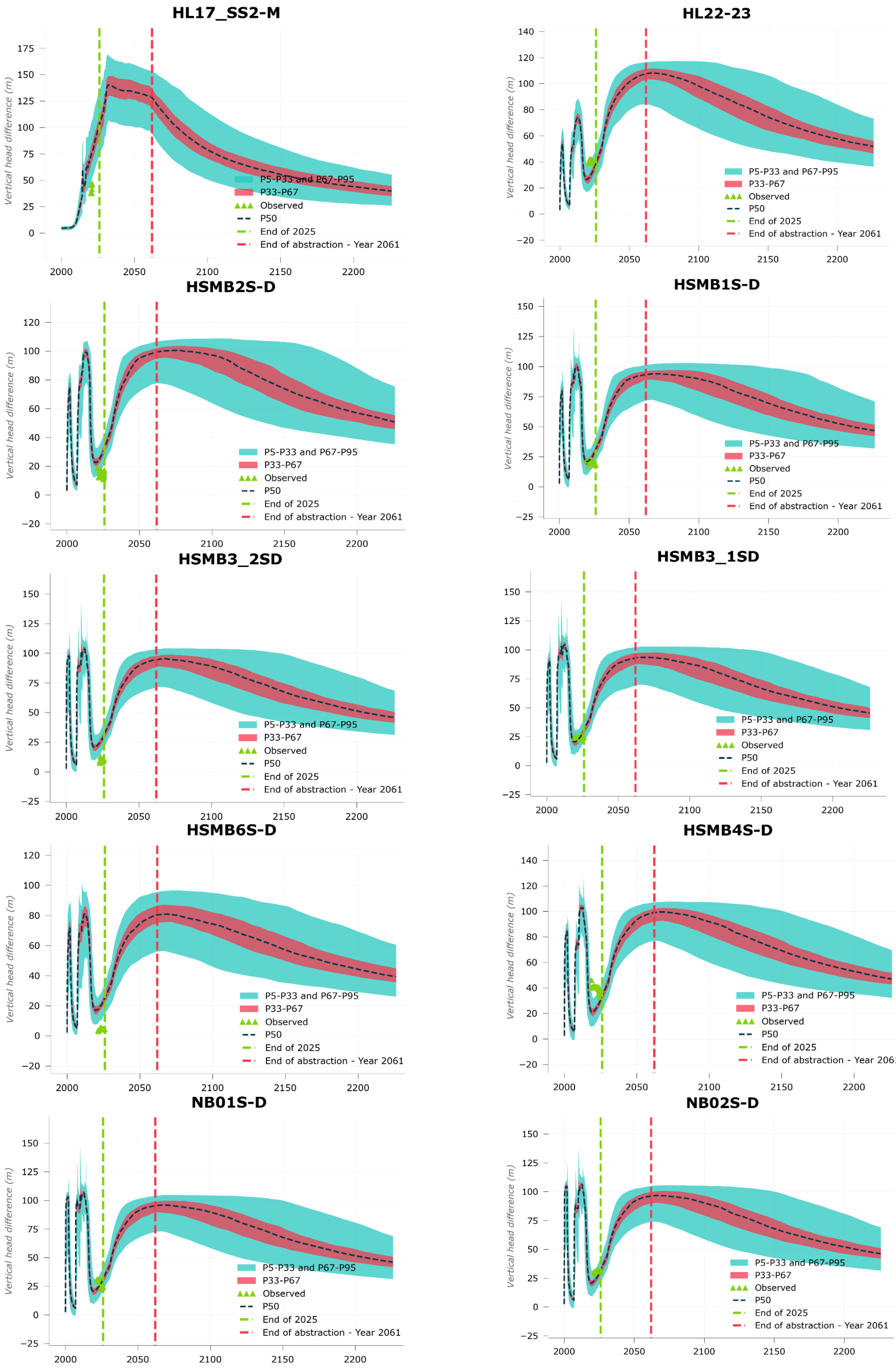


Figure 5-5 Predicted vertical hydraulic gradient between the Springbok sandstone and Macalister coal seam at paired monitoring locations

5.4 Particle tracking

Particle tracking was undertaken as a conservative approach to assess the maximum potential extent of contaminant movement under simulated groundwater flow conditions. Unlike solute transport modelling, particle tracking does not account for attenuation processes such as sorption, degradation, or dilution, and therefore represents an upper-bound estimate of advective contaminant migration. Particles were released in 2019 from the following locations:

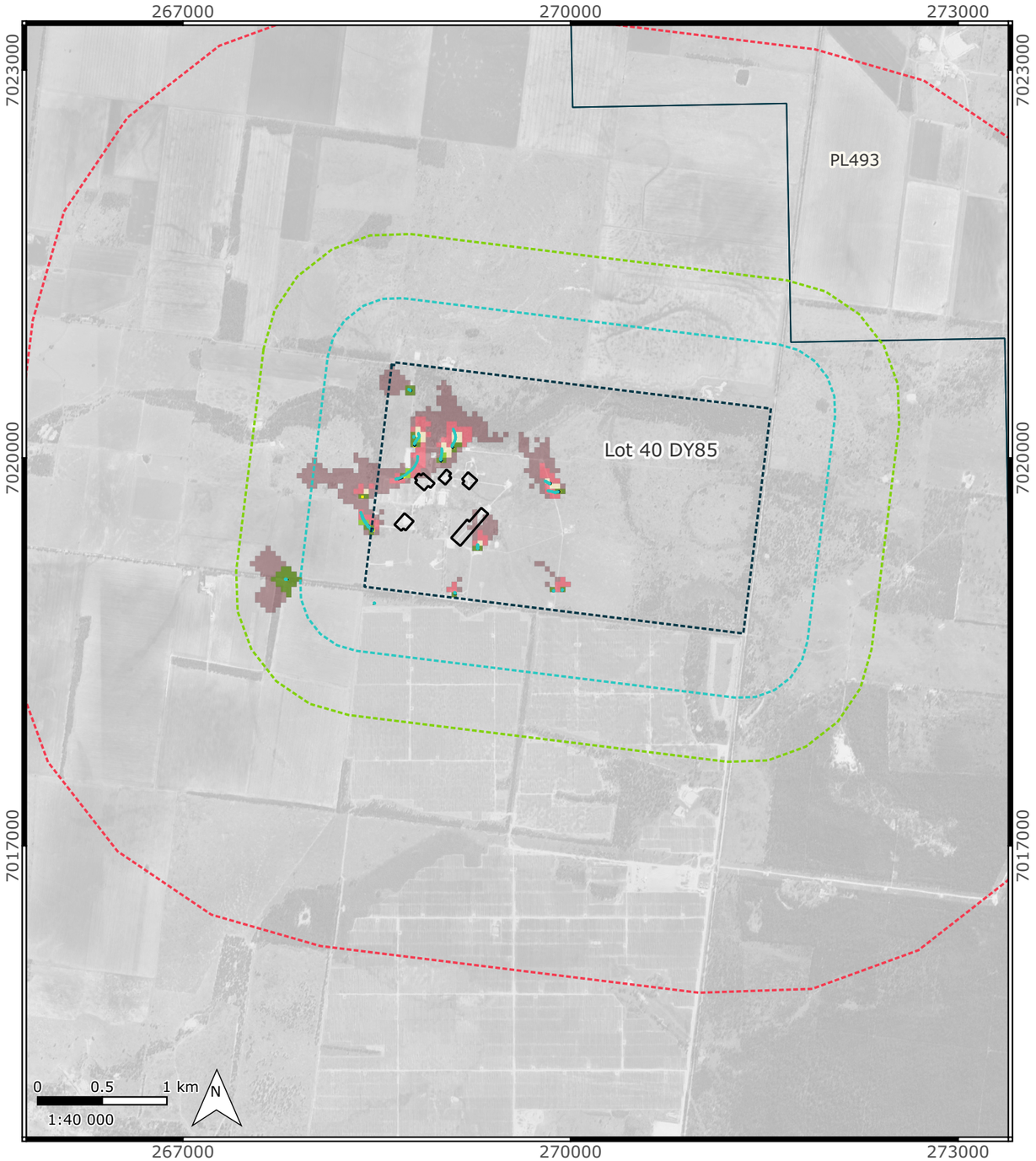
- Monitoring bores,
- Gasifier locations, and
- Lot 40 DY85 boundaries.

Particle movement was simulated under transient conditions from January 2019 through to the end of December 2225 for both scenario 2 and scenario 3.

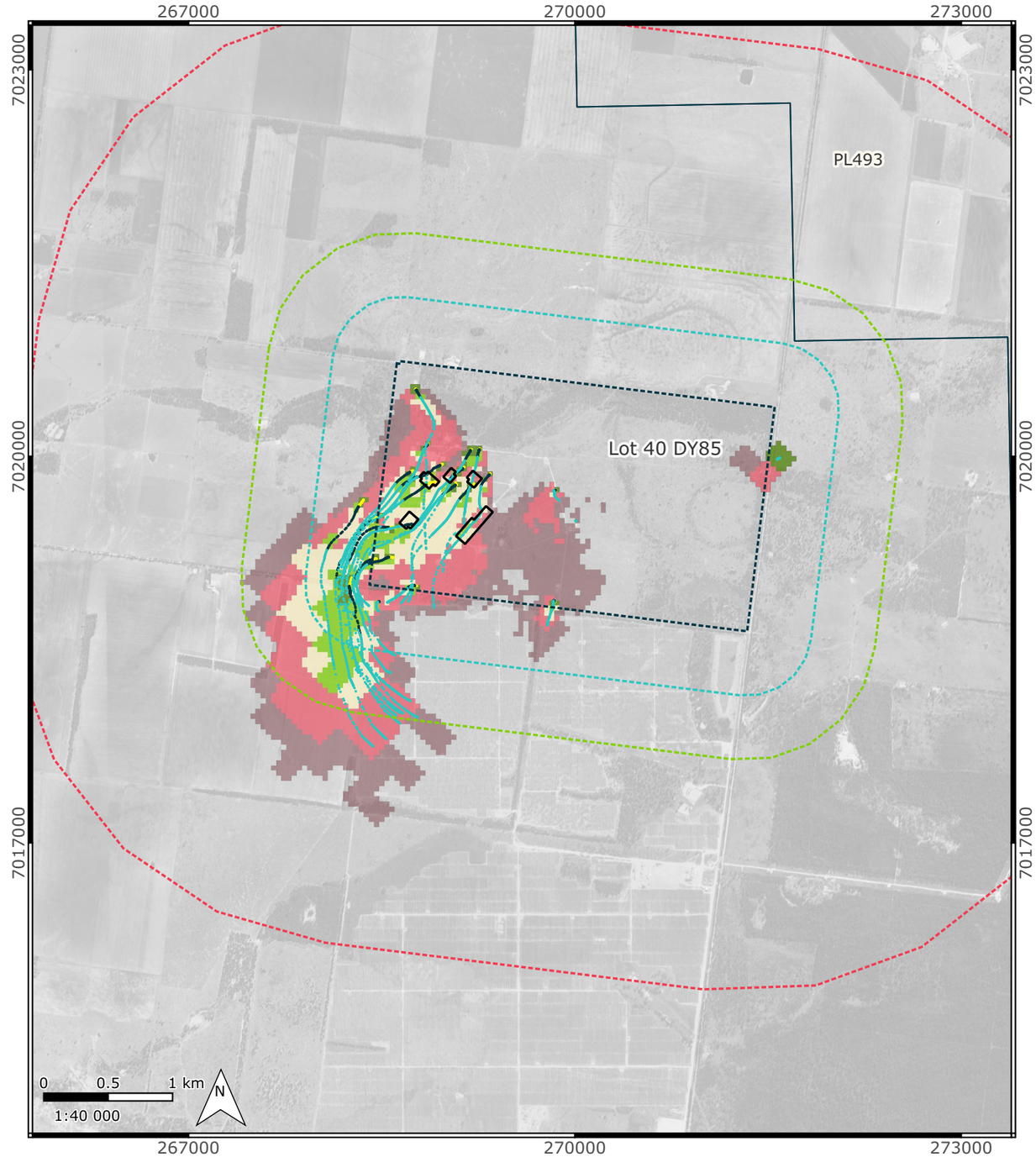
For scenario 3, the probability of particle pathlines intersecting each model cell within the Springbok sandstone and Macalister coal seam is presented in Figure 5-6 to Figure 5-8, for particles released from monitoring bores, gasifier locations, and the Lot 40 DY85 boundaries, based on ensemble predictions from 216 model realisations. These figures also show representative particle pathlines extracted from the reference case. The results indicate that:

- Particles released in the Springbok sandstone generally travel shorter distances than those released in the Macalister coal seam, reflecting lower hydraulic conductivity, reduced transmissivity, and weaker advective flow conditions in the Springbok sandstone compared to the more transmissive and regionally depressurised Macalister coal seam.
- Groundwater flow within the Macalister coal seam is predominantly directed toward the south-southwest, consistent with regional groundwater flow patterns, whereas flow directions within the Springbok sandstone vary at a more localised scale and are mostly directed inward toward Lot 40 DY85, reflecting the influence of historical depressurisation associated with former UCG activities.
- It is very unlikely (probability of less than 5%) that, by the end of the recovery period in 2225, particles released at or near the gasifier locations will travel beyond:
  - Lot 40 DY85 boundary within the Springbok sandstone, and
  - Approximately 1,250 m beyond the Lot 40 DY85 boundary within the Macalister coal seam.
- Particle movement was limited during the historical period (2015 to 2019), compared with greater migration occurring during the abstraction period in response to groundwater extraction from CSG wells. Reference case simulations indicate that particles released within the gasifiers remained within Lot 40 DY85 throughout the abstraction period, with migration extending beyond the Lot 40 DY85 boundary during the post-abstraction recovery period. Ensemble predictions across all particle release locations indicate that the greatest particle movement occurs during the post-abstraction recovery period (2062 to 2225), reflecting the longer travel times associated with this phase of the simulation. Given the considerable natural attenuation of contaminants observed in groundwater monitoring data (discussed in section 2.4.2), by the year 2062 these predictions represent a conservative estimate of the likelihood and extent of contaminant movement from Lot 40 DY85.

Springbok sandstone



Macalister coal seam



Legend

- Groundwater model extent
- Lot 40 DY85
- Gasifiers
- Petroleum Leases

Lot 40 DY85 buffer zones:

- 500 m
- 1000 m
- 2800 m

Particle travel period:

- 2019-2025
- 2026-2061
- 2062-2225

Pathline probability

- Very unlikely (<5%)
- Unlikely (5-33%)
- As likely as not (33-67%)
- Likely (67-95%)
- Very likely (>95%)

Probability of particle tracking pathlines in Springbok sandstone and Macalister coal seam for scenario 3 (particles released at monitoring bores)

Project No.	Client	Figure No.
411001-00917	Arrow	5-6

Notes:
Project CRS: GDA94 / MGA zone 56
Last Saved: 22:42 04/08/2026
Filename: Figure_5-6_PT_probability_bores_v2

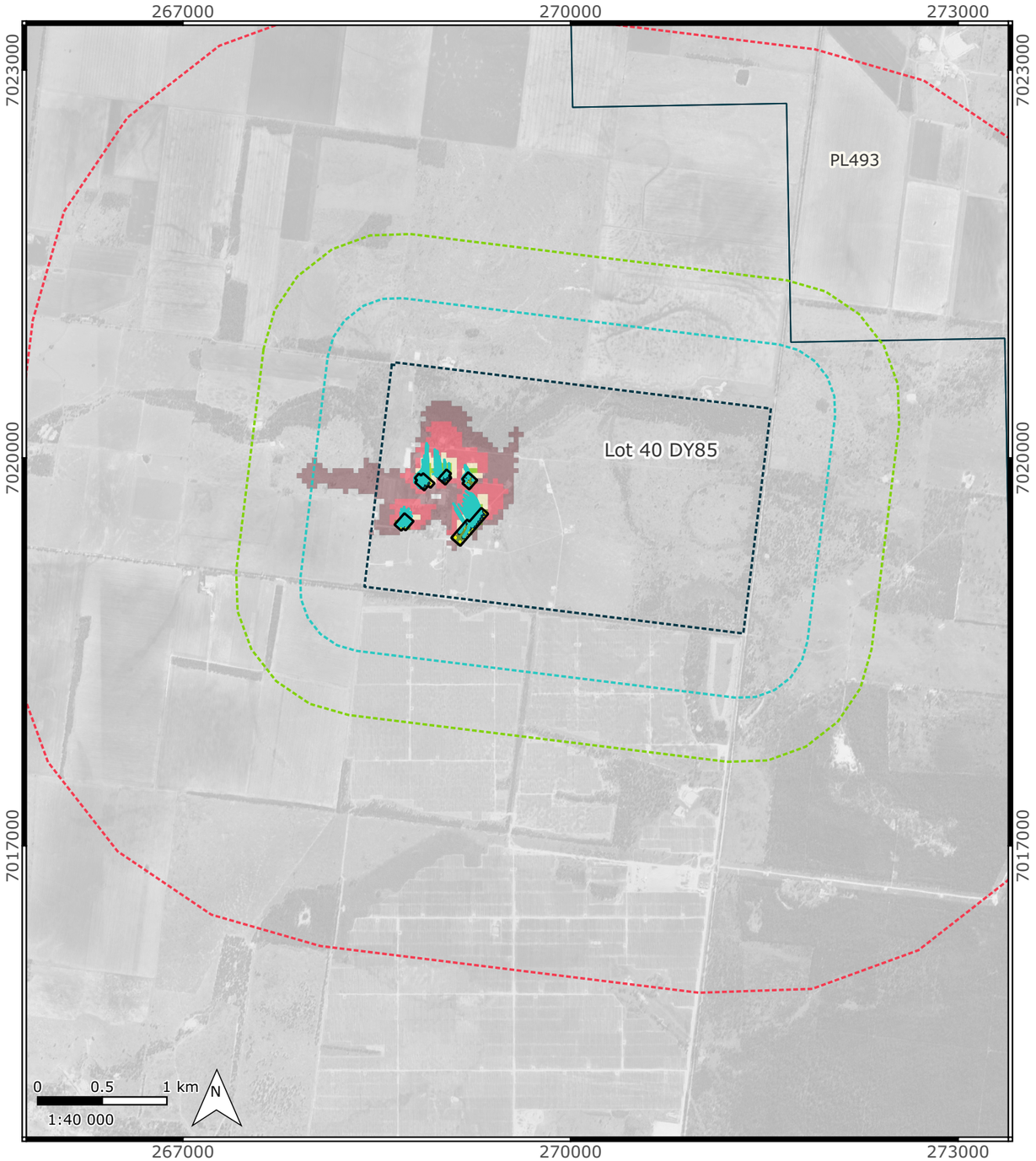
Exported by User: Mohsen.Azadi
Project Exported: 22:48 04/08/2026

References:
N/A

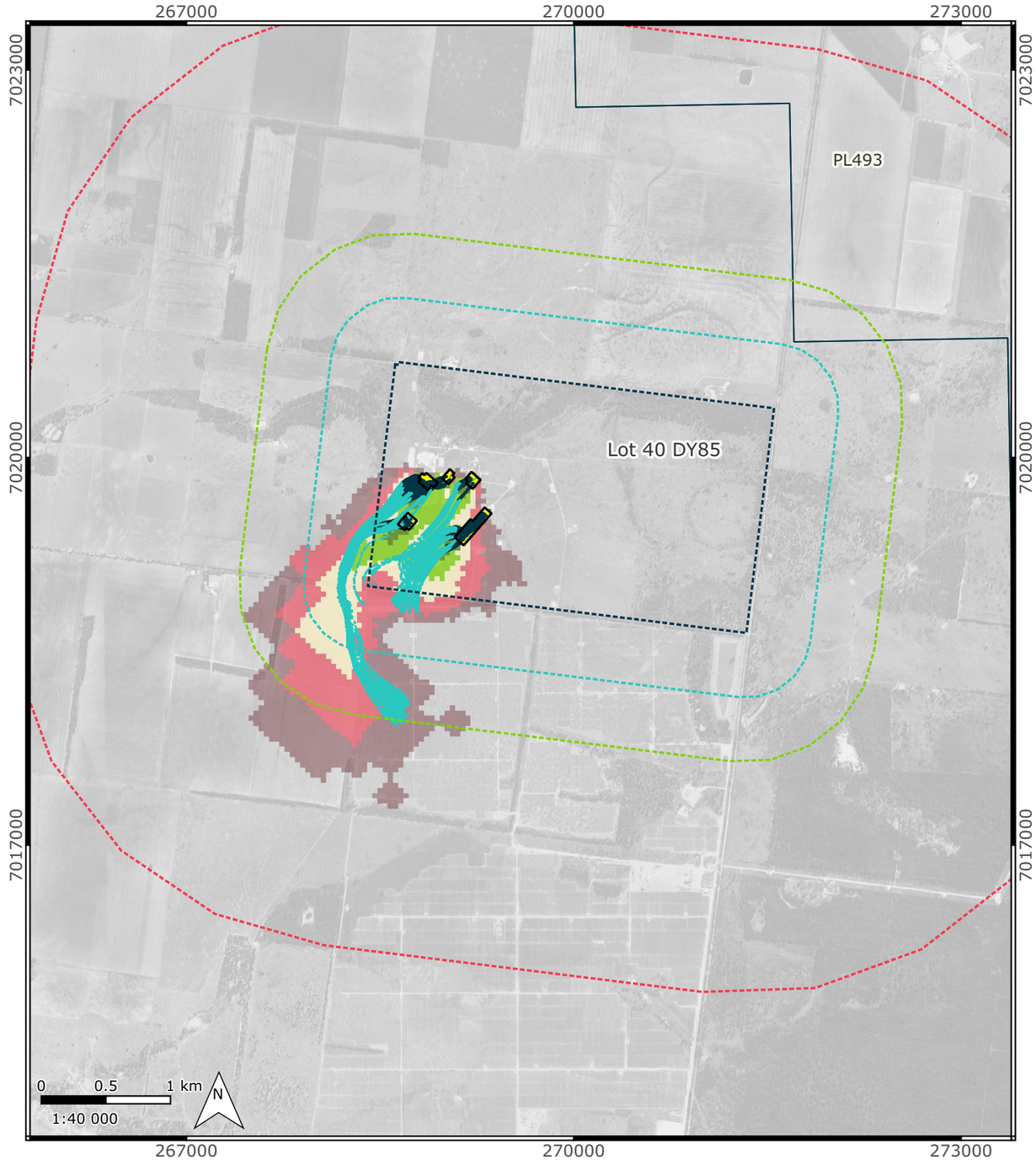
File Path: C:\modelling\Arrow\deliverables\Figures_REP-HG-002\Figure_5-6_PT_probability_bores_v2.qgz

© Worley Pty Ltd While every care is taken to ensure the accuracy of this data, Worley makes no representations or warranties aboutits accuracy, reliability, completeness or suitability for any particular purpose and disclaims all responsibility and all liability (including without limitation liability in negligence) for all expenses, losses, damages (including indirect or consequential damage) and costs which might be incurred as a result of the data being inaccurate or incomplete in any way and for any reason.

Springbok sandstone



Macalister coal seam



Legend

- Groundwater model extent
- Lot 40 DY85
- Gasifiers
- Petroleum Leases

Lot 40 DY85 buffer zones:

- 500 m
- 1000 m
- 2800 m

Particle travel period:

- 2019-2025
- 2026-2061
- 2062-2225

Pathline probability

- Very unlikely (<5%)
- Unlikely (5-33%)
- As likely as not (33-67%)
- Likely (67-95%)
- Very likely (>95%)

Probability of particle tracking pathlines in Springbok sandstone and Macalister coal seam for scenario 3 (particles released at gasifiers)

Project No.	Client	Figure No.
411001-00917	Arrow	5-7

Notes:
Project CRS: GDA94 / MGA zone 56
Last Saved: 22:34 04/08/2026
Filename: Figure_5-6_PT_probability_bores_v2

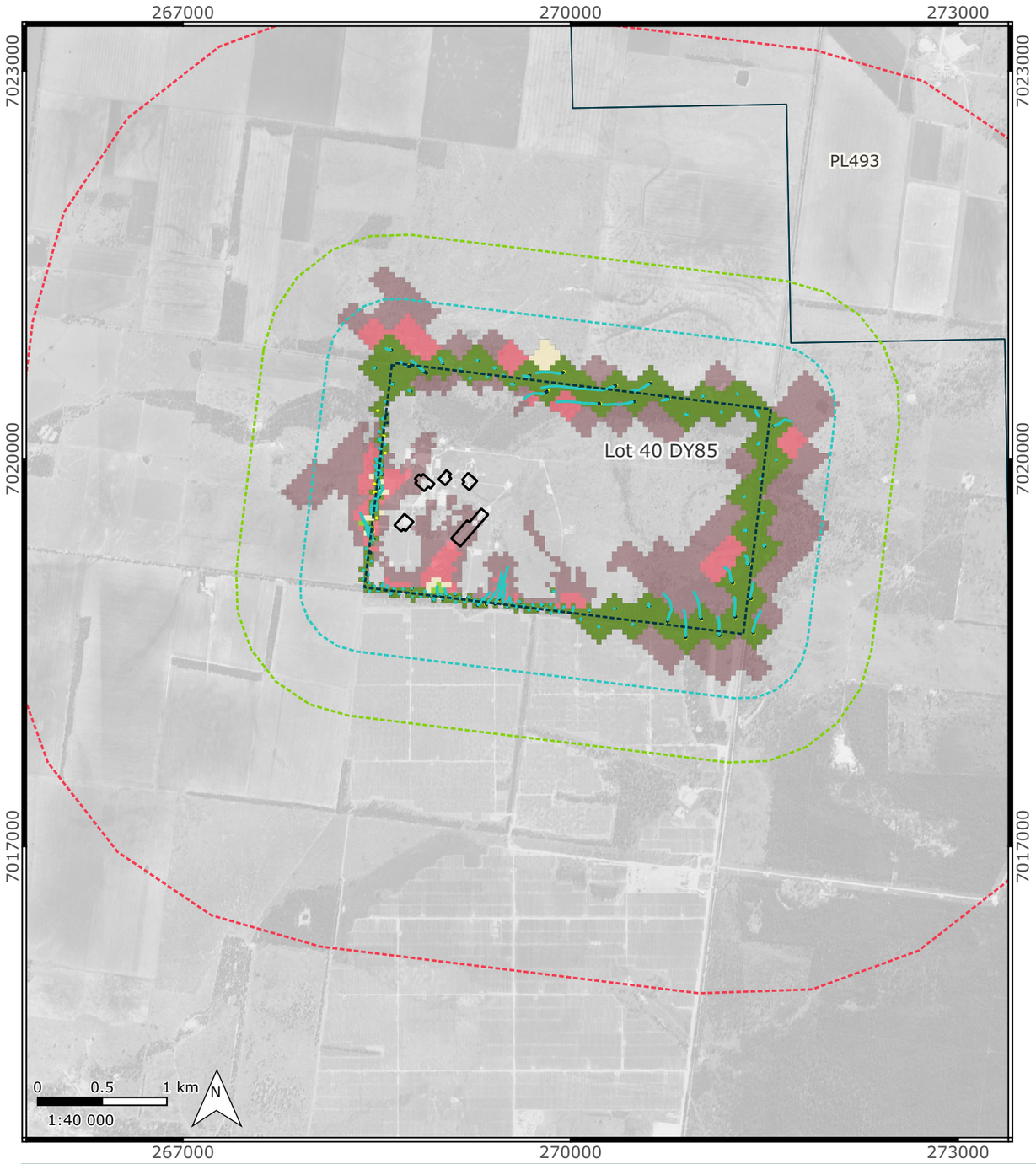
Exported by User: Mohsen.Azadi
Project Exported: 22:41 04/08/2026

References:
N/A

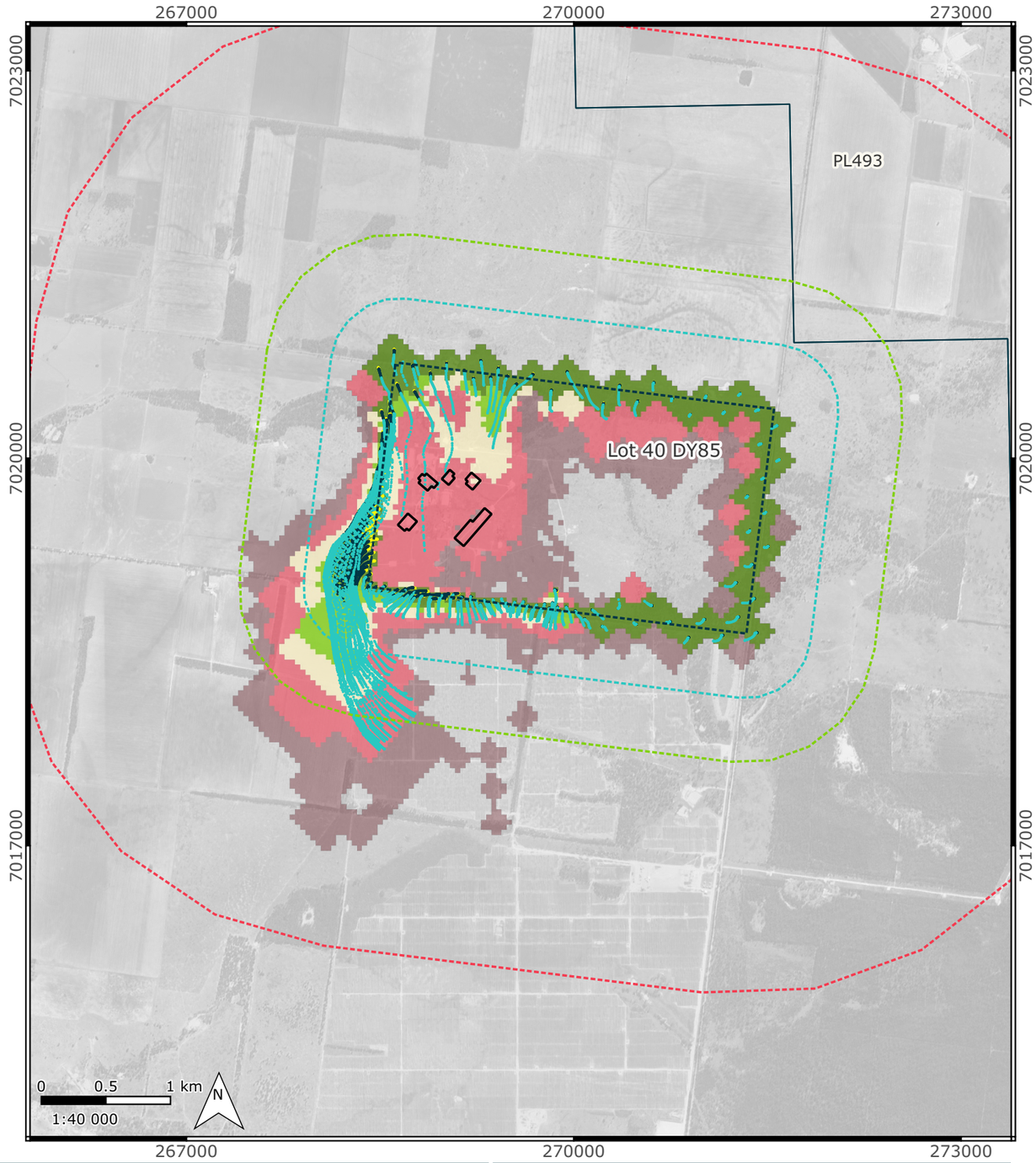
File Path: C:\modelling\Arrow\deliverables\Figures_REP-HG-002\Figure_5-6_PT_probability_bores_v2.qgz

© Worley Pty Ltd While every care is taken to ensure the accuracy of this data, Worley makes no representations or warranties aboutits accuracy, reliability, completeness or suitability for any particular purpose and disclaims all responsibility and all liability (including without limitation liability in negligence) for all expenses, losses, damages (including indirect or consequential damage) and costs which might be incurred as a result of the data being inaccurate or incomplete in any way and for any reason.

Springbok sandstone



Macalister coal seam



Legend

- Groundwater model extent
- Lot 40 DY85
- Gasifiers
- Petroleum Leases

Lot 40 DY85 buffer zones:
- 500 m
- 1000 m
- 2800 m

Particle travel period:
- 2019-2025
- 2026-2061
- 2062-2225

Pathline probability
- Very unlikely (<5%)
- Unlikely (5-33%)
- As likely as not (33-67%)
- Likely (67-95%)
- Very likely (>95%)

Probability of particle tracking pathlines in Springbok sandstone and Macalister coal seam for scenario 3 (particles released at Lot 40 DY85 boundaries)

Project No.	Client	Figure No.
411001-00917	Arrow	5-8

Notes:
Project CRS: GDA94 / MGA zone 56
Last Saved: 22:12 04/08/2026
Filename: Figure_5-6_PT_probability_bores_v2

Exported by User: Mohsen.Azadi
Project Exported: 22:28 04/08/2026

References:
N/A

File Path: C:\modelling\Arrow\deliverables\Figures_REP-HG-002\Figure_5-6_PT_probability_bores_v2.qgz

© Worley Pty Ltd While every care is taken to ensure the accuracy of this data, Worley makes no representations or warranties aboutits accuracy, reliability, completeness or suitability for any particular purpose and disclaims all responsibility and all liability (including without limitation liability in negligence) for all expenses, losses, damages (including indirect or consequential damage) and costs which might be incurred as a result of the data being inaccurate or incomplete in any way and for any reason.

To assess the potential influence of the proposed Clynes Road wells, particle travel distances were compared across the ensemble of model realisations for scenario 2 (approved development) and scenario 3 (approved plus proposed wells). The assessment focused on differences in particle travel distances (simulated to the end of the recovery period) to evaluate whether abstraction from the proposed wells materially modifies advective transport behaviour of the residual contaminants in Lot 40 DY85. This scenario-based comparison allows the potential effect of the Clynes Road wells on maximum contaminant migration to be evaluated independently of attenuation processes, while accounting for parameter uncertainty.

Summary statistics of particle travel distances (from 2019 to 2225) for particles released within the Springbok sandstone and Macalister coal seam under scenario 2, scenario 3, and their incremental differences are presented in Table 5-3. The particle tracking predictions indicate that, by the end of the recovery period in 2225:

- Particle travel distances are consistently greater within the Macalister coal seam than within the Springbok Sandstone, as discussed previously.
- For the ensemble median results:
  - A maximum particle travel distance of approximately 131 m was predicted within the Springbok sandstone,
  - A maximum particle travel distance of approximately 1,130 m was predicted within the Macalister coal seam,
  - A maximum incremental particle travel distance increase of approximately 2 m was predicted in the Springbok sandstone associated with the proposed Clynes Road wells, and
  - A maximum incremental particle travel distance increase of approximately 75 m was predicted in the Macalister coal seam associated with the proposed Clynes Road wells.
- It is very unlikely (based on P95 percentile results) that addition of the proposed Clynes Road wells would result in an increase in particle travel distance exceeding of approximately 7 m in the Springbok sandstone and 81 m in the Macalister coal seam.

Table 5-3 Summary statistics of particle travel distances (from 2019 and 2225) for particles released within Springbok sandstone and Macalister coal seam

Modelling scenario	Layer	Particle location	P5			P50			P95		
			Min	Mean	Max	Min	Mean	Max	Min	Mean	Max
Scenario 2 (approved)	Springbok	Bores	<1	10	47	1	40	115	4	195	1002
		Gasifiers	<1	15	33	20	79	130	117	284	444
		Boundaries	<1	3	40	<1	17	97	5	100	767
	Macalister	Bores	9	217	534	40	653	985	129	1400	1944
		Gasifiers	129	322	538	529	752	875	1032	1573	1850
		Boundaries	<1	75	382	10	306	1082	45	793	1870
Scenario 3 (Clynes Rd)	Springbok	Bores	<1	10	44	1	41	117	4	197	1004
		Gasifiers	<1	15	33	21	80	131	120	287	446
		Boundaries	<1	3	41	<1	17	98	5	101	775
	Macalister	Bores	10	223	533	40	676	993	129	1451	1923
		Gasifiers	138	331	540	561	782	950	1106	1642	1931
		Boundaries	<1	78	392	11	321	1130	37	815	1908
Predicted impacted	Springbok	Bores	<1	<1	-3	<1	1	2	<1	2	2
		Gasifiers	<1	<1	1	<1	1	1	3	2	3
		Boundaries	<1	<1	1	<1	<1	1	<1	1	7
	Macalister	Bores	1	7	-1	<1	23	8	<1	51	-22
		Gasifiers	9	8	2	31	30	75	74	69	81
		Boundaries	<1	3	10	<1	15	48	-8	22	38

5.5 Contaminant transport and fate

The contaminant transport and fate were evaluated based on long-term evolution of benzene and naphthalene concentrations under simulated groundwater flow, source depletion, and natural attenuation processes (discussed in section 3.3). Predictions are based on the ensemble of calibrated model realisations and are interpreted using percentile statistics (P5, P50, and P95) to characterise uncertainty and provide a risk-based assessment of contaminant attenuation and migration within the Springbok sandstone and Macalister coal seam. The assessment focuses on concentration trends at monitoring locations, the timing of concentration depletion below LOR, and the spatial distribution of residual concentrations.

Ensemble predictions indicate a consistent decline in benzene and naphthalene concentrations at monitoring locations across both formations, reflecting the combined effects of source dilution and natural attenuation (shown in Appendices F and G). For benzene, concentration trends show progressive reductions over time, with variability between monitoring locations diminishing as source contributions decrease. Naphthalene concentrations decline more rapidly across the ensemble, consistent with its lower source strength and stronger attenuation characteristics. Overall, the ensemble results demonstrate convergence toward declining concentrations at monitoring bores.

The year in which contaminant concentrations are predicted to decline below the LOR was evaluated across the ensemble of model realisations for both HSUs and contaminants, as summarised in Table 5-4. Ensemble results indicate that the median (P50) predictions are as follows:

- Benzene concentrations are predicted to fall below the LOR in:
  - 2049 for the Springbok sandstone, and
  - 2035 for the Macalister coal seam.
- Naphthalene concentrations are predicted to fall below the LOR in:
  - January 2027 for the Springbok sandstone, and
  - April 2024 for the Macalister coal seam.

Upper-bound ensemble predictions (P95) further indicate that it is very unlikely that the year of depletion below the LOR will exceed the following:

- For benzene:
  - 2053 for the Springbok sandstone, and
  - 2043 for the Macalister coal seam.
- For naphthalene:
  - 2037 for the Springbok sandstone, and
  - June 2025 for the Macalister coal seam, consistent with current groundwater monitoring observations.

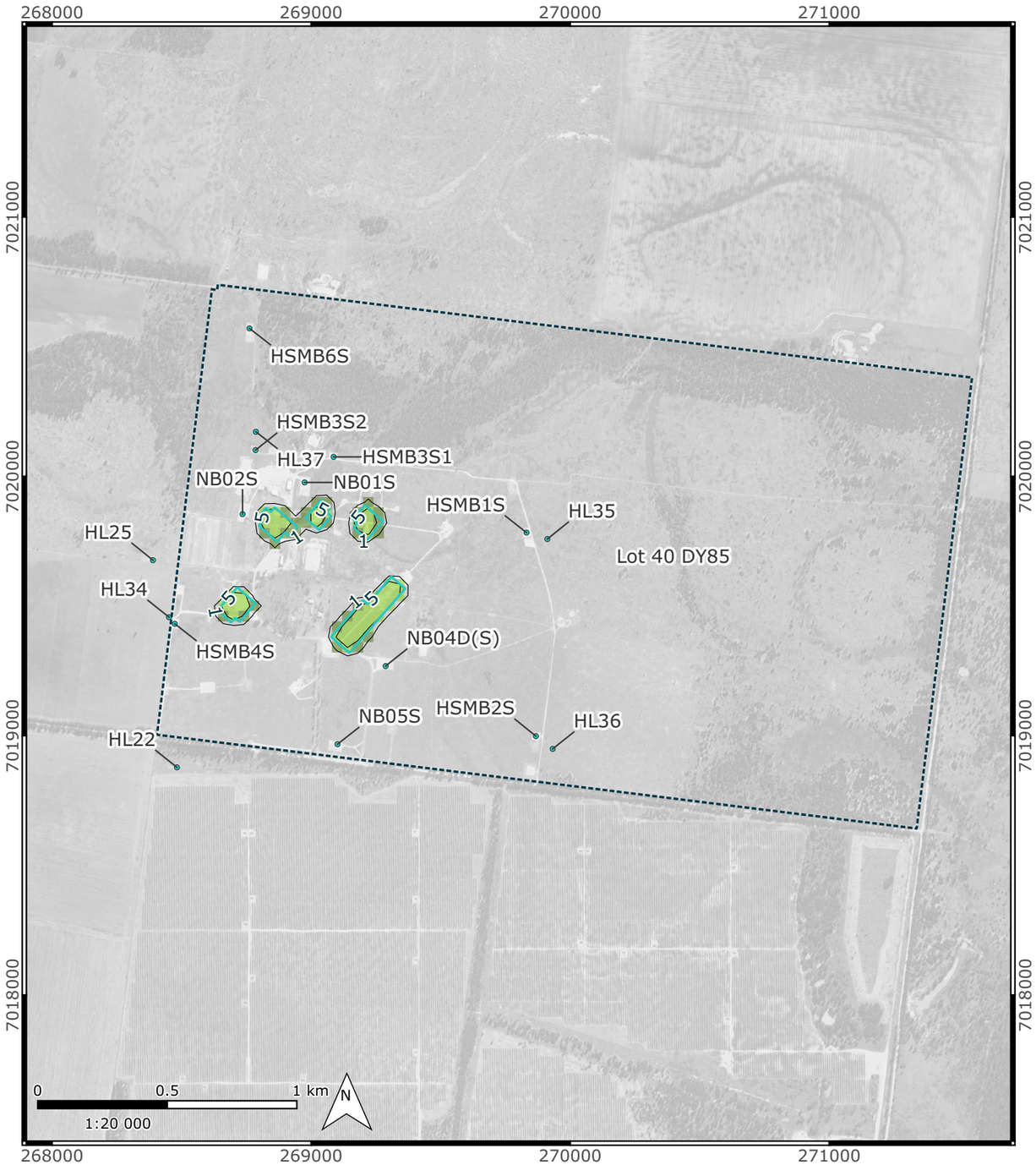
Comparison of predicted depletion timing between scenarios 2 and 3 indicates no change in the year at which concentrations are predicted to fall below the LOR for either contaminant or formation. This outcome indicates that inclusion of the proposed Clynes Road wells is not expected to materially influence natural attenuation or long-term depletion of benzene or naphthalene concentrations.

Based on the ensemble depletion timing, median (P50) benzene concentration distributions were examined for future years, including year 2030 in the Macalister coal seam and year 2040 in the Springbok sandstone (Figure 5-9). These years were chosen based on the median years discussed above to better understand the plume distribution before reaching below LOR. The benzene distribution in the final years before reaching below the LOR are predominantly present within or near gasifier releasing source depletion term. This also indicates that removal of the source terms will likely result in earlier timing when the contaminants concentrations reach below the LOR.

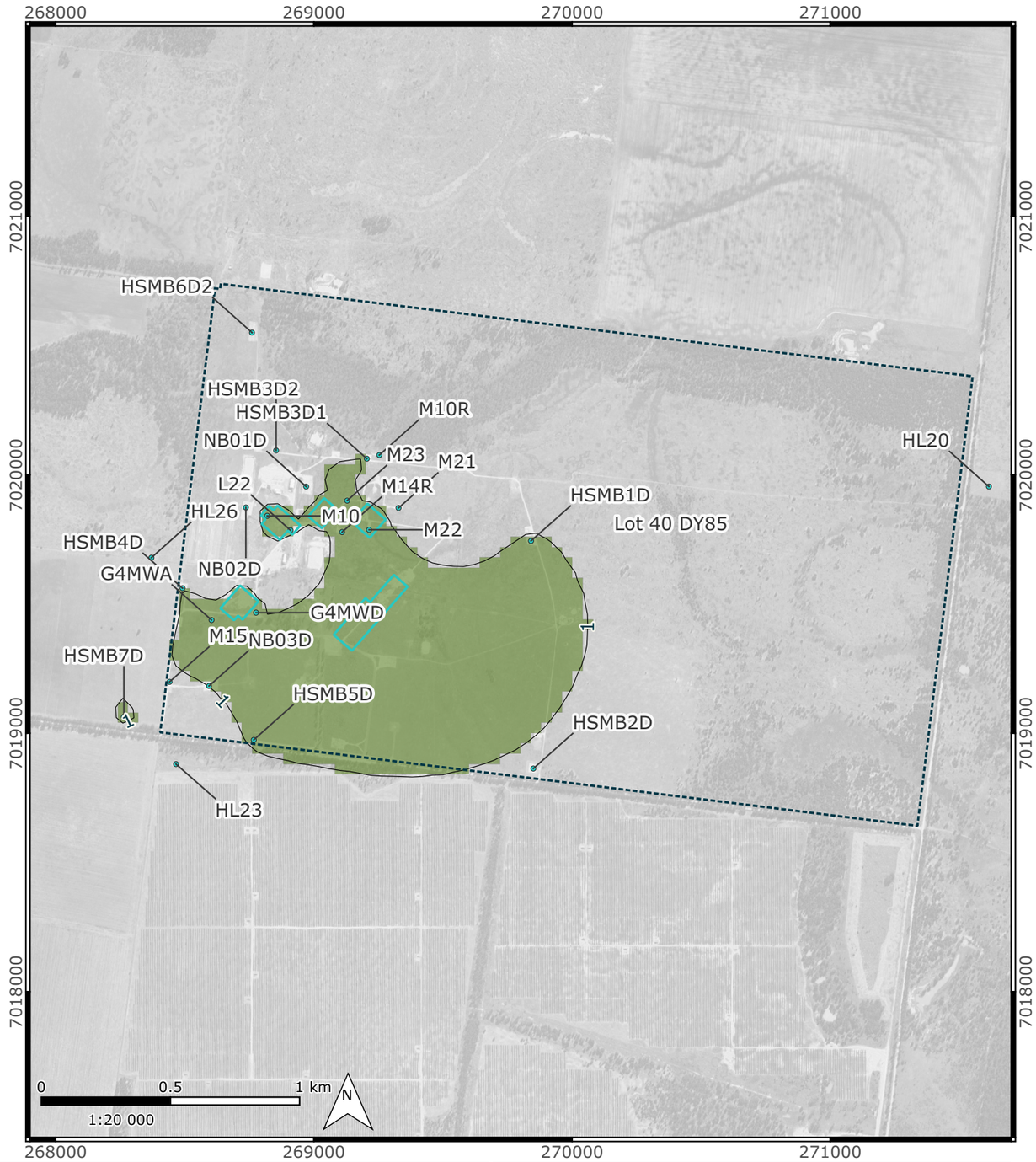
Table 5-4 Predicted year of contaminant concentration reaching below the LOR

Modelling scenario	Compound	Springbok sandstone			Macalister coal		
		P5	P50	P95	P5	P50	P95
Scenario 2 (approved)	Benzene	Jan 2049	Jan 2049	Jan 2053	Jan 2033	Jan 2035	Jan 2043
	Naphthalene	Jan 2026	Jan 2027	Jan 2037	Jan 2024	Apr 2024	Jun 2025
Scenario 3 (Clynes Rd)	Benzene	Jan 2049	Jan 2049	Jan 2053	Jan 2033	Jan 2035	Jan 2043
	Naphthalene	Jan 2026	Jan 2027	Jan 2037	Jan 2024	Apr 2024	Jun 2025

Springbok sandstone (end of 2040)



Macalister coal seam (end of 2030)



Legend

- Lot 40 DY85
- Gasifier
- Monitoring bores

Concentration (ug/L)

- 1 - 5
- 5 - 10
- 10 - 50
- 50 - 100
- 100 - 500
- 500 - 1000
- 1000 - 5000

Predicted median benzene concentrations in the Springbok sandstone (end of December 2040) and Macalister coal seam (end of December 2030)

Project No.	Client	Figure No.
411001-00917	Arrow	5-9

Notes:
Project CRS: GDA94 / MGA zone 56
Last Saved: 23:08 04/08/2026
Filename: Figure_5-9_benzene_pred_v2

Exported by User: Mohsen.Azadi
Project Exported: 23:10 04/08/2026

References:
N/A

File Path: C:\modelling\Arrow\deliverables\Figures_REP-HG-002\Figure_5-9_benzene_pred_v2.qgz

© Worley Pty Ltd While every care is taken to ensure the accuracy of this data, Worley makes no representations or warranties aboutits accuracy, reliability, completeness or suitability for any particular purpose and disclaims all responsibility and all liability (including without limitation liability in negligence) for all expenses, losses, damages (including indirect or consequential damage) and costs which might be incurred as a result of the data being inaccurate or incomplete in any way and for any reason.

worley consulting

5.6 Impact assessment

This impact assessment evaluates the incremental effects of the proposed Clynes Road wells (scenario 3) relative to the currently approved FDP (scenario 2) on groundwater flow, hydraulic gradients, contaminant transport and fate within the Springbok sandstone and Macalister coal seam. The assessment is based on the predictive ensemble modelling results presented in sections 5.2 to 5.5, using uncertainty analysis results (for P5, P50, and P95 percentiles) to provide a conservative, risk-based assessment.

Groundwater levels and flow directions

Predictive groundwater level simulations indicate that cumulative abstraction under both scenarios results in drawdown centered on abstraction areas, with groundwater flow directed predominantly toward the south to southwest at the regional scale. At the end of 2025, groundwater flow shows inward gradients toward Lot 40 DY85 in the Springbok sandstone, while flow in the Macalister coal seam converges toward the gasifiers and continues toward the southwest of the site.

Comparison of median groundwater levels between scenarios 2 and 3 demonstrates that the incremental drawdown attributable to the proposed Clynes Road wells is small and spatially limited. At the end of the abstraction period (2061), predicted median differences are generally less than 1 m, with a localised zone of approximately 1–2 m difference in the Macalister coal seam near the proposed wells. By the end of the recovery period (2225), differences in median groundwater levels between scenarios are less than 1 m across both formations, indicating that inclusion of the Clynes Road wells is not expected to result in a material change to long-term groundwater level recovery relative to the approved development.

Assessment of horizontal hydraulic gradients across 1,500 m sections of the southern and western boundaries of Lot 40 DY85 shows stronger inward gradients in the Springbok sandstone compared to partially-inward gradients in the Macalister coal seam. Comparison between scenarios indicates that incremental changes in these gradients are negligible, with differences generally within ±1% across all percentiles. These results demonstrate that it is unlikely that the proposed Clynes Road wells will materially alter regional or site-scale groundwater flow directions relevant to contaminant migration beyond Lot 40 DY85.

Vertical hydraulic gradient

Evaluation of vertical hydraulic gradients between the Springbok sandstone and the Macalister coal seam was undertaken under scenario 3 to confirm the direction of vertical groundwater flow under the maximum proposed development. Analysis of groundwater level differences at 10 pairs of monitoring locations indicates continuous positive head differences from 2026 through to 2225, corresponding to a constant downward vertical gradient from the Springbok sandstone into the Macalister coal seam.

This outcome is consistent across the ensemble and throughout both abstraction and recovery phases, indicating that vertical groundwater flow remains directed downward under scenario 3. These results predict that the proposed Clynes Road wells do not cause upward vertical flow from the Macalister coal seam into the overlying Springbok sandstone, supporting a very low likelihood of upward contaminant migration under the maximum development scenario.

Particle tracking – conservative assessment of contaminants

Particle tracking was undertaken as a conservative assessment of maximum potential contaminant movement, independent of attenuation processes such as sorption, degradation, and dilution. Comparison of ensemble particle travel distances between scenarios 2 and 3 provides a measure of the incremental impact of the proposed Clynes Road wells on potential migration pathways.

Results indicate that particle travel distances are consistently greater in the Macalister coal seam than in the Springbok sandstone, reflecting higher formation transmissivity and CSG abstraction within WCM. For ensemble median (P50) results, maximum particle travel distances of approximately 131 m were predicted in the Springbok sandstone and approximately 1,130 m in the Macalister coal seam. The incremental impact associated with the proposed Clynes Road wells is small, with maximum increases in median particle travel distance of approximately 2 m in the Springbok sandstone and approximately 75 m in the Macalister coal seam.

Upper-bound (P95) results further indicate that it is very unlikely that inclusion of the proposed Clynes Road wells would result in an increase in particle travel distance exceeding of approximately 7 m in the Springbok sandstone or approximately 81 m in the Macalister coal seam. These incremental changes are small relative to overall travel distances (between 2019 and 2225) and do not materially change particle migration pathways beyond those predicted under the approved scenario.

Contaminant transport and fate

Contaminant transport modelling indicates continued long-term decline in benzene and naphthalene concentrations across both formations due to dilution and natural attenuation. Ensemble results show consistent depletion trends at monitoring locations, with naphthalene attenuating more rapidly than benzene and reaching below the laboratory limit of reporting (LOR) earlier across all percentiles.

Predicted depletion timing indicates that, at the ensemble median (P50), benzene concentrations fall below the LOR by approximately 2049 in the Springbok sandstone and approximately 2035 in the Macalister coal seam, while naphthalene concentrations fall below the LOR by approximately January 2027 and April 2024, respectively. Upper-bound (P95) predictions indicate that it is very unlikely for benzene depletion to extend beyond approximately 2053 for Springbok sandstone or 2043 for Macalister coal seam, and for naphthalene beyond approximately 2037 and mid-2025, respectively.

Comparison of depletion timing between scenarios 2 and 3 indicates no change in predicted years at which concentrations fall below the LOR for either contaminant or formation. This outcome indicates that inclusion of the proposed Clynes Road wells is not expected to materially influence natural attenuation or long-term depletion of benzene or naphthalene concentrations.

Overall impact assessment

Collectively, results from groundwater level predictions, hydraulic gradient assessments, particle tracking, and contaminant transport modelling demonstrate that the proposed Clynes

Road wells (scenario 3) result in minor localised incremental changes relative to the approved development (scenario 2). No material changes are predicted in groundwater flow directions, vertical gradients, contaminant migration, or contaminant depletion timing. The assessment indicates that the proposed development is unlikely to increase the risk of off-site contaminant migration or compromise long-term groundwater recovery and containment of residual contamination associated with the former Hopeland UCG site.

6. Conclusions and recommendations

This groundwater impact assessment presents the results of an updated numerical groundwater flow and contaminant transport modelling study undertaken to support Arrow Energy's proposed Field Development Plan (FDP) for Clynes Road (scenario 3) within PL253. The study builds on a sequence of previous investigations and modelling studies (AGE, 2021; AGE, 2023; Intera, 2024; Intera, 2025), incorporating updated monitoring data, revised conceptual model and hydrostratigraphic interpretation, and improved representation of boundary conditions and modelling assumptions. The modelling has been undertaken in accordance with Environmental Authority EA0001401, OGIA (2021a) regional groundwater modelling approach, Australian Groundwater Modelling Guidelines (Barnett et al., 2012), and using the risk-based terminology outlined in Peeters & Middlemis (2023) with a focus on groundwater flow behaviour, contaminant migration, uncertainty analysis, and long-term recovery associated with the former Hopeland UCG site on Lot 40 DY85.

Hydrogeological conceptualisation of the PL253 area and the former Hopeland UCG site was updated building upon, and refining, the conceptual understanding established in earlier studies (including AGE and Intera investigations). The updated conceptualisation incorporates the latest groundwater level and groundwater quality monitoring data, revised hydrostratigraphic interpretation, and updated regional groundwater incorporation to better represent current groundwater conditions. The Springbok sandstone and the Walloon Coal Measures (WCM), particularly the Macalister coal seam, remain the key hydrostratigraphic units governing groundwater flow and contaminant behaviour, with monitoring data confirming persistent downward vertical hydraulic gradients from the Springbok sandstone toward the WCM. Updated groundwater level and quality datasets indicate that residual effects of historical UCG activities remain localised within Lot 40 DY85, with declining benzene and naphthalene concentrations. Regionally, groundwater flow is expected to be directed predominantly toward the south to southwest, consistent with OGIA (2021) conceptualisation, while local scale variability reflects historical UCG depressurisation and formation heterogeneity near gasifier locations.

The groundwater flow and contaminant transport models, consistent with recent studies (Intera, 2024 and 2025), were developed in MODFLOW 6 to better replicate the groundwater flow regime and contaminant transport processes, while targeted refinements were introduced to improve representation of hydrostratigraphic units, boundary conditions, and historical UCG related activities. Key improvements include alignment of General Head Boundary (GHB) and drain boundary conditions with OGIA (2021) regional model datasets for non-Arrow CSG extraction, updated boundary condition for simulation of Arrow CSG extraction, adjusted simulation of Hopeland pilot wells using the Multi Aquifer Well package, and incorporation of time varying hydraulic properties to represent UCG related fracturing and material alteration. For contaminant transport, the model implements data driven source depletion terms, dual domain porosity, mechanical dispersion, molecular diffusion, sorption, and degradation processes using MODFLOW 6 transport packages and aligned with the conceptual understanding of concentration distributions.

The groundwater flow and contaminant transport models achieved a good history-matching fit, with simulated groundwater levels and contaminant concentrations showing good agreement

with the observed data. A total of 216 model realisations satisfied convergence and history matching performance criteria, with scaled root mean square errors less than 10% consistent with Australian Groundwater Modelling Guidelines threshold. History matching successfully reproduced observed temporal trends, spatial groundwater level patterns, vertical hydraulic gradients, and benzene and naphthalene concentration behaviour in both the Springbok sandstone and the Macalister coal seam. History matching also reasonably replicated the current groundwater flow regimes and contaminant transport processes aligned with the conceptual understanding of the study area utilised as history matching targets.

Predictive modelling indicates that inclusion of the proposed Clynes Road wells results in minor and localised incremental impacts relative to the approved development (scenario 2). Differences in predicted median groundwater levels between scenarios 2 and 3 are generally less than 1 m at the end of abstraction and recovery, with localised differences (of approximately 1–2 m) confined to areas near the proposed wells in the Macalister coal seam. Horizontal hydraulic gradient assessments along the southern and western boundaries of Lot 40 DY85 show incremental changes generally within ±1%, indicating no material alteration to Lot 40 DY85 flow directions relevant to contaminant migration beyond the site boundary.

Predictive modelling indicates that inclusion of the proposed Clynes Road wells results in minor and localised incremental impacts relative to the approved development (scenario 2). Differences in predicted median groundwater levels between scenarios 2 and 3 are generally less than 1 m at the end of abstraction and recovery, with localised differences of up to approximately 1-2 m confined to areas near the proposed wells in the Macalister coal seam. Assessment of horizontal hydraulic gradients along the southern and western boundaries of Lot 40 DY85 indicates incremental changes generally within ±1%, demonstrating no material alteration to site-scale flow directions relevant to contaminant migration beyond the site boundary. In addition, predictive results indicate that a downward vertical hydraulic gradient from the Springbok sandstone to the Macalister coal seam is maintained throughout both the abstraction and recovery periods.

Particle tracking and contaminant transport simulations further demonstrate that the proposed Clynes Road wells is unlikely to materially alter contaminant transport pathways, travel distances or contaminant depletion timing. Incremental increases in particle travel distance are small relative to total travel distances and remain spatially limited for the simulation period between 2019 and 2225. Ensemble contaminant transport predictions indicate continued decline in benzene and naphthalene concentrations across both formations, with no change in the predicted year of depletion below the laboratory limit of reporting between scenarios 2 and 3. Residual concentrations predicted during the abstraction period remain confined to areas proximal to former gasifier locations, consistent with the observed monitoring data.

While the current modelling reasonably replicates the magnitude and trends in the observed groundwater level and contaminants' concentrations, continued model update is recommended to further reduce prediction uncertainty over time. Ongoing groundwater level and groundwater quality monitoring should be maintained within the Springbok sandstone and Macalister coal seam, with particular focus on groundwater flow directions, vertical gradients, and any areas of persistent elevated concentrations near former gasifier locations or beyond Lot 40 DY 85. Periodic review and incorporation of new monitoring data into the numerical model would allow reassessment of predictions and confirmation of long-term trends.

It is also recommended that future updates to the groundwater model consider refinement of source representation as additional data becomes available regarding the persistence or removal of residual contamination zones. Should any site-scale alterations occur to the current declining trends across monitoring bores within and around Lot 40 DY85, updated groundwater flow and contaminant transport modelling is recommended to be undertaken to reassess contaminant movement and depletion timing. Continued alignment with OGIA regional model updates is recommended to ensure future modelling remains consistent with updated basin-scale conceptualisation and regional flow directions.

7. References

AGE, (2021). Production Licensing Modelling Support prepared for Arrow Energy by Australasian Groundwater and Environmental Consultants Pty Ltd. June 2021.

AGE, (2023). PL 253 Environmental Approval Amendment Support – Contaminant transport validation – Addendum to AGE (2022) by Australasian Groundwater and Environmental Consultants Pty Ltd. 19th January 2023.

Ahangar, A.G. (2010). Sorption of PAHs in the soil environment with emphasis on the role of soil organic matter: A review. World Applied Sciences Journal, 11(7), 759–765.

Aguilera, R. (2004). A triple porosity model for petrophysical analysis of naturally fractured reservoirs. Petrophysics (SPWLA Journal), 45(2).

Anderson, R.T., Rooney-Varga, J.N., Gaw, C.V. & Lovley, D.R. (1998). Anaerobic benzene oxidation in the Fe(III) reduction zone of petroleum-contaminated aquifers. Environmental Science & Technology, 32(9), 1222–1229.

American Petroleum Institute (API). (1998). Delineation and characterization of the Borden MTBE plume: An evaluation of eight years of natural attenuation processes. Health and Environmental Sciences Department, Publication No. 4668.

Agency for Toxic Substances and Disease Registry (ATSDR). (2024). Toxicological profile for benzene (Draft for public comment). Atlanta, GA: U.S. Department of Health and Human Services, Public Health Service.

Barnett, B., Townley, L., Post, V., Evans, R., Hunt, R., Peeters, L., Richardson, S., Werner, A., Knapton, A., & Boronkay, A. (2012). Australian groundwater modelling guidelines. National Water Commission.

Bayard, R., Barna, L., Mahjoub, B., and Gourdon, R., (2020). Influence of the presence of PAHs and coal tar on naphthalene sorption in soils. Journal of Contaminant Hydrology, Volume 46, Issues 1–2, pp. 61-80. https://doi.org/10.1016/S0169-7722(00)00125-X.

Bjerg, P.L., Rügge, K., Cortsen, J., Nielsen, P.H. & Christensen, T.H. (1999). Degradation of aromatic and chlorinated aliphatic hydrocarbons in the anaerobic part of the Grindsted landfill leachate plume: In situ microcosm and laboratory batch experiments. Ground Water, 37, 113–121.

Bjerg, P.L., Bøllingtoft, A. & Mosthaf, K. (2025). Lecture Note: Dispersion in Aquifers. DTU Sustain.

Doherty, J., (2024). Tutorial: Ensemble Space Inversion. GMDSI. https://gmdsi.org/blog/ensemble-space-inversion/.

Dong, S., Dai, Z., Li, J. & Zhou, W. (2018). The scale dependence of dispersivity in multi-facies heterogeneous formations. Carbonates and Evaporites, 33, 161–165.

ECETOC (European Centre for Ecotoxicology and Toxicology of Chemicals). (2013). Environmental Exposure Assessment of Ionisable Organic Compounds. Technical Report No. 123, Brussels: ECETOC.

Epic, (2020). Former Underground Coal Gasification Plant, Hopeland - Updated Conceptual Site Model. 17 December 2020.

Gelhar, L.W., Welty, C. & Rehfeldt, K.R. (1992). A critical review of data on field-scale dispersion in aquifers. Water Resources Research, 28(7), 1955–1974.

GHD, (2019). Arrow Hopeland Groundwater Study Groundwater Modelling Report – PL253.

Grathwohl, P., Eberhardt, C., Klenk, I., Rügner, H. & Maier, U. (2000). Transverse vertical dispersivity in aquifer materials: Implications on mass transfer across the capillary fringe and the length of steady state plumes. In: Bjerg, P.L. (ed.), Groundwater 2000: Proceedings of the International Conference on Groundwater Research, Copenhagen, Denmark, 6–8 June 2000. Rotterdam: A.A. Balkema.

Gustafson, K.E. & Dickhut, R.M. (1994). Molecular diffusivity of polycyclic aromatic hydrocarbons in air. Journal of Chemical & Engineering Data, 39(2), 286–289.

Intera (2024). PL253 –Site Conceptual Model, and Groundwater Flow, Contaminant Transport and Predictive Modelling.

Intera (2025). PL253 Groundwater Flow and Contaminant Transport Modelling Report. Prepared for Arrow Energy Pty Ltd.

King, G.R., Ertekin, T. & Schwerer, F.C. (1986). Numerical simulation of the transient behavior of coal-seam degasification wells. SPE Formation Evaluation, 1(2), 165–183.

Langevin, C.D., Provost, A.M., Panday, S. & Hughes, J.D. (2022). Documentation for the MODFLOW 6 Groundwater Transport Model. U.S. Geological Survey, Techniques and Methods, Book 6, Chap. A61.

Musat, F., Galushko, A., Jacob, J., Widdel, F., Kube, M., Reinhardt, R., Wilkes, H., Schink, B. & Rabus, R. (2009). Anaerobic degradation of naphthalene and 2-methylnaphthalene by strains of marine sulfate-reducing bacteria. Environmental Microbiology, 11(1), 209–219.

Newell, C.J., Rifai, H.S., Wilson, J.T., Connor, J.A., Aziz, J.A. & Suarez, M.P. (2002). Calculation and use of first-order rate constants for monitored natural attenuation studies. U.S. Environmental Protection Agency, Ground Water Issue.

Odermatt, J.R., (1994). Natural chromatographic separation of benzene, toluene, ethylbenzene and xylenes (BTEX compounds) in a gasoline contaminated ground water aquifer. Organic Chemistry v. 21, 10-11; p 1141-1150.

OGIA, (2021a). Modelling of Cumulative Groundwater Impacts in the Surat CMA: Approach and Methods. Version 1.0.

OGIA, (2021b). Regional Flow Systems and Potentiometry in Queensland's Surat and Southern Bowen Basins. Version 1.0.

Osagie, E.I. & Owabor, C.N. (2015a). Adsorption of benzene in batch system in natural clay and sandy soil. Advances in Chemical Engineering and Science, 5, 352–361.

Osagie, E.I. & Owabor, C.N. (2015b). Adsorption of naphthalene on clay and sandy soil from aqueous solution. Advances in Chemical Engineering and Science, 5, 345–351.

Peeters, L.J.M. and Middlemis, H. (2023). Information Guidelines Explanatory Note: Uncertainty analysis for groundwater modelling. Independent Expert Scientific Committee on Coal Seam Gas and Large Coal Mining Development, Commonwealth of Australia.

Prommer, H., Davis G.B., Barry D.A., Miller C.T., (2003). Modelling the Fate of Petroleum Hydrocarbons in Groundwater. Proceedings of the Fifth National Workshop on the Assessment of Site Contamination.

Pruess, K. & Narasimhan, T.N. (1985). A practical method for modeling fluid and heat flow in fractured porous media. Society of Petroleum Engineers Journal, 25(1), 14–26.

Schulze-Makuch, D. (2005). Longitudinal dispersivity data and implications for scaling behavior. Ground Water, 43(3), 443–456.

Shi, B., Ngueleu, S.K., Rezanezhad, F., Slowinski, S., Pronk, G.J., Smeaton, C.M., Stevenson, K., Al-Raoush, R.I. & Van Cappellen, P. (2020). Sorption and desorption of the model aromatic hydrocarbons naphthalene and benzene: Effects of temperature and soil composition. Frontiers in Environmental Chemistry, 1, 581103.

Ukalska-Jaruga, A. & Smreczak, B. (2020). The impact of organic matter on polycyclic aromatic hydrocarbon (PAH) availability and persistence in soils. Molecules, 25(11), 2470.

U.S. Environmental Protection Agency (U.S. EPA). (1996). A citizen's guide to natural attenuation. EPA 542-F-96-015, Office of Solid Waste and Emergency Response.

U.S. Environmental Protection Agency (US EPA). (1999). Monitored natural attenuation of petroleum hydrocarbons. EPA 600/F-98/021.

Warren, J.E. & Root, P.J. (1963). The behavior of naturally fractured reservoirs. Society of Petroleum Engineers Journal, 3(3), 245–255.

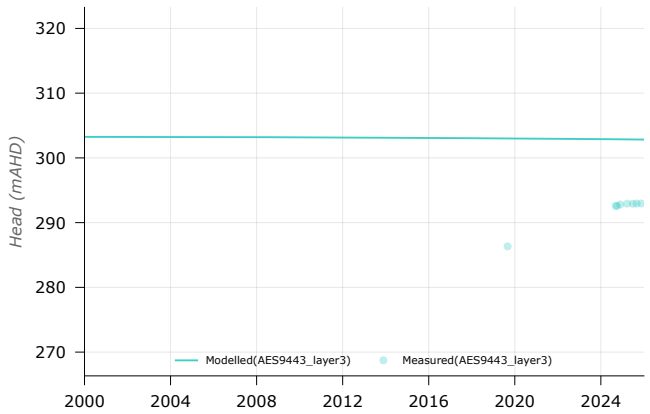
White, J.T., (2018). A model-independent iterative ensemble smoother for efficient history-matching and uncertainty quantification in very high dimensions. Environmental Modelling & Software, vol. 109.

Wiedemeier, T.H., Rifai, H.S., Newell, C.J., and Wilson, J.T. (1999). Natural Attenuation of Fuels and Chlorinated Solvents in the Subsurface. John Wiley & Sons, New York, 617 pp.

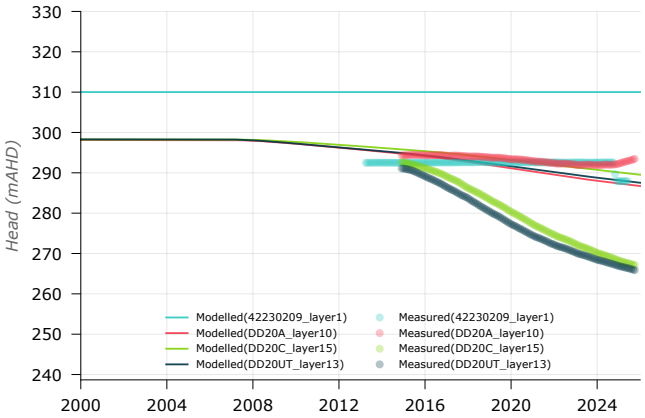
Zhang, T., [et al.] (2005). Hydroxylation and carboxylation—two crucial steps of anaerobic benzene degradation by Dechloromonas strain RCB. Applied and Environmental Microbiology, 71(9), 5427–5432.

Appendix A. Modelled versus observed hydrographs

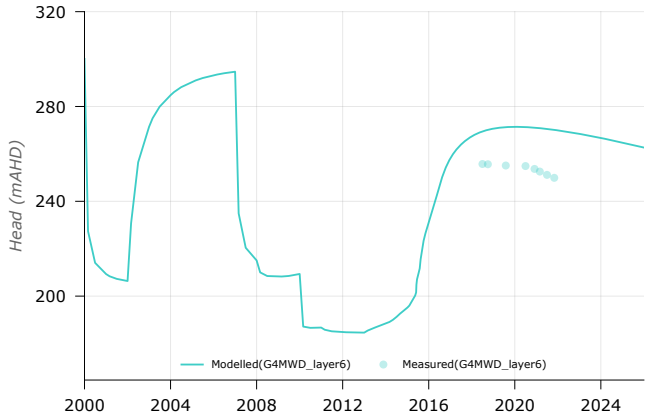
AES9443



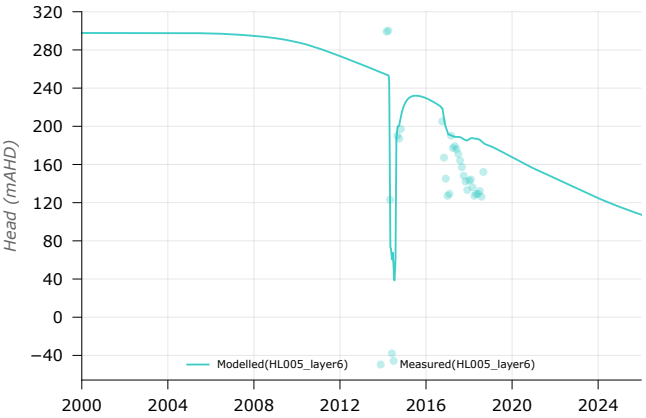
DD20



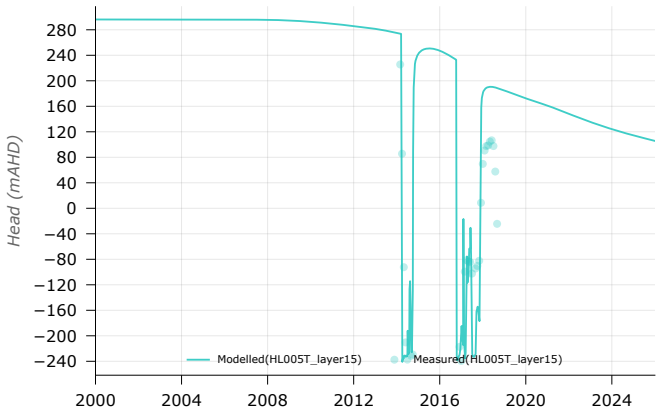
G4MWD



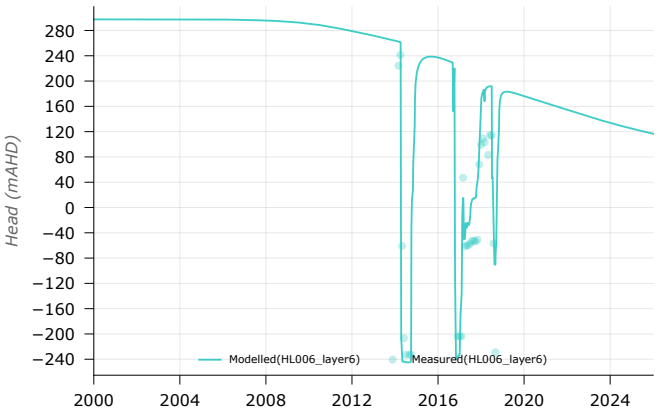
HL005



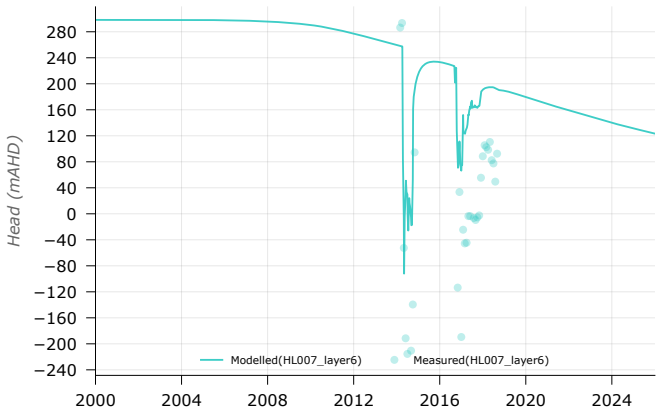
HL005T



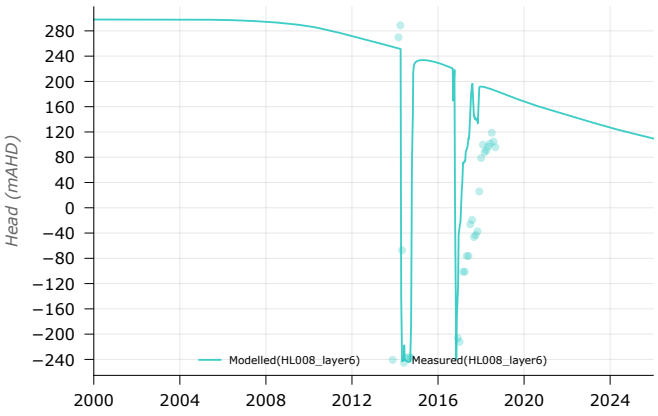
HL006



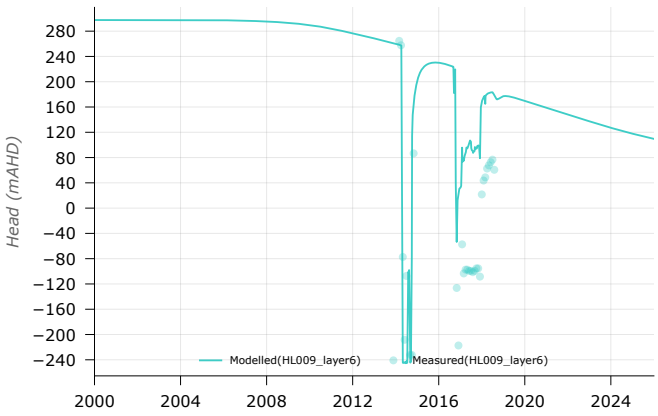
HL007



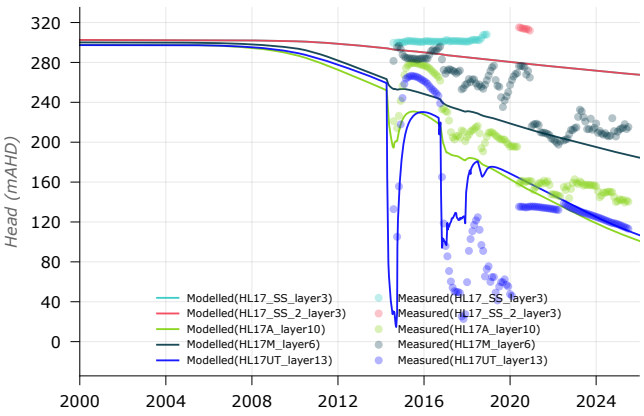
HL008



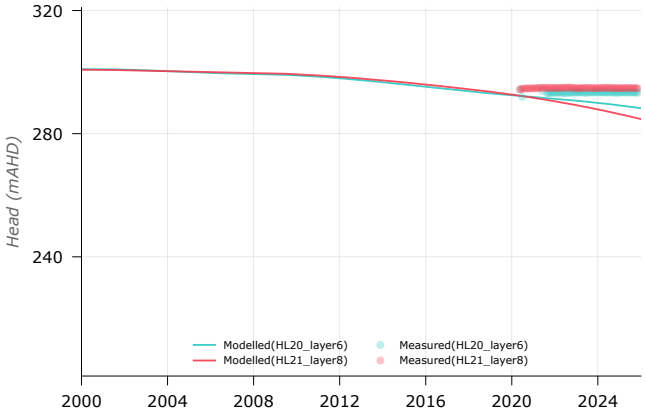
HL009



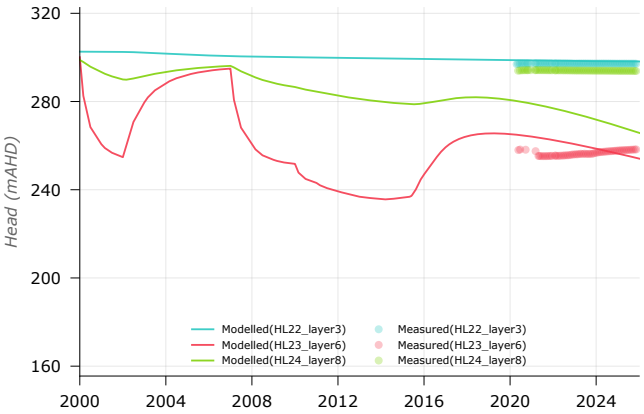
HL17



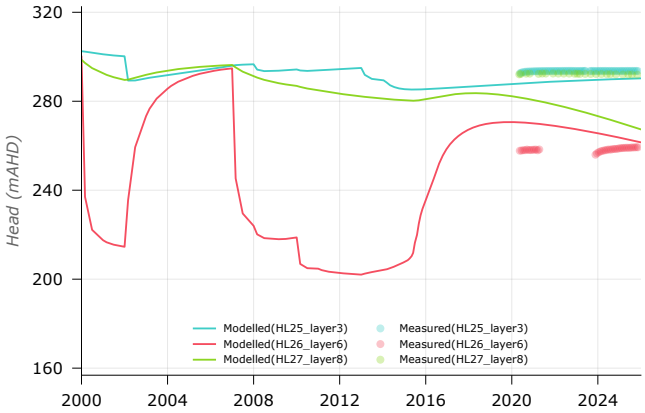
HL20-21



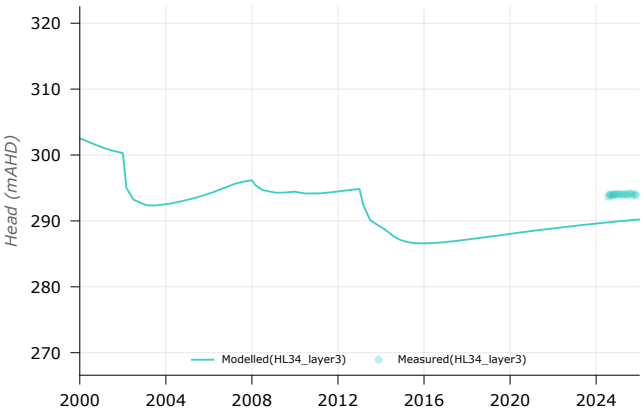
HL22-24



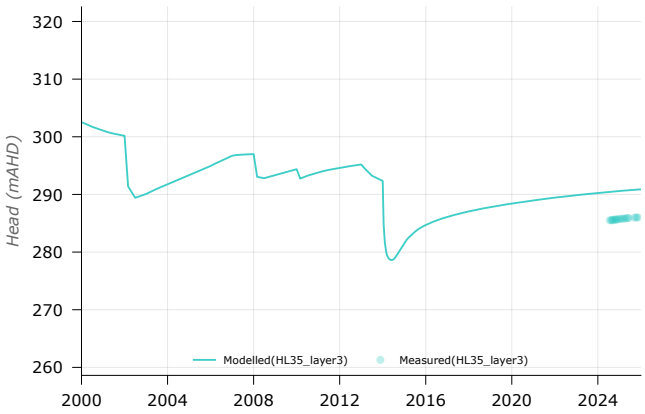
HL25-27



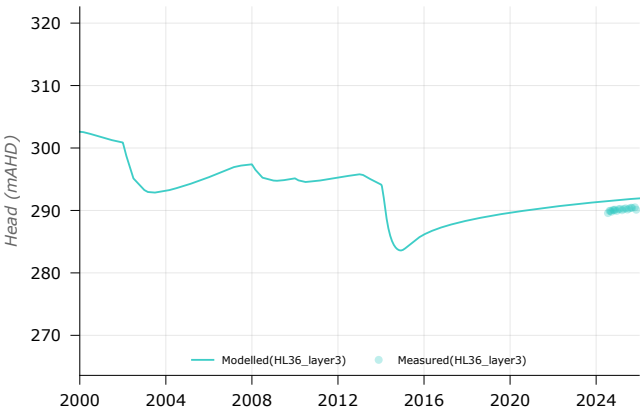
HL34

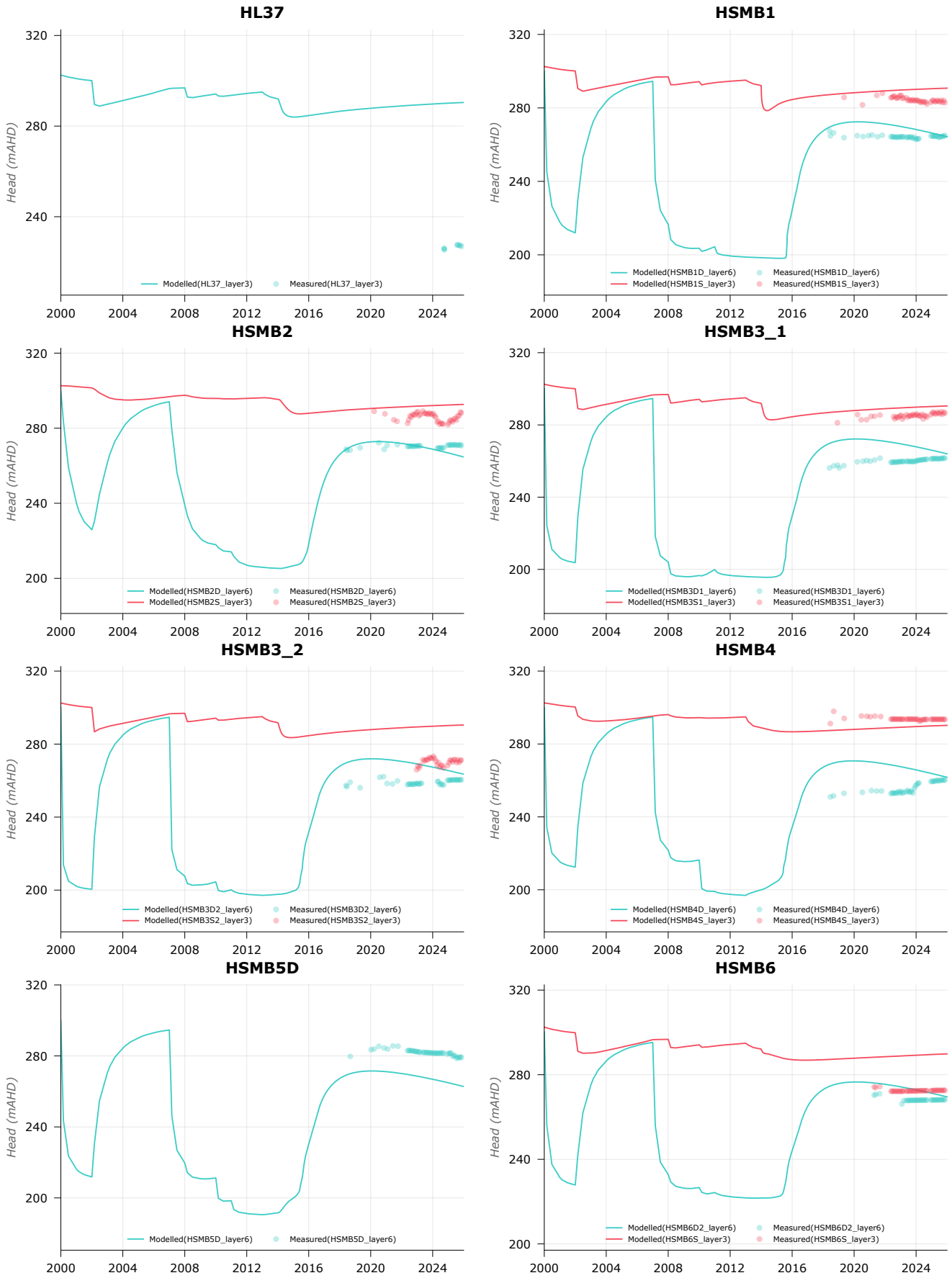


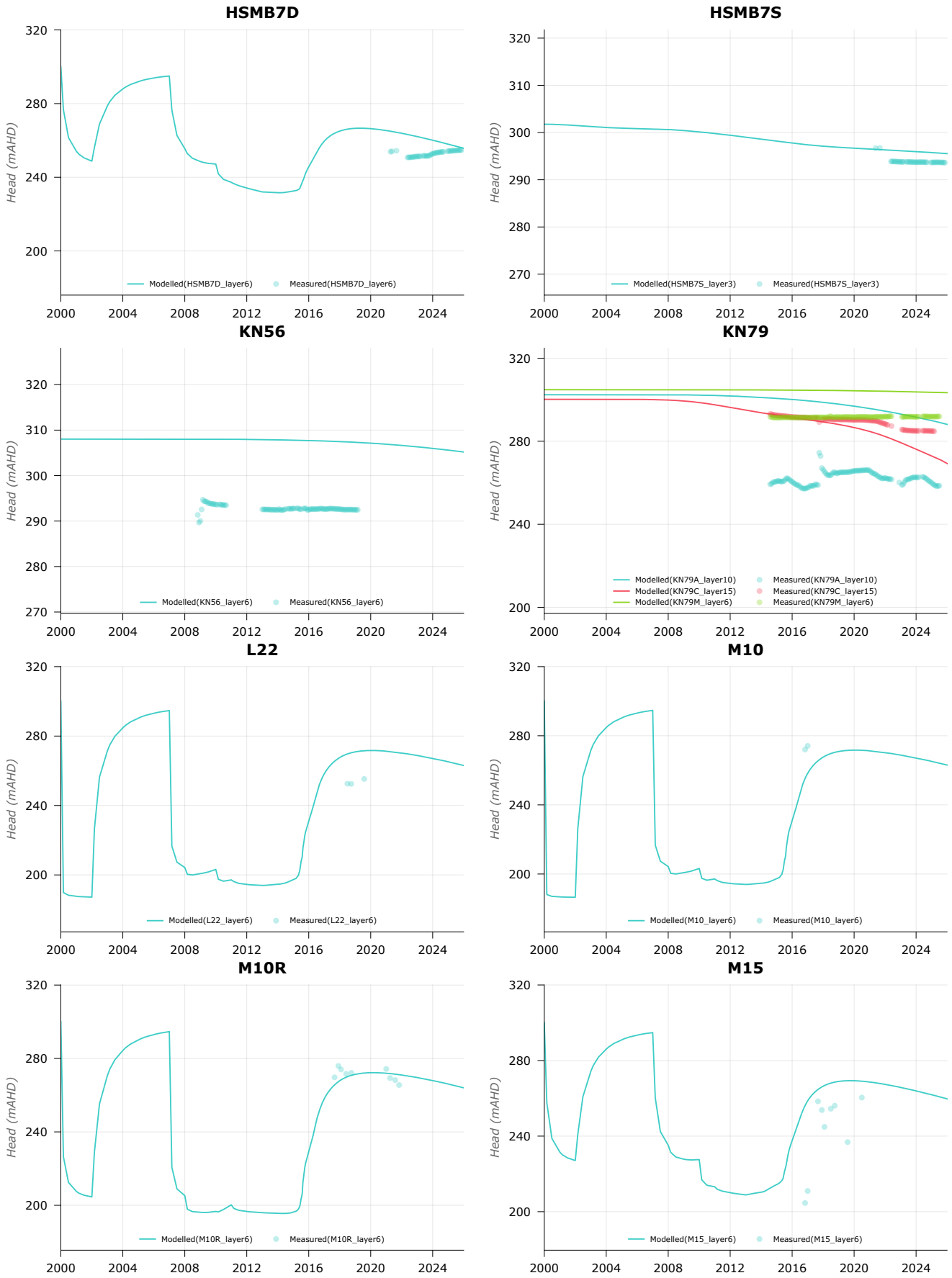
HL35

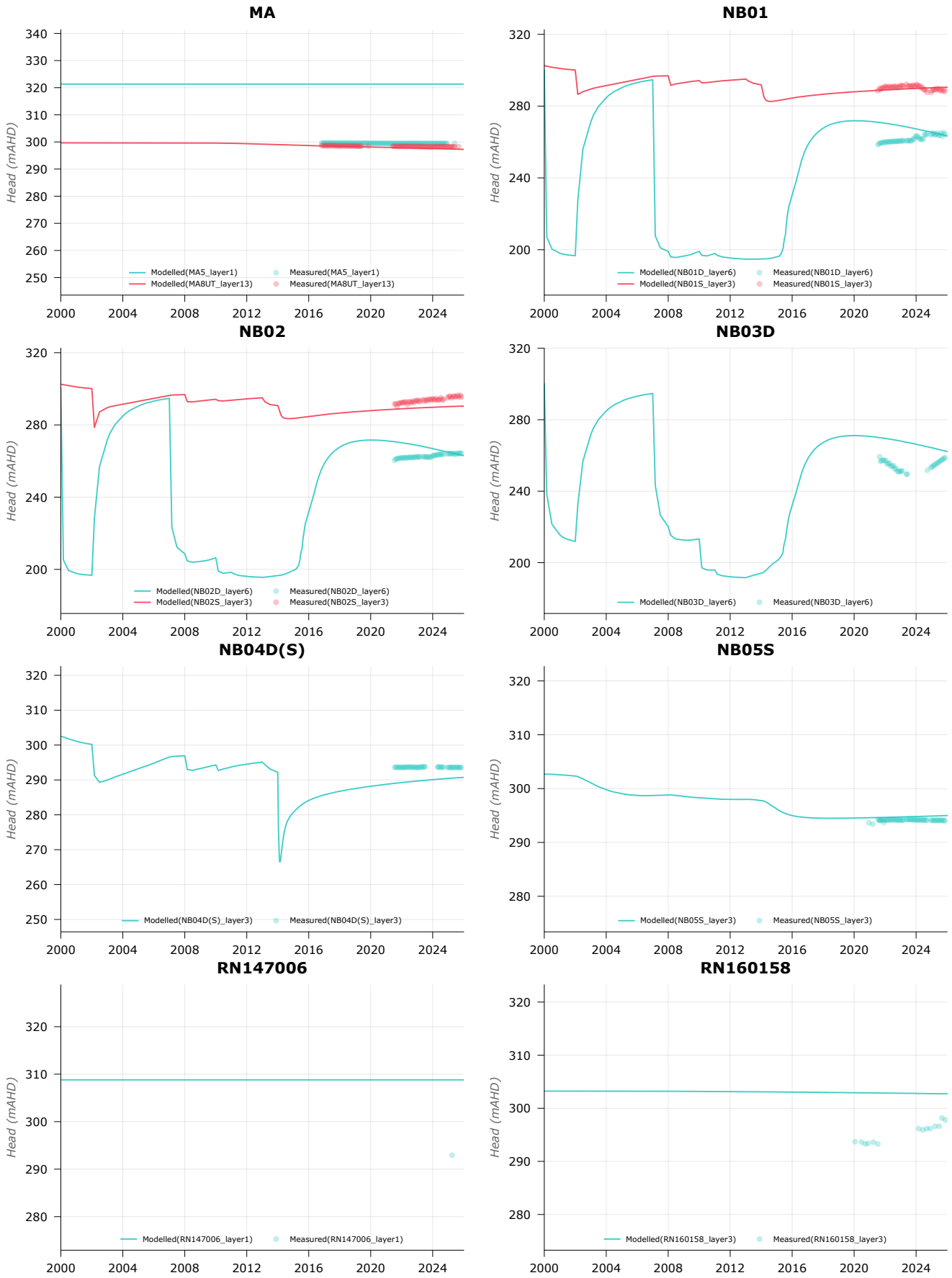


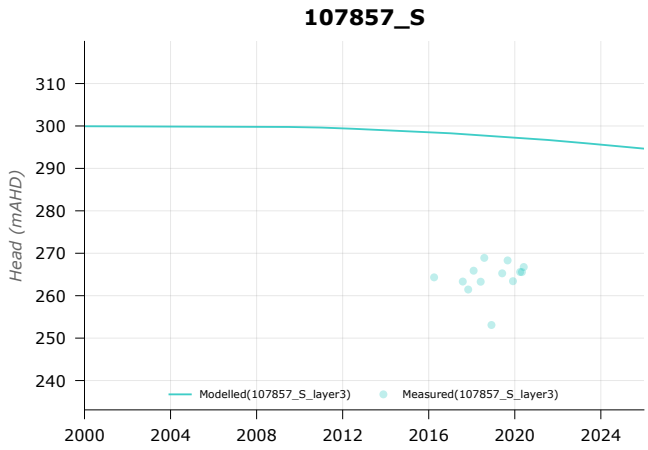
HL36

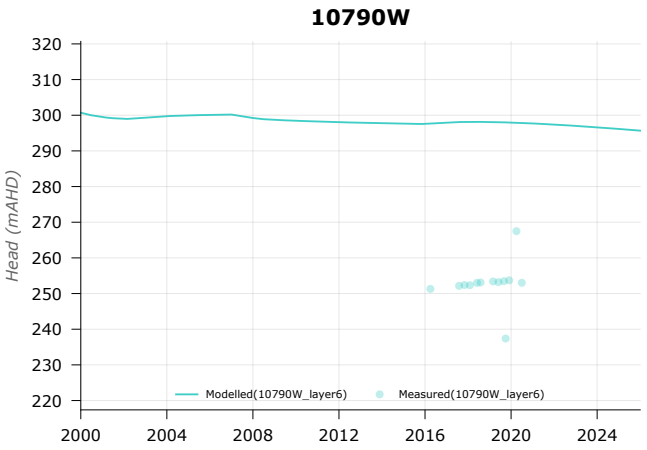


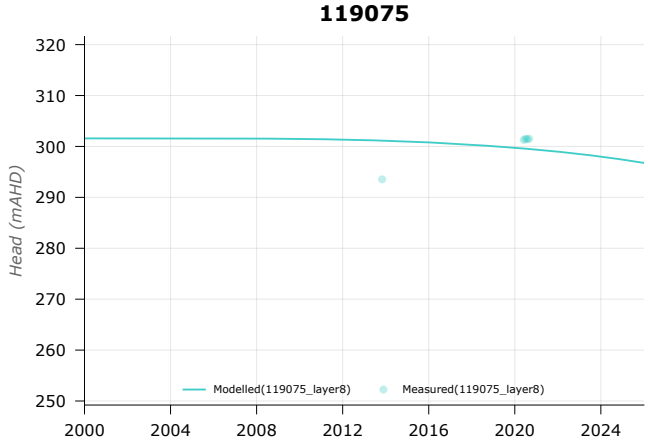

HL37
Head (mAHD)
320
280
240
2000
2004
2008
2012
2016
2020
2024
Modelled(HL37_layer3)
Measured(HL37_layer3)
HSMB1
200
Modelled(HSMB1D_layer6)
Measured(HSMB1D_layer6)
Modelled(HSMB1S_layer3)
Measured(HSMB1S_layer3)
HSMB2
Modelled(HSMB2D_layer6)
Measured(HSMB2D_layer6)
Modelled(HSMB2S_layer3)
Measured(HSMB2S_layer3)
HSMB3_1
Modelled(HSMB3D1_layer6)
Measured(HSMB3D1_layer6)
Modelled(HSMB3S1_layer3)
Measured(HSMB3S1_layer3)
HSMB3_2
Modelled(HSMB3D2_layer6)
Measured(HSMB3D2_layer6)
Modelled(HSMB3S2_layer3)
Measured(HSMB3S2_layer3)
HSMB4
Modelled(HSMB4D_layer6)
Measured(HSMB4D_layer6)
Modelled(HSMB4S_layer3)
Measured(HSMB4S_layer3)
HSMB5D
Modelled(HSMB5D_layer6)
Measured(HSMB5D_layer6)
HSMB6
Modelled(HSMB6D2_layer6)
Measured(HSMB6D2_layer6)
Modelled(HSMB6S_layer3)
Measured(HSMB6S_layer3)

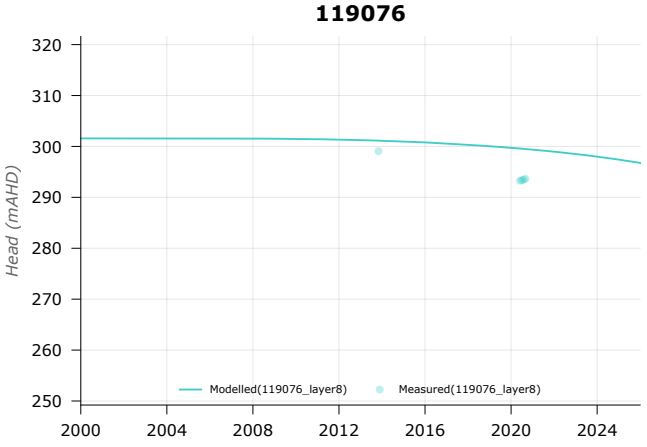

HSMB7D
Head (mAHD)
320
280
240
200
2000
2004
2008
2012
2016
2020
2024
Modelled(HSMB7D_layer6)
Measured(HSMB7D_layer6)
HSMB7S
Head (mAHD)
320
310
300
290
280
270
Modelled(HSMB7S_layer3)
Measured(HSMB7S_layer3)
KN56
Head (mAHD)
320
310
300
290
280
270
Modelled(KN56_layer6)
Measured(KN56_layer6)
KN79
Head (mAHD)
320
280
240
200
Modelled(KN79A_layer10)
Modelled(KN79C_layer15)
Modelled(KN79M_layer6)
Measured(KN79A_layer10)
Measured(KN79C_layer15)
Measured(KN79M_layer6)
L22
Head (mAHD)
320
280
240
200
Modelled(L22_layer6)
Measured(L22_layer6)
M10
Head (mAHD)
320
280
240
200
Modelled(M10_layer6)
Measured(M10_layer6)
M10R
Head (mAHD)
320
280
240
200
Modelled(M10R_layer6)
Measured(M10R_layer6)
M15
Head (mAHD)
320
280
240
200
Modelled(M15_layer6)
Measured(M15_layer6)

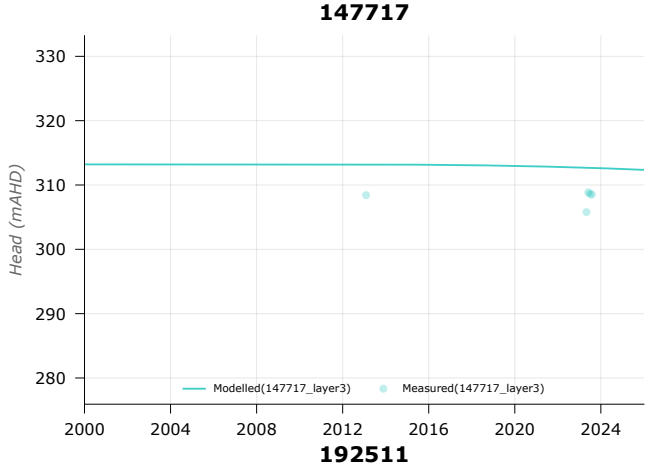

MA
Head (mAHD)
Modelled(MA5_layer1)
Measured(MA5_layer1)
Modelled(MA8UT_layer13)
Measured(MA8UT_layer13)
NB01
Modelled(NB01D_layer6)
Measured(NB01D_layer6)
Modelled(NB01S_layer3)
Measured(NB01S_layer3)
NB02
Modelled(NB02D_layer6)
Measured(NB02D_layer6)
Modelled(NB02S_layer3)
Measured(NB02S_layer3)
NB03D
Modelled(NB03D_layer6)
Measured(NB03D_layer6)
NB04D(S)
Modelled(NB04D(S)_layer3)
Measured(NB04D(S)_layer3)
NB05S
Modelled(NB05S_layer3)
Measured(NB05S_layer3)
RN147006
Modelled(RN147006_layer1)
Measured(RN147006_layer1)
RN160158
Modelled(RN160158_layer3)
Measured(RN160158_layer3)

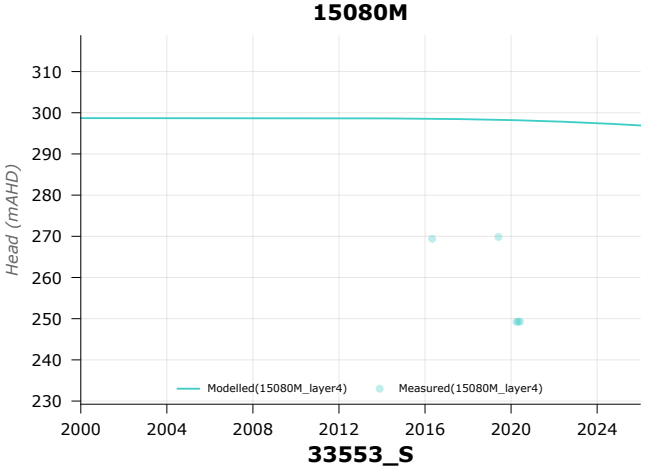

107857_S
Head (mAHD)
Modelled(107857_S_layer3)
Measured(107857_S_layer3)

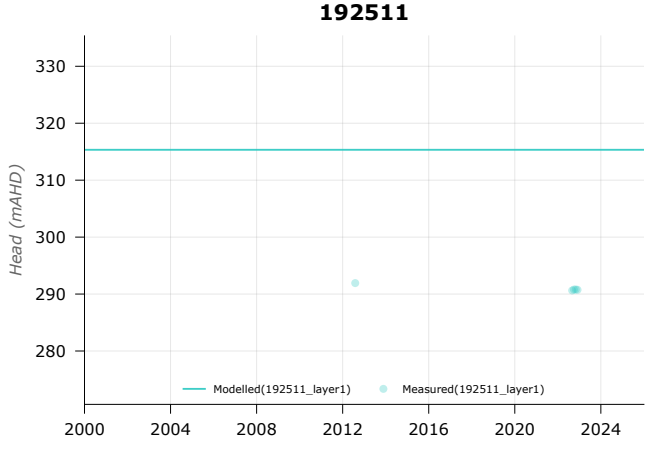

10790W
Head (mAHD)
Modelled(10790W_layer6)
Measured(10790W_layer6)

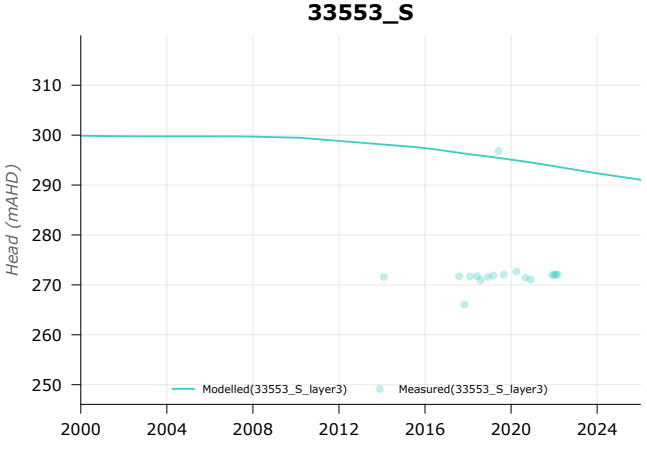

119075
Head (mAHD)
Modelled(119075_layer8)
Measured(119075_layer8)

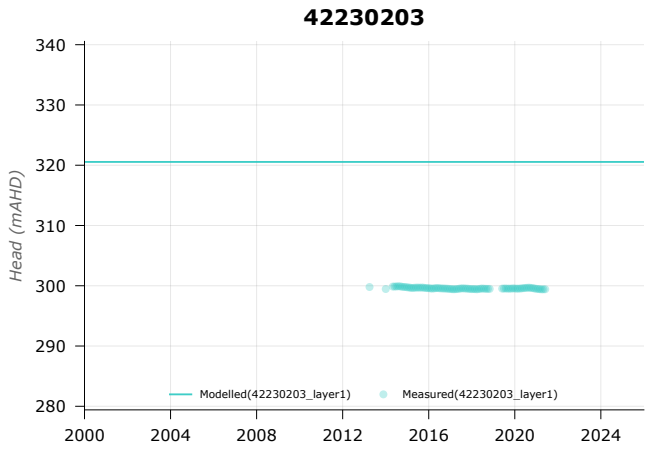

119076
Head (mAHD)
Modelled(119076_layer8)
Measured(119076_layer8)

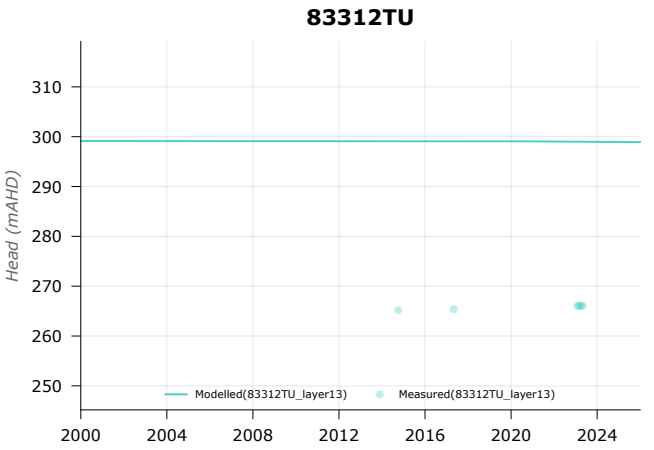

147717
Head (mAHD)
Modelled(147717_layer3)
Measured(147717_layer3)

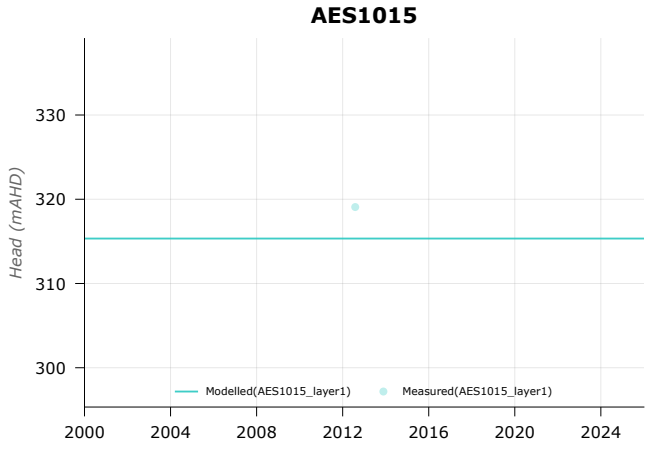

15080M
Head (mAHD)
Modelled(15080M_layer4)
Measured(15080M_layer4)

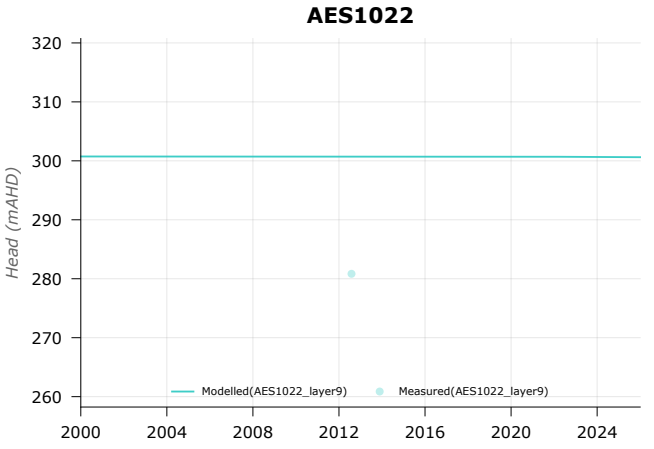

192511
Head (mAHD)
Modelled(192511_layer1)
Measured(192511_layer1)

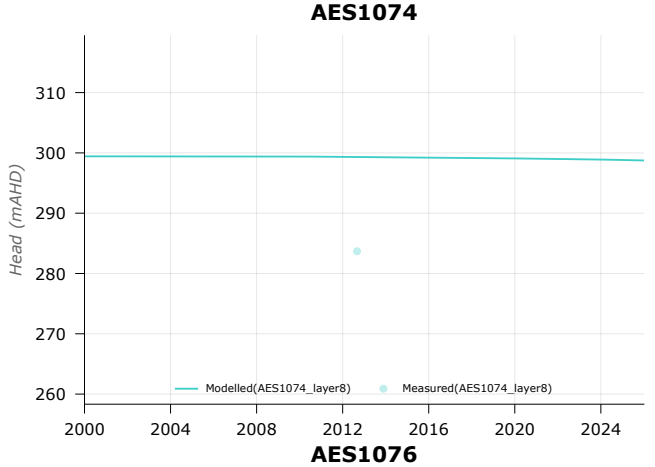

33553_S
Head (mAHD)
Modelled(33553_S_layer3)
Measured(33553_S_layer3)

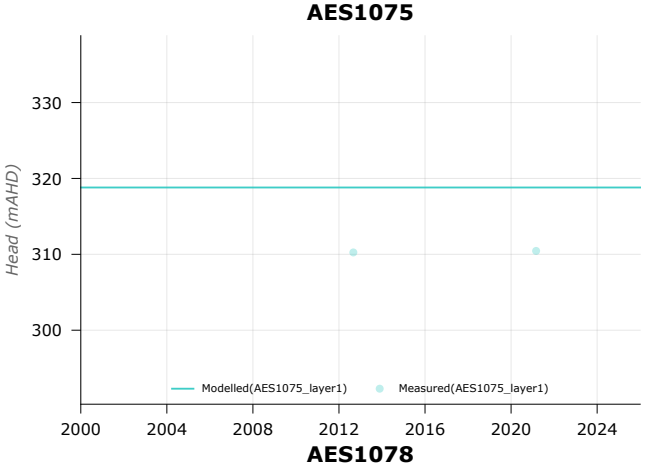

42230203
Head (mAHD)
340
330
320
310
300
290
280
2000
2004
2008
2012
2016
2020
2024
Modelled(42230203_layer1)
Measured(42230203_layer1)

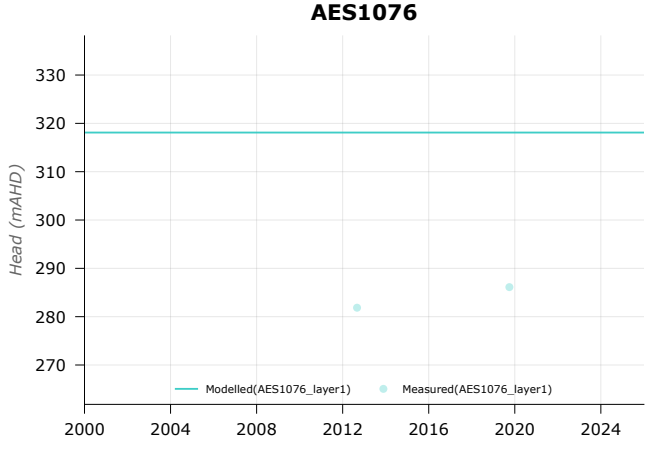

83312TU
Head (mAHD)
310
300
290
280
270
260
250
2000
2004
2008
2012
2016
2020
2024
Modelled(83312TU_layer13)
Measured(83312TU_layer13)

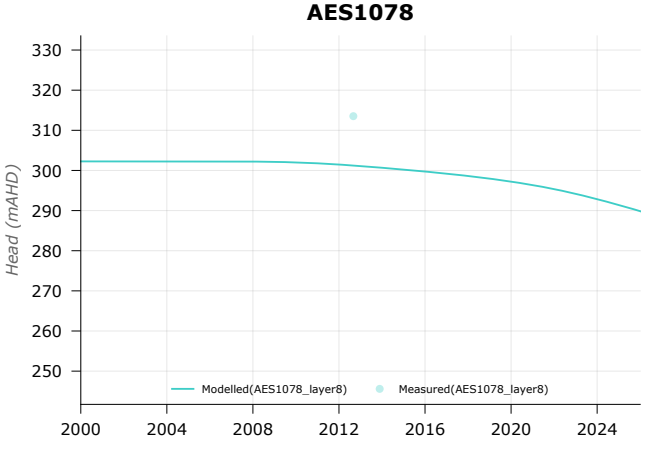

AES1015
Head (mAHD)
330
320
310
300
2000
2004
2008
2012
2016
2020
2024
Modelled(AES1015_layer1)
Measured(AES1015_layer1)

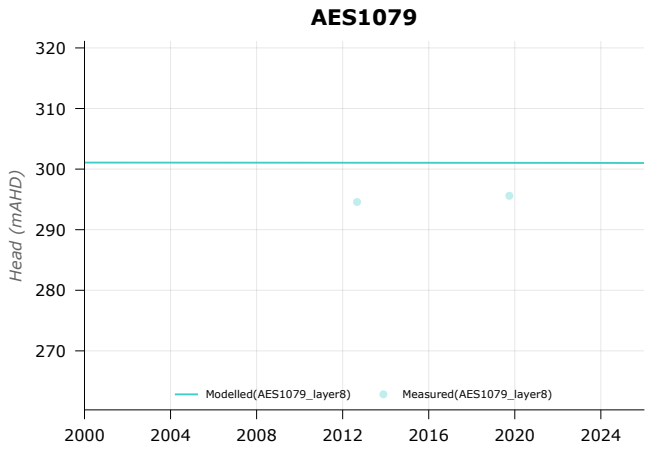

AES1022
Head (mAHD)
320
310
300
290
280
270
260
2000
2004
2008
2012
2016
2020
2024
Modelled(AES1022_layer9)
Measured(AES1022_layer9)

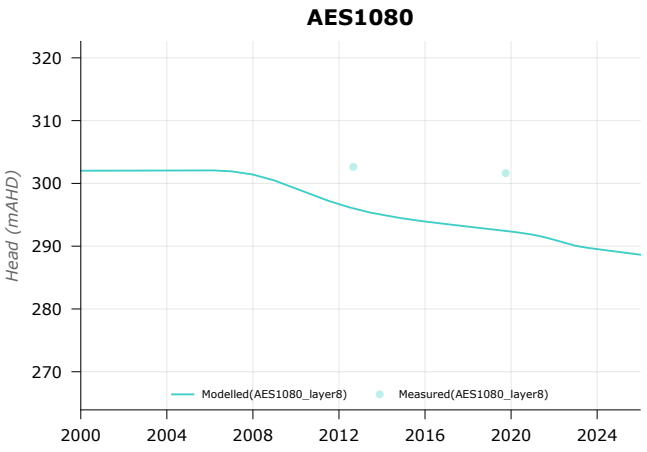

AES1074
Head (mAHD)
310
300
290
280
270
260
2000
2004
2008
2012
2016
2020
2024
Modelled(AES1074_layer8)
Measured(AES1074_layer8)

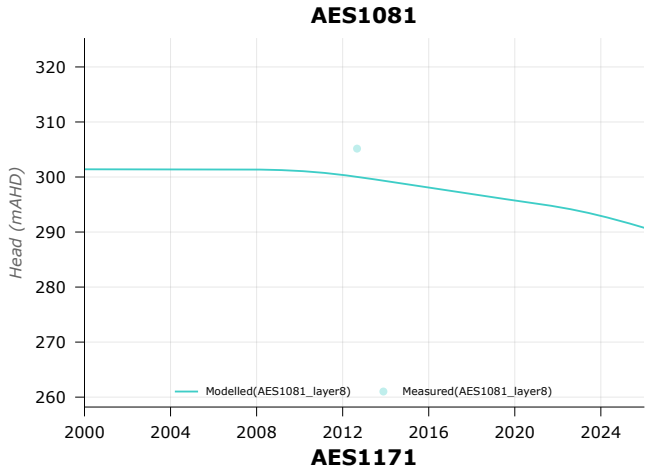

AES1075
Head (mAHD)
330
320
310
300
2000
2004
2008
2012
2016
2020
2024
Modelled(AES1075_layer1)
Measured(AES1075_layer1)

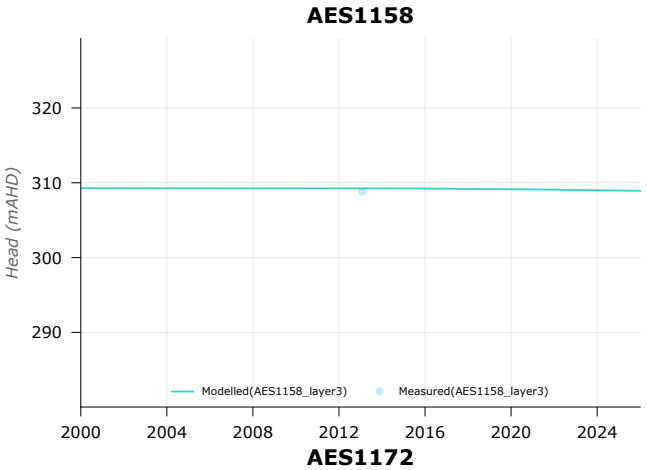

AES1076
Head (mAHD)
330
320
310
300
290
280
270
2000
2004
2008
2012
2016
2020
2024
Modelled(AES1076_layer1)
Measured(AES1076_layer1)

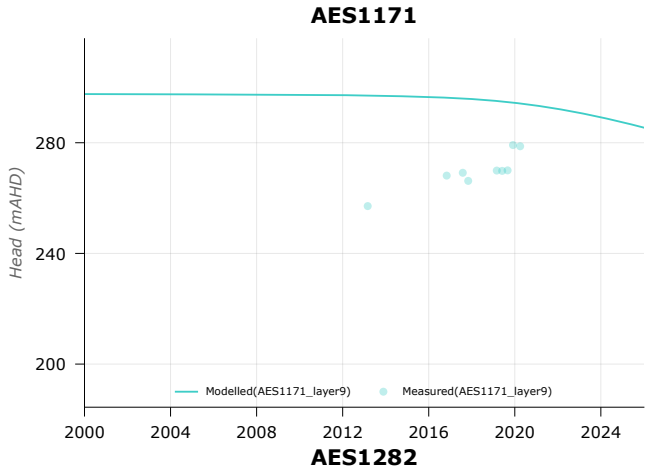

AES1078
Head (mAHD)
330
320
310
300
290
280
270
260
250
2000
2004
2008
2012
2016
2020
2024
Modelled(AES1078_layer8)
Measured(AES1078_layer8)

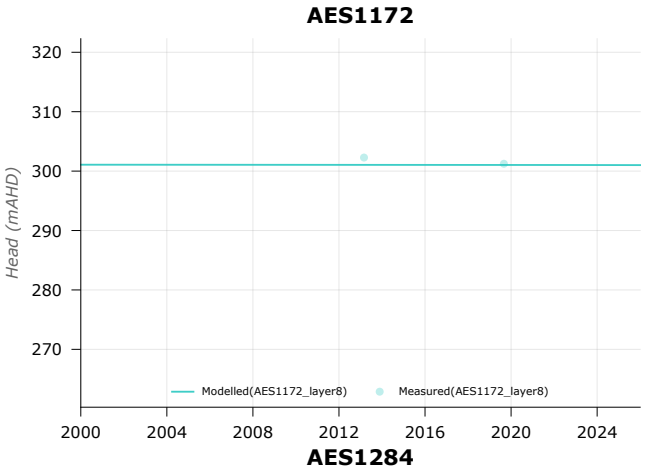

AES1079
Head (mAHD)
320
310
300
290
280
270
2000
2004
2008
2012
2016
2020
2024
Modelled(AES1079_layer8)
Measured(AES1079_layer8)

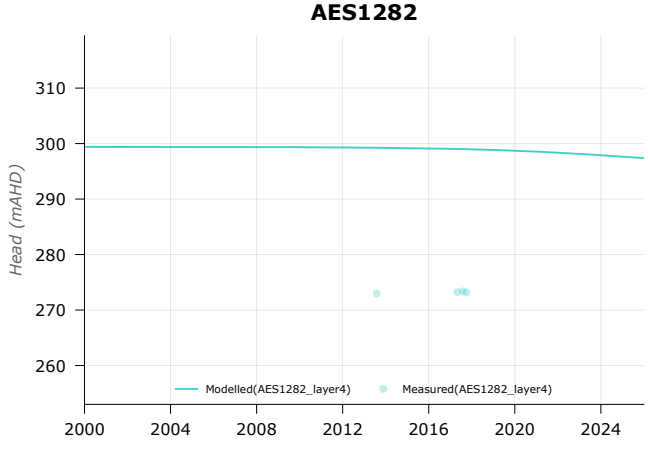

AES1080
Head (mAHD)
320
310
300
290
280
270
2000
2004
2008
2012
2016
2020
2024
Modelled(AES1080_layer8)
Measured(AES1080_layer8)

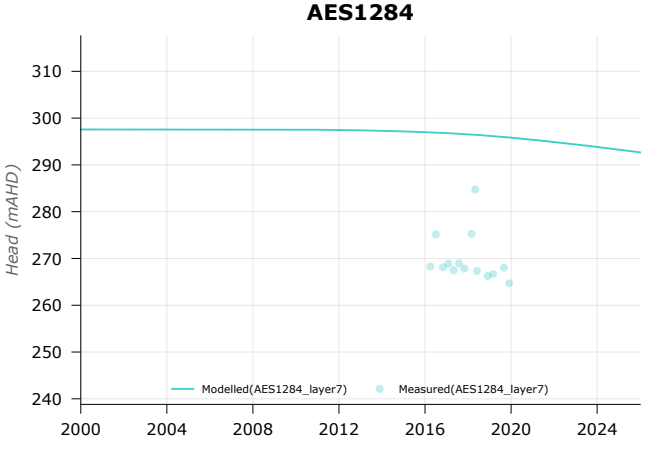

AES1081
Head (mAHD)
320
310
300
290
280
270
260
2000
2004
2008
2012
2016
2020
2024
Modelled(AES1081_layer8)
Measured(AES1081_layer8)

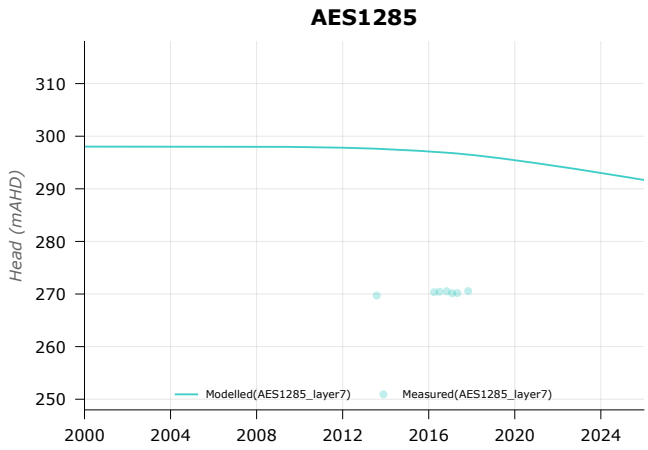

AES1158
Head (mAHD)
320
310
300
290
2000
2004
2008
2012
2016
2020
2024
Modelled(AES1158_layer3)
Measured(AES1158_layer3)

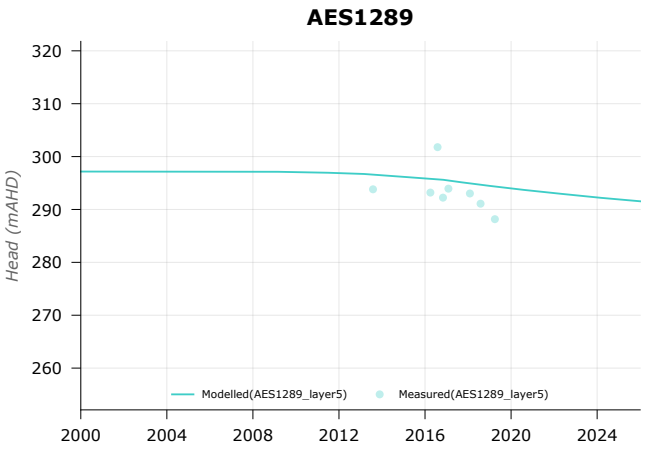

AES1171
Head (mAHD)
280
240
200
2000
2004
2008
2012
2016
2020
2024
Modelled(AES1171_layer9)
Measured(AES1171_layer9)

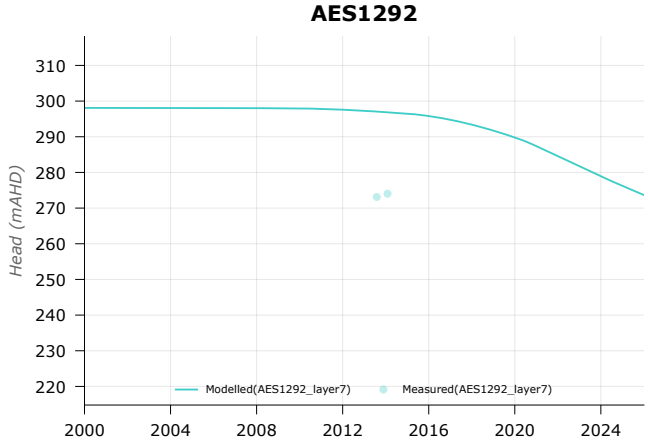

AES1172
Head (mAHD)
320
310
300
290
280
270
2000
2004
2008
2012
2016
2020
2024
Modelled(AES1172_layer8)
Measured(AES1172_layer8)

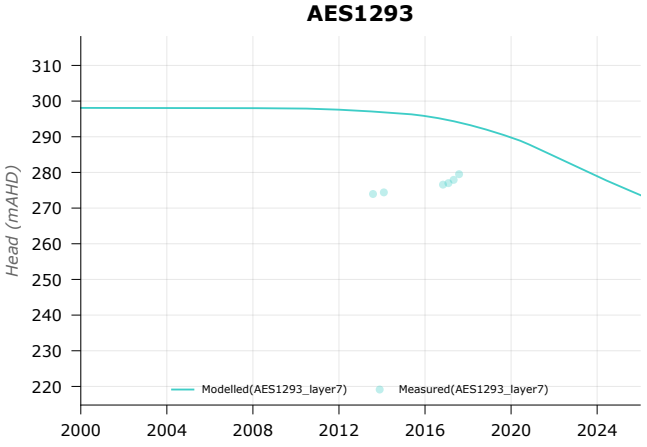

AES1282
Head (mAHD)
310
300
290
280
270
260
2000
2004
2008
2012
2016
2020
2024
Modelled(AES1282_layer4)
Measured(AES1282_layer4)

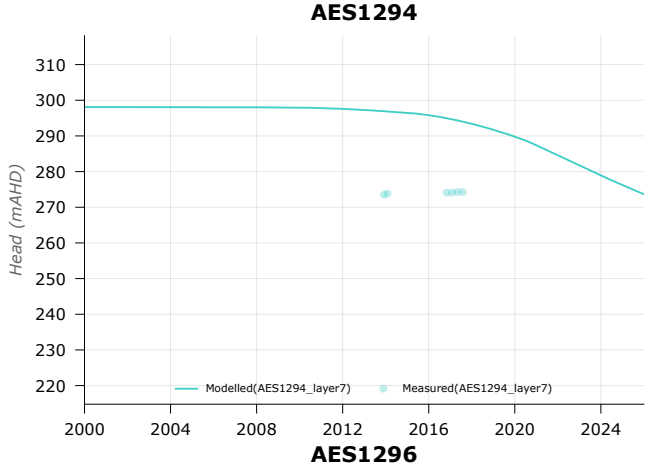

AES1284
Head (mAHD)
310
300
290
280
270
260
250
240
2000
2004
2008
2012
2016
2020
2024
Modelled(AES1284_layer7)
Measured(AES1284_layer7)

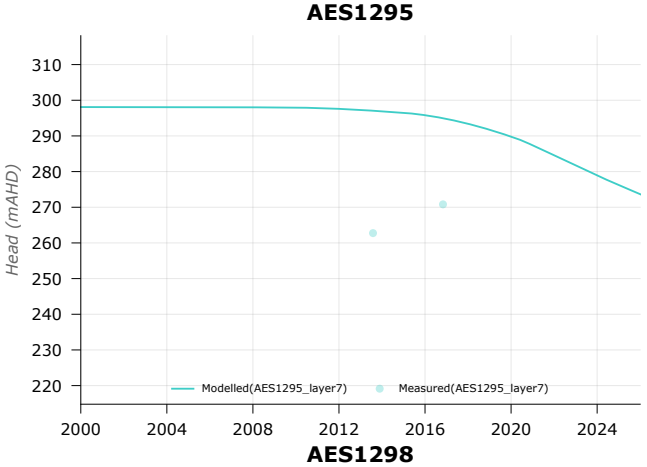

AES1285
Head (mAHD)
Modelled(AES1285_layer7)
Measured(AES1285_layer7)

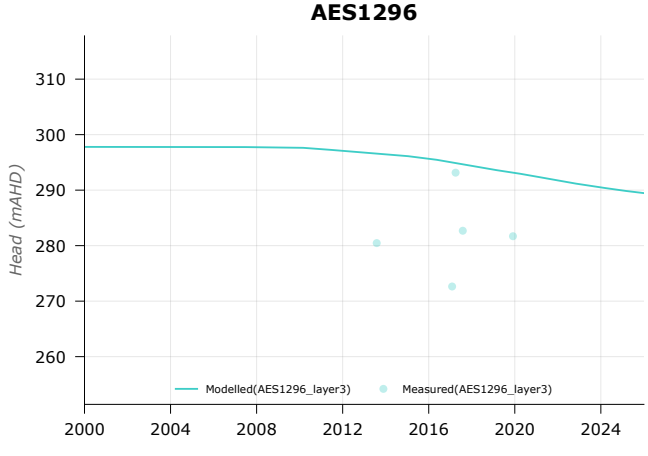

AES1289
Head (mAHD)
Modelled(AES1289_layer5)
Measured(AES1289_layer5)

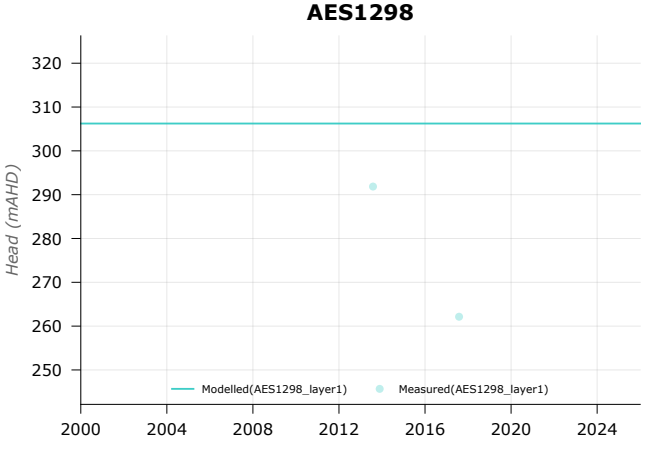

AES1292
Head (mAHD)
Modelled(AES1292_layer7)
Measured(AES1292_layer7)

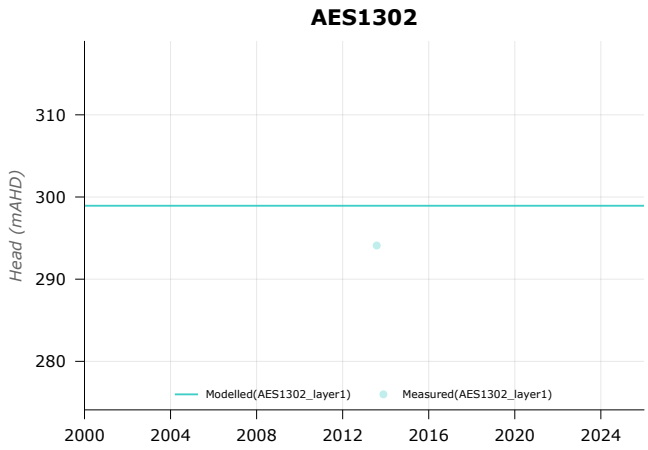

AES1293
Head (mAHD)
Modelled(AES1293_layer7)
Measured(AES1293_layer7)

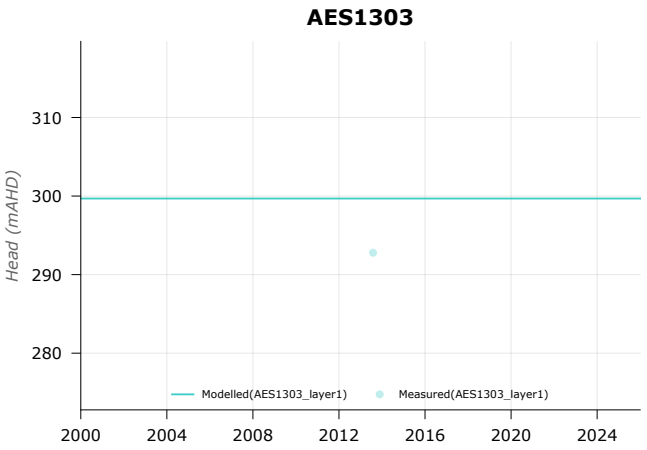

AES1294
Head (mAHD)
Modelled(AES1294_layer7)
Measured(AES1294_layer7)

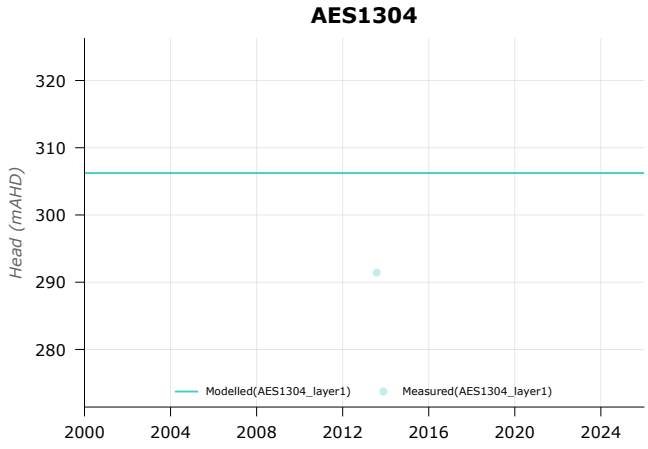

AES1295
Head (mAHD)
Modelled(AES1295_layer7)
Measured(AES1295_layer7)

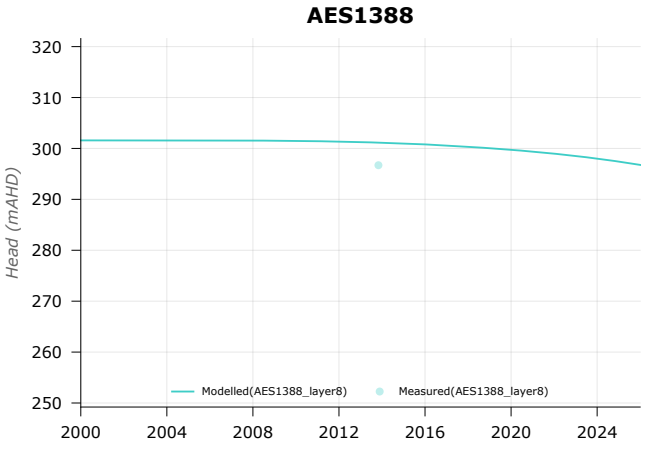

AES1296
Head (mAHD)
Modelled(AES1296_layer3)
Measured(AES1296_layer3)

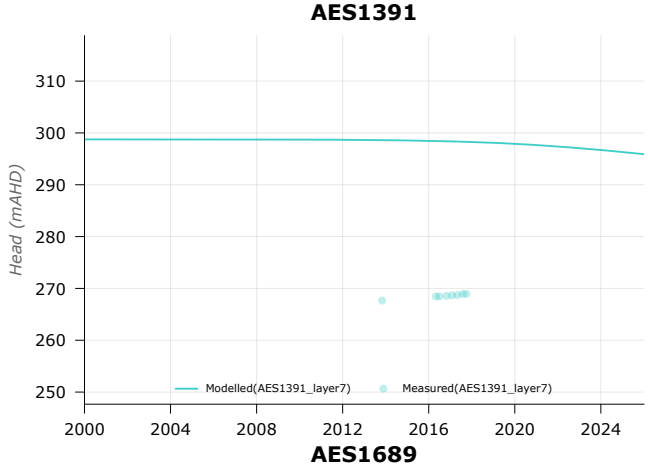

AES1298
Head (mAHD)
Modelled(AES1298_layer1)
Measured(AES1298_layer1)

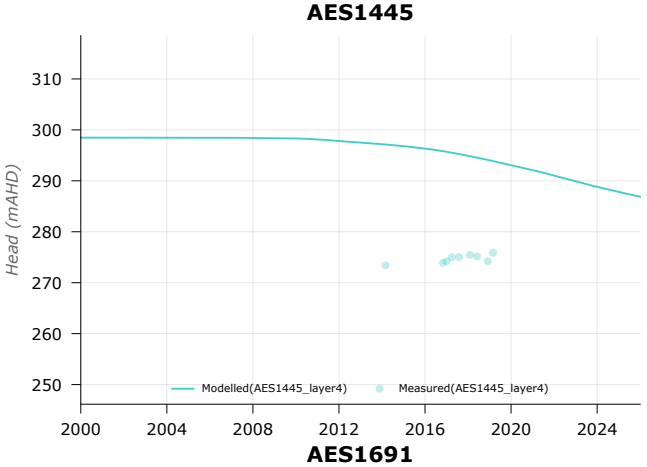

AES1302
Head (mAHD)
310
300
290
280
2000
2004
2008
2012
2016
2020
2024
Modelled(AES1302_layer1)
Measured(AES1302_layer1)

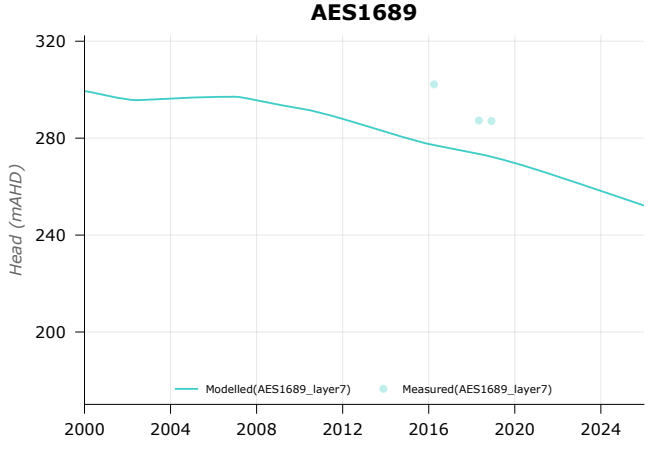

AES1303
Head (mAHD)
310
300
290
280
2000
2004
2008
2012
2016
2020
2024
Modelled(AES1303_layer1)
Measured(AES1303_layer1)

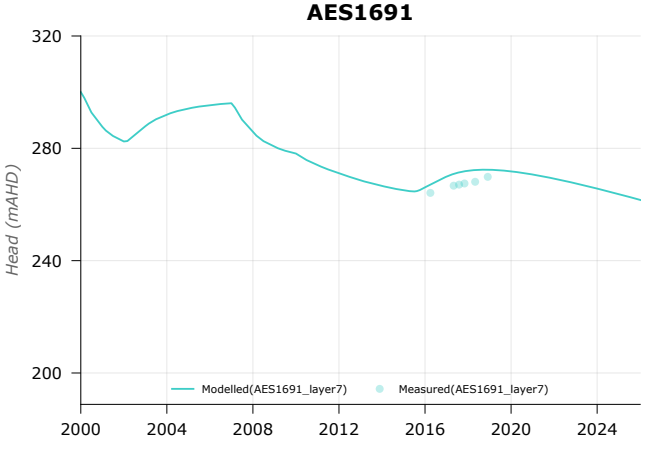

AES1304
Head (mAHD)
320
310
300
290
280
2000
2004
2008
2012
2016
2020
2024
Modelled(AES1304_layer1)
Measured(AES1304_layer1)

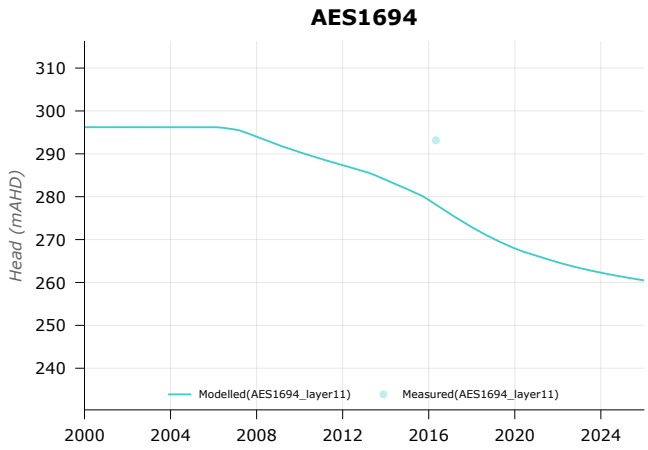

AES1388
Head (mAHD)
320
310
300
290
280
270
260
250
2000
2004
2008
2012
2016
2020
2024
Modelled(AES1388_layer8)
Measured(AES1388_layer8)

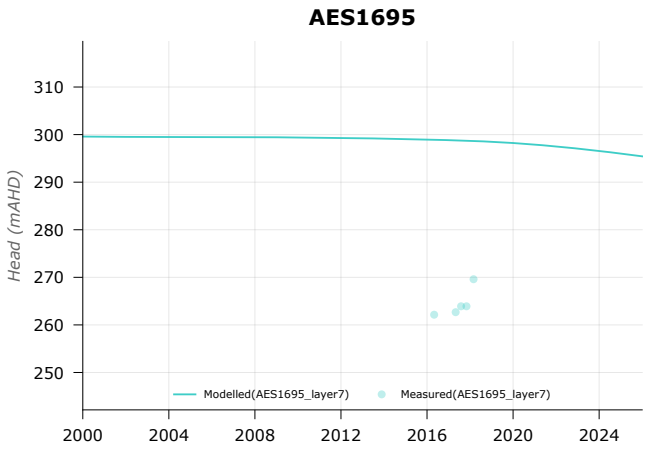

AES1391
Head (mAHD)
310
300
290
280
270
260
250
2000
2004
2008
2012
2016
2020
2024
Modelled(AES1391_layer7)
Measured(AES1391_layer7)

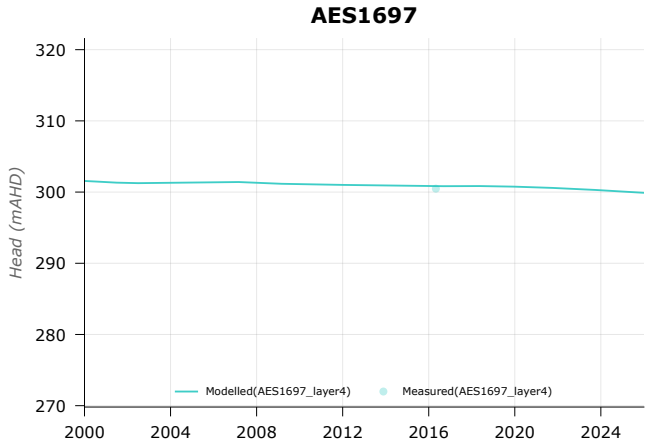

AES1445
Head (mAHD)
310
300
290
280
270
260
250
2000
2004
2008
2012
2016
2020
2024
Modelled(AES1445_layer4)
Measured(AES1445_layer4)

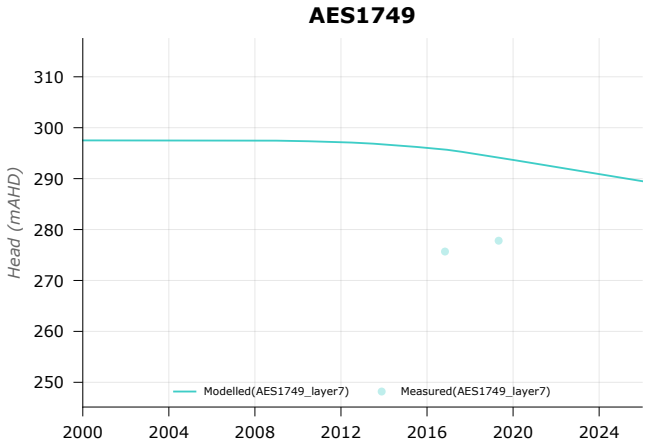

AES1689
Head (mAHD)
320
280
240
200
2000
2004
2008
2012
2016
2020
2024
Modelled(AES1689_layer7)
Measured(AES1689_layer7)

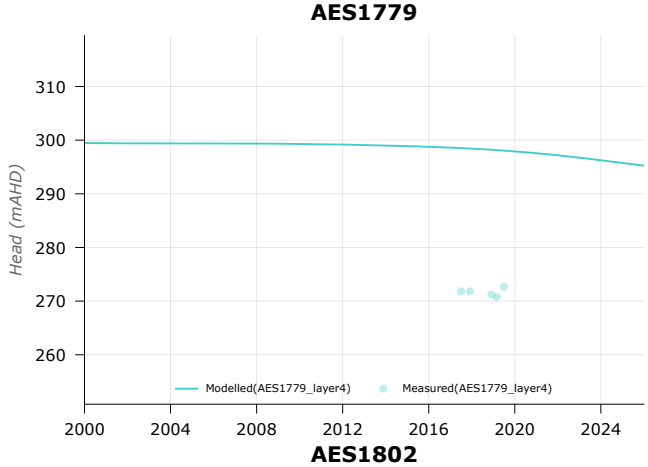

AES1691
Head (mAHD)
320
280
240
200
2000
2004
2008
2012
2016
2020
2024
Modelled(AES1691_layer7)
Measured(AES1691_layer7)

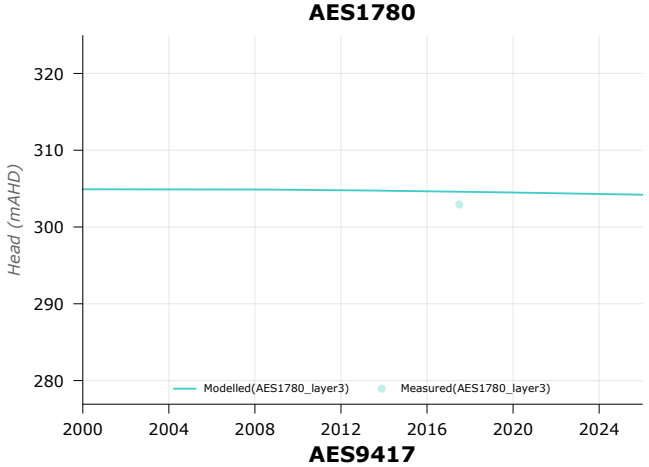

AES1694
Head (mAHD)
Modelled(AES1694_layer11)
Measured(AES1694_layer11)

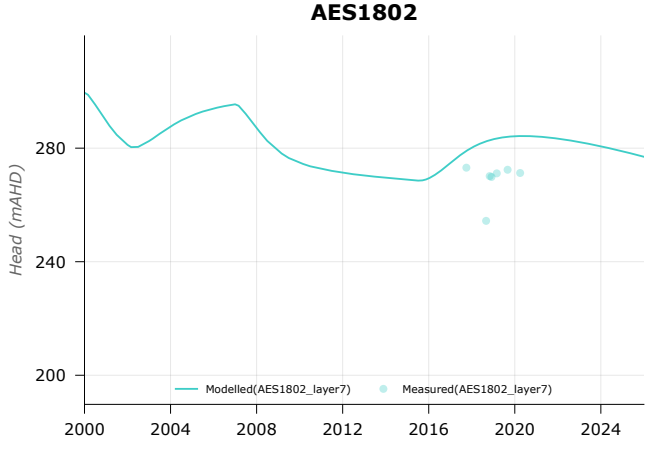

AES1695
Head (mAHD)
Modelled(AES1695_layer7)
Measured(AES1695_layer7)

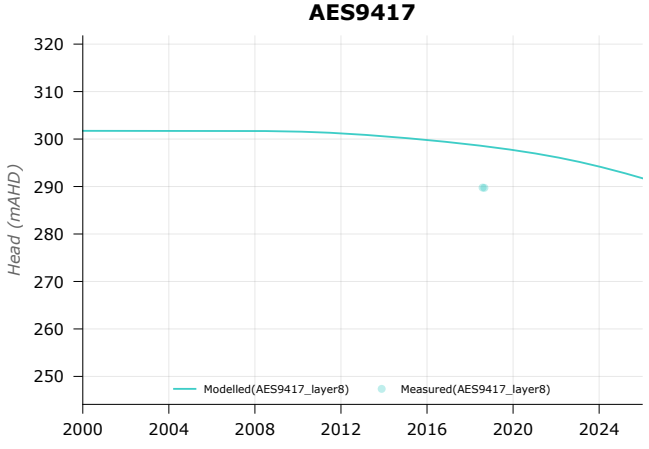

AES1697
Head (mAHD)
Modelled(AES1697_layer4)
Measured(AES1697_layer4)

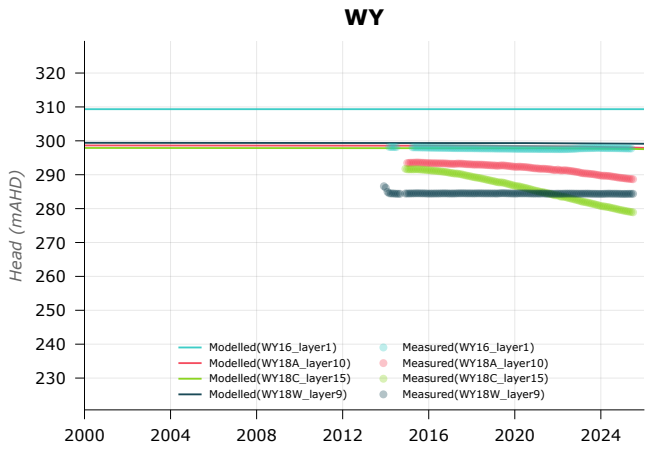

AES1749
Head (mAHD)
Modelled(AES1749_layer7)
Measured(AES1749_layer7)


AES1779
Head (mAHD)
Modelled(AES1779_layer4)
Measured(AES1779_layer4)


AES1780
Head (mAHD)
Modelled(AES1780_layer3)
Measured(AES1780_layer3)

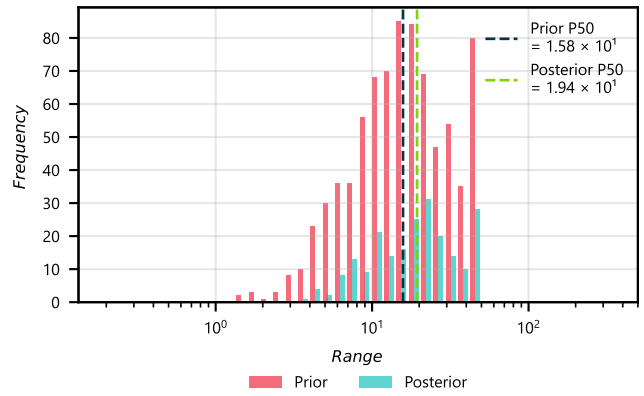

AES1802
Head (mAHD)
Modelled(AES1802_layer7)
Measured(AES1802_layer7)


AES9417
Head (mAHD)
Modelled(AES9417_layer8)
Measured(AES9417_layer8)

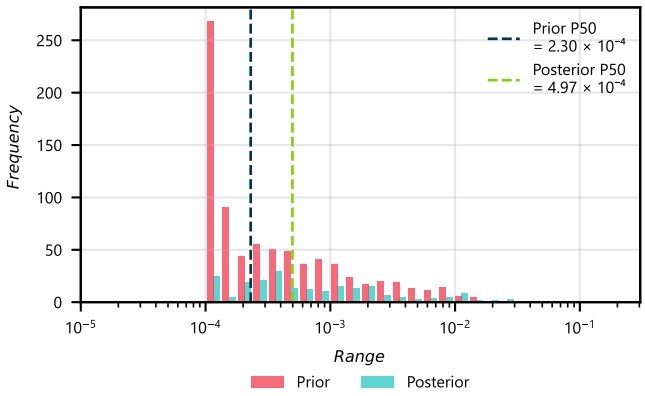

WY
Head (mAHD)
320
310
300
290
280
270
260
250
240
230
2000
2004
2008
2012
2016
2020
2024
Modelled(WY16_layer1)
Modelled(WY18A_layer10)
Modelled(WY18C_layer15)
Modelled(WY18W_layer9)
Measured(WY16_layer1)
Measured(WY18A_layer10)
Measured(WY18C_layer15)
Measured(WY18W_layer9)

Appendix B. Median prior and posterior parameter distributions

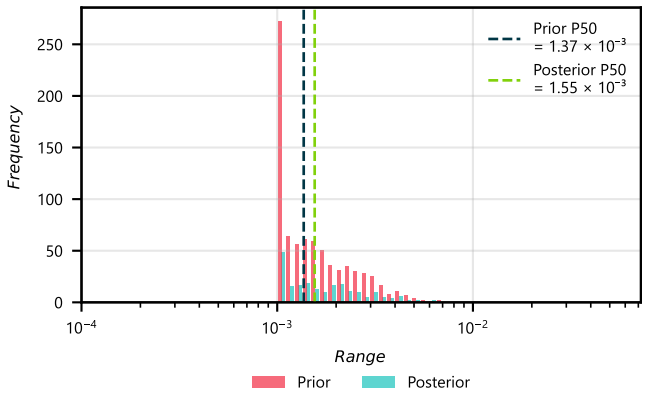
Kh:CondamineAlv



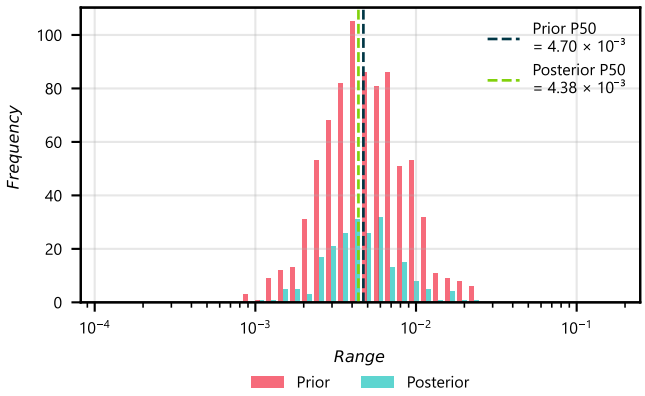
Kh:Gubb.Sst



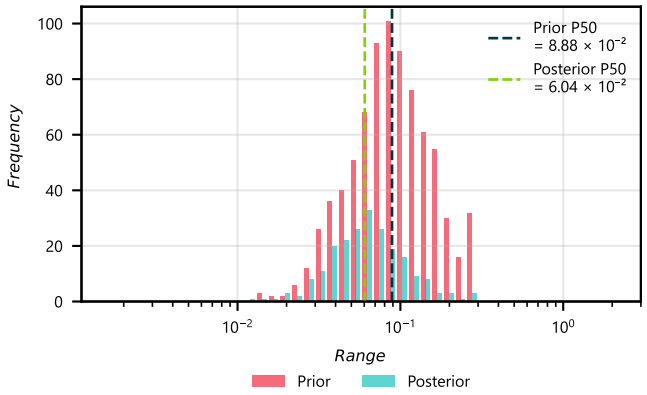
Kh:WestbourneFm



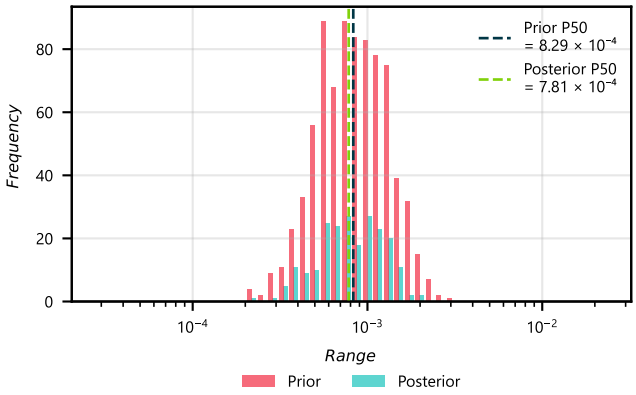
Kh:SpringbokSst



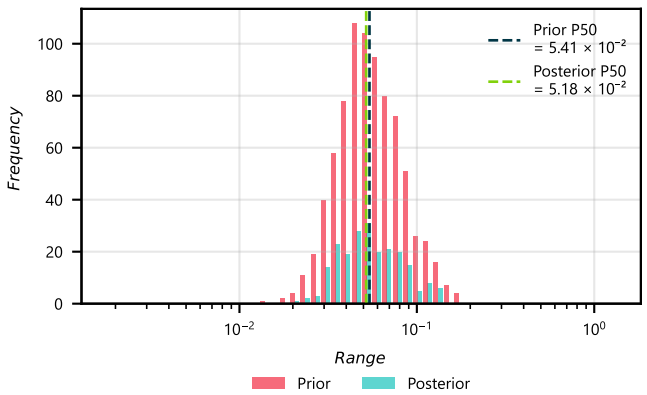
Kh:KoganC



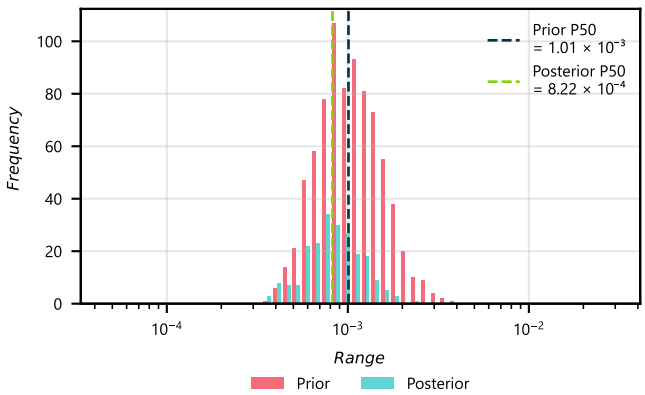
Kh:KoganIB

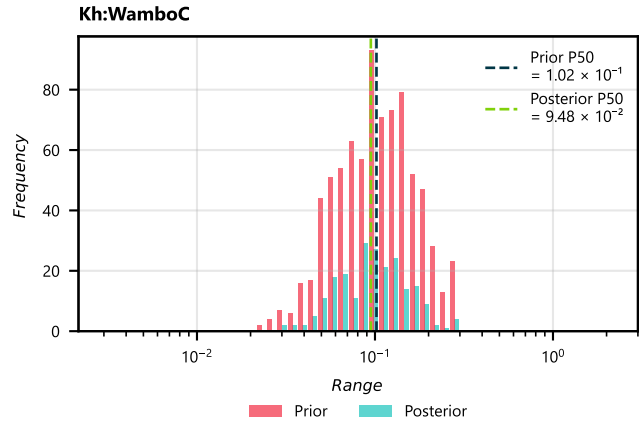


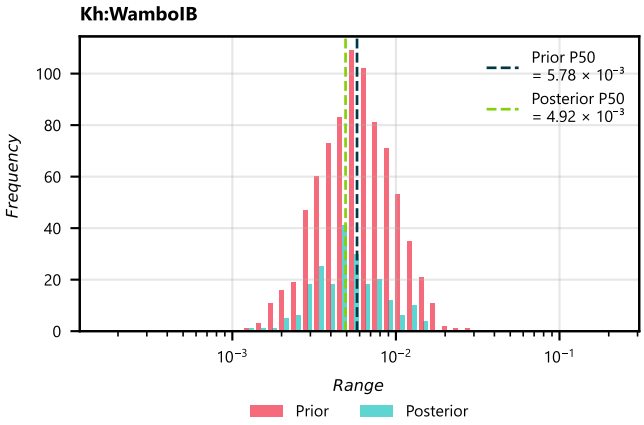
Kh:MacalisterC

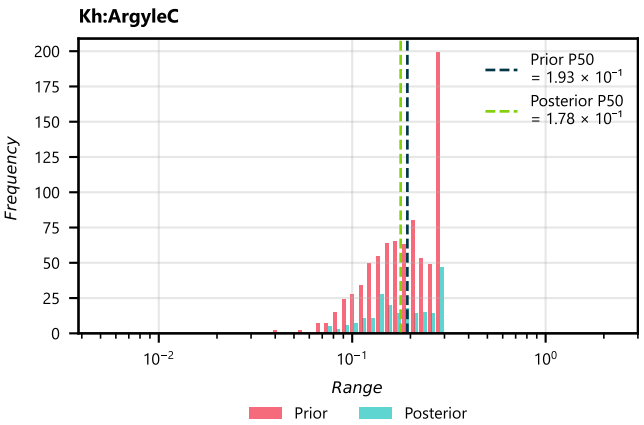


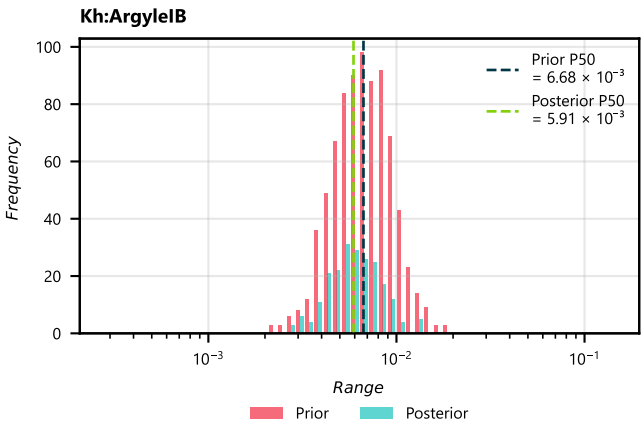
Kh:MacalisterIB

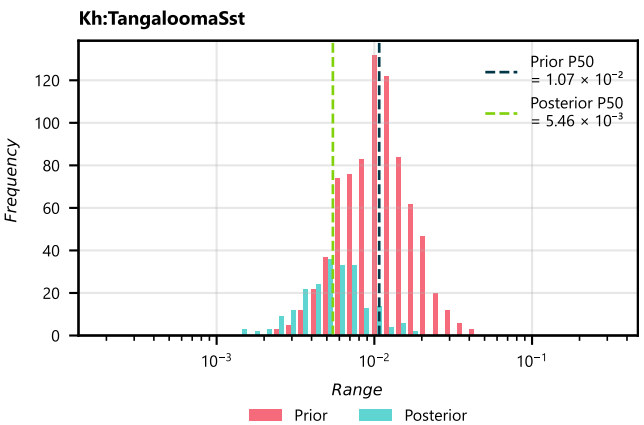


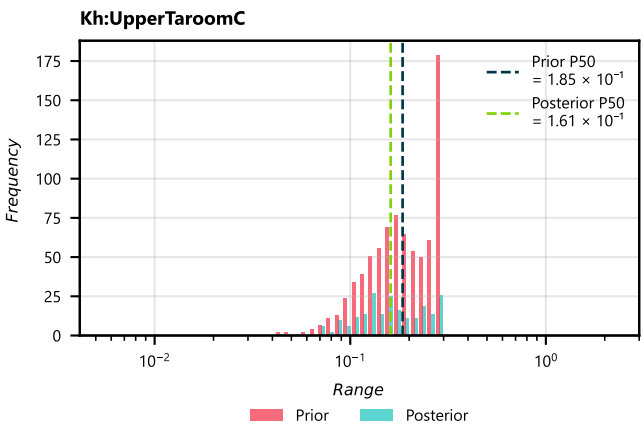

Kh:WamboC
Prior P50
= 1.02 × 10⁻¹
Posterior P50
= 9.48 × 10⁻²
Frequency
Range
Prior
Posterior

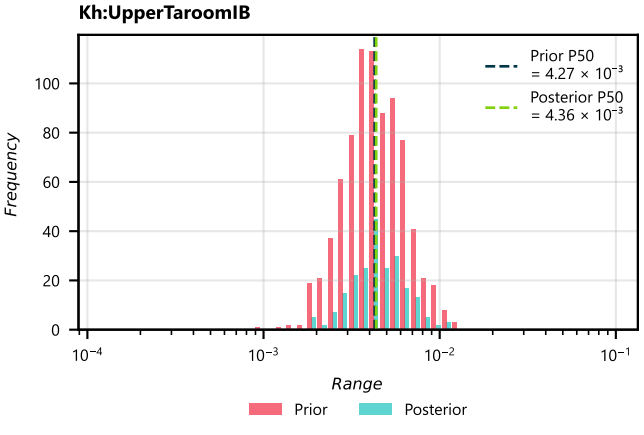

Kh:WamboIB
Prior P50
= 5.78 × 10⁻³
Posterior P50
= 4.92 × 10⁻³
Frequency
Range
Prior
Posterior

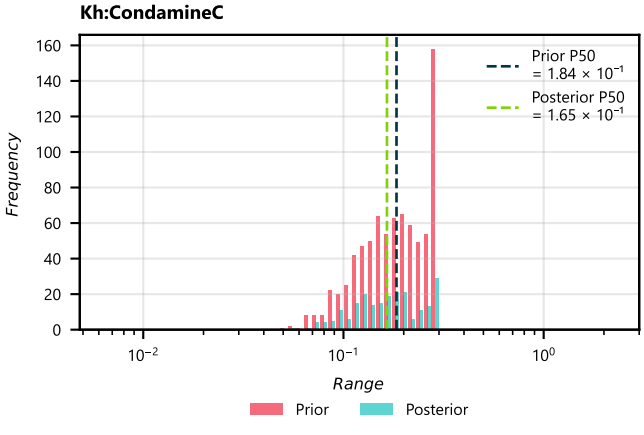

Kh:ArgyleC
Prior P50
= 1.93 × 10⁻¹
Posterior P50
= 1.78 × 10⁻¹
Frequency
Range
Prior
Posterior

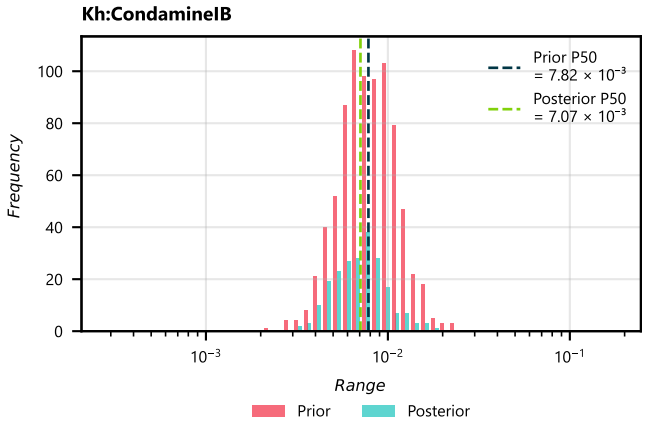

Kh:ArgyleIB
Prior P50
= 6.68 × 10⁻³
Posterior P50
= 5.91 × 10⁻³
Frequency
Range
Prior
Posterior

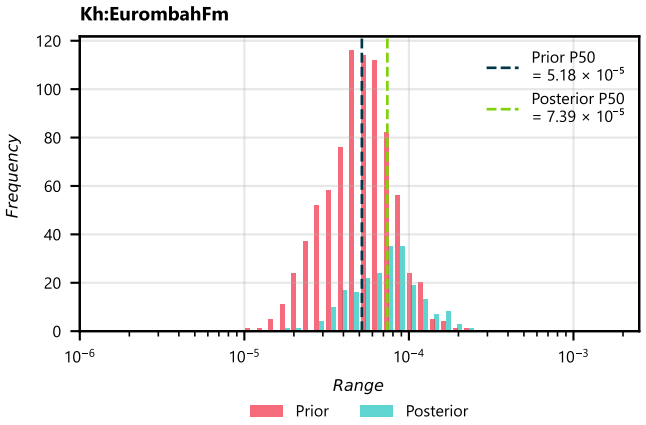

Kh:TangaloomaSst
Prior P50
= 1.07 × 10⁻²
Posterior P50
= 5.46 × 10⁻³
Frequency
Range
Prior
Posterior

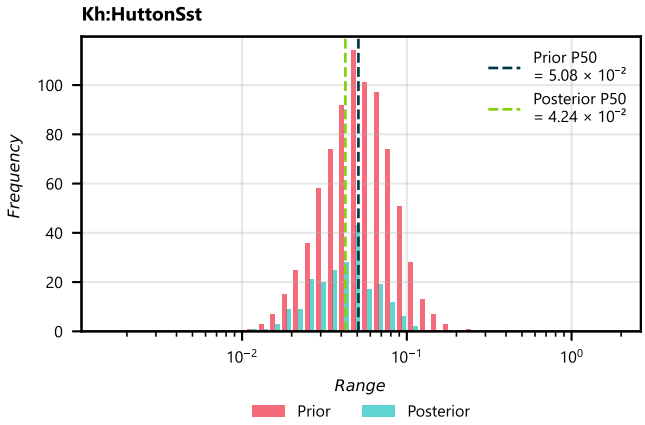

Kh:UpperTaroomC
Prior P50
= 1.85 × 10⁻¹
Posterior P50
= 1.61 × 10⁻¹
Frequency
Range
Prior
Posterior

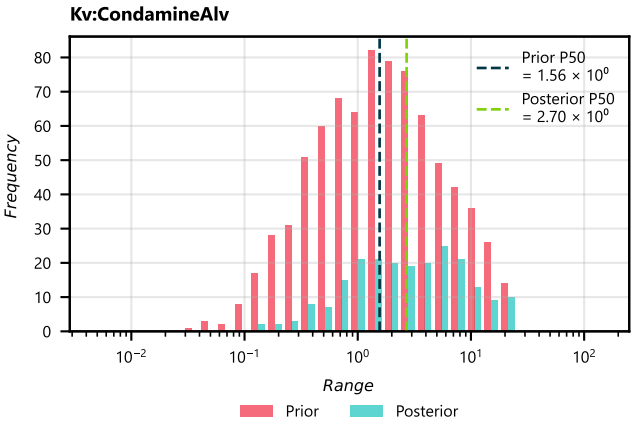

Kh:UpperTaroomIB
Prior P50
= 4.27 × 10⁻³
Posterior P50
= 4.36 × 10⁻³
Frequency
Range
Prior
Posterior

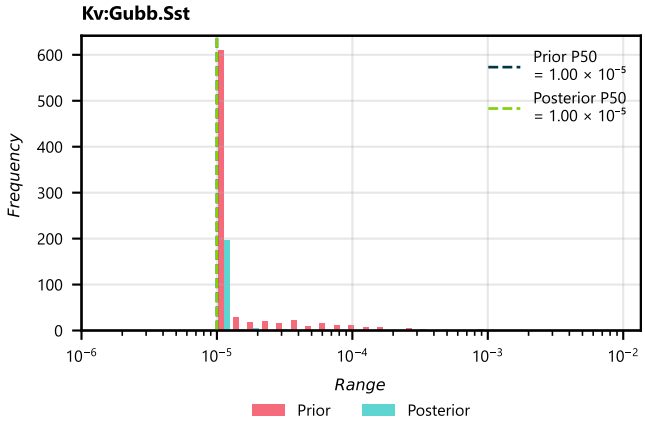

Kh:CondamineC
Prior P50
= 1.84 × 10⁻¹
Posterior P50
= 1.65 × 10⁻¹
Frequency
Range
Prior
Posterior

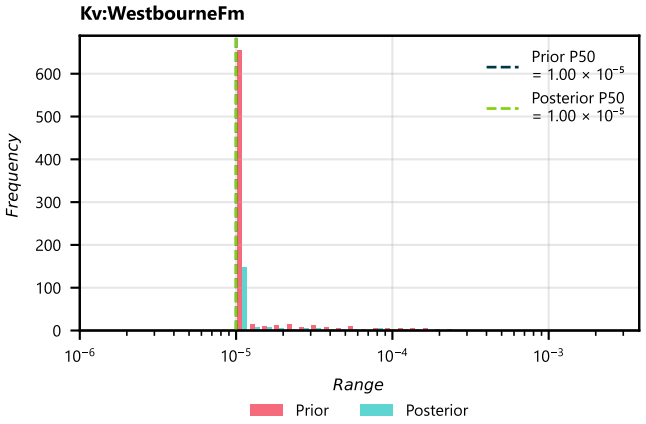

Kh:CondamineIB
Prior P50
= 7.82 × 10⁻³
Posterior P50
= 7.07 × 10⁻³
Frequency
Range
Prior
Posterior

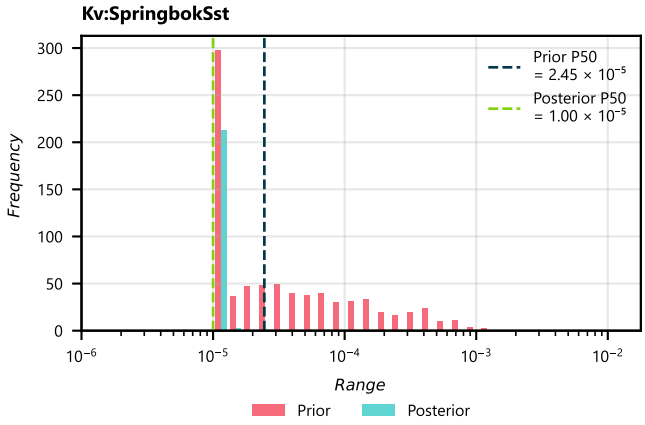

Kh:EurombahFm
Prior P50
= 5.18 × 10⁻⁵
Posterior P50
= 7.39 × 10⁻⁵
Frequency
Range
Prior
Posterior

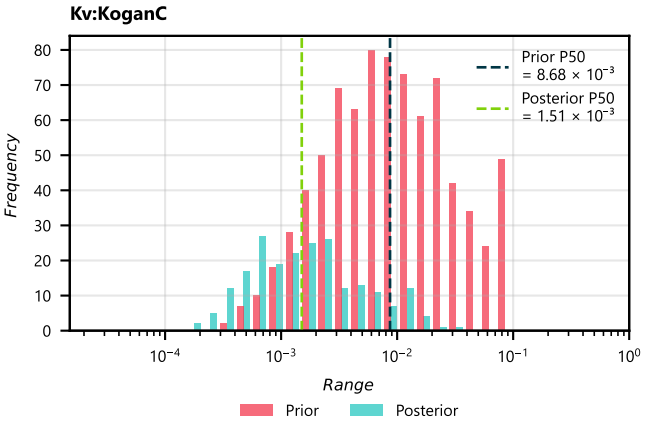

Kh:HuttonSst
Prior P50
= 5.08 × 10⁻²
Posterior P50
= 4.24 × 10⁻²
Frequency
Range
Prior
Posterior

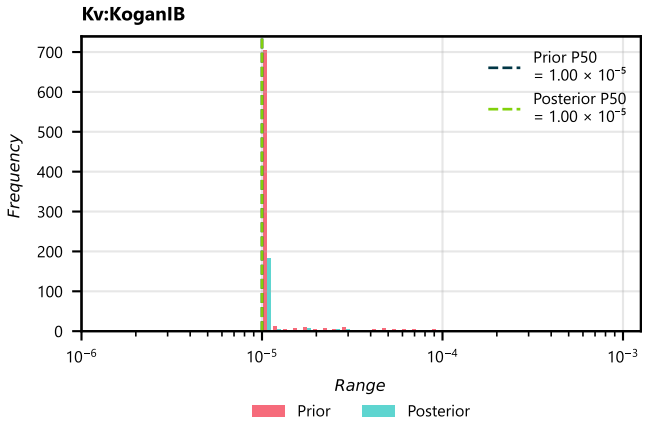

Kv:CondamineAlv
Prior P50
= 1.56 × 10⁰
Posterior P50
= 2.70 × 10⁰
Frequency
Range
Prior
Posterior

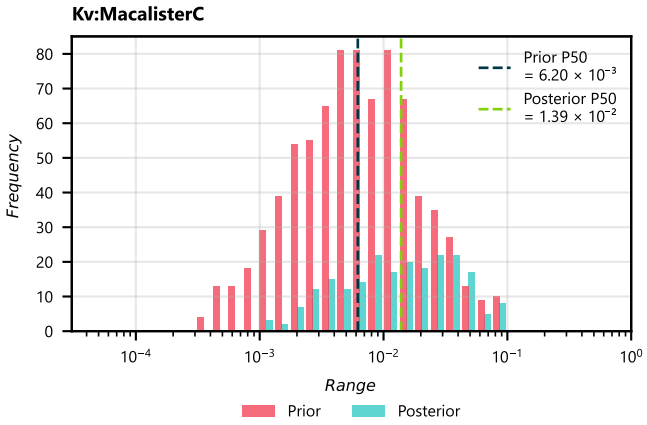

Kv:Gubb.Sst
Prior P50
= 1.00 × 10⁻⁵
Posterior P50
= 1.00 × 10⁻⁵
Frequency
Range
Prior
Posterior

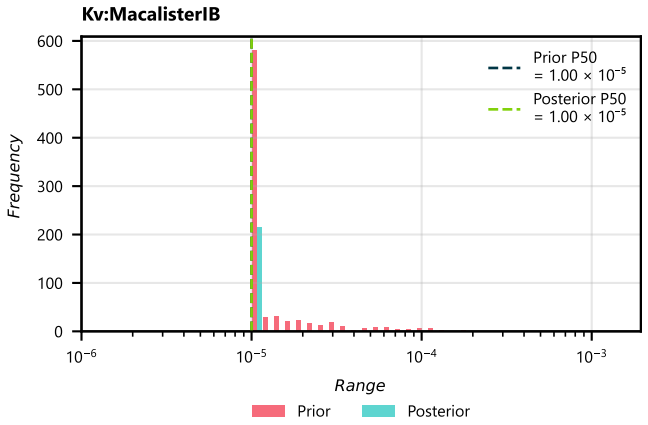

Kv:WestbourneFm
Prior P50
= 1.00 × 10⁻⁵
Posterior P50
= 1.00 × 10⁻⁵
Frequency
Range
Prior
Posterior

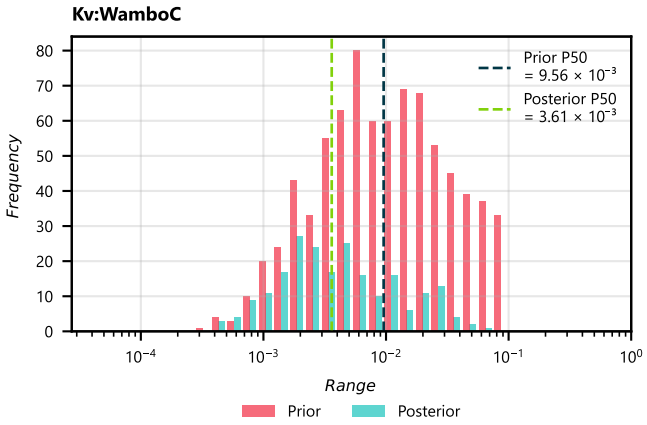

Kv:SpringbokSst
Prior P50
= 2.45 × 10⁻⁵
Posterior P50
= 1.00 × 10⁻⁵
Frequency
Range
Prior
Posterior

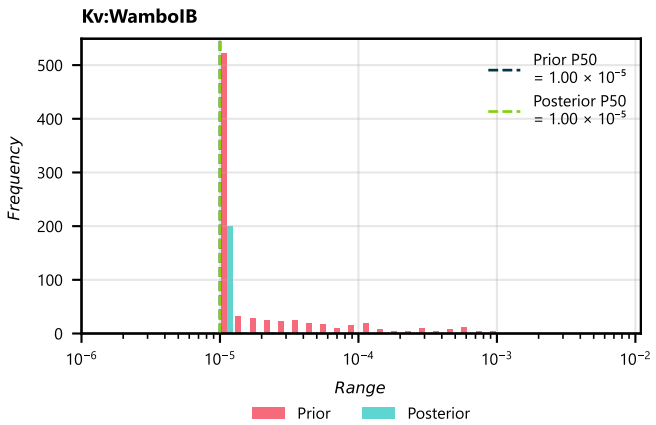

Kv:KoganC
Prior P50
= 8.68 × 10⁻³
Posterior P50
= 1.51 × 10⁻³
Frequency
Range
Prior
Posterior

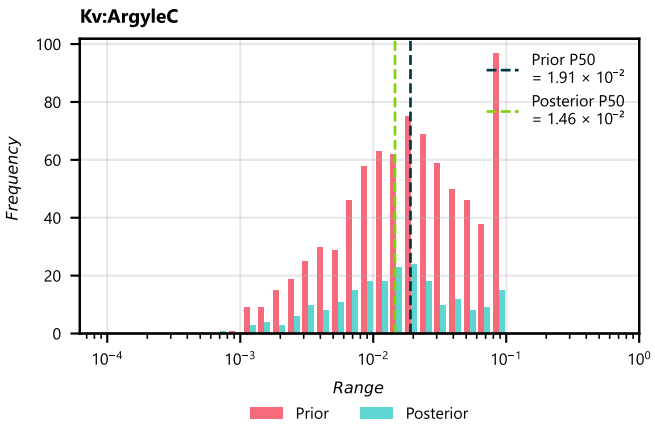

Kv:KoganIB
Prior P50
= 1.00 × 10⁻⁵
Posterior P50
= 1.00 × 10⁻⁵
Frequency
Range
Prior
Posterior

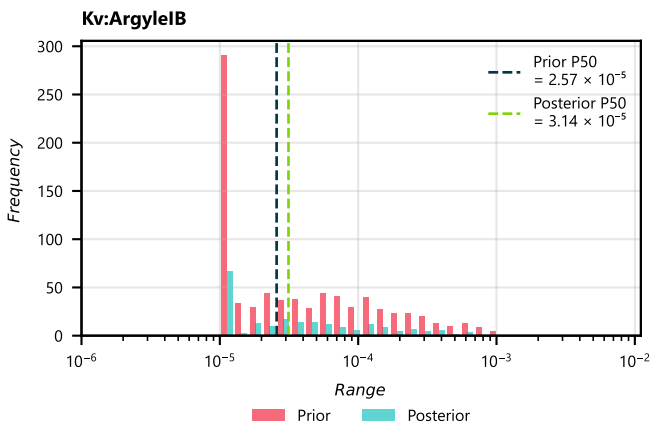

Kv:MacalisterC
Prior P50
= 6.20 × 10⁻³
Posterior P50
= 1.39 × 10⁻²
Frequency
Range
Prior
Posterior

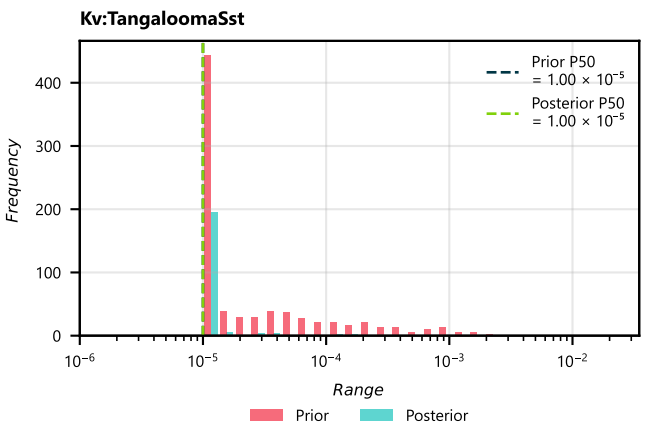

Kv:MacalisterIB
Prior P50
= 1.00 × 10⁻⁵
Posterior P50
= 1.00 × 10⁻⁵
Frequency
Range
Prior
Posterior


Kv:WamboC
Prior P50
= 9.56 × 10⁻³
Posterior P50
= 3.61 × 10⁻³
Frequency
Range
Prior
Posterior

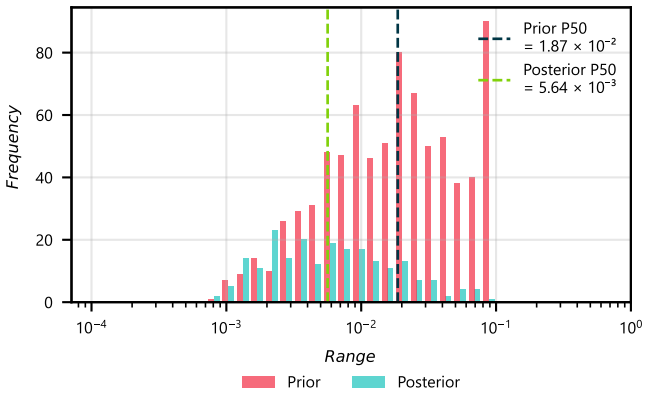

Kv:WamboIB
Prior P50
= 1.00 × 10⁻⁵
Posterior P50
= 1.00 × 10⁻⁵
Frequency
Range
Prior
Posterior


Kv:ArgyleC
Prior P50
= 1.91 × 10⁻²
Posterior P50
= 1.46 × 10⁻²
Frequency
Range
Prior
Posterior

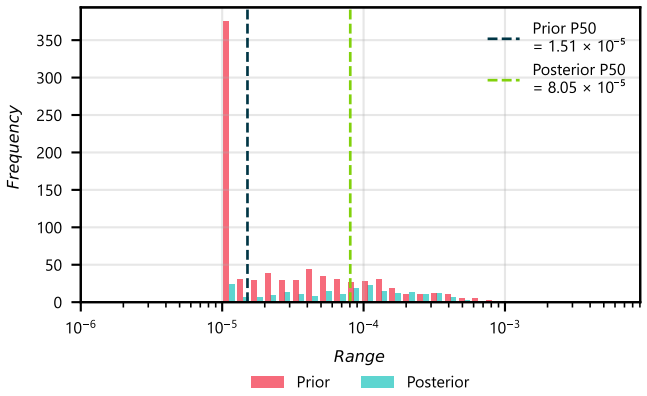

Kv:ArgyleIB
Prior P50
= 2.57 × 10⁻⁵
Posterior P50
= 3.14 × 10⁻⁵
Frequency
Range
Prior
Posterior


Kv:TangaloomaSst
Prior P50
= 1.00 × 10⁻⁵
Posterior P50
= 1.00 × 10⁻⁵
Frequency
Range
Prior
Posterior

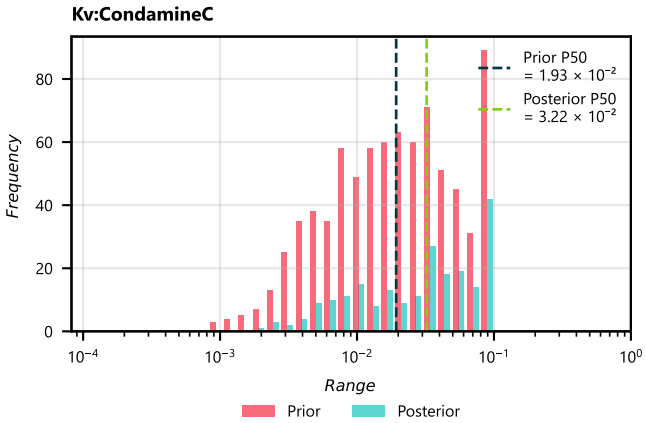
Kv:UpperTaroomC



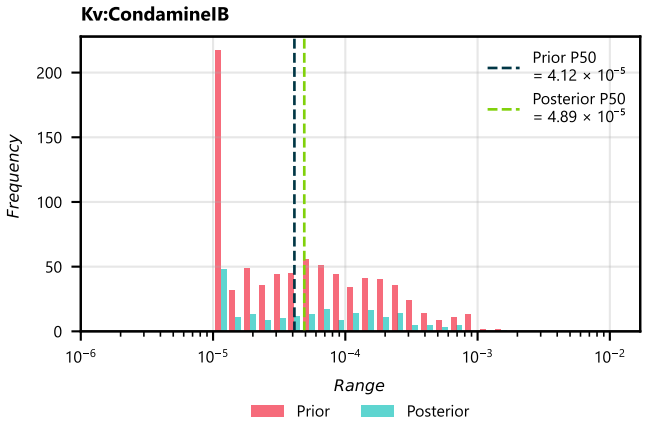
Kv:UpperTaroomIB



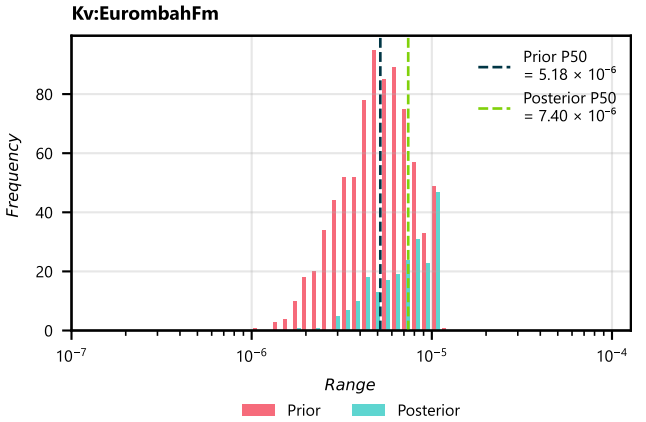
Kv:CondamineC



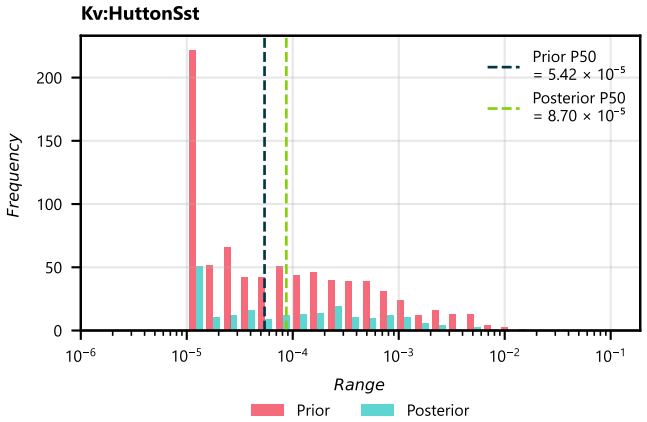
Kv:CondamineIB



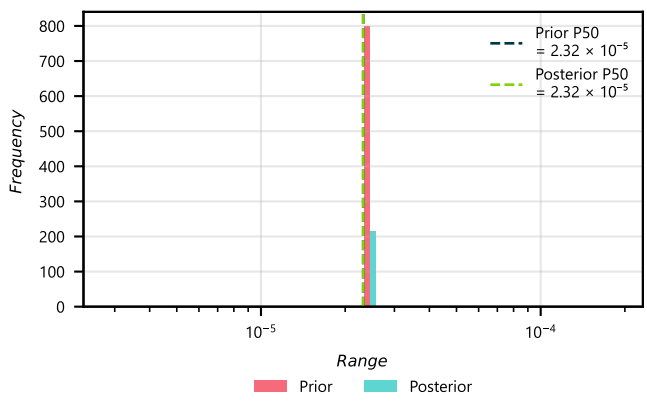
Kv:EurombahFm



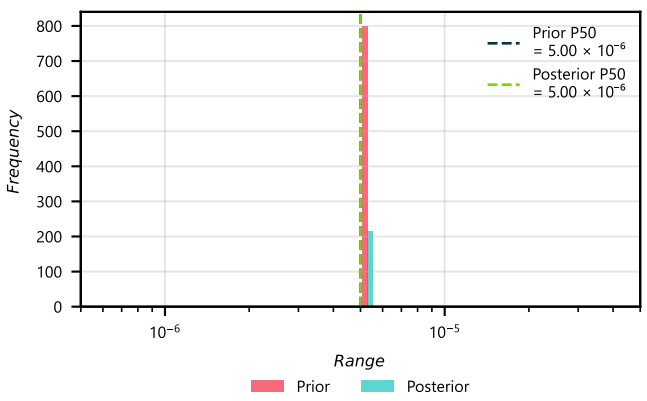
Kv:HuttonSst



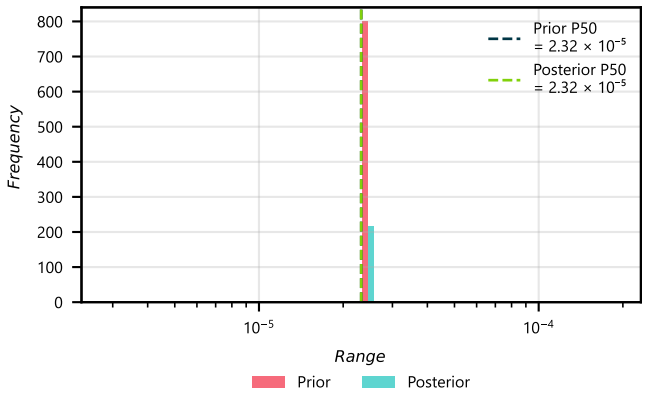
Ss:CondamineAlv



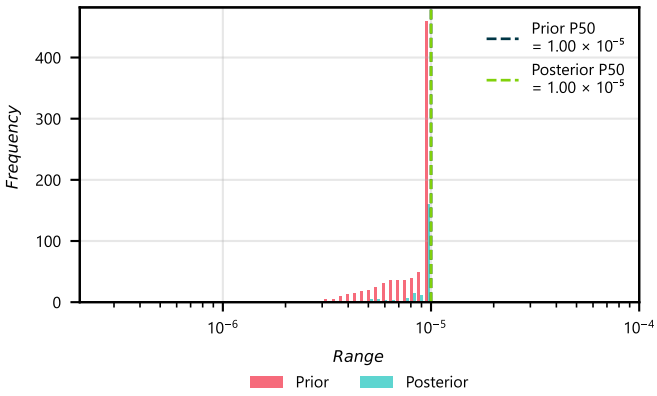
Ss:Gubb.Sst



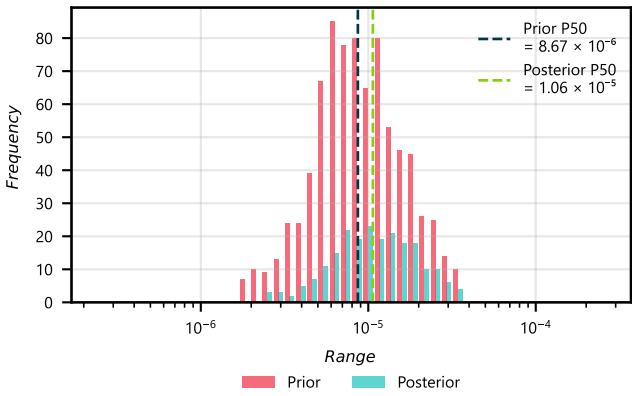
Ss:WestbourneFm



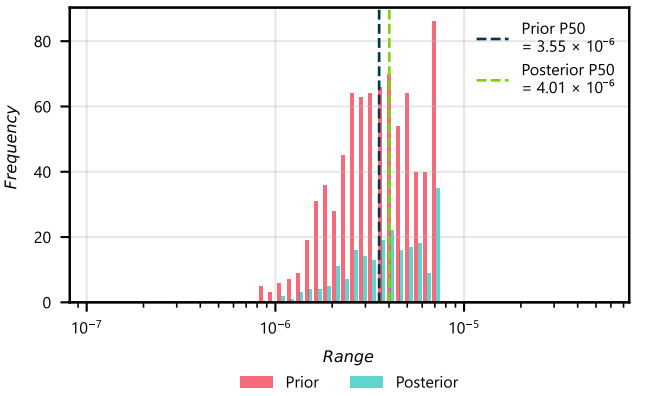
Ss:SpringbokSst



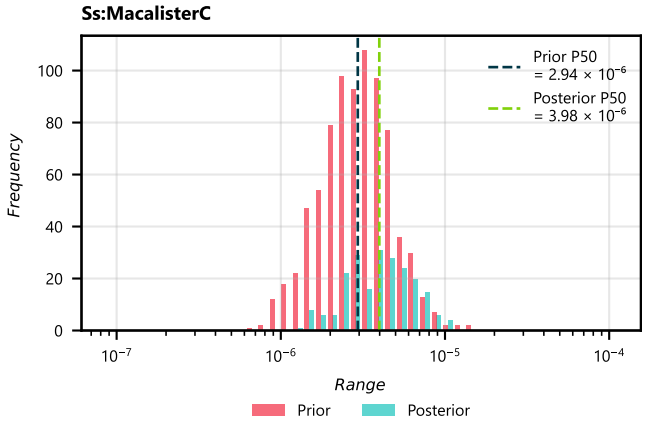
Ss:KoganC



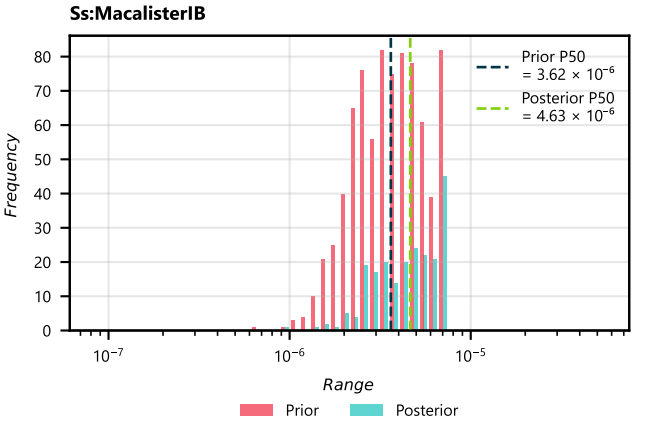
Ss:KoganIB



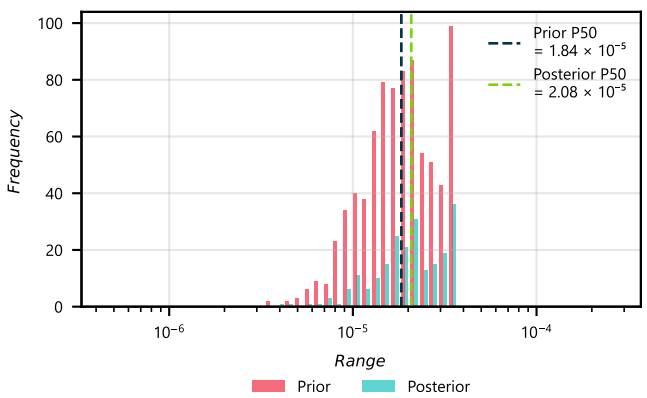
Ss:MacalisterC



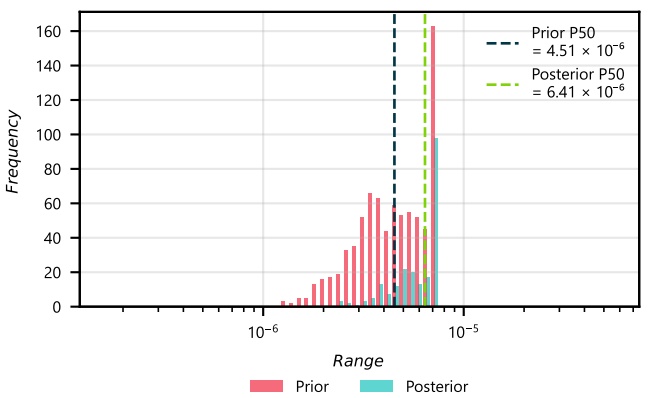
Ss:MacalisterIB



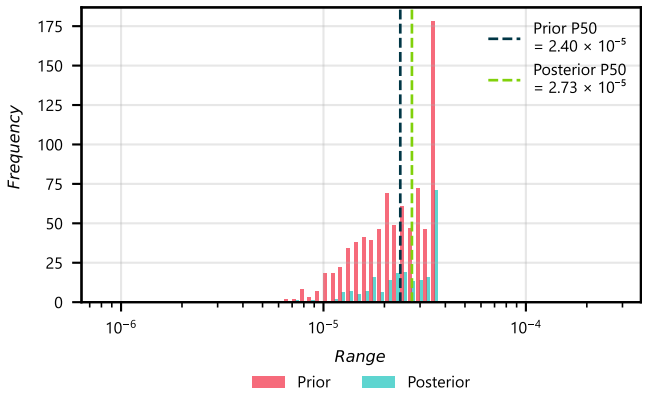
Ss:WamboC



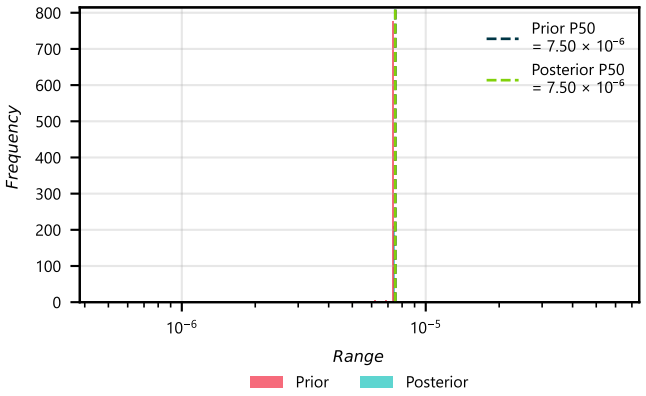
Ss:WamboIB



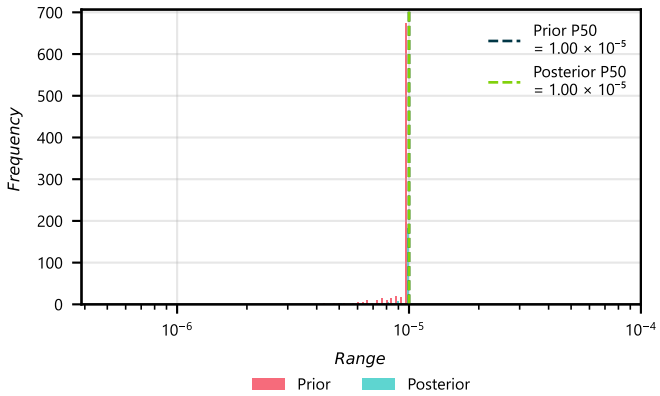
Ss:ArgyleC



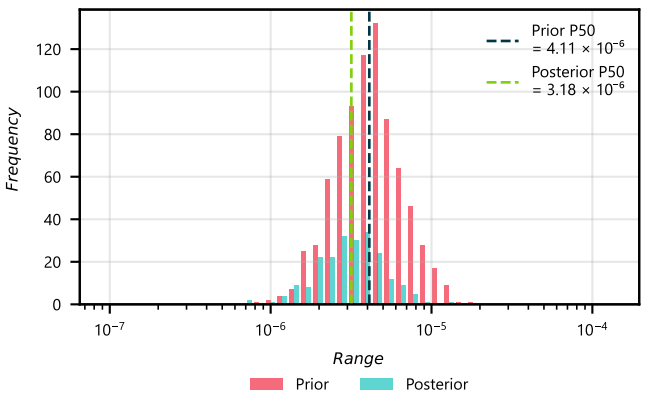
Ss:ArgyleIB



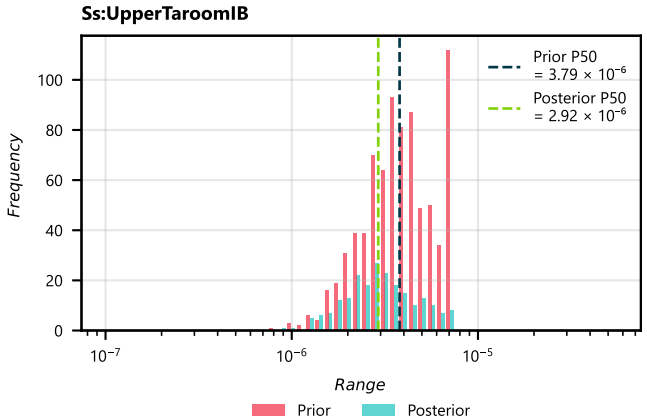
Ss:TangaloomaSst



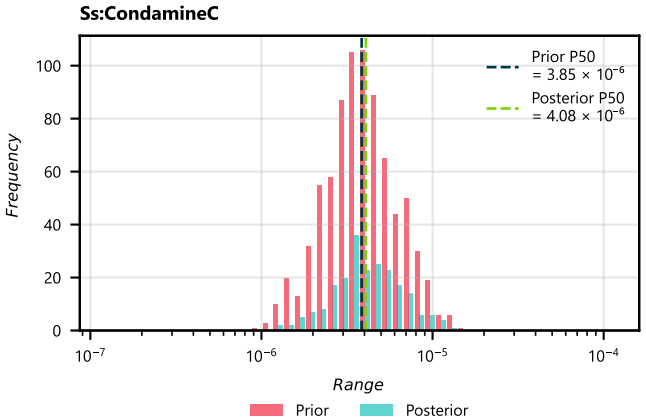
Ss:UpperTaroomC



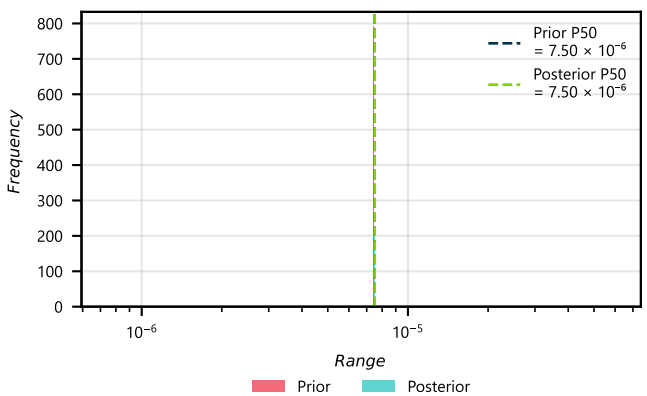
Ss:UpperTaroomIB



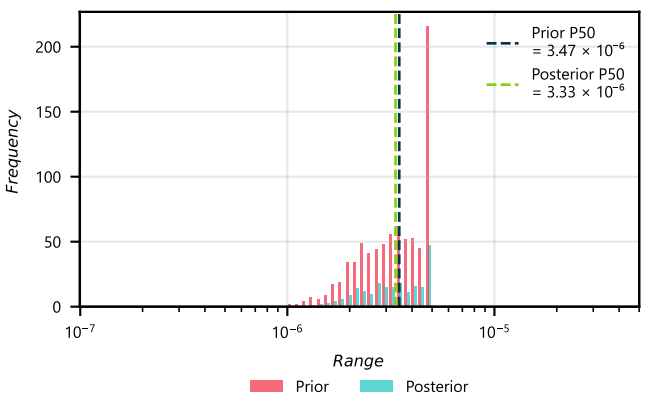
Ss:CondamineC



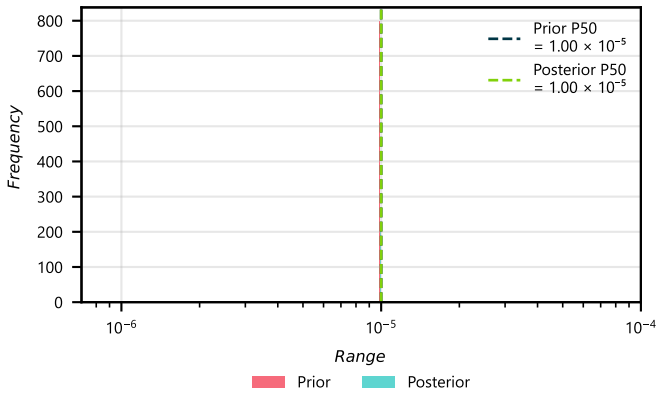
Ss:CondamineIB



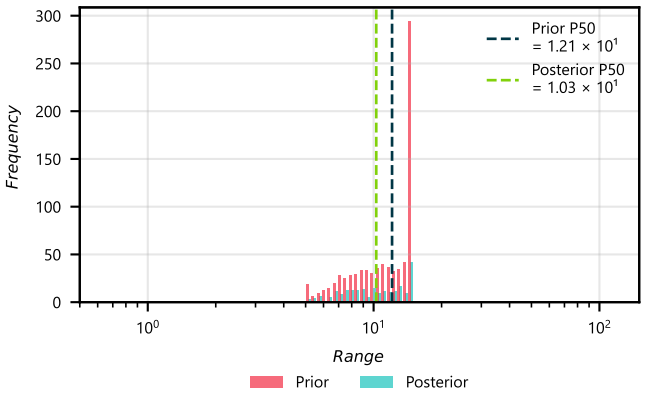
Ss:EurombahFm



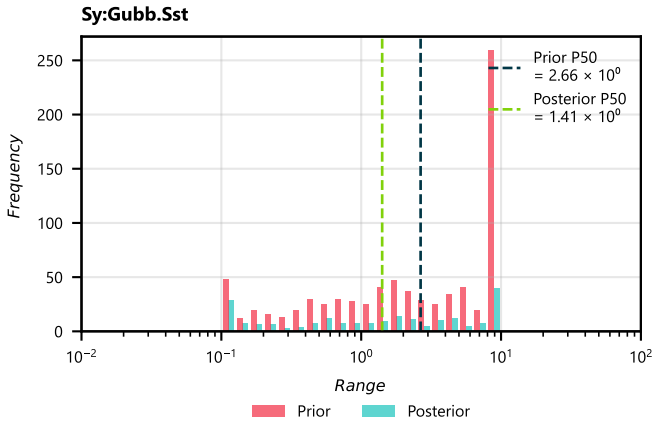
Ss:HuttonSst



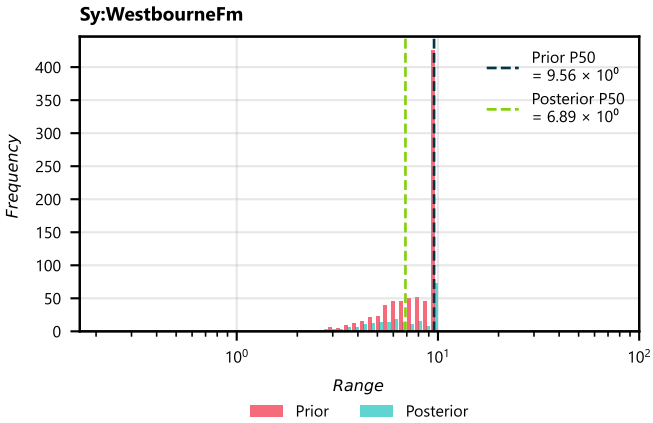
Sy:CondamineAlv



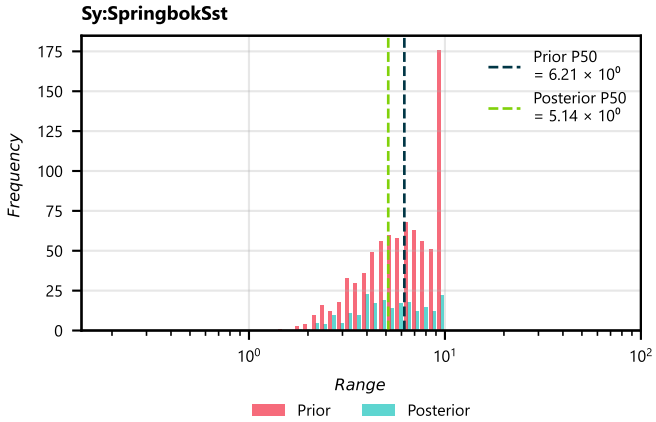
Sy:Gubb.Sst



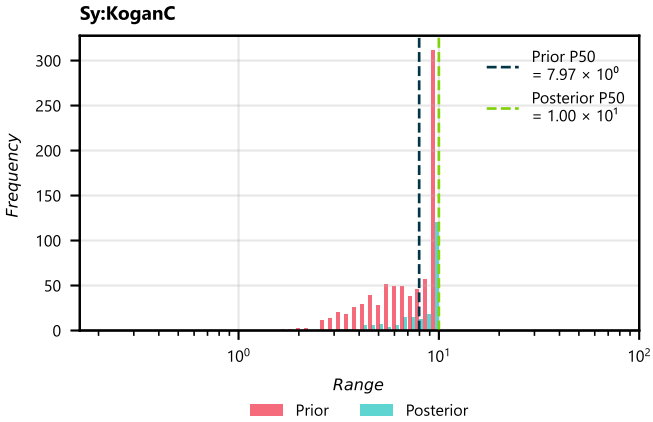
Sy:WestbourneFm



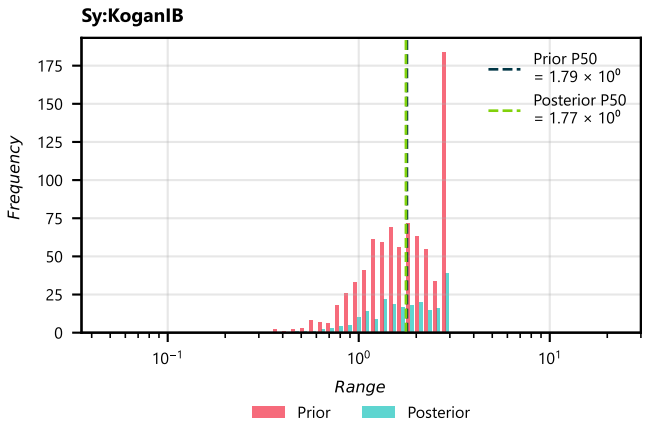
Sy:SpringbokSst



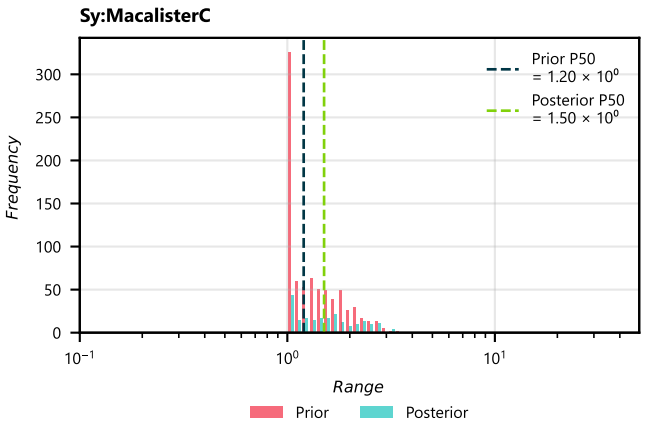
Sy:KoganC

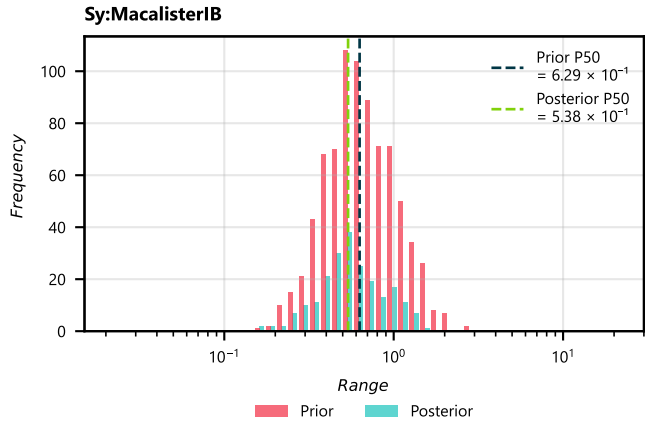


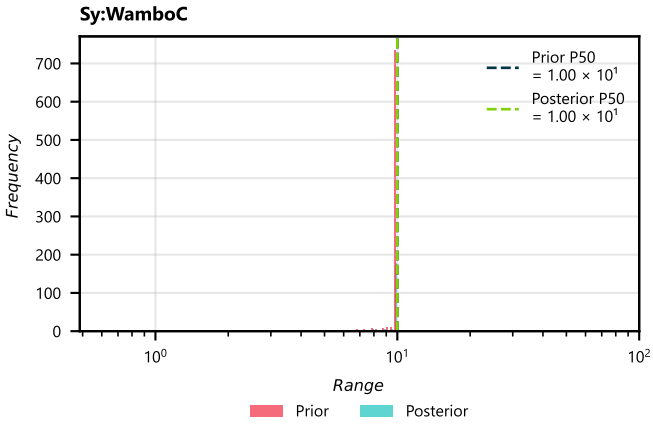
Sy:KoganIB

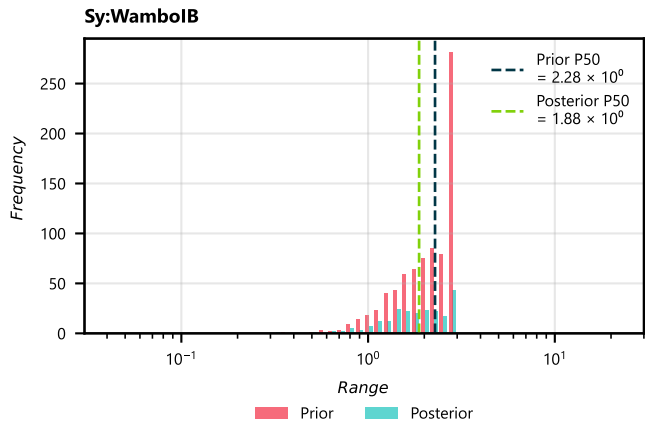


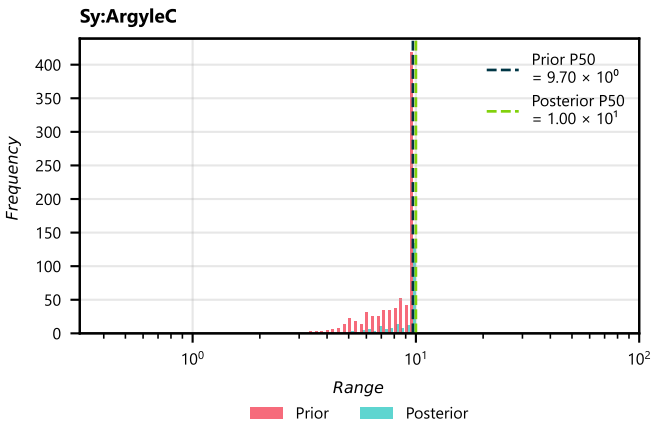
Sy:MacalisterC

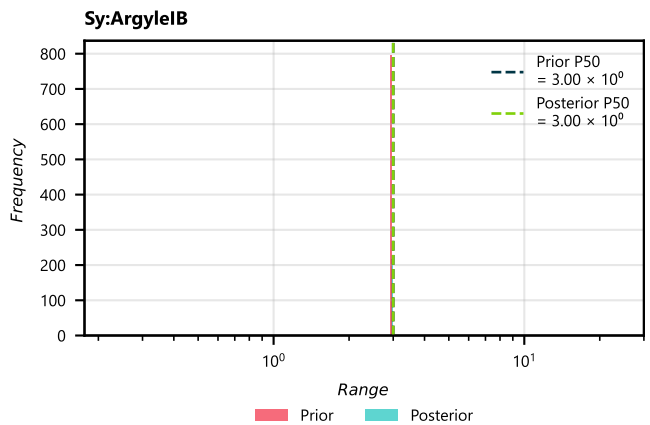


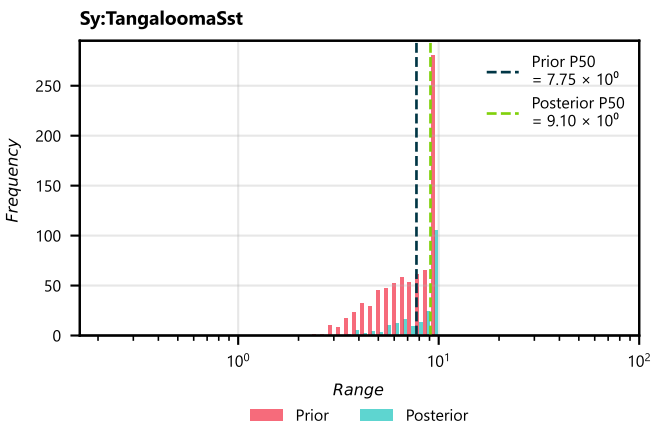

Sy:MacalisterIB
Prior P50
= 6.29 × 10⁻¹
Posterior P50
= 5.38 × 10⁻¹
Frequency
Range
Prior
Posterior

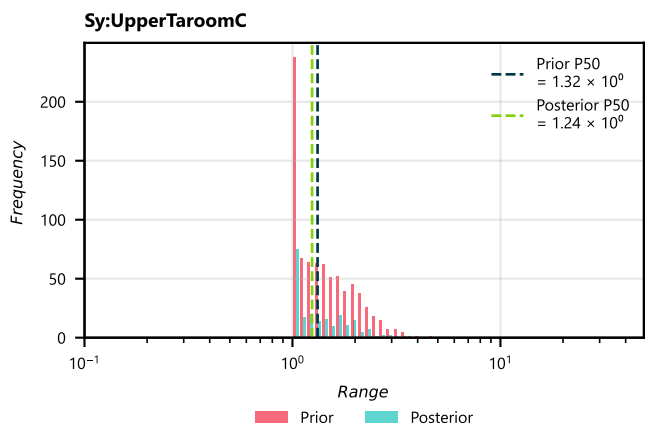

Sy:WamboC
Prior P50
= 1.00 × 10¹
Posterior P50
= 1.00 × 10¹
Frequency
Range
Prior
Posterior

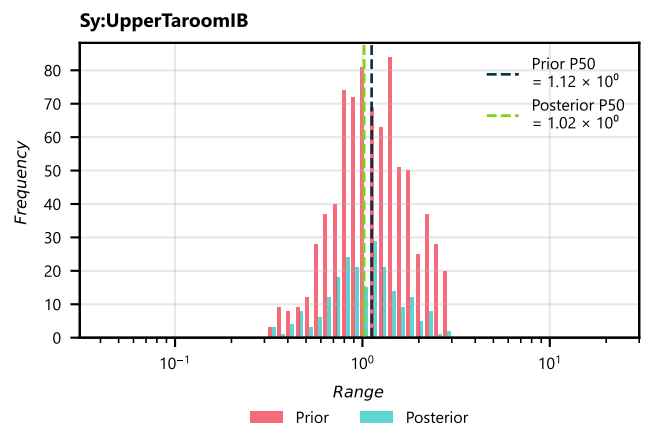

Sy:WamboIB
Prior P50
= 2.28 × 10⁰
Posterior P50
= 1.88 × 10⁰
Frequency
Range
Prior
Posterior

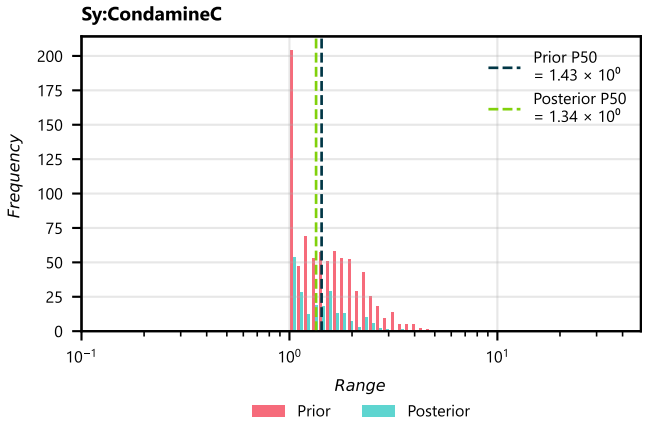

Sy:ArgyleC
Prior P50
= 9.70 × 10⁰
Posterior P50
= 1.00 × 10¹
Frequency
Range
Prior
Posterior

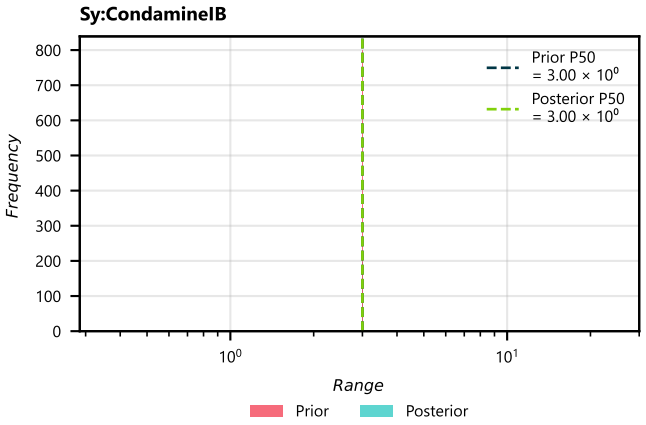

Sy:ArgyleIB
Prior P50
= 3.00 × 10⁰
Posterior P50
= 3.00 × 10⁰
Frequency
Range
Prior
Posterior

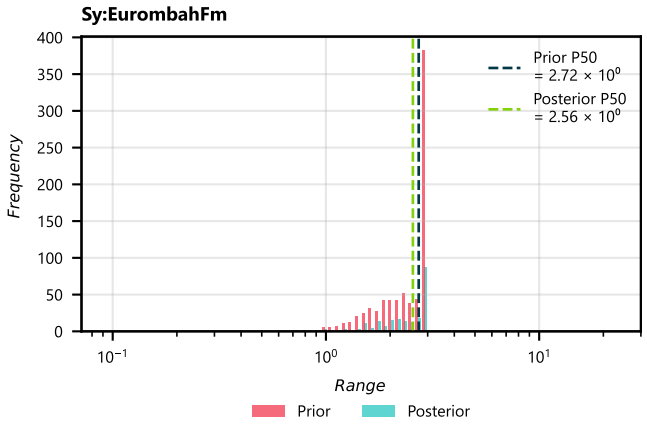

Sy:TangaloomaSst
Prior P50
= 7.75 × 10⁰
Posterior P50
= 9.10 × 10⁰
Frequency
Range
Prior
Posterior

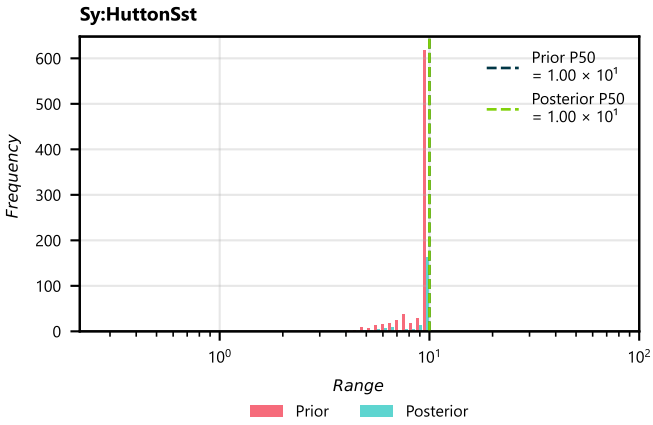

Sy:UpperTaroomC
Prior P50
= 1.32 × 10⁰
Posterior P50
= 1.24 × 10⁰
Frequency
Range
Prior
Posterior

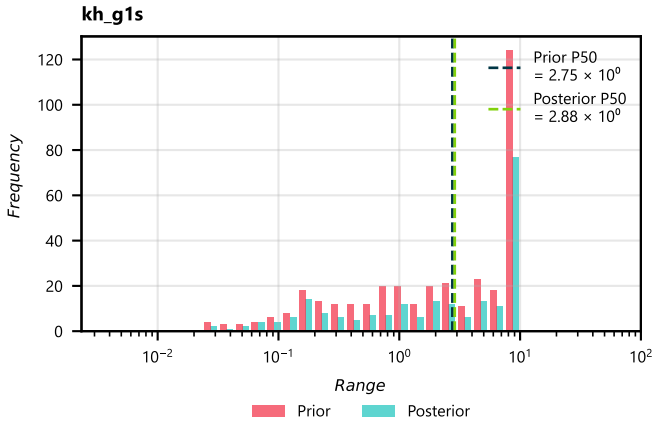

Sy:UpperTaroomIB
Prior P50
= 1.12 × 10⁰
Posterior P50
= 1.02 × 10⁰
Frequency
Range
Prior
Posterior

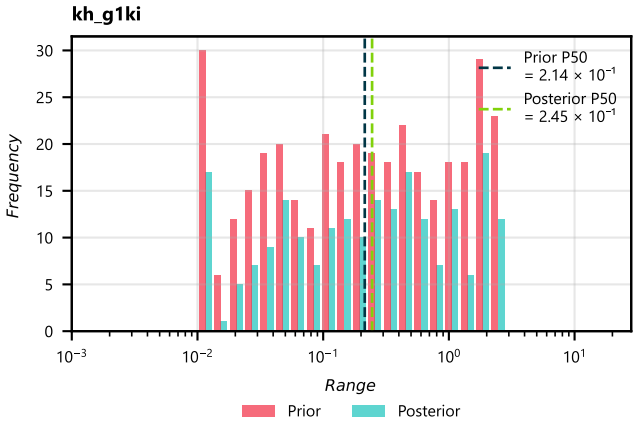

Sy:CondamineC
Prior P50
= 1.43 × 10⁰
Posterior P50
= 1.34 × 10⁰
Frequency
Range
Prior
Posterior

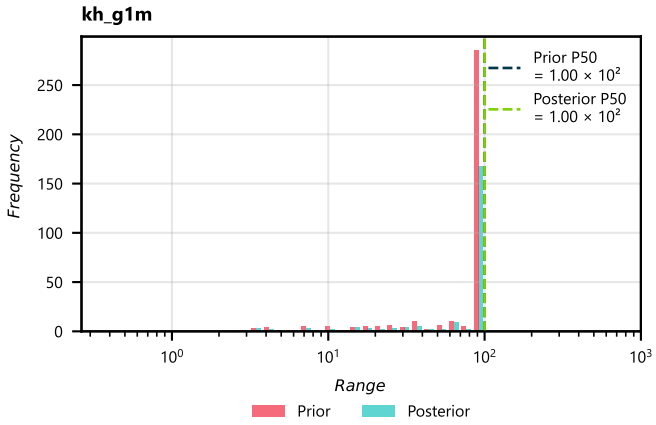

Sy:CondamineIB
Prior P50
= 3.00 × 10⁰
Posterior P50
= 3.00 × 10⁰
Frequency
Range
Prior
Posterior

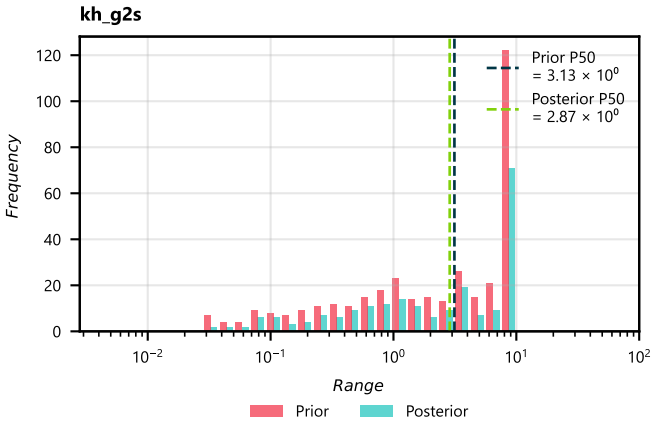

Sy:EurombahFm
Prior P50
= 2.72 × 10⁰
Posterior P50
= 2.56 × 10⁰
Frequency
Range
Prior
Posterior

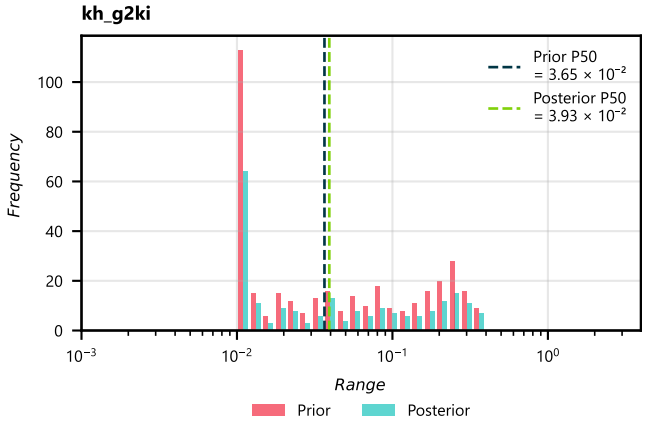

Sy:HuttonSst
Prior P50
= 1.00 × 10¹
Posterior P50
= 1.00 × 10¹
Frequency
Range
Prior
Posterior

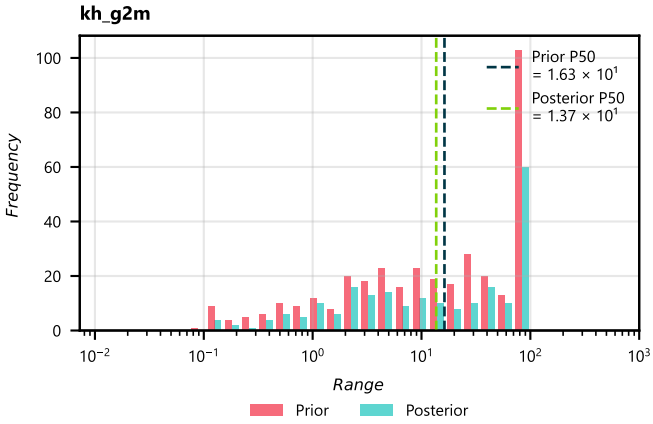

kh_g1s
Prior P50
= 2.75 × 10^0
Posterior P50
= 2.88 × 10^0
Frequency
Range
Prior
Posterior

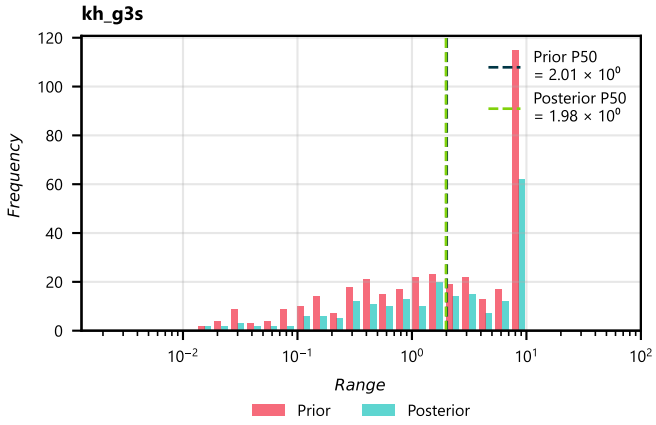

kh_g1ki
Prior P50
= 2.14 × 10^-1
Posterior P50
= 2.45 × 10^-1
Frequency
Range
Prior
Posterior

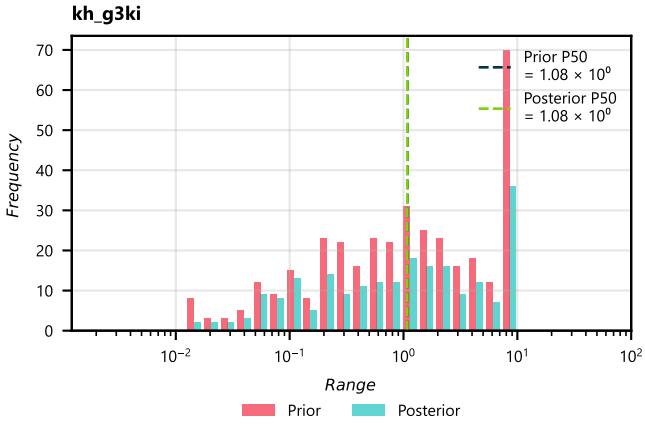

kh_g1m
Prior P50
= 1.00 × 10^2
Posterior P50
= 1.00 × 10^2
Frequency
Range
Prior
Posterior

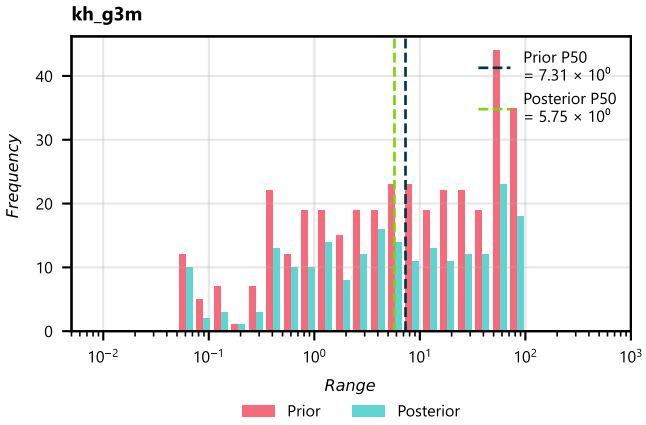

kh_g2s
Prior P50
= 3.13 × 10^0
Posterior P50
= 2.87 × 10^0
Frequency
Range
Prior
Posterior

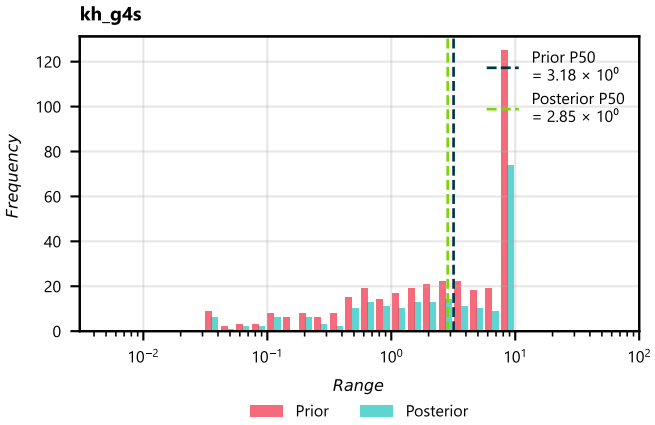

kh_g2ki
Prior P50
= 3.65 × 10^-2
Posterior P50
= 3.93 × 10^-2
Frequency
Range
Prior
Posterior

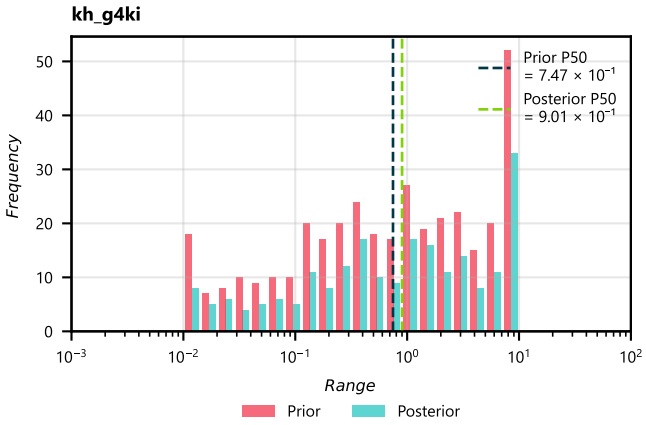

kh_g2m
Prior P50
= 1.63 × 10^1
Posterior P50
= 1.37 × 10^1
Frequency
Range
Prior
Posterior

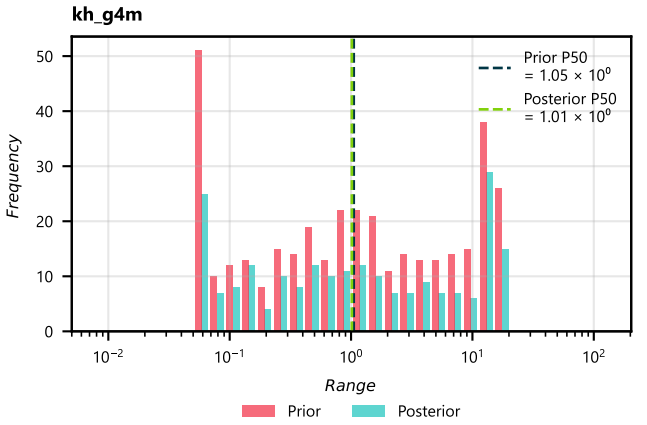

kh_g3s
Prior P50
= 2.01 × 10^0
Posterior P50
= 1.98 × 10^0
Frequency
Range
Prior
Posterior

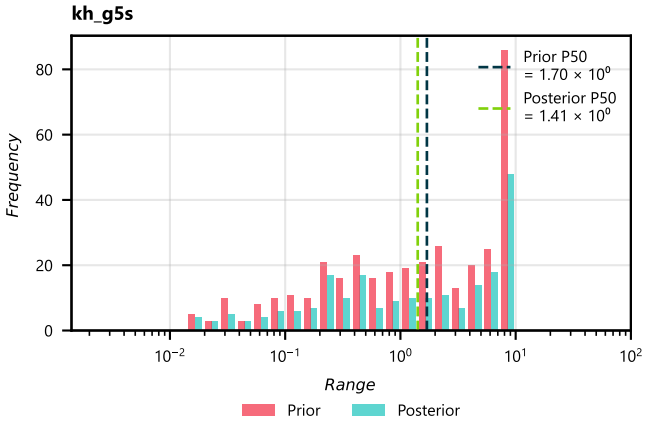

kh_g3ki
Prior P50
= 1.08 × 10^0
Posterior P50
= 1.08 × 10^0
Frequency
Range
Prior
Posterior

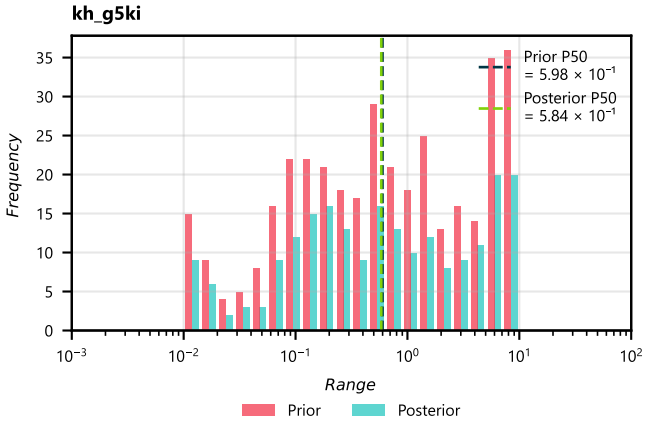

kh_g3m
Prior P50
= 7.31 × 10^0
Posterior P50
= 5.75 × 10^0
Frequency
Range
Prior
Posterior

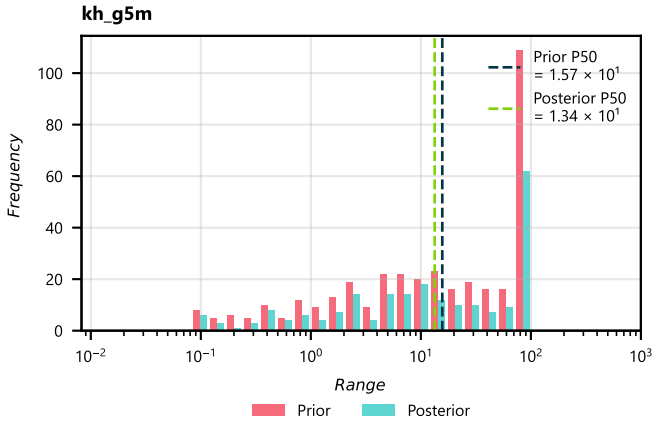

kh_g4s
Prior P50
= 3.18 × 10^0
Posterior P50
= 2.85 × 10^0
Frequency
Range
Prior
Posterior

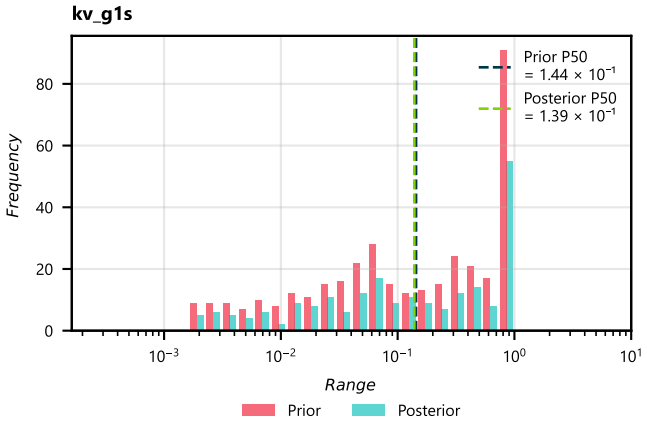

kh_g4ki
Prior P50
= 7.47 × 10^-1
Posterior P50
= 9.01 × 10^-1
Frequency
Range
Prior
Posterior

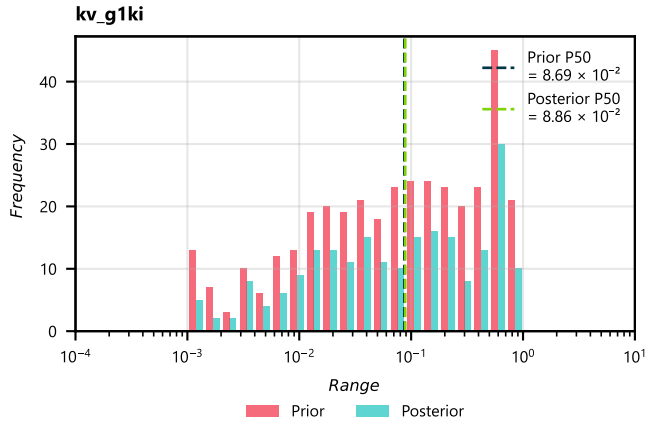

kh_g4m
Prior P50
= 1.05 × 10^0
Posterior P50
= 1.01 × 10^0
Frequency
Range
Prior
Posterior

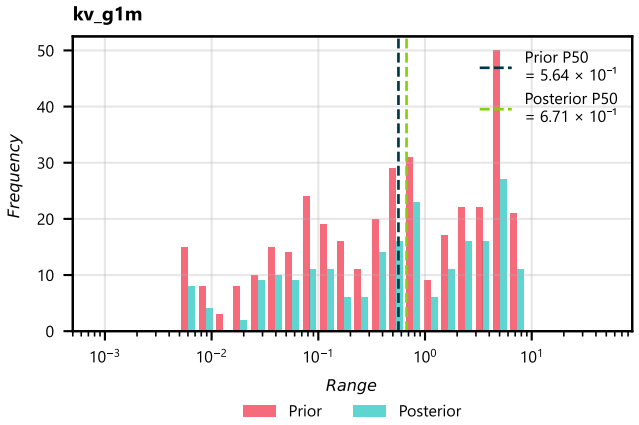

kh_g5s
Prior P50
= 1.70 × 10^0
Posterior P50
= 1.41 × 10^0
Frequency
Range
Prior
Posterior

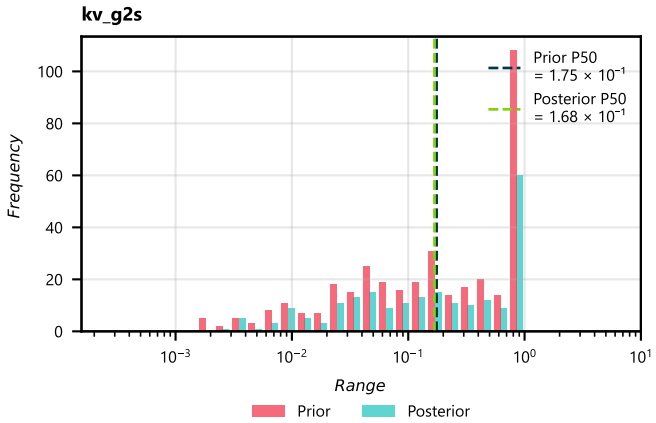

kh_g5ki
Prior P50
= 5.98 × 10^-1
Posterior P50
= 5.84 × 10^-1
Frequency
Range
Prior
Posterior

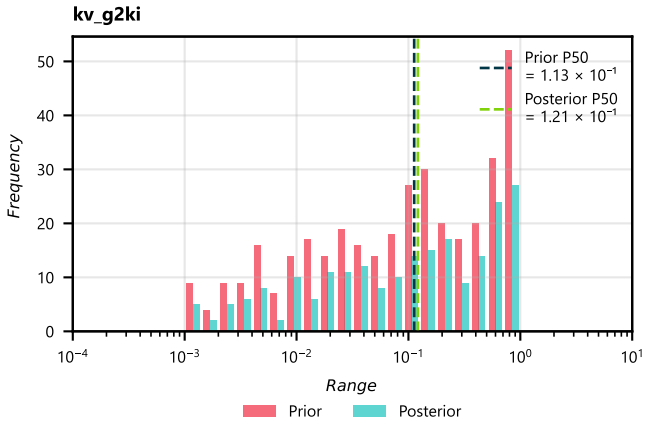

kh_g5m
Prior P50
= 1.57 × 10^1
Posterior P50
= 1.34 × 10^1
Frequency
Range
Prior
Posterior

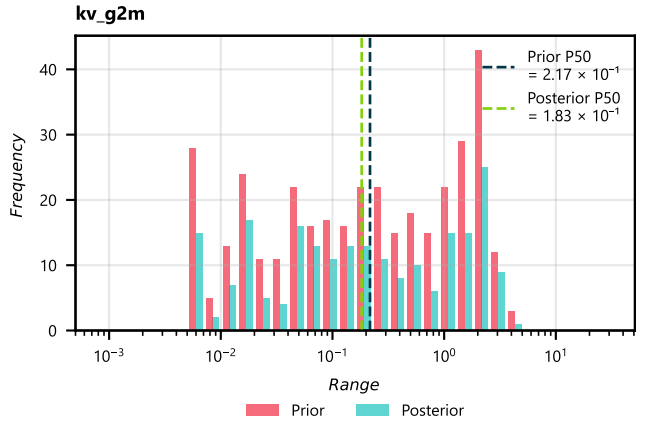

kv_g1s
Prior P50
= 1.44 × 10^-1
Posterior P50
= 1.39 × 10^-1
Frequency
Range
Prior
Posterior

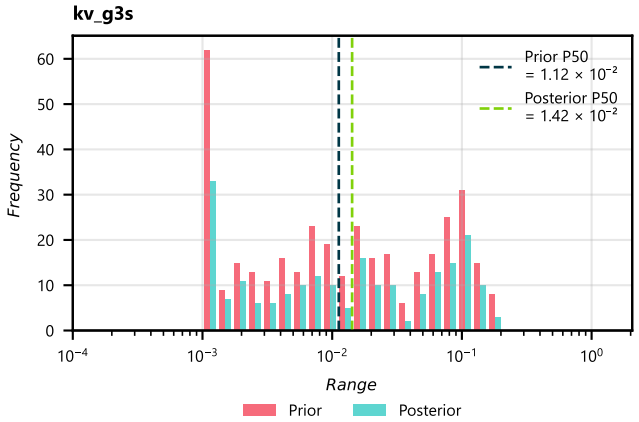

kv_g1ki
Prior P50
= 8.69 × 10⁻²
Posterior P50
= 8.86 × 10⁻²
Frequency
Range
Prior
Posterior

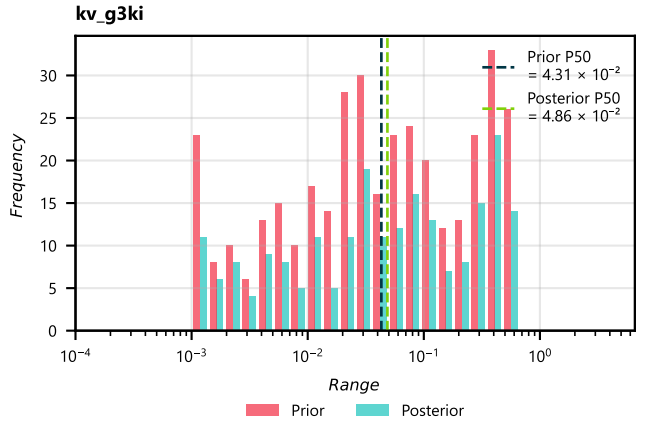

kv_g1m
Prior P50
= 5.64 × 10⁻¹
Posterior P50
= 6.71 × 10⁻¹
Frequency
Range
Prior
Posterior

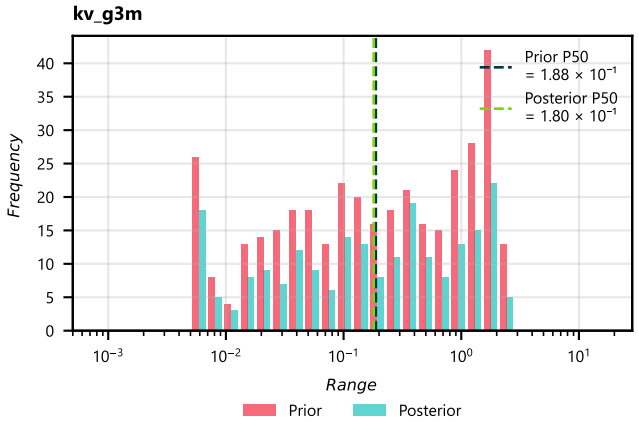

kv_g2s
Prior P50
= 1.75 × 10⁻¹
Posterior P50
= 1.68 × 10⁻¹
Frequency
Range
Prior
Posterior

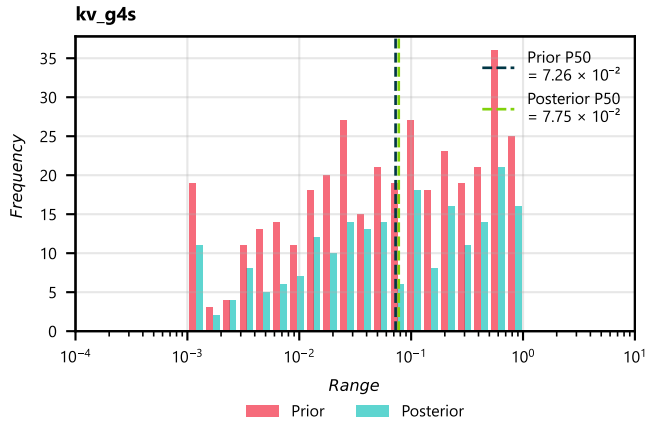

kv_g2ki
Prior P50
= 1.13 × 10⁻¹
Posterior P50
= 1.21 × 10⁻¹
Frequency
Range
Prior
Posterior

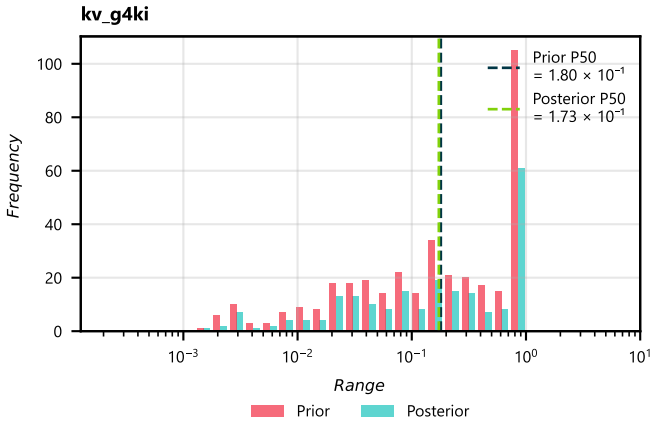

kv_g2m
Prior P50
= 2.17 × 10⁻¹
Posterior P50
= 1.83 × 10⁻¹
Frequency
Range
Prior
Posterior

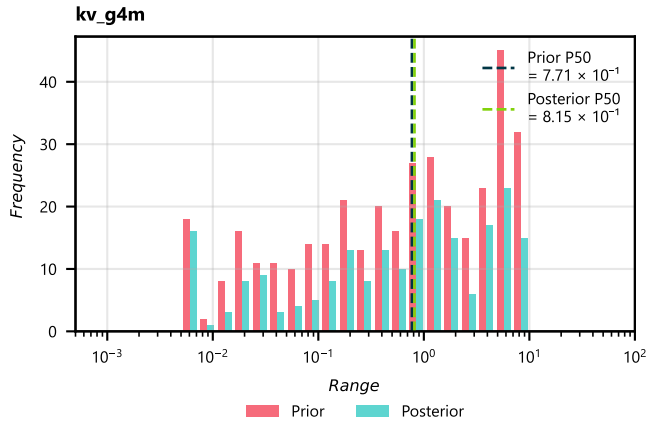

kv_g3s
Prior P50
= 1.12 × 10⁻²
Posterior P50
= 1.42 × 10⁻²
Frequency
Range
Prior
Posterior

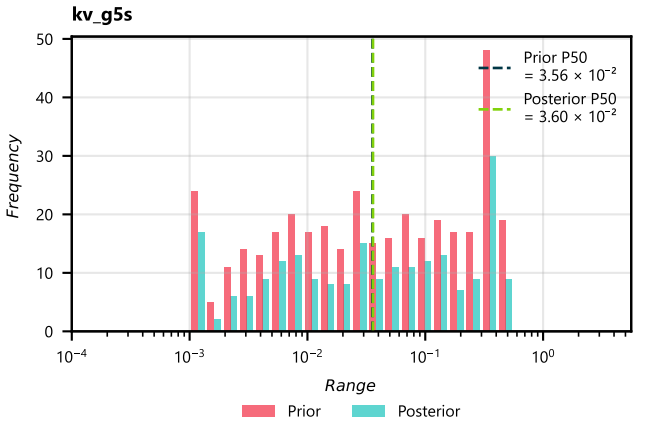

kv_g3ki
Prior P50
= 4.31 × 10⁻²
Posterior P50
= 4.86 × 10⁻²
Frequency
Range
Prior
Posterior

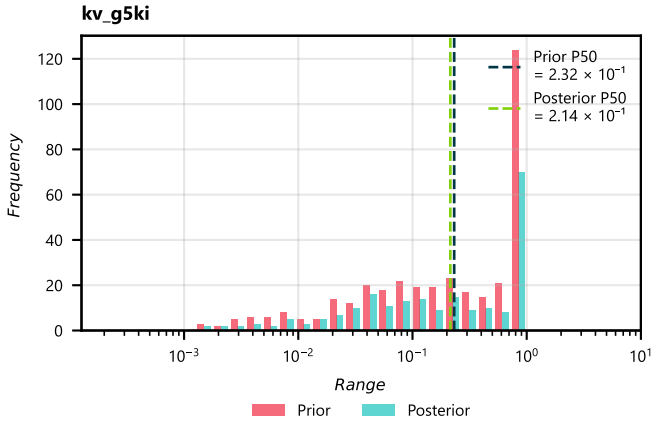

kv_g3m
Prior P50
= 1.88 × 10⁻¹
Posterior P50
= 1.80 × 10⁻¹
Frequency
Range
Prior
Posterior

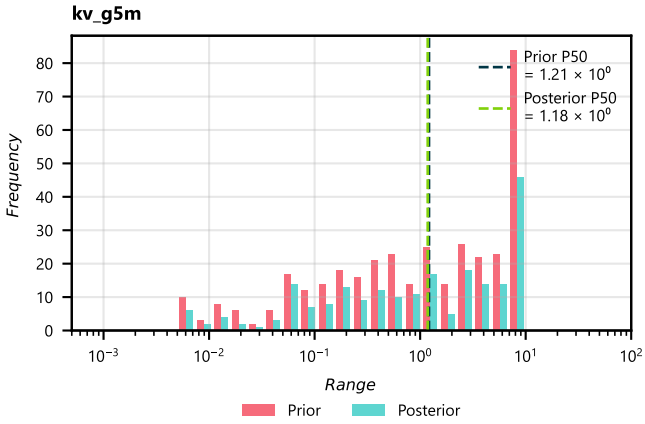

kv_g4s
Prior P50
= 7.26 × 10⁻²
Posterior P50
= 7.75 × 10⁻²
Frequency
Range
Prior
Posterior

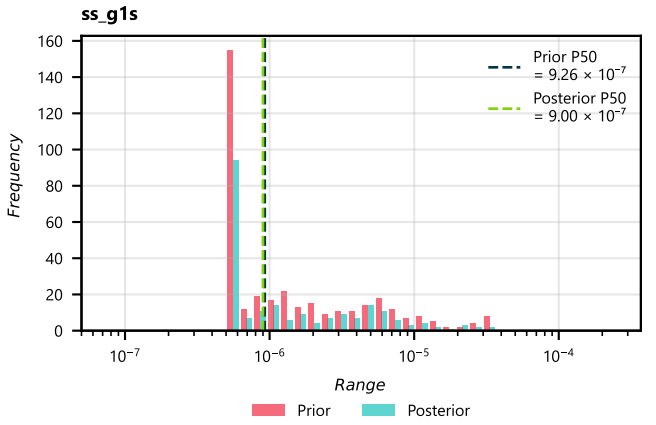

kv_g4ki
Prior P50
= 1.80 × 10⁻¹
Posterior P50
= 1.73 × 10⁻¹
Frequency
Range
Prior
Posterior

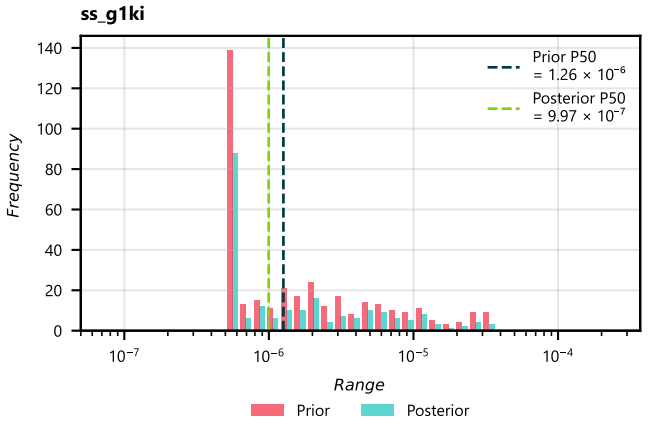

kv_g4m
Prior P50
= 7.71 × 10⁻¹
Posterior P50
= 8.15 × 10⁻¹
Frequency
Range
Prior
Posterior

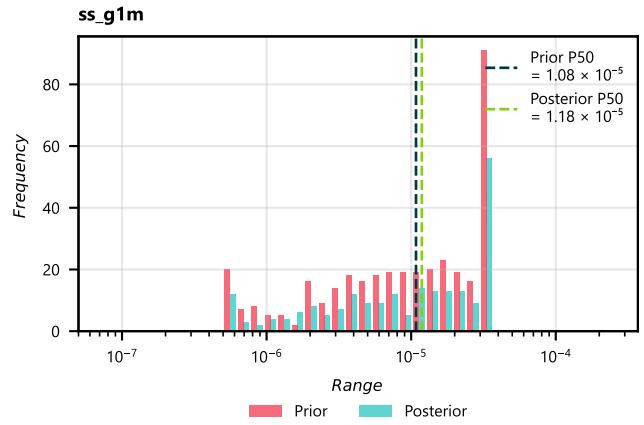

kv_g5s
Prior P50
= 3.56 × 10⁻²
Posterior P50
= 3.60 × 10⁻²
Frequency
Range
Prior
Posterior

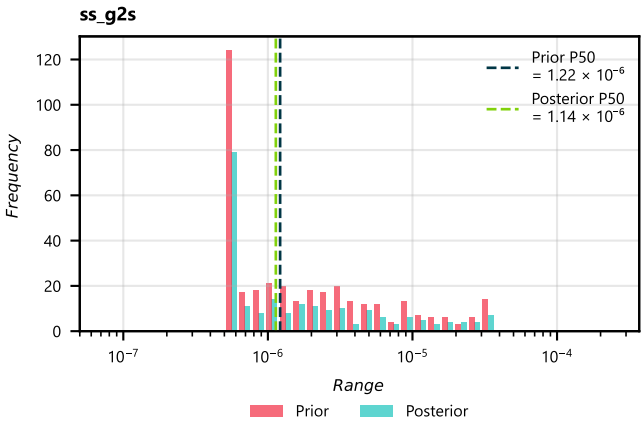

kv_g5ki
Prior P50
= 2.32 × 10⁻¹
Posterior P50
= 2.14 × 10⁻¹
Frequency
Range
Prior
Posterior

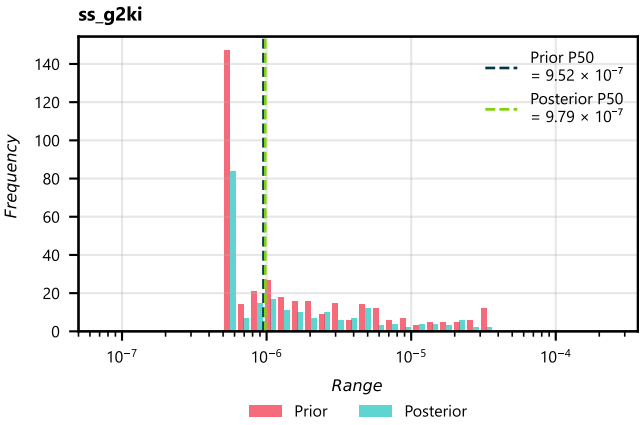

kv_g5m
Prior P50
= 1.21 × 10⁰
Posterior P50
= 1.18 × 10⁰
Frequency
Range
Prior
Posterior

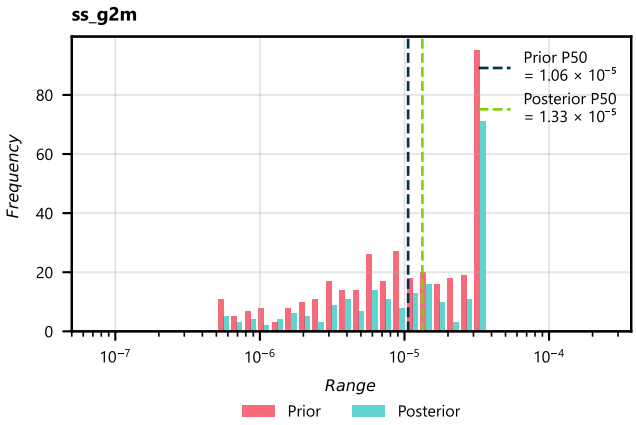

ss_g1s
Prior P50
= 9.26 × 10⁻⁷
Posterior P50
= 9.00 × 10⁻⁷
Frequency
Range
Prior
Posterior

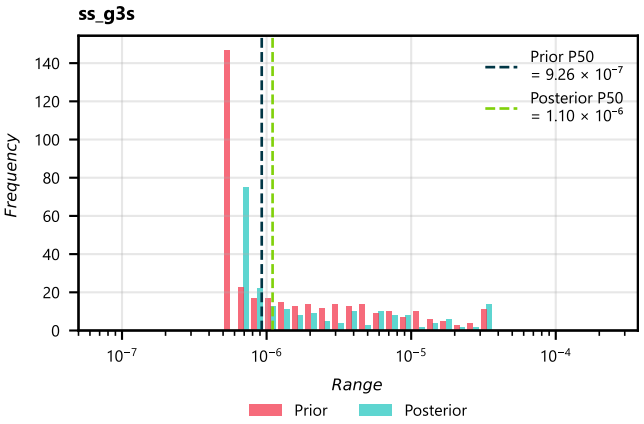

ss_g1ki
Prior P50
= 1.26 × 10⁻⁶
Posterior P50
= 9.97 × 10⁻⁷
Frequency
Range
Prior
Posterior

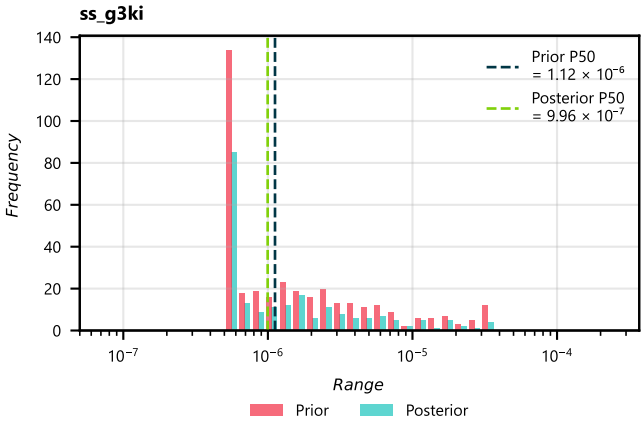

ss_g1m
Prior P50
= 1.08 × 10⁻⁵
Posterior P50
= 1.18 × 10⁻⁵
Frequency
Range
Prior
Posterior

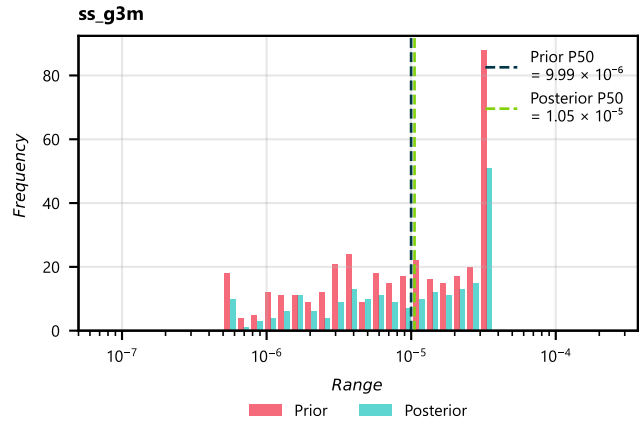

ss_g2s
Prior P50
= 1.22 × 10⁻⁶
Posterior P50
= 1.14 × 10⁻⁶
Frequency
Range
Prior
Posterior

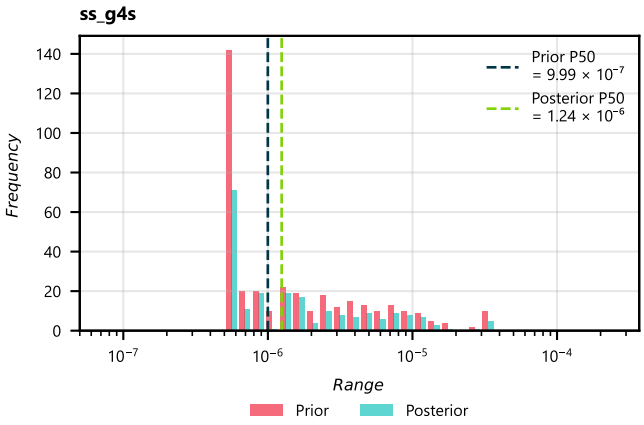

ss_g2ki
Prior P50
= 9.52 × 10⁻⁷
Posterior P50
= 9.79 × 10⁻⁷
Frequency
Range
Prior
Posterior

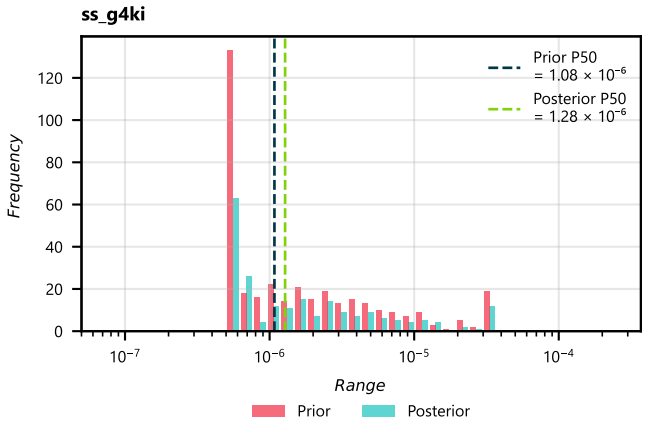

ss_g2m
Prior P50
= 1.06 × 10⁻⁵
Posterior P50
= 1.33 × 10⁻⁵
Frequency
Range
Prior
Posterior

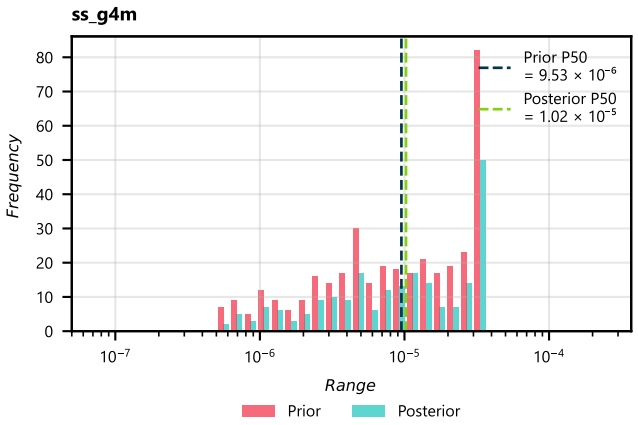

ss_g3s
Prior P50
= 9.26 × 10⁻⁷
Posterior P50
= 1.10 × 10⁻⁶
Frequency
Range
Prior
Posterior

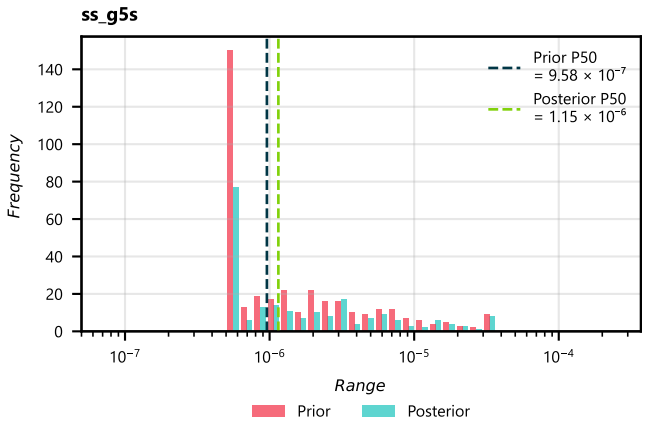

ss_g3ki
Prior P50
= 1.12 × 10⁻⁶
Posterior P50
= 9.96 × 10⁻⁷
Frequency
Range
Prior
Posterior

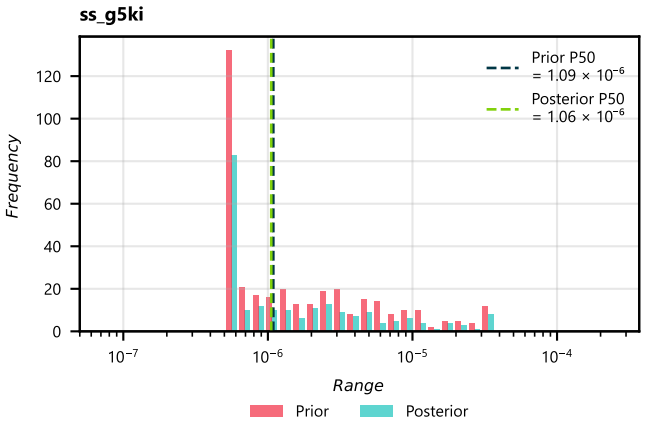

ss_g3m
Prior P50
= 9.99 × 10⁻⁶
Posterior P50
= 1.05 × 10⁻⁵
Frequency
Range
Prior
Posterior

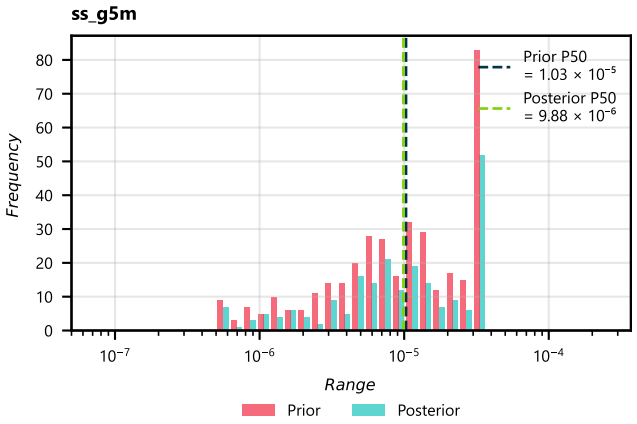

ss_g4s
Prior P50
= 9.99 × 10⁻⁷
Posterior P50
= 1.24 × 10⁻⁶
Frequency
Range
Prior
Posterior

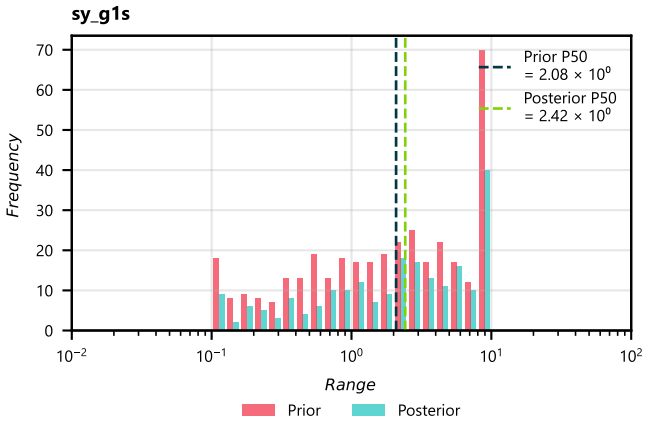

ss_g4ki
Prior P50
= 1.08 × 10⁻⁶
Posterior P50
= 1.28 × 10⁻⁶
Frequency
Range
Prior
Posterior

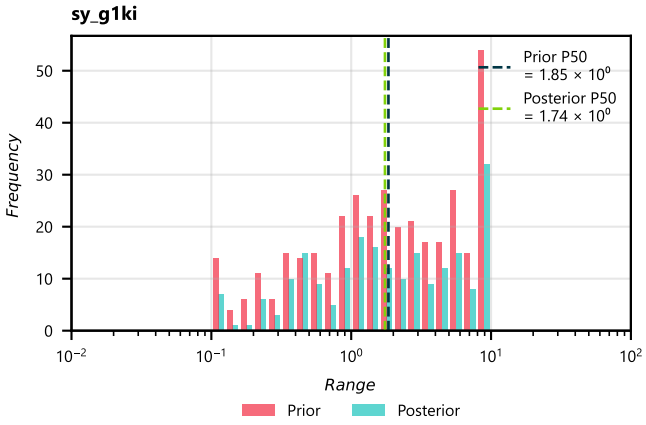

ss_g4m
Prior P50
= 9.53 × 10⁻⁶
Posterior P50
= 1.02 × 10⁻⁵
Frequency
Range
Prior
Posterior

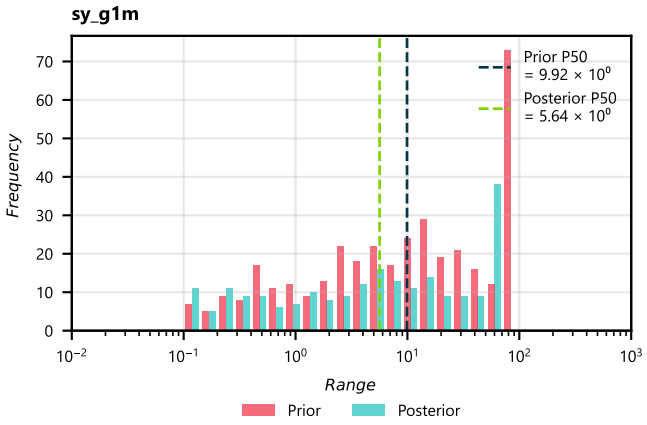

ss_g5s
Prior P50
= 9.58 × 10⁻⁷
Posterior P50
= 1.15 × 10⁻⁶
Frequency
Range
Prior
Posterior


ss_g5ki
Prior P50
= 1.09 × 10⁻⁶
Posterior P50
= 1.06 × 10⁻⁶
Frequency
Range
Prior
Posterior

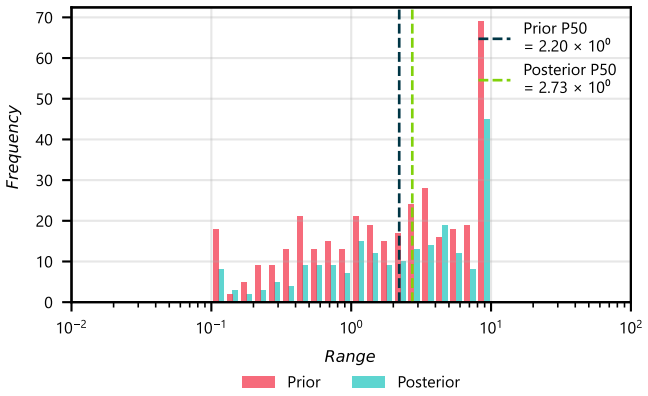

ss_g5m
Prior P50
= 1.03 × 10⁻⁵
Posterior P50
= 9.88 × 10⁻⁶
Frequency
Range
Prior
Posterior


sy_g1s
Prior P50
= 2.08 × 10⁰
Posterior P50
= 2.42 × 10⁰
Frequency
Range
Prior
Posterior

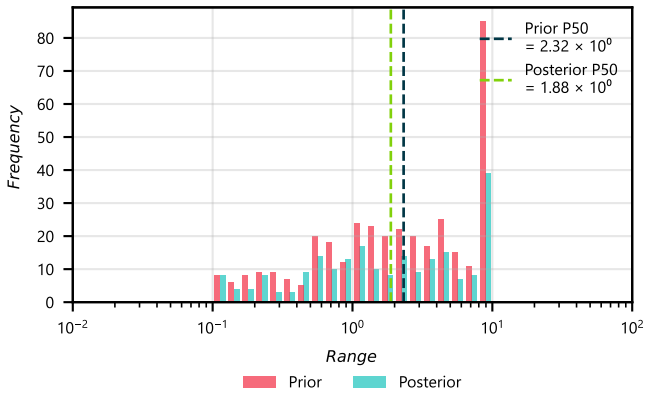

sy_g1ki
Prior P50
= 1.85 × 10⁰
Posterior P50
= 1.74 × 10⁰
Frequency
Range
Prior
Posterior


sy_g1m
Prior P50
= 9.92 × 10⁰
Posterior P50
= 5.64 × 10⁰
Frequency
Range
Prior
Posterior

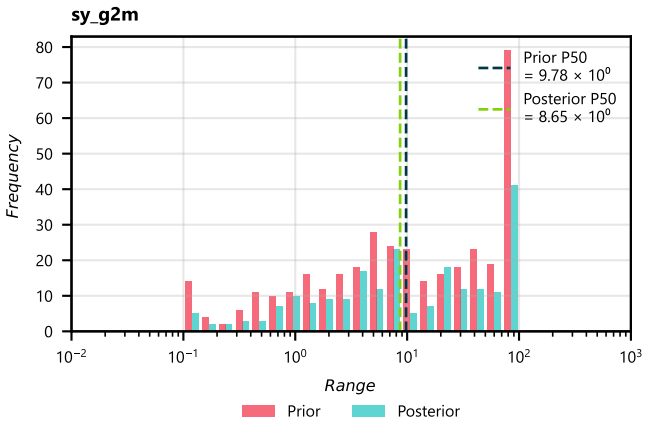
sy_g2s



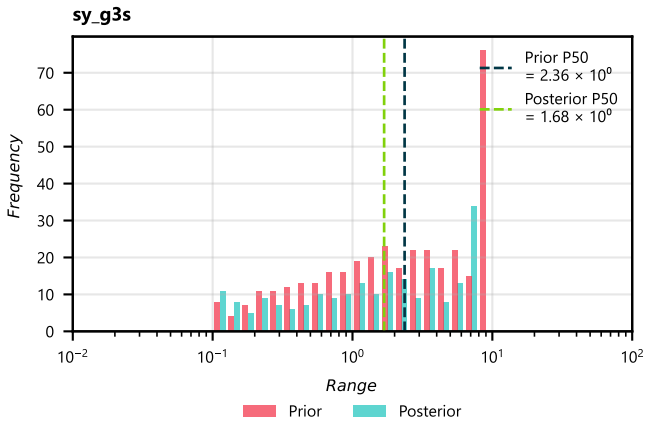
sy_g2ki



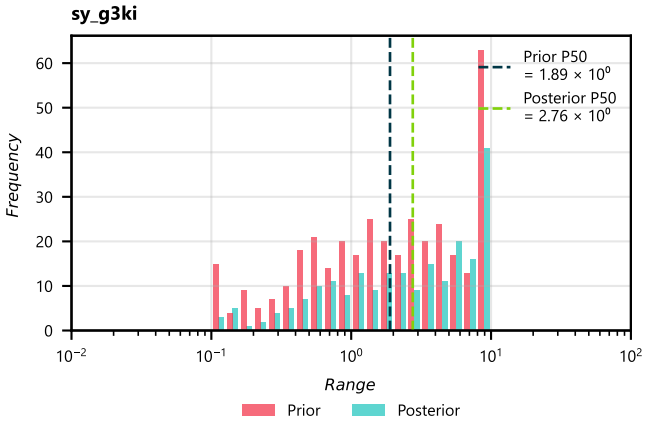
sy_g2m



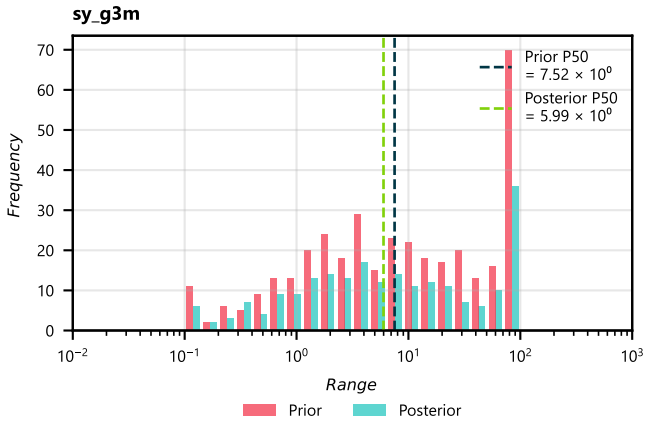
sy_g3s



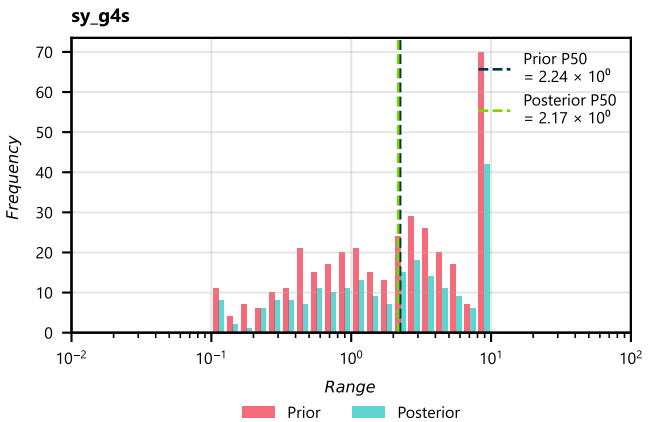
sy_g3ki



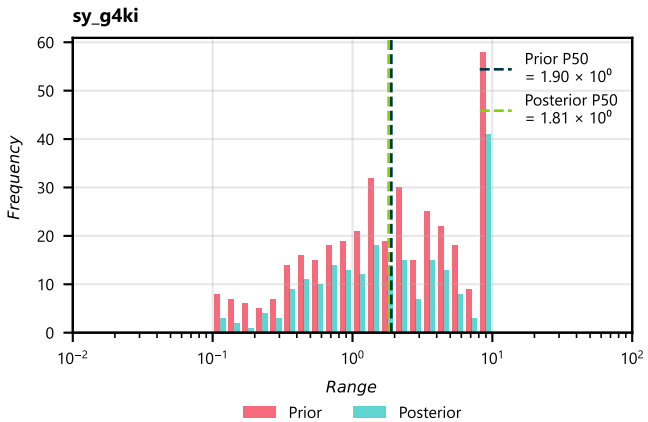
sy_g3m

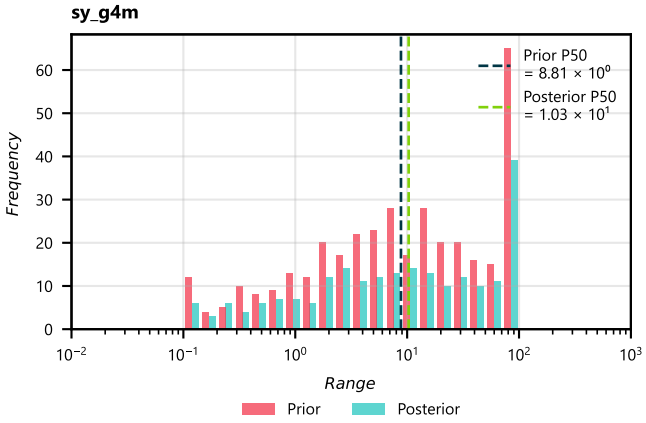


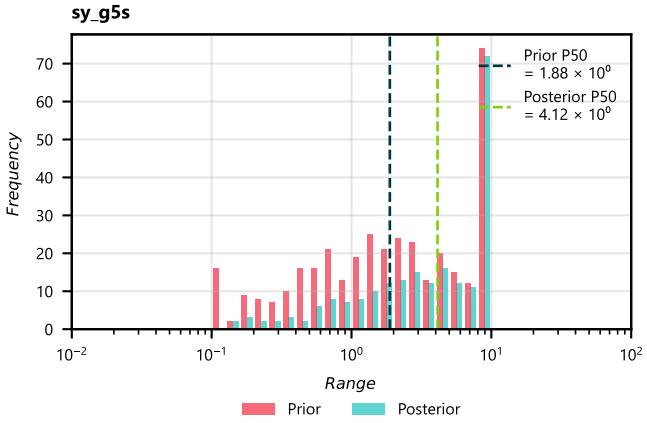
sy_g4s

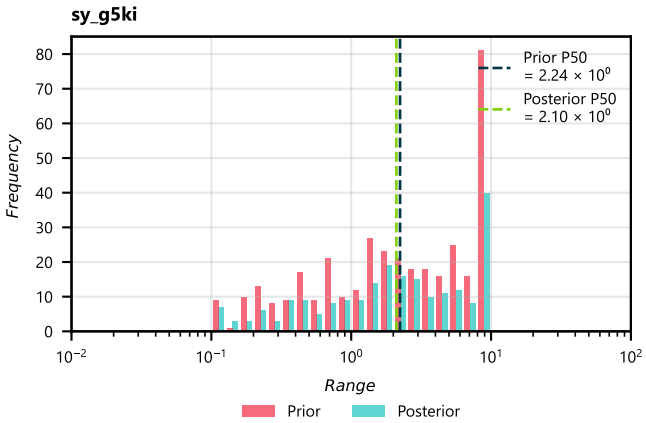


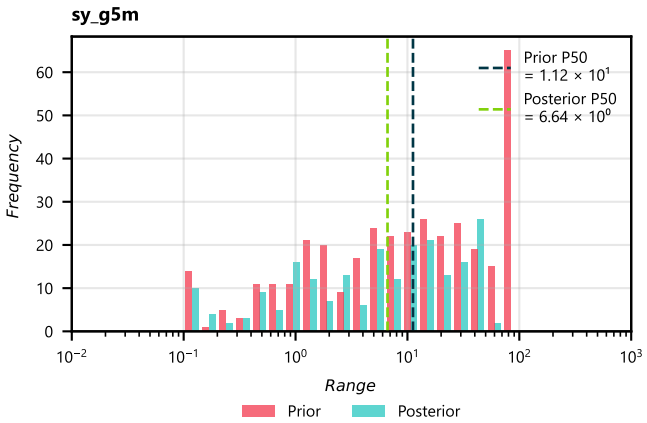
sy_g4ki

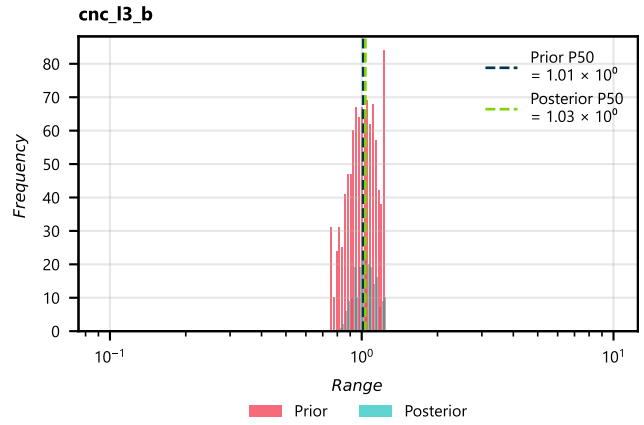


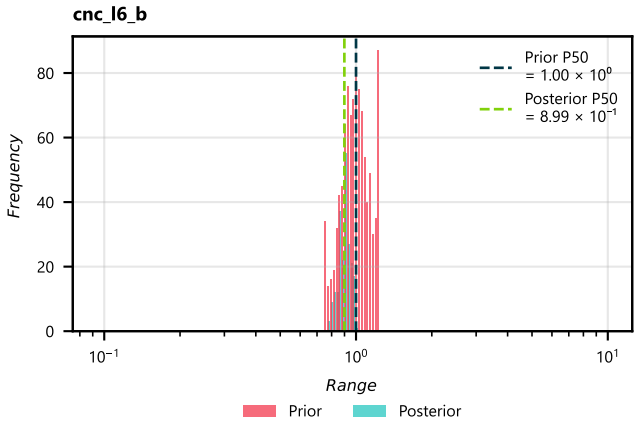

sy_g4m
Prior P50
= 8.81 × 10⁰
Posterior P50
= 1.03 × 10¹
Frequency
Range
Prior
Posterior

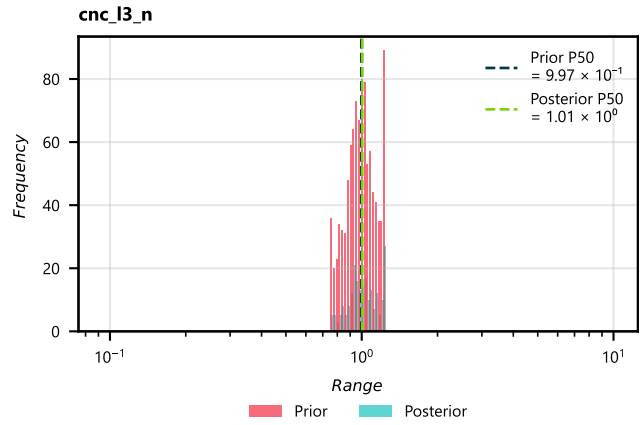

sy_g5s
Prior P50
= 1.88 × 10⁰
Posterior P50
= 4.12 × 10⁰
Frequency
Range
Prior
Posterior

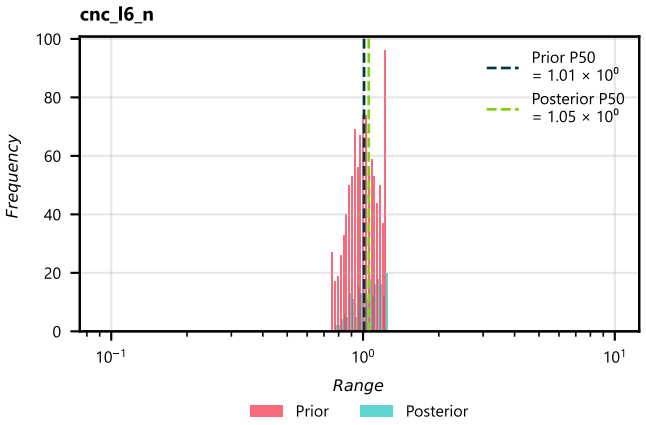

sy_g5ki
Prior P50
= 2.24 × 10⁰
Posterior P50
= 2.10 × 10⁰
Frequency
Range
Prior
Posterior

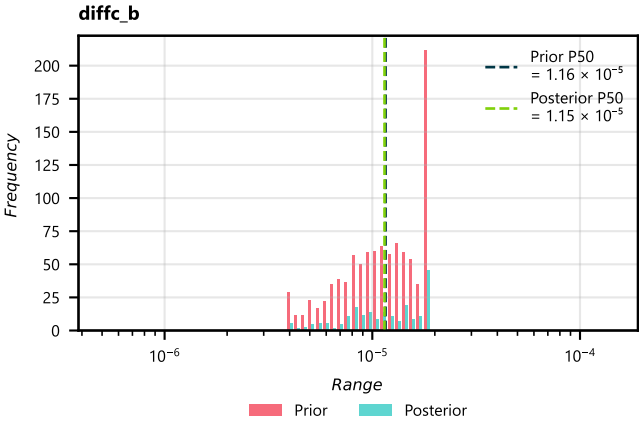

sy_g5m
Prior P50
= 1.12 × 10¹
Posterior P50
= 6.64 × 10⁰
Frequency
Range
Prior
Posterior

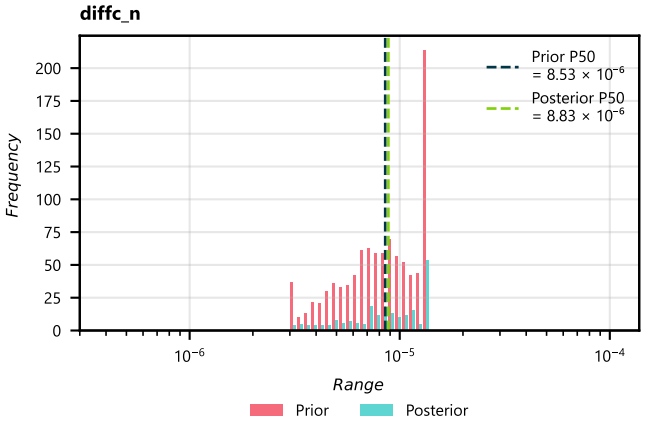

cnc_l3_b
Prior P50
= 1.01 × 10^0
Posterior P50
= 1.03 × 10^0
Frequency
Range
Prior
Posterior

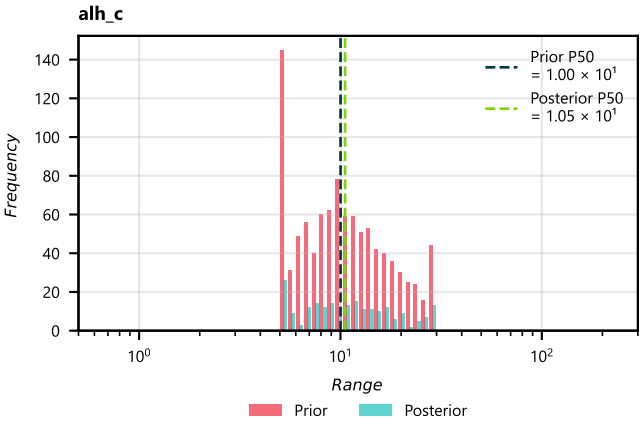

cnc_l6_b
Prior P50
= 1.00 × 10^0
Posterior P50
= 8.99 × 10^-1
Frequency
Range
Prior
Posterior

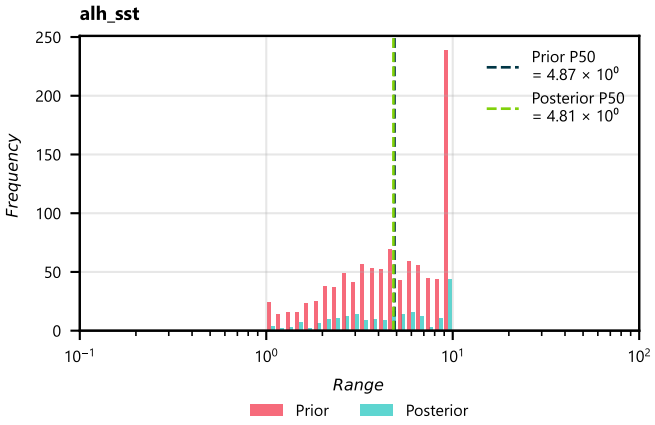

cnc_l3_n
Prior P50
= 9.97 × 10^-1
Posterior P50
= 1.01 × 10^0
Frequency
Range
Prior
Posterior

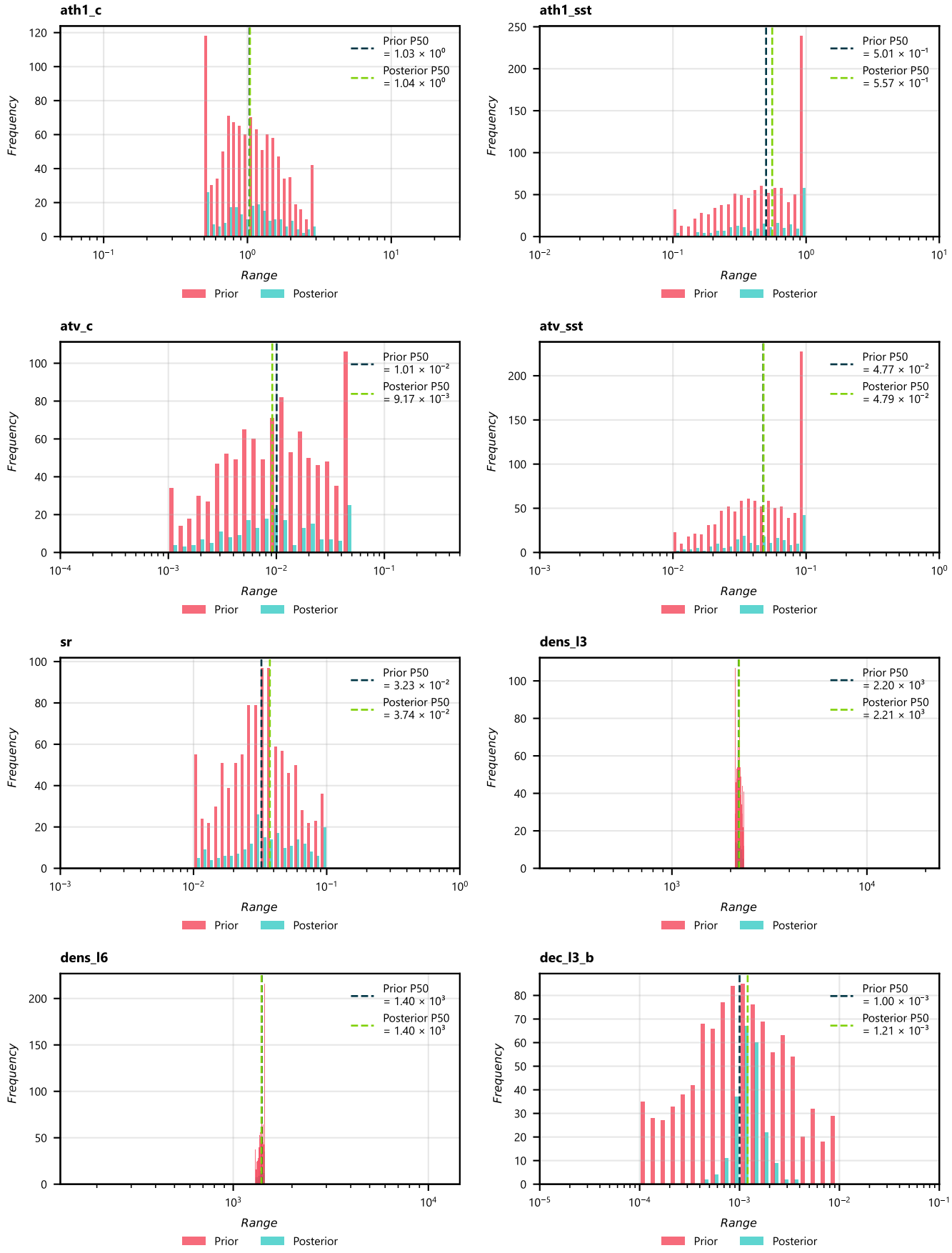

cnc_l6_n
Prior P50
= 1.01 × 10^0
Posterior P50
= 1.05 × 10^0
Frequency
Range
Prior
Posterior

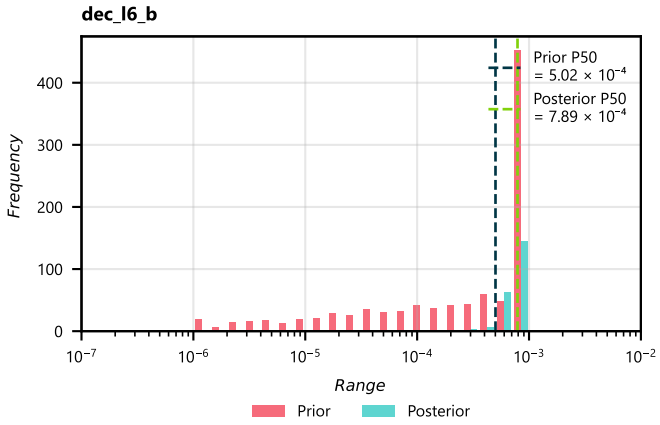

diffc_b
Prior P50
= 1.16 × 10^-5
Posterior P50
= 1.15 × 10^-5
Frequency
Range
Prior
Posterior

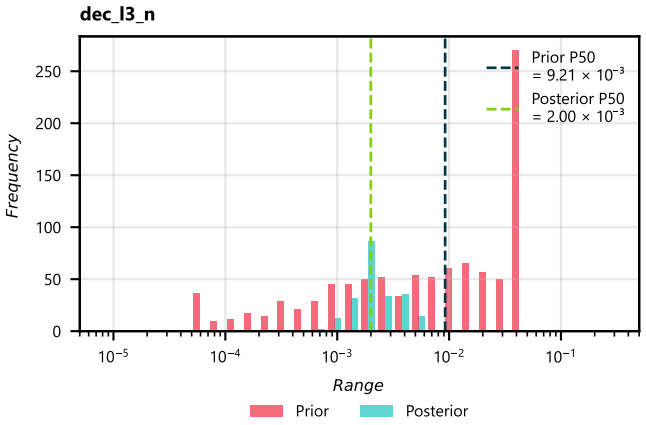

diffc_n
Prior P50
= 8.53 × 10^-6
Posterior P50
= 8.83 × 10^-6
Frequency
Range
Prior
Posterior

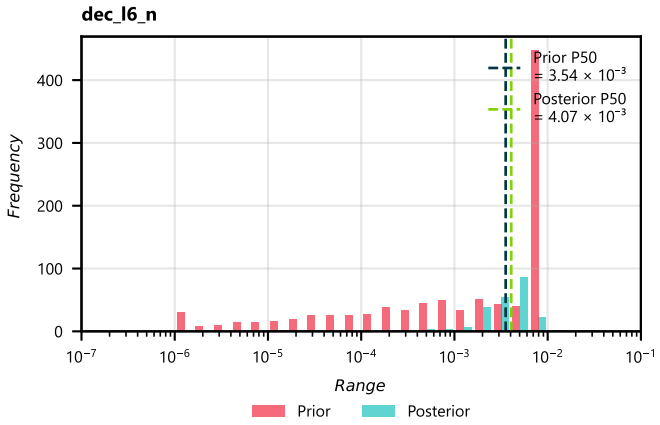

alh_c
Prior P50
= 1.00 × 10^1
Posterior P50
= 1.05 × 10^1
Frequency
Range
Prior
Posterior

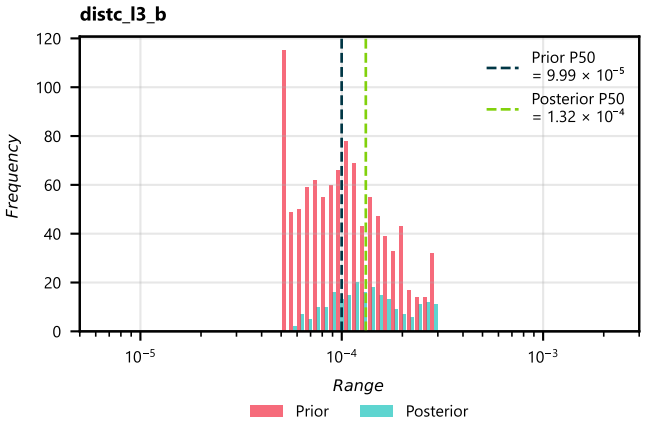

alh_sst
Prior P50
= 4.87 × 10^0
Posterior P50
= 4.81 × 10^0
Frequency
Range
Prior
Posterior

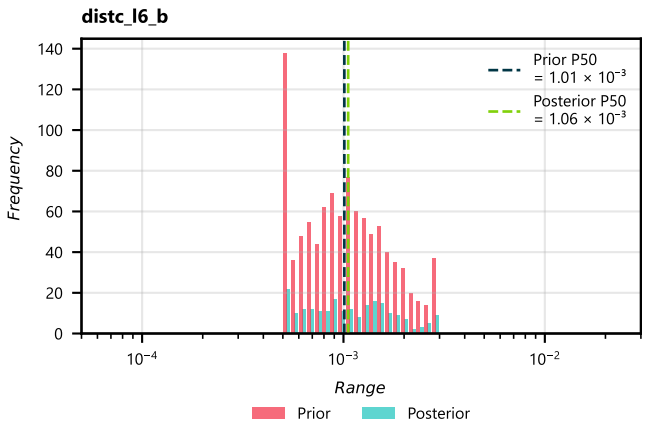

ath1_c
Prior P50 = 1.03 × 10^0
Posterior P50 = 1.04 × 10^0
ath1_sst
Prior P50 = 5.01 × 10^-1
Posterior P50 = 5.57 × 10^-1
atv_c
Prior P50 = 1.01 × 10^-2
Posterior P50 = 9.17 × 10^-3
atv_sst
Prior P50 = 4.77 × 10^-2
Posterior P50 = 4.79 × 10^-2
sr
Prior P50 = 3.23 × 10^-2
Posterior P50 = 3.74 × 10^-2
dens_l3
Prior P50 = 2.20 × 10^3
Posterior P50 = 2.21 × 10^3
dens_l6
Prior P50 = 1.40 × 10^3
Posterior P50 = 1.40 × 10^3
dec_l3_b
Prior P50 = 1.00 × 10^-3
Posterior P50 = 1.21 × 10^-3
Frequency
Range
Prior
Posterior

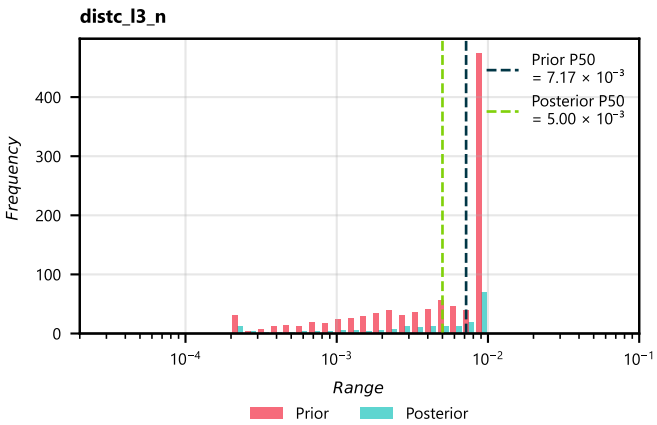

dec_l6_b
Prior P50
= 5.02 × 10⁻⁴
Posterior P50
= 7.89 × 10⁻⁴
Frequency
Range
Prior
Posterior

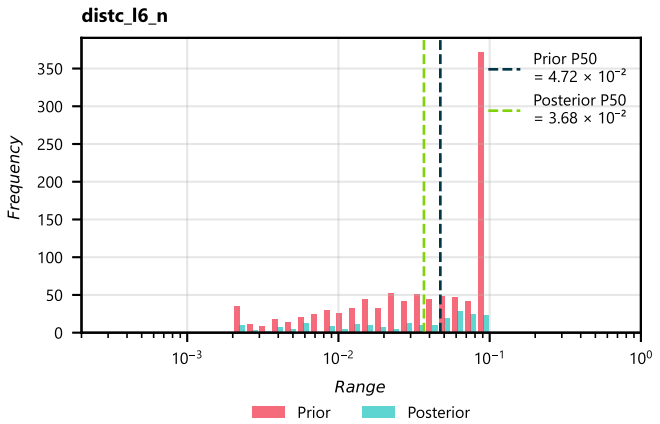

dec_l3_n
Prior P50
= 9.21 × 10⁻³
Posterior P50
= 2.00 × 10⁻³
Frequency
Range
Prior
Posterior

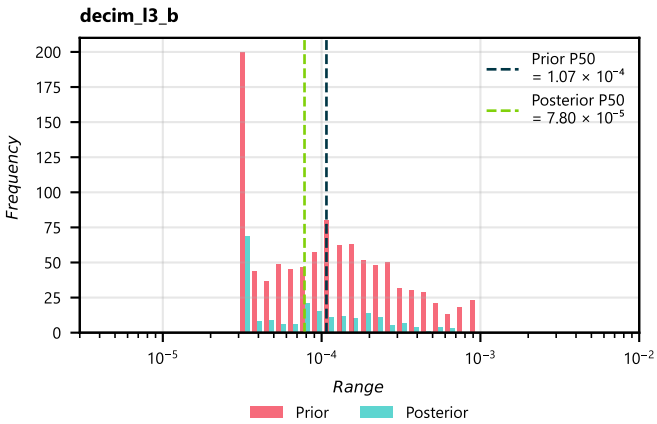

dec_l6_n
Prior P50
= 3.54 × 10⁻³
Posterior P50
= 4.07 × 10⁻³
Frequency
Range
Prior
Posterior

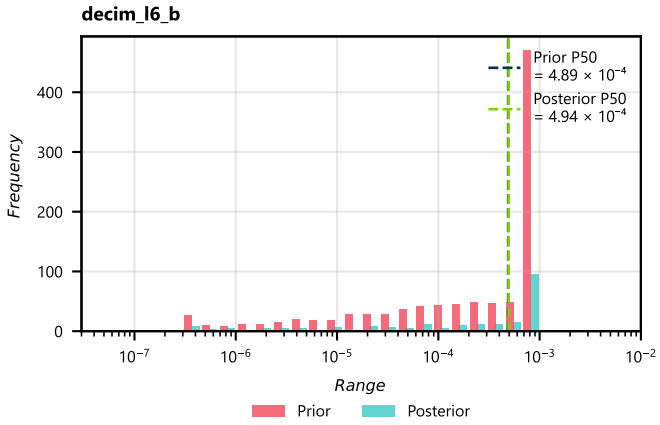

distc_l3_b
Prior P50
= 9.99 × 10⁻⁵
Posterior P50
= 1.32 × 10⁻⁴
Frequency
Range
Prior
Posterior

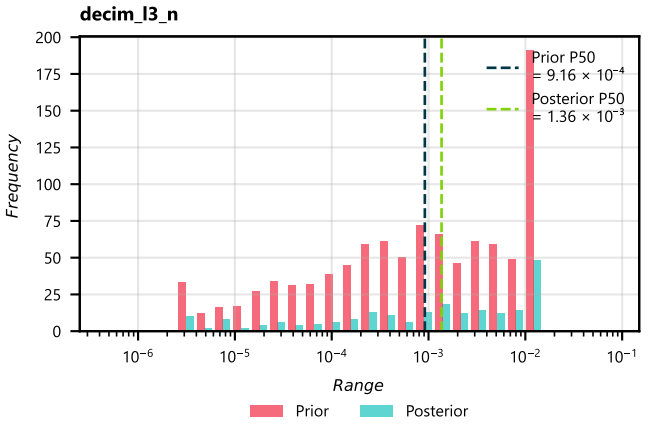

distc_l6_b
Prior P50
= 1.01 × 10⁻³
Posterior P50
= 1.06 × 10⁻³
Frequency
Range
Prior
Posterior

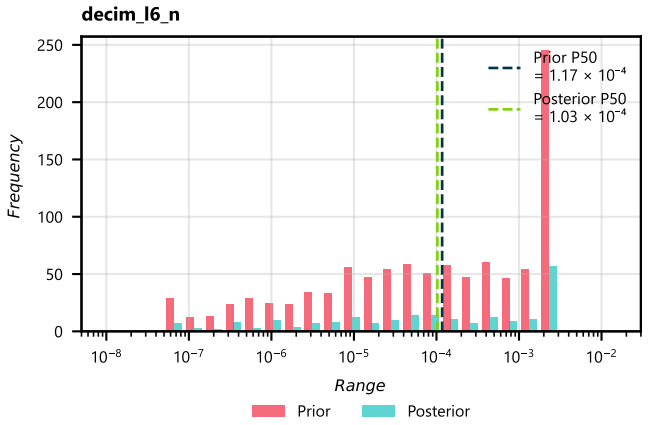

distc_l3_n
Prior P50
= 7.17 × 10⁻³
Posterior P50
= 5.00 × 10⁻³
Frequency
Range
Prior
Posterior

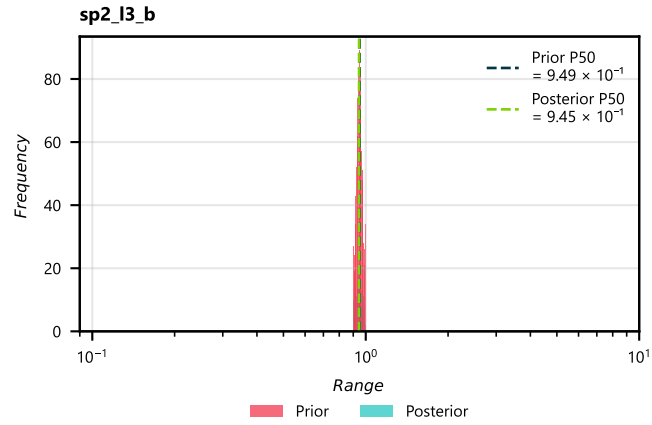

distc_l6_n
Prior P50
= 4.72 × 10⁻²
Posterior P50
= 3.68 × 10⁻²
Frequency
Range
Prior
Posterior

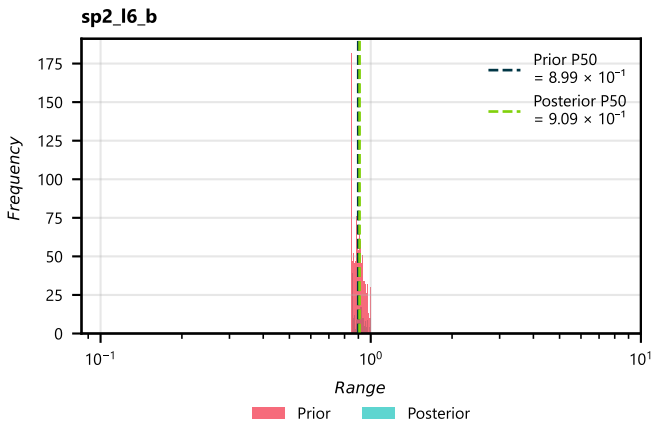

decim_l3_b
Prior P50
= 1.07 × 10⁻⁴
Posterior P50
= 7.80 × 10⁻⁵
Frequency
Range
Prior
Posterior

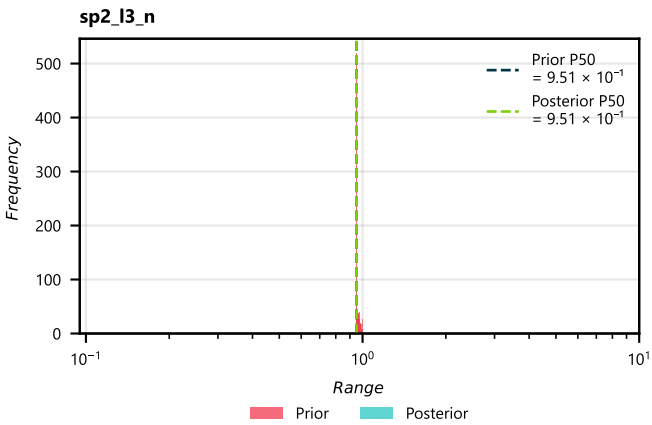

decim_l6_b
Prior P50
= 4.89 × 10⁻⁴
Posterior P50
= 4.94 × 10⁻⁴
Frequency
Range
Prior
Posterior

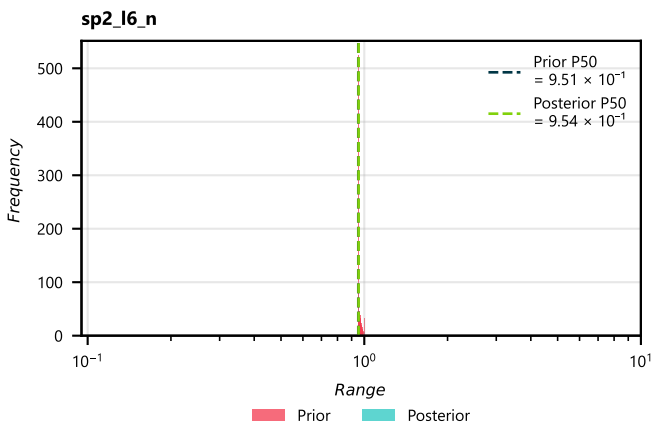

decim_l3_n
Prior P50
= 9.16 × 10⁻⁴
Posterior P50
= 1.36 × 10⁻³
Frequency
Range
Prior
Posterior

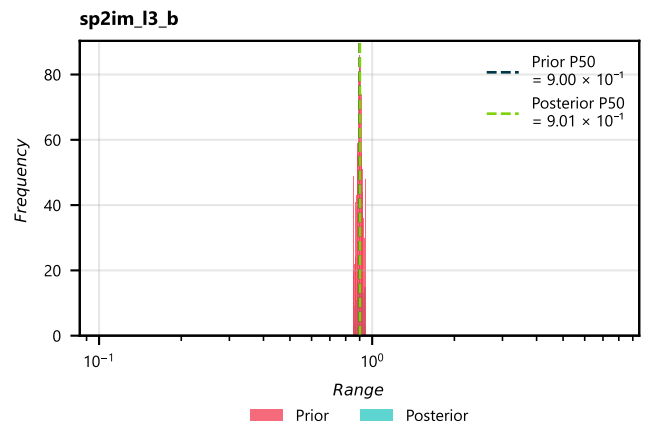

decim_l6_n
Prior P50
= 1.17 × 10⁻⁴
Posterior P50
= 1.03 × 10⁻⁴
Frequency
Range
Prior
Posterior


sp2_l3_b
Prior P50
= 9.49 × 10⁻¹
Posterior P50
= 9.45 × 10⁻¹
Frequency
Range
Prior
Posterior

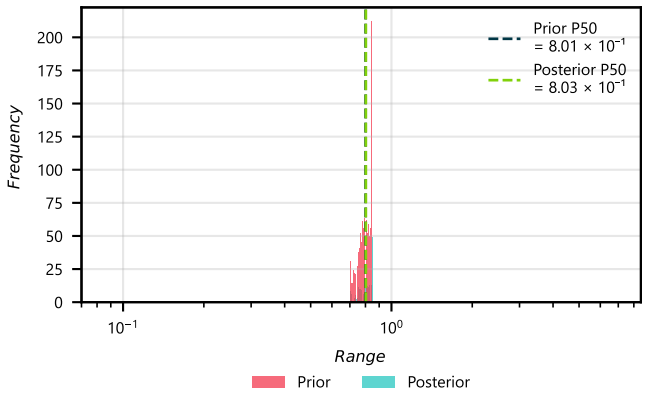

sp2_l6_b
Prior P50
= 8.99 × 10⁻¹
Posterior P50
= 9.09 × 10⁻¹
Frequency
Range
Prior
Posterior


sp2_l3_n
Prior P50
= 9.51 × 10⁻¹
Posterior P50
= 9.51 × 10⁻¹
Frequency
Range
Prior
Posterior

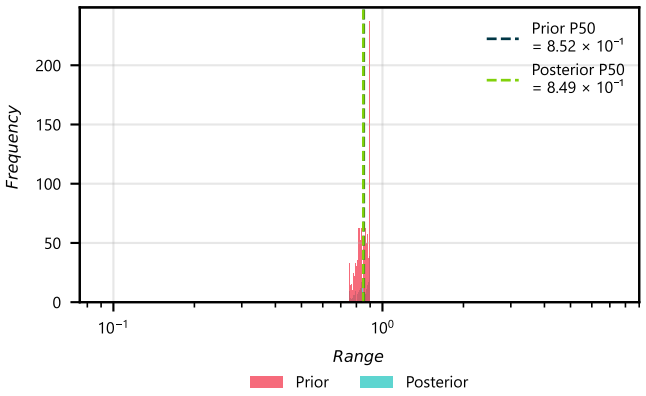

sp2_l6_n
Prior P50
= 9.51 × 10⁻¹
Posterior P50
= 9.54 × 10⁻¹
Frequency
Range
Prior
Posterior


sp2im_l3_b
Prior P50
= 9.00 × 10⁻¹
Posterior P50
= 9.01 × 10⁻¹
Frequency
Range
Prior
Posterior

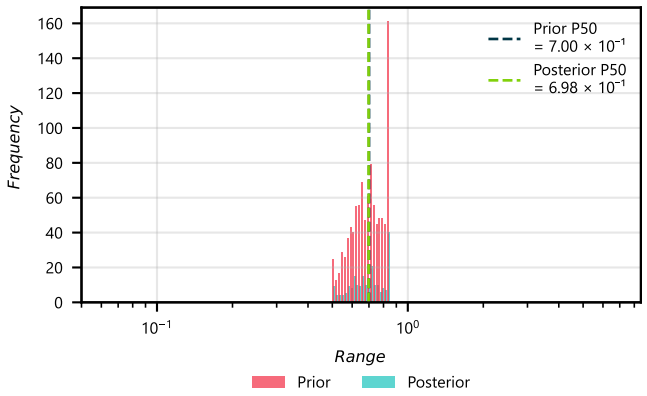
sp2im_l6_b



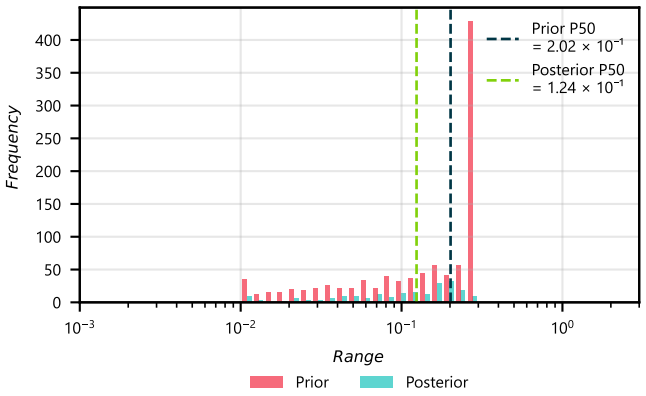
sp2im_l3_n



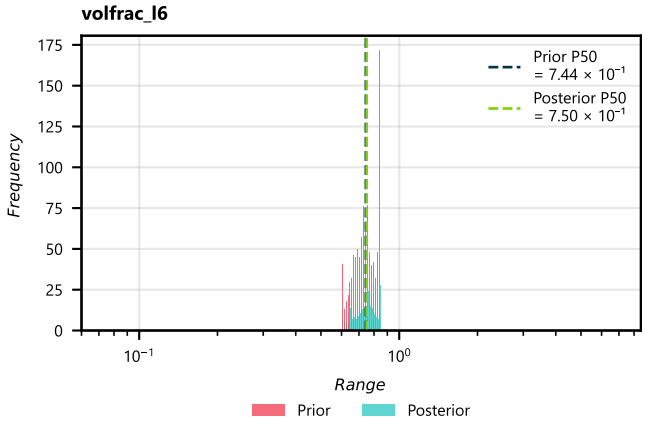
sp2im_l6_n



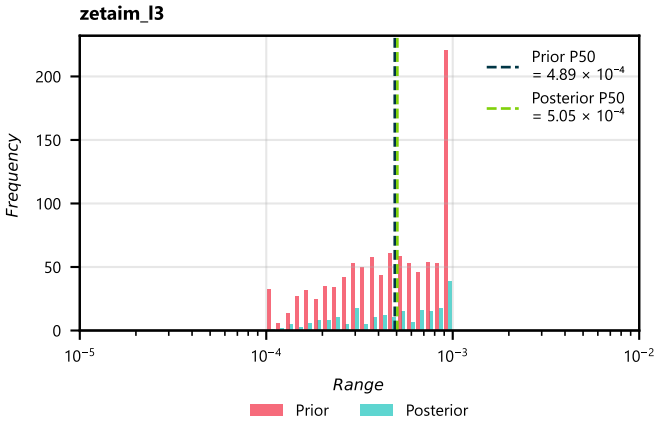
volfrac_l3



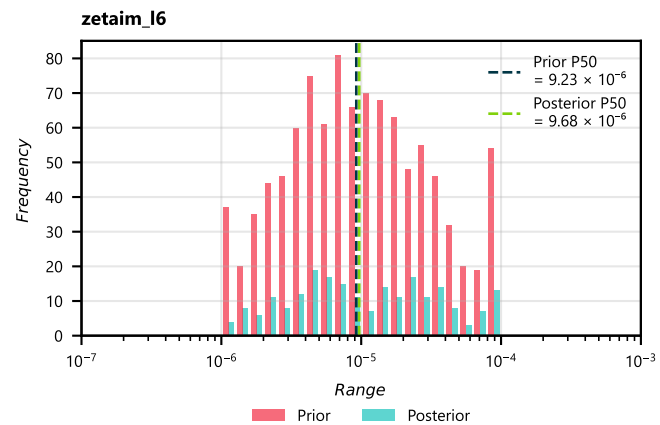
volfrac_l6



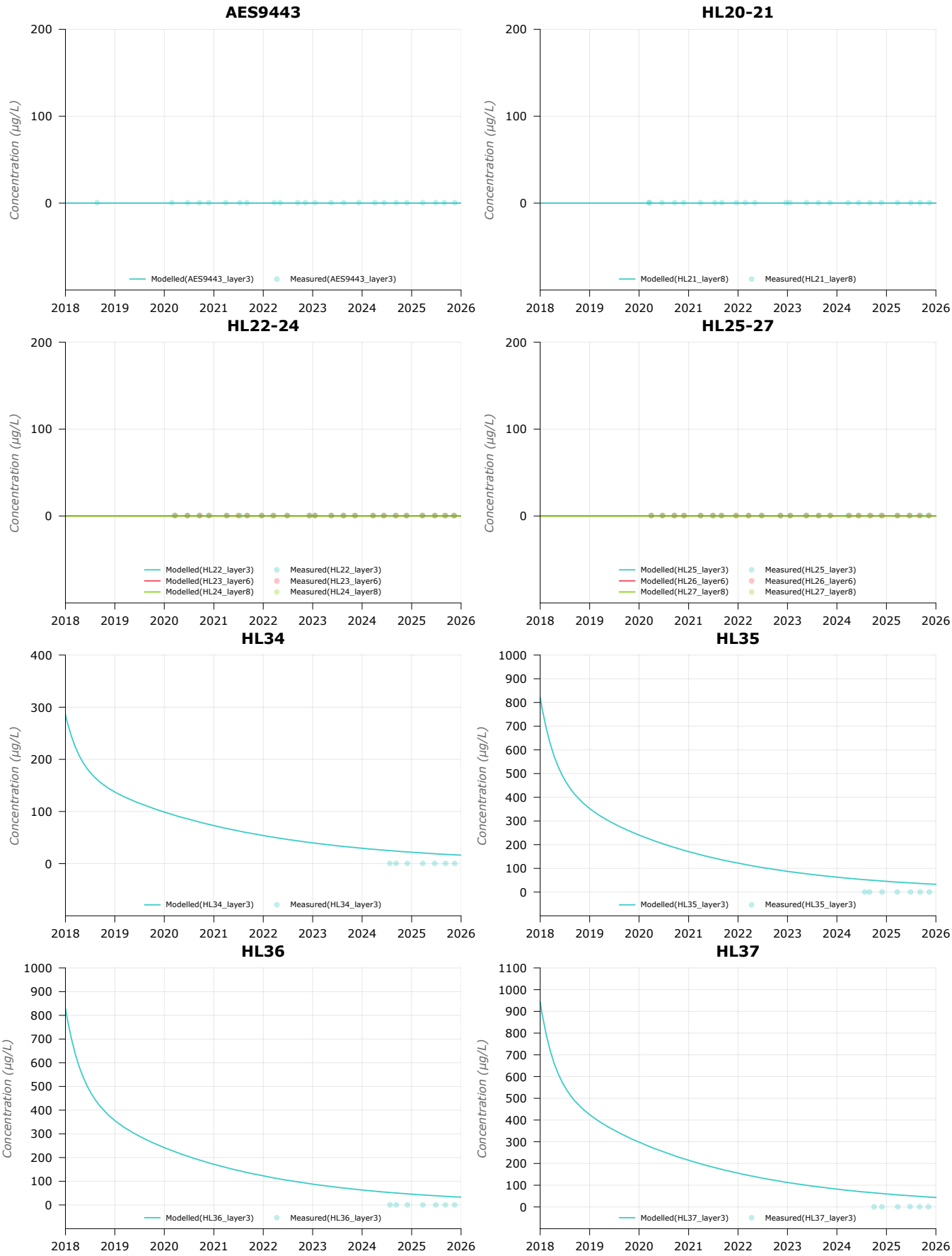
zetaim_l3

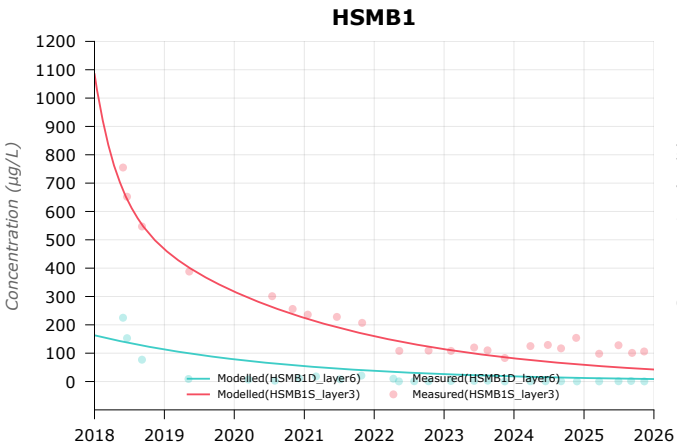


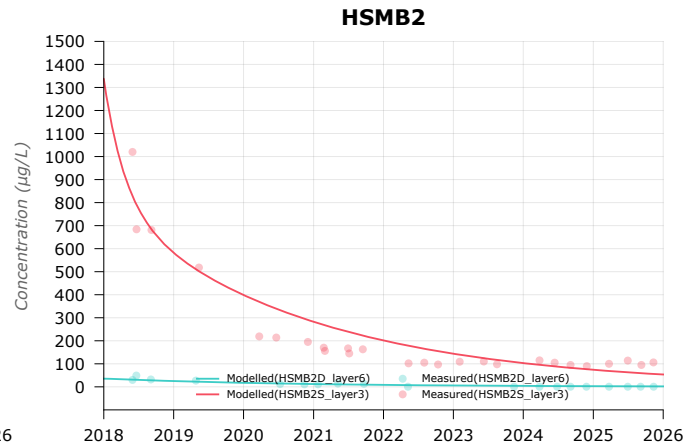
zetaim_l6

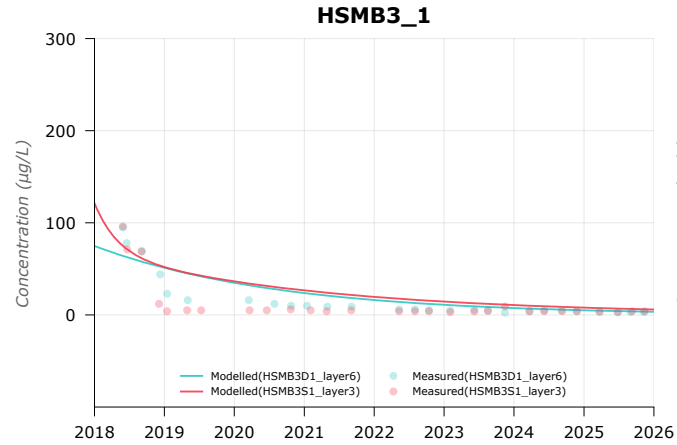


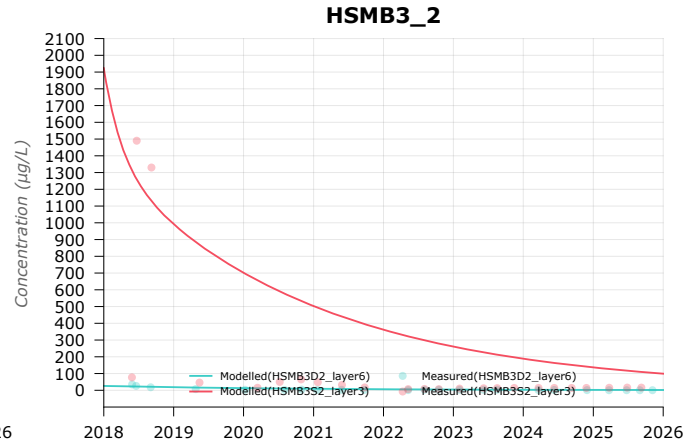
Appendix C. Modelled versus observed concentration time series plots – Benzene

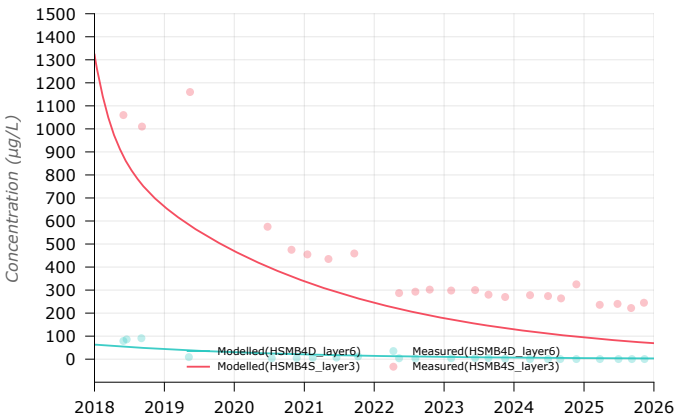

AES9443
Concentration (µg/L)
Modelled(AES9443_layer3)
Measured(AES9443_layer3)
HL20-21
Modelled(HL21_layer8)
Measured(HL21_layer8)
HL22-24
Modelled(HL22_layer3)
Modelled(HL23_layer6)
Modelled(HL24_layer8)
Measured(HL22_layer3)
Measured(HL23_layer6)
Measured(HL24_layer8)
HL25-27
Modelled(HL25_layer3)
Modelled(HL26_layer6)
Modelled(HL27_layer8)
Measured(HL25_layer3)
Measured(HL26_layer6)
Measured(HL27_layer8)
HL34
Modelled(HL34_layer3)
Measured(HL34_layer3)
HL35
Modelled(HL35_layer3)
Measured(HL35_layer3)
HL36
Modelled(HL36_layer3)
Measured(HL36_layer3)
HL37
Modelled(HL37_layer3)
Measured(HL37_layer3)

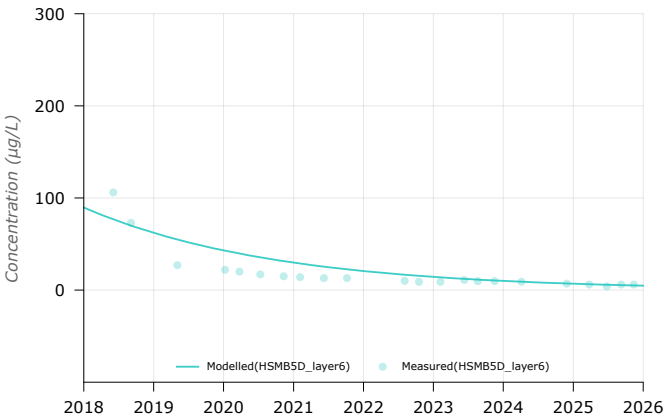

HSMB1
Concentration (µg/L)
Modelled(HSMB1D_layer6)
Modelled(HSMB1S_layer3)
Measured(HSMB1D_layer6)
Measured(HSMB1S_layer3)

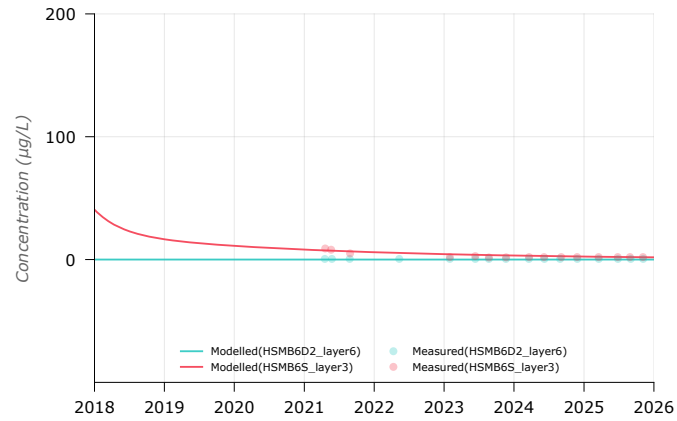

HSMB2
Concentration (µg/L)
Modelled(HSMB2D_layer6)
Modelled(HSMB2S_layer3)
Measured(HSMB2D_layer6)
Measured(HSMB2S_layer3)

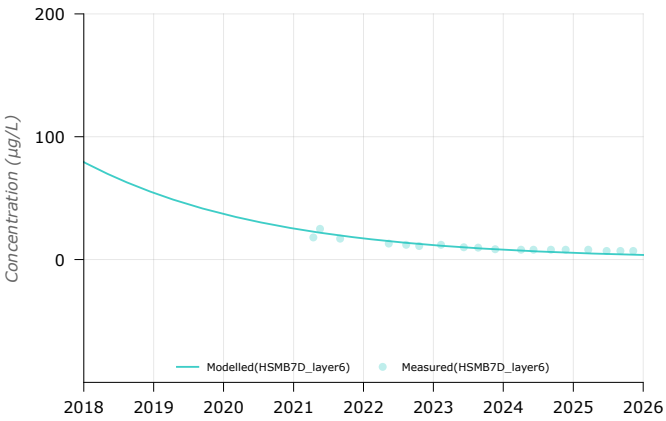

HSMB3_1
Concentration (µg/L)
Modelled(HSMB3D1_layer6)
Modelled(HSMB3S1_layer3)
Measured(HSMB3D1_layer6)
Measured(HSMB3S1_layer3)

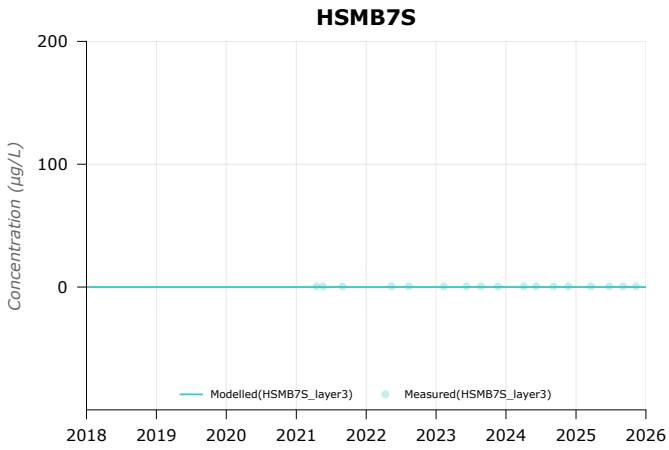

HSMB3_2
Concentration (µg/L)
Modelled(HSMB3D2_layer6)
Modelled(HSMB3S2_layer3)
Measured(HSMB3D2_layer6)
Measured(HSMB3S2_layer3)

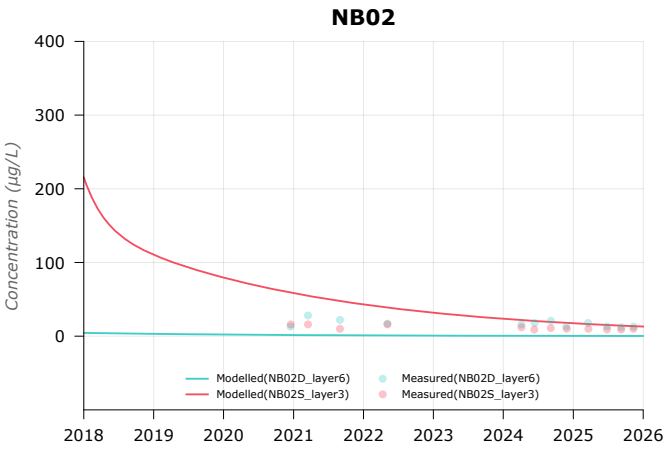

HSMB4
Concentration (µg/L)
Modelled(HSMB4D_layer6)
Modelled(HSMB4S_layer3)
Measured(HSMB4D_layer6)
Measured(HSMB4S_layer3)

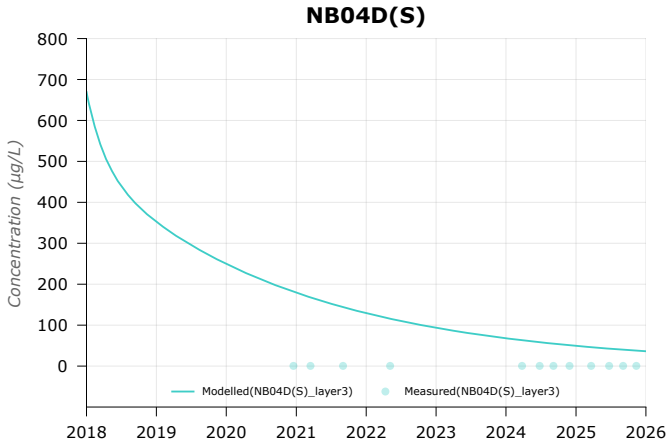

HSMB5D
Concentration (µg/L)
Modelled(HSMB5D_layer6)
Measured(HSMB5D_layer6)

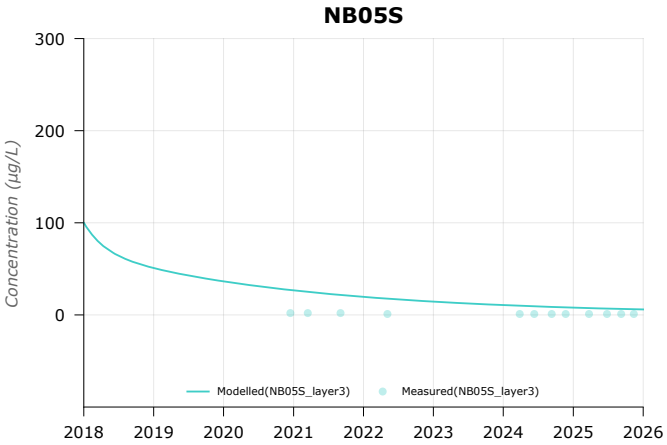

HSMB6
Concentration (µg/L)
Modelled(HSMB6D2_layer6)
Modelled(HSMB6S_layer3)
Measured(HSMB6D2_layer6)
Measured(HSMB6S_layer3)

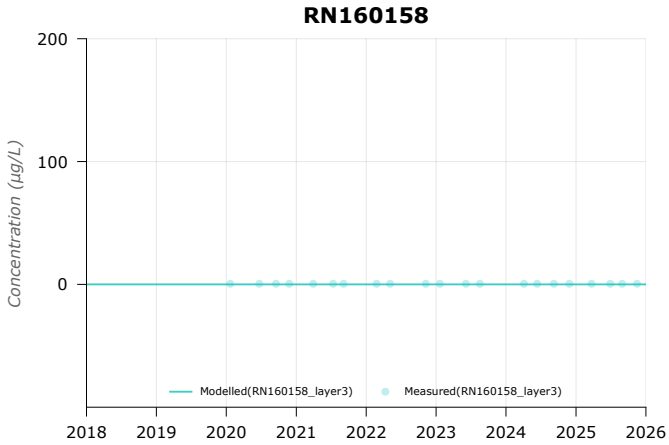

HSMB7D
Concentration (µg/L)
Modelled(HSMB7D_layer6)
Measured(HSMB7D_layer6)


HSMB7S
Concentration (µg/L)
200
100
0
Modelled(HSMB7S_layer3)
Measured(HSMB7S_layer3)
2018
2019
2020
2021
2022
2023
2024
2025
2026

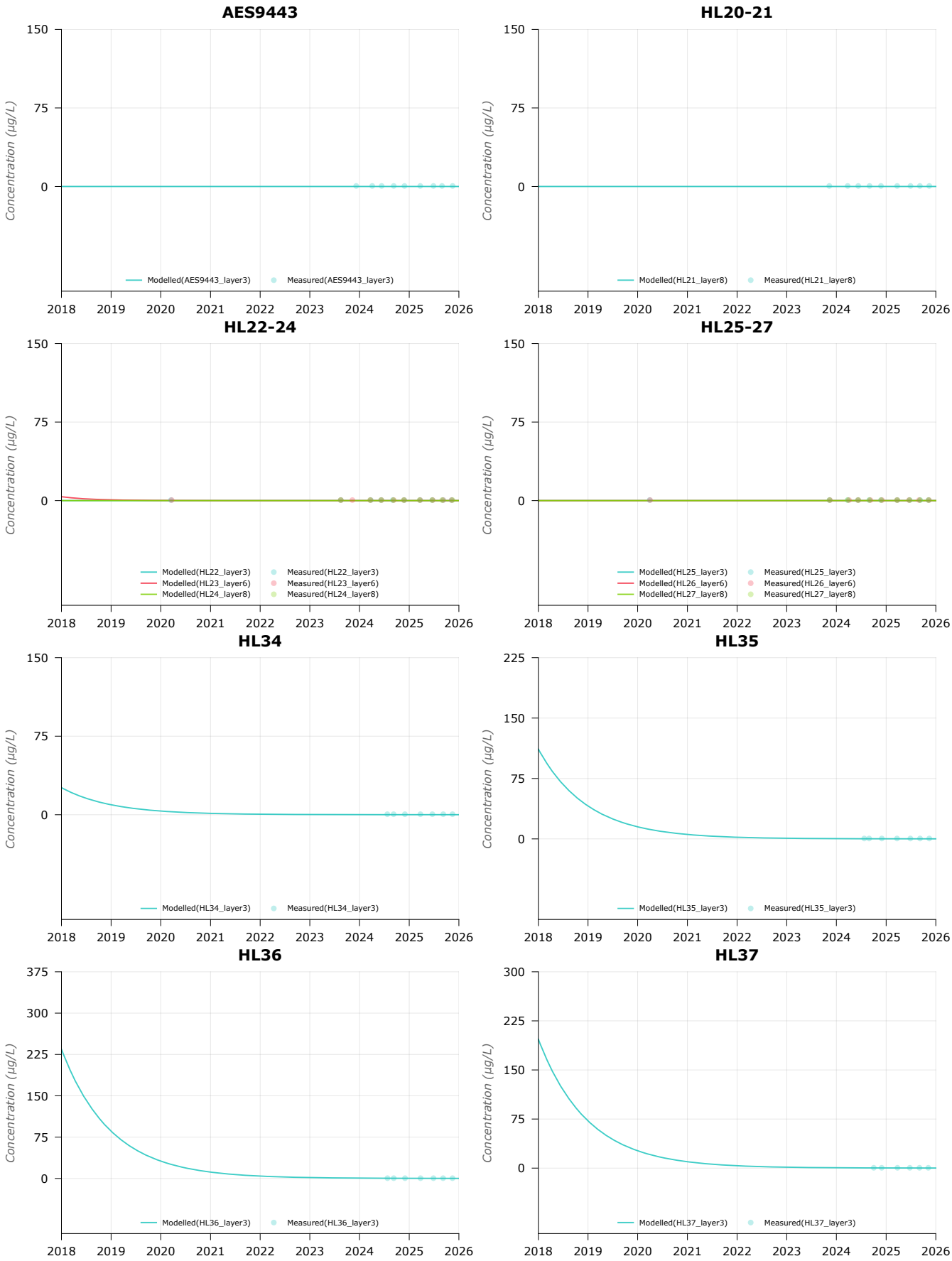

NB02
Concentration (µg/L)
400
300
200
100
0
Modelled(NB02D_layer6)
Measured(NB02D_layer6)
Modelled(NB02S_layer3)
Measured(NB02S_layer3)
2018
2019
2020
2021
2022
2023
2024
2025
2026

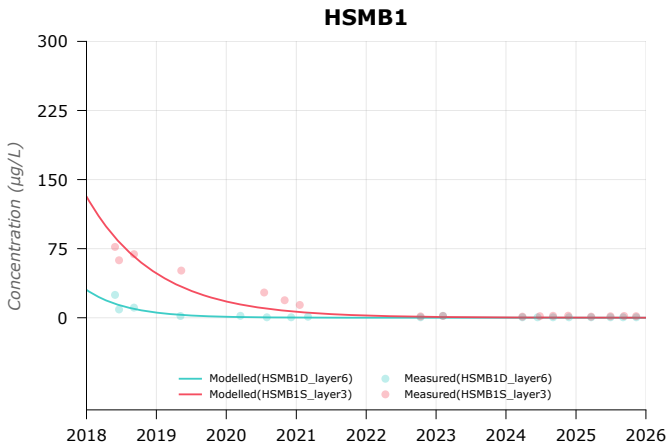

NB04D(S)
Concentration (µg/L)
800
700
600
500
400
300
200
100
0
Modelled(NB04D(S)_layer3)
Measured(NB04D(S)_layer3)
2018
2019
2020
2021
2022
2023
2024
2025
2026

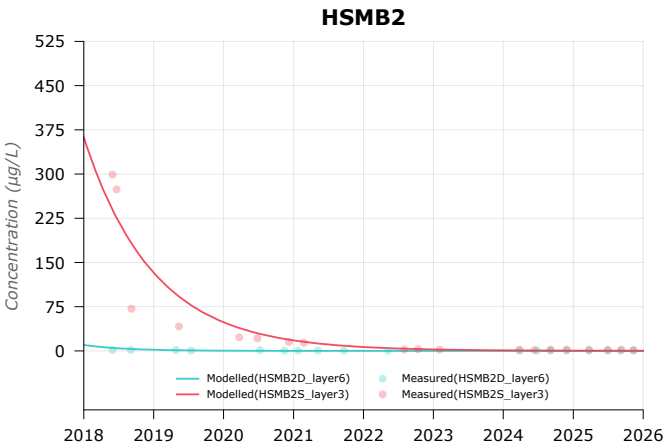

NB05S
Concentration (µg/L)
300
200
100
0
Modelled(NB05S_layer3)
Measured(NB05S_layer3)
2018
2019
2020
2021
2022
2023
2024
2025
2026

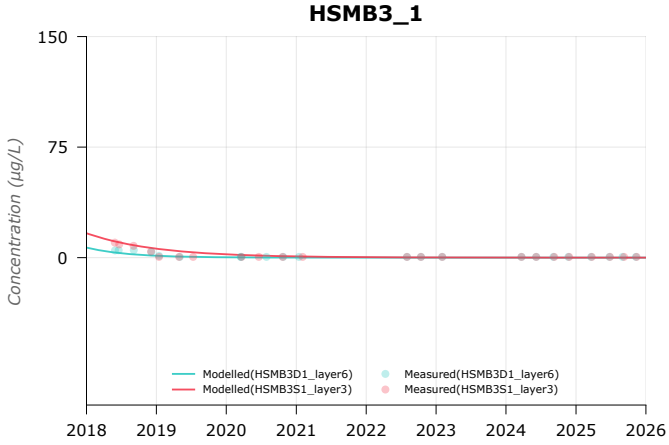

RN160158
Concentration (µg/L)
200
100
0
Modelled(RN160158_layer3)
Measured(RN160158_layer3)
2018
2019
2020
2021
2022
2023
2024
2025
2026

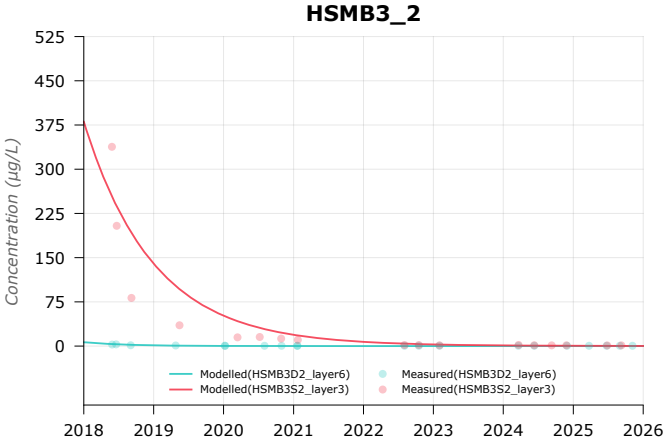
Appendix D. Modelled versus observed concentration time series plots - Naphthalene

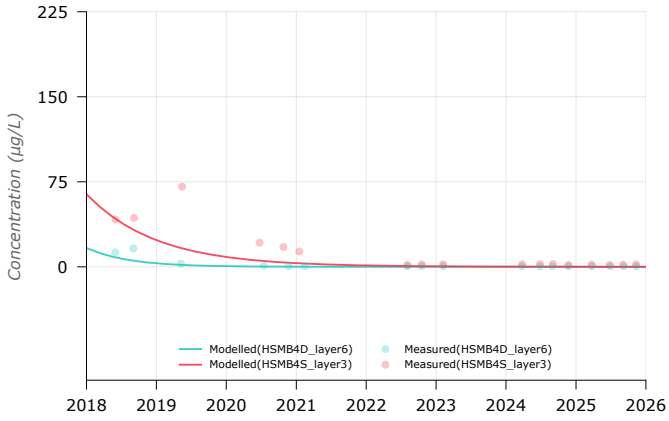

AES9443
Concentration (µg/L)
150
75
0
Modelled(AES9443_layer3)
Measured(AES9443_layer3)
2018
2019
2020
2021
2022
2023
2024
2025
2026
HL20-21
Concentration (µg/L)
150
75
0
Modelled(HL21_layer8)
Measured(HL21_layer8)
2018
2019
2020
2021
2022
2023
2024
2025
2026
HL22-24
Concentration (µg/L)
150
75
0
Modelled(HL22_layer3)
Modelled(HL23_layer6)
Modelled(HL24_layer8)
Measured(HL22_layer3)
Measured(HL23_layer6)
Measured(HL24_layer8)
2018
2019
2020
2021
2022
2023
2024
2025
2026
HL25-27
Concentration (µg/L)
150
75
0
Modelled(HL25_layer3)
Modelled(HL26_layer6)
Modelled(HL27_layer8)
Measured(HL25_layer3)
Measured(HL26_layer6)
Measured(HL27_layer8)
2018
2019
2020
2021
2022
2023
2024
2025
2026
HL34
Concentration (µg/L)
150
75
0
Modelled(HL34_layer3)
Measured(HL34_layer3)
2018
2019
2020
2021
2022
2023
2024
2025
2026
HL35
Concentration (µg/L)
225
150
75
0
Modelled(HL35_layer3)
Measured(HL35_layer3)
2018
2019
2020
2021
2022
2023
2024
2025
2026
HL36
Concentration (µg/L)
375
300
225
150
75
0
Modelled(HL36_layer3)
Measured(HL36_layer3)
2018
2019
2020
2021
2022
2023
2024
2025
2026
HL37
Concentration (µg/L)
300
225
150
75
0
Modelled(HL37_layer3)
Measured(HL37_layer3)
2018
2019
2020
2021
2022
2023
2024
2025
2026

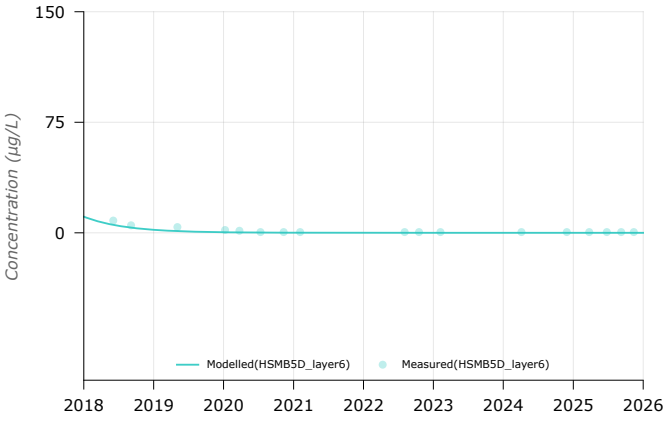

HSMB1
Concentration (µg/L)
300
225
150
75
0
2018
2019
2020
2021
2022
2023
2024
2025
2026
Modelled(HSMB1D_layer6)
Modelled(HSMB1S_layer3)
Measured(HSMB1D_layer6)
Measured(HSMB1S_layer3)

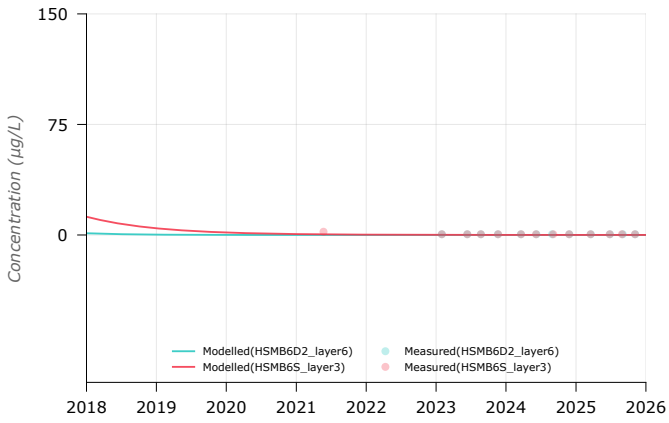

HSMB2
Concentration (µg/L)
525
450
375
300
225
150
75
0
2018
2019
2020
2021
2022
2023
2024
2025
2026
Modelled(HSMB2D_layer6)
Modelled(HSMB2S_layer3)
Measured(HSMB2D_layer6)
Measured(HSMB2S_layer3)

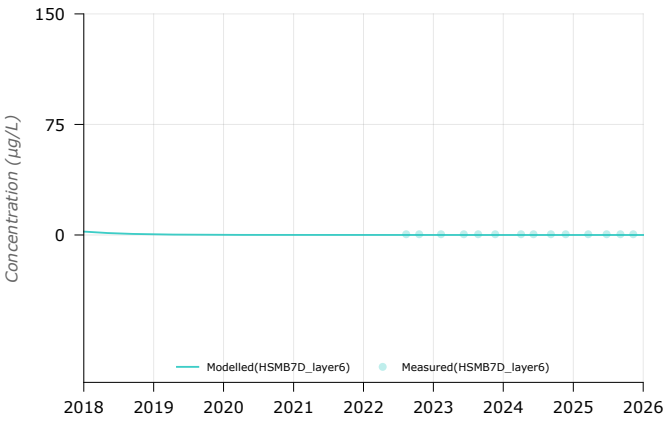

HSMB3_1
Concentration (µg/L)
150
75
0
2018
2019
2020
2021
2022
2023
2024
2025
2026
Modelled(HSMB3D1_layer6)
Modelled(HSMB3S1_layer3)
Measured(HSMB3D1_layer6)
Measured(HSMB3S1_layer3)

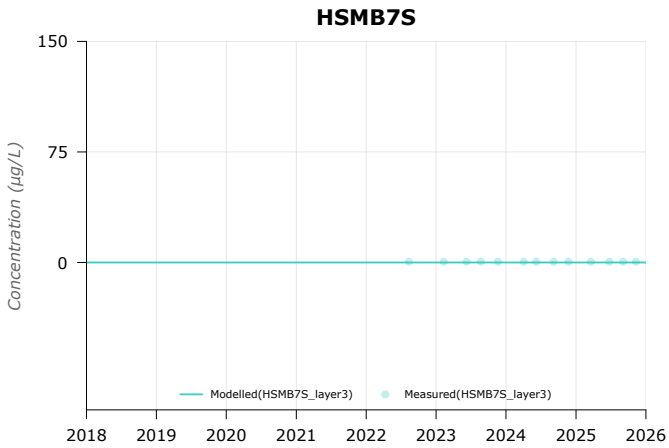

HSMB3_2
Concentration (µg/L)
525
450
375
300
225
150
75
0
2018
2019
2020
2021
2022
2023
2024
2025
2026
Modelled(HSMB3D2_layer6)
Modelled(HSMB3S2_layer3)
Measured(HSMB3D2_layer6)
Measured(HSMB3S2_layer3)

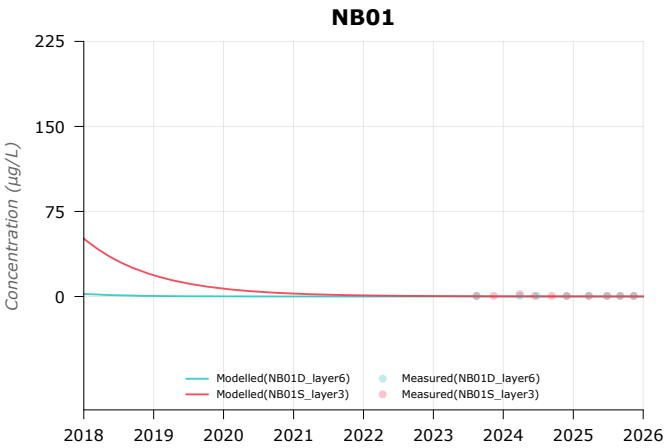

HSMB4
Concentration (µg/L)
225
150
75
0
2018
2019
2020
2021
2022
2023
2024
2025
2026
Modelled(HSMB4D_layer6)
Modelled(HSMB4S_layer3)
Measured(HSMB4D_layer6)
Measured(HSMB4S_layer3)

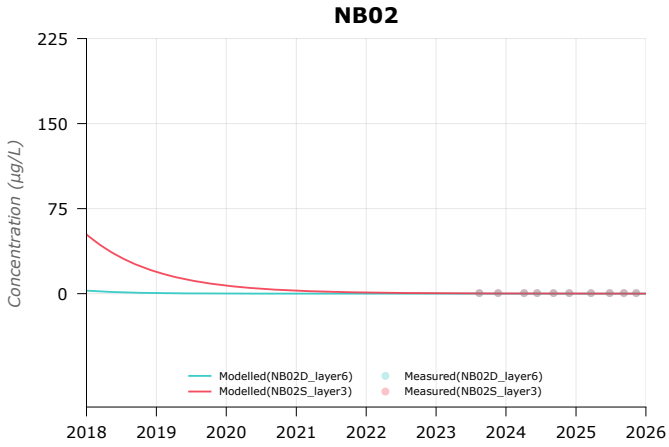

HSMB5D
Concentration (µg/L)
150
75
0
2018
2019
2020
2021
2022
2023
2024
2025
2026
Modelled(HSMB5D_layer6)
Measured(HSMB5D_layer6)

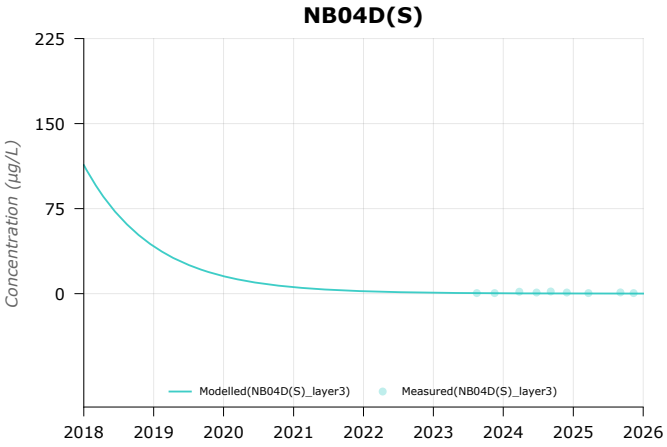

HSMB6
Concentration (µg/L)
150
75
0
2018
2019
2020
2021
2022
2023
2024
2025
2026
Modelled(HSMB6D2_layer6)
Modelled(HSMB6S_layer3)
Measured(HSMB6D2_layer6)
Measured(HSMB6S_layer3)

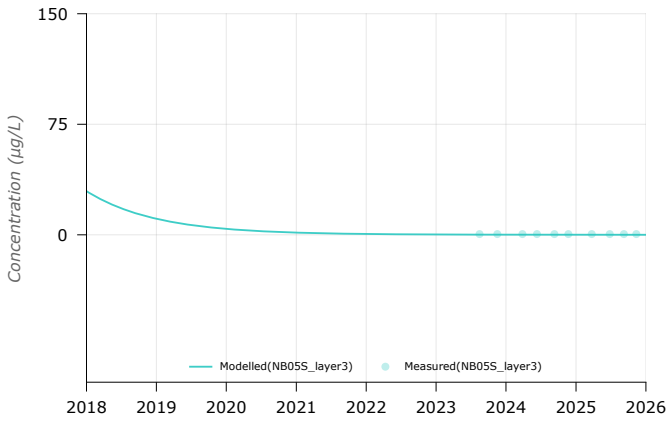

HSMB7D
Concentration (µg/L)
150
75
0
2018
2019
2020
2021
2022
2023
2024
2025
2026
Modelled(HSMB7D_layer6)
Measured(HSMB7D_layer6)

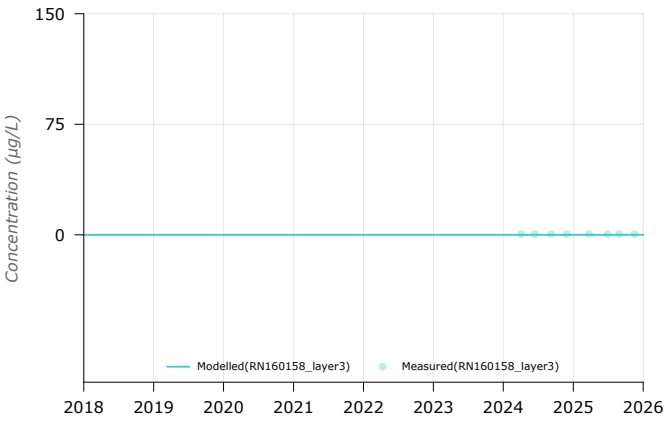

HSMB7S
Concentration (µg/L)
150
75
0
Modelled(HSMB7S_layer3)
Measured(HSMB7S_layer3)
2018
2019
2020
2021
2022
2023
2024
2025
2026


NB01
Concentration (µg/L)
225
150
75
0
Modelled(NB01D_layer6)
Modelled(NB01S_layer3)
Measured(NB01D_layer6)
Measured(NB01S_layer3)
2018
2019
2020
2021
2022
2023
2024
2025
2026

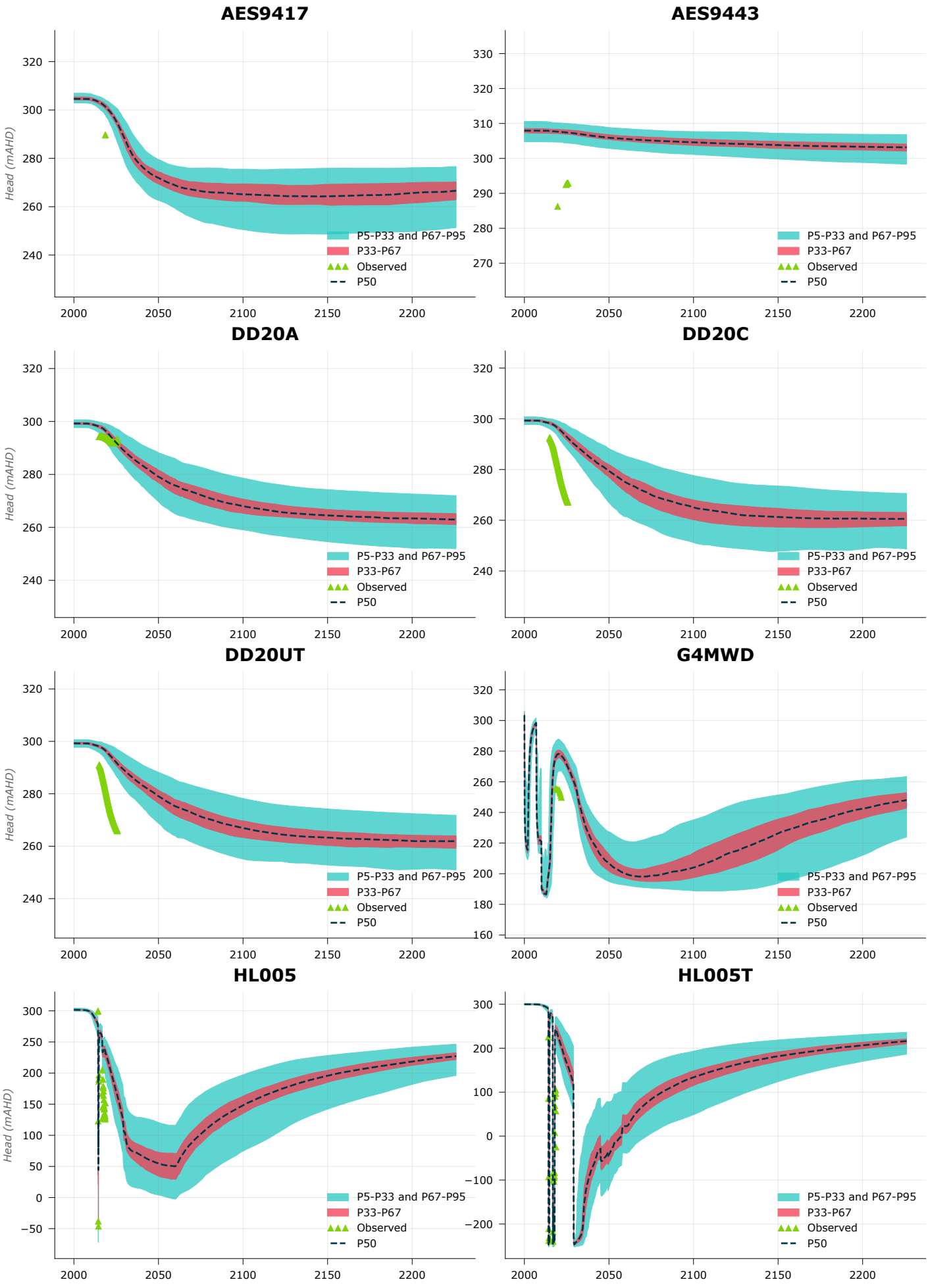

NB02
Concentration (µg/L)
225
150
75
0
Modelled(NB02D_layer6)
Modelled(NB02S_layer3)
Measured(NB02D_layer6)
Measured(NB02S_layer3)
2018
2019
2020
2021
2022
2023
2024
2025
2026

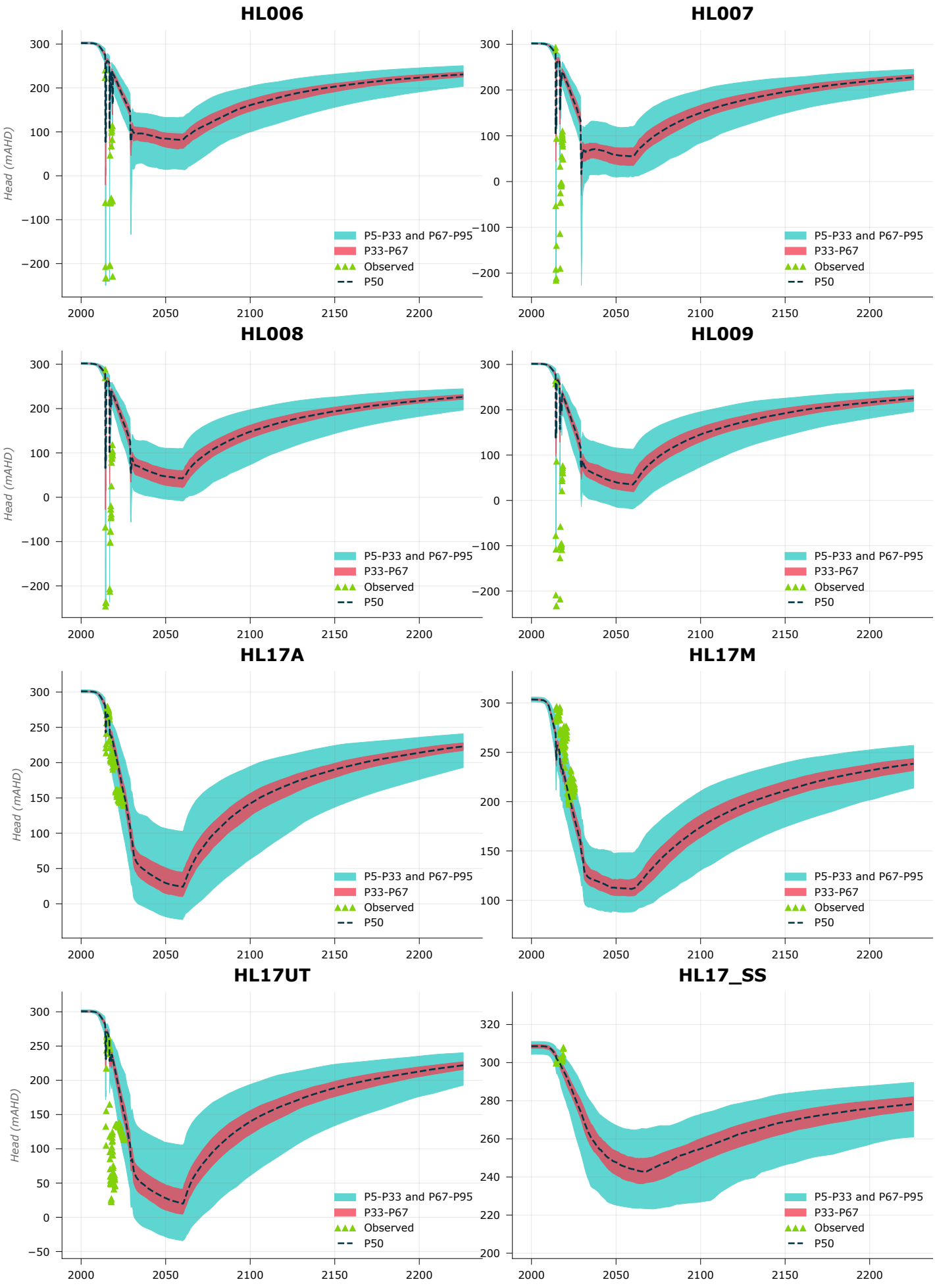

NB04D(S)
Concentration (µg/L)
225
150
75
0
Modelled(NB04D(S)_layer3)
Measured(NB04D(S)_layer3)
2018
2019
2020
2021
2022
2023
2024
2025
2026

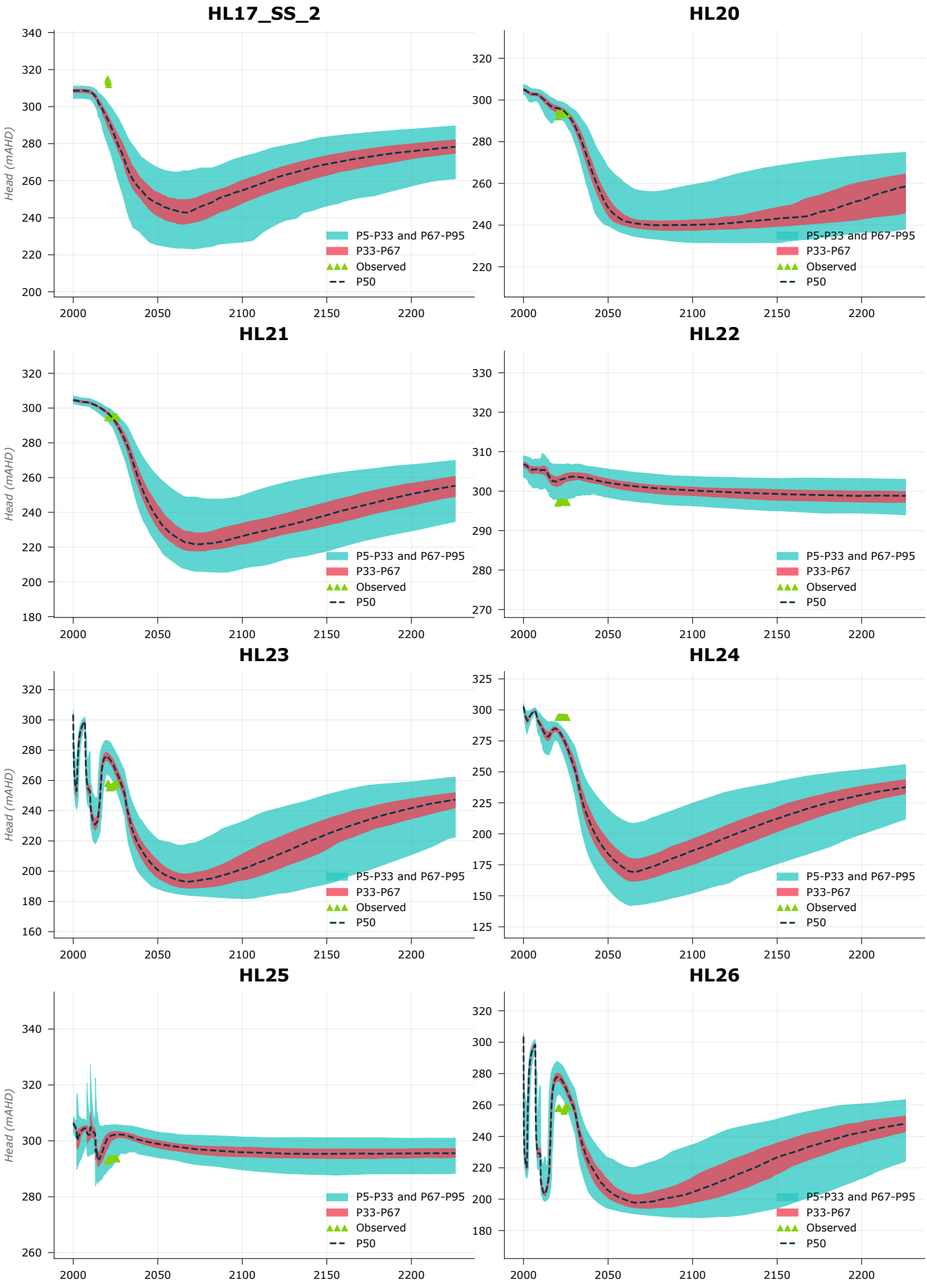

NB05S
Concentration (µg/L)
150
75
0
Modelled(NB05S_layer3)
Measured(NB05S_layer3)
2018
2019
2020
2021
2022
2023
2024
2025
2026

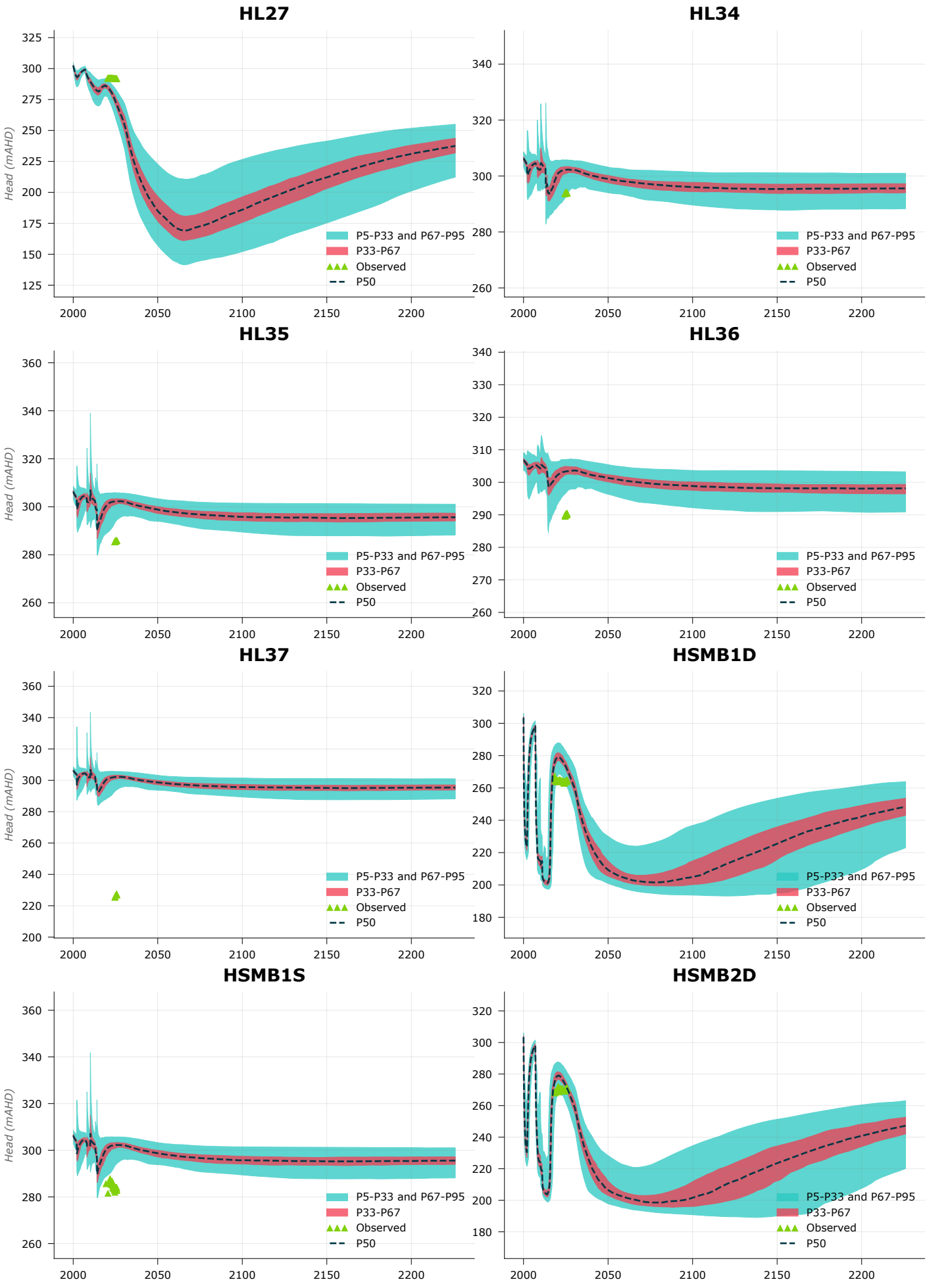

RN160158
Concentration (µg/L)
150
75
0
Modelled(RN160158_layer3)
Measured(RN160158_layer3)
2018
2019
2020
2021
2022
2023
2024
2025
2026

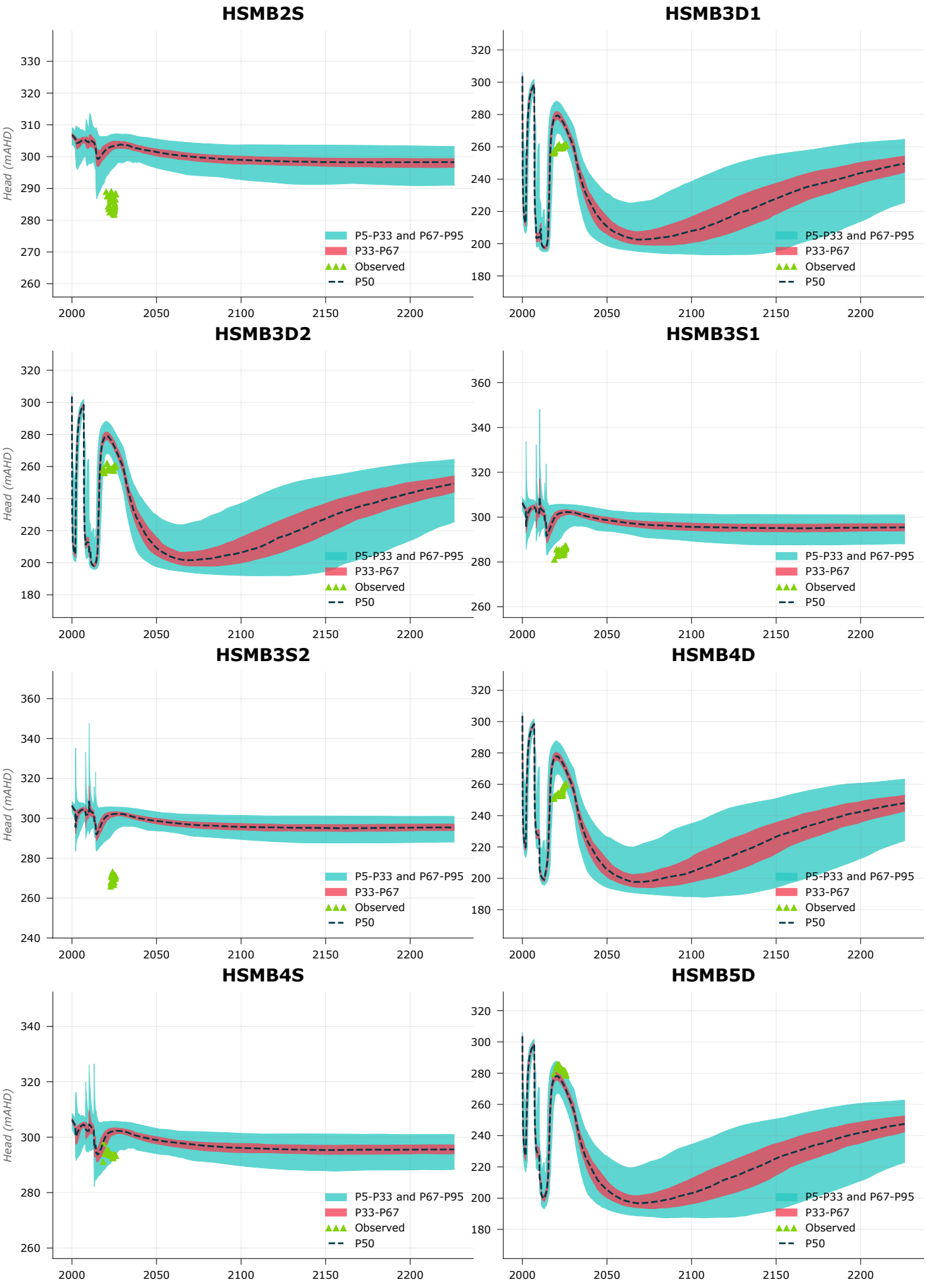
Appendix E. Predictive uncertainty - groundwater levels

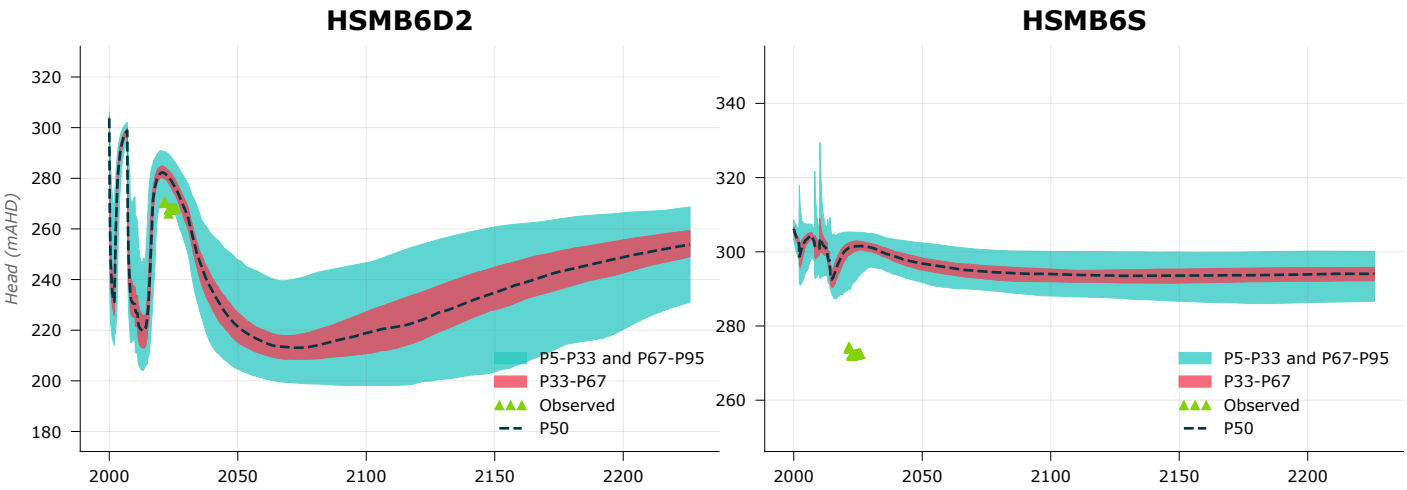

AES9417
AES9443
DD20A
DD20C
DD20UT
G4MWD
HL005
HL005T
Head (mAHD)
P5-P33 and P67-P95
P33-P67
Observed
P50

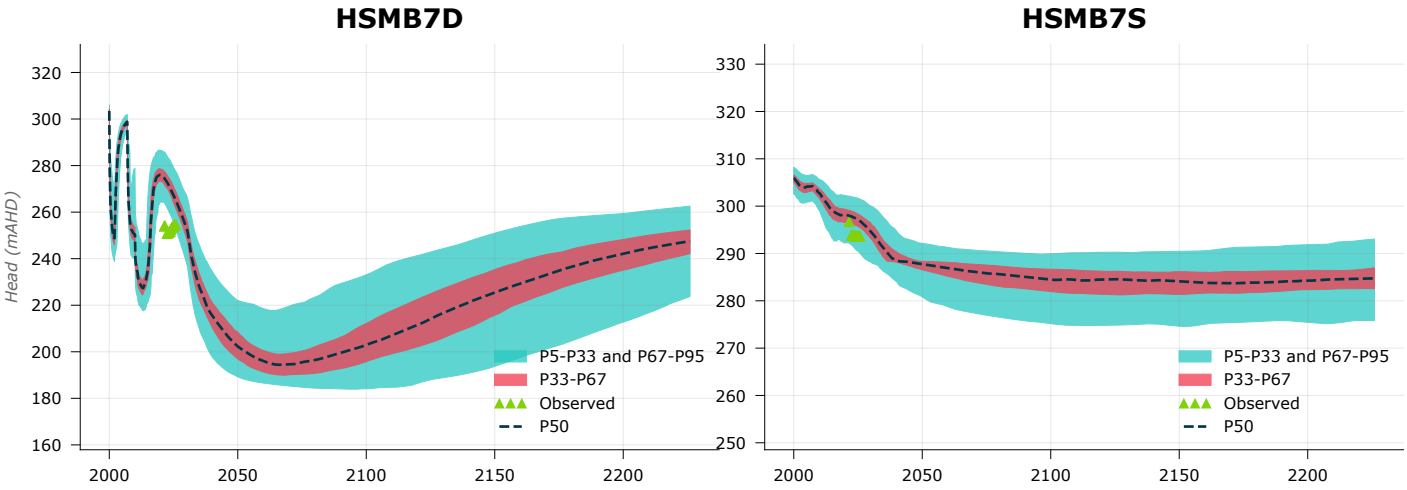

HL006
HL007
HL008
HL009
HL17A
HL17M
HL17UT
HL17_SS
Head (mAHD)
P5-P33 and P67-P95
P33-P67
Observed
P50


HL17_SS_2
HL20
HL21
HL22
HL23
HL24
HL25
HL26
Head (mAHD)
P5-P33 and P67-P95
P33-P67
Observed
P50
2000
2050
2100
2150
2200


HL27
HL34
HL35
HL36
HL37
HSMB1D
HSMB1S
HSMB2D
Head (mAHD)
P5-P33 and P67-P95
P33-P67
Observed
P50
2000
2050
2100
2150
2200

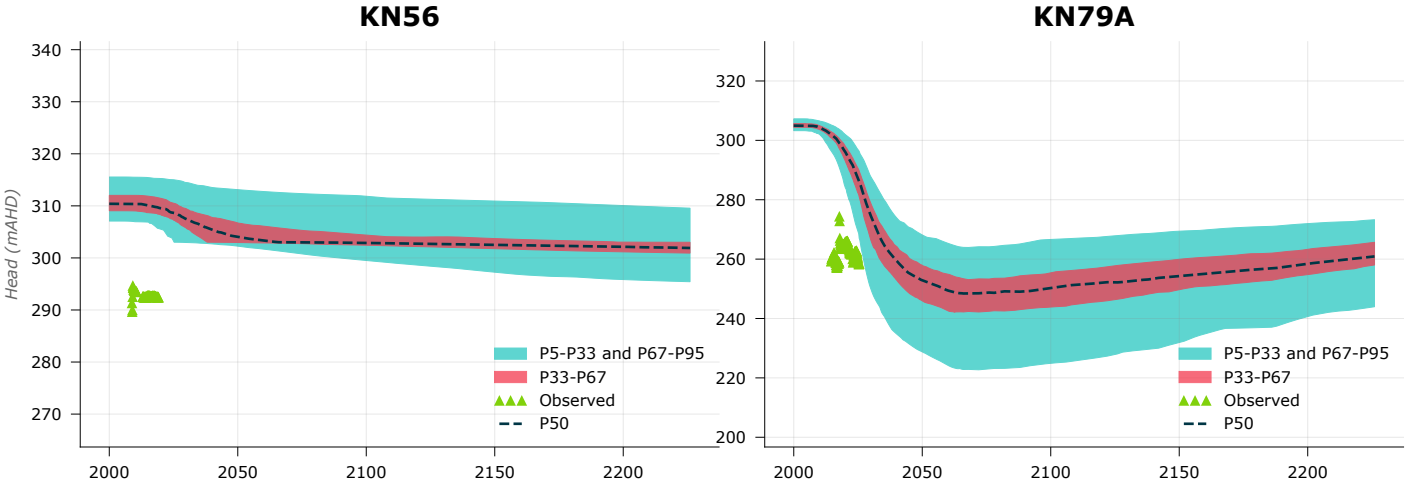

HSMB2S
HSMB3D1
HSMB3D2
HSMB3S1
HSMB3S2
HSMB4D
HSMB4S
HSMB5D
Head (mAHD)
P5-P33 and P67-P95
P33-P67
Observed
P50
2000
2050
2100
2150
2200


HSMB6D2
Head (mAHD)
320
300
280
260
240
220
200
180
2000
2050
2100
2150
2200
P5-P33 and P67-P95
P33-P67
Observed
P50

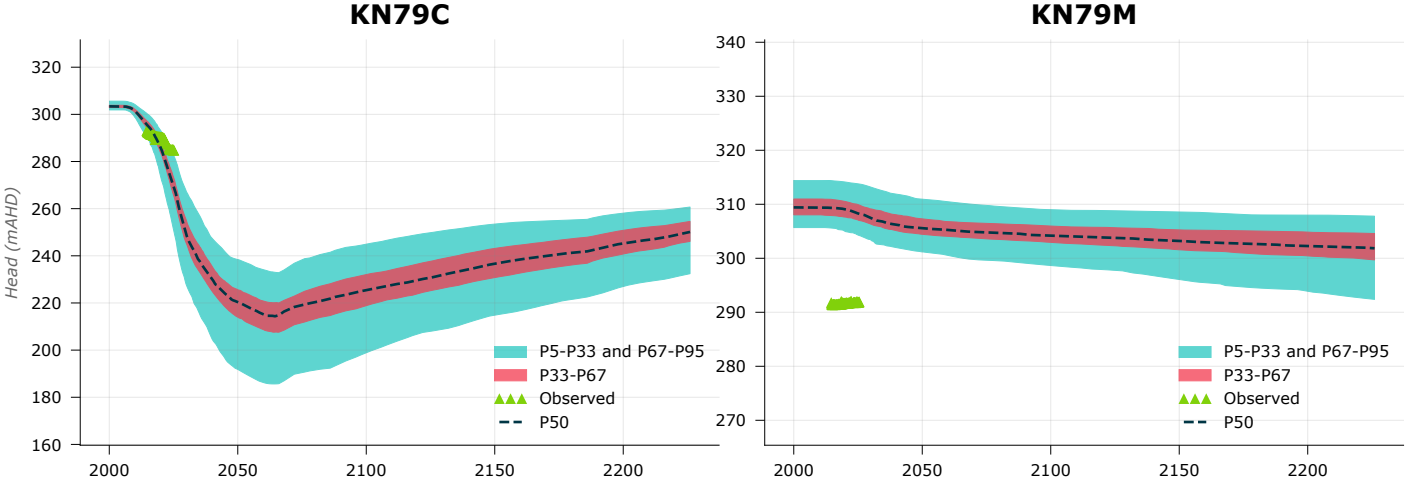

HSMB6S
Head (mAHD)
340
320
300
280
260
2000
2050
2100
2150
2200
P5-P33 and P67-P95
P33-P67
Observed
P50

HSMB7D
Head (mAHD)
320
300
280
260
240
220
200
180
160
2000
2050
2100
2150
2200
P5-P33 and P67-P95
P33-P67
Observed
P50

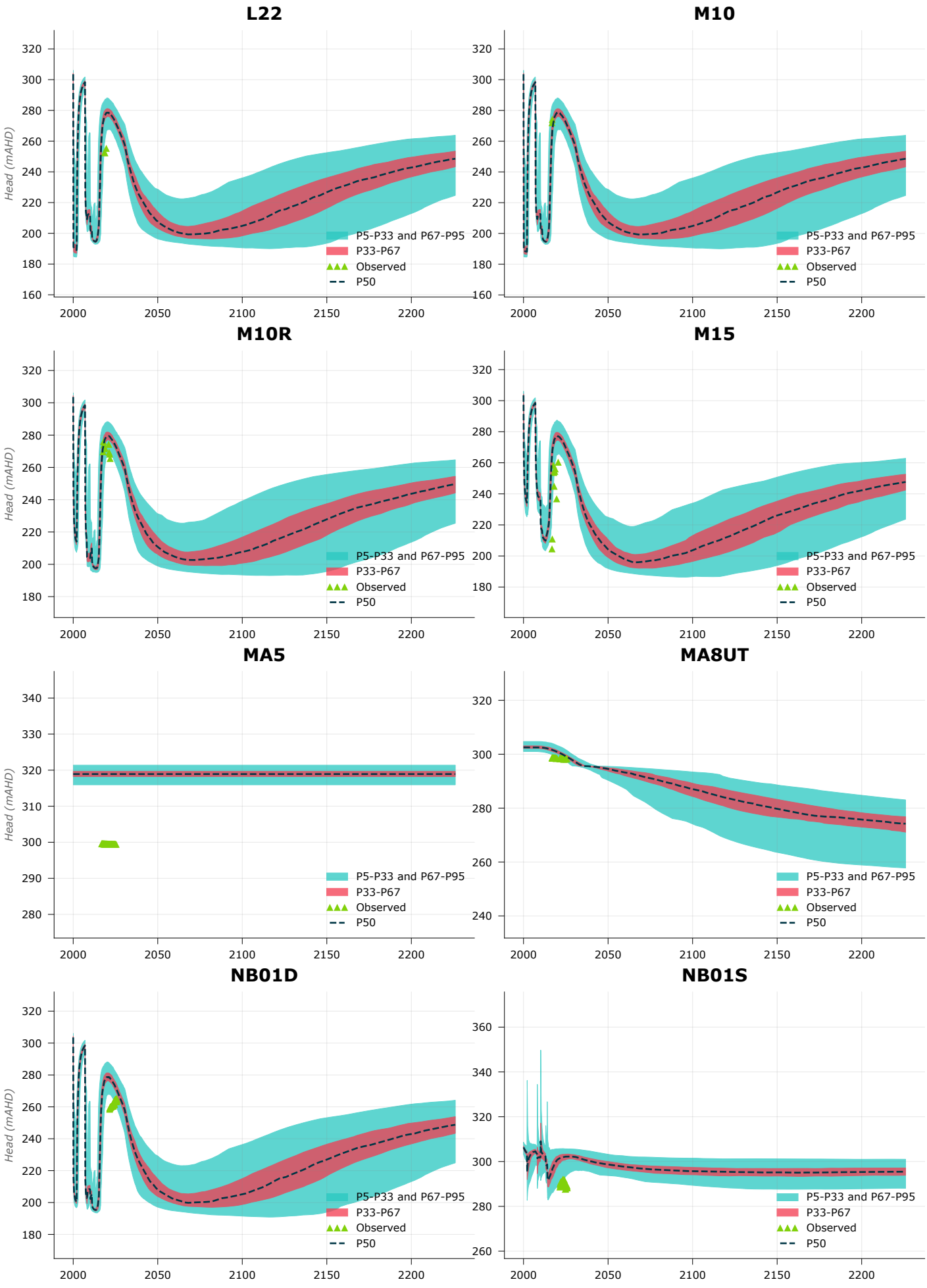
HSMB7S
Head (mAHD)
330
320
310
300
290
280
270
260
250
2000
2050
2100
2150
2200
P5-P33 and P67-P95
P33-P67
Observed
P50

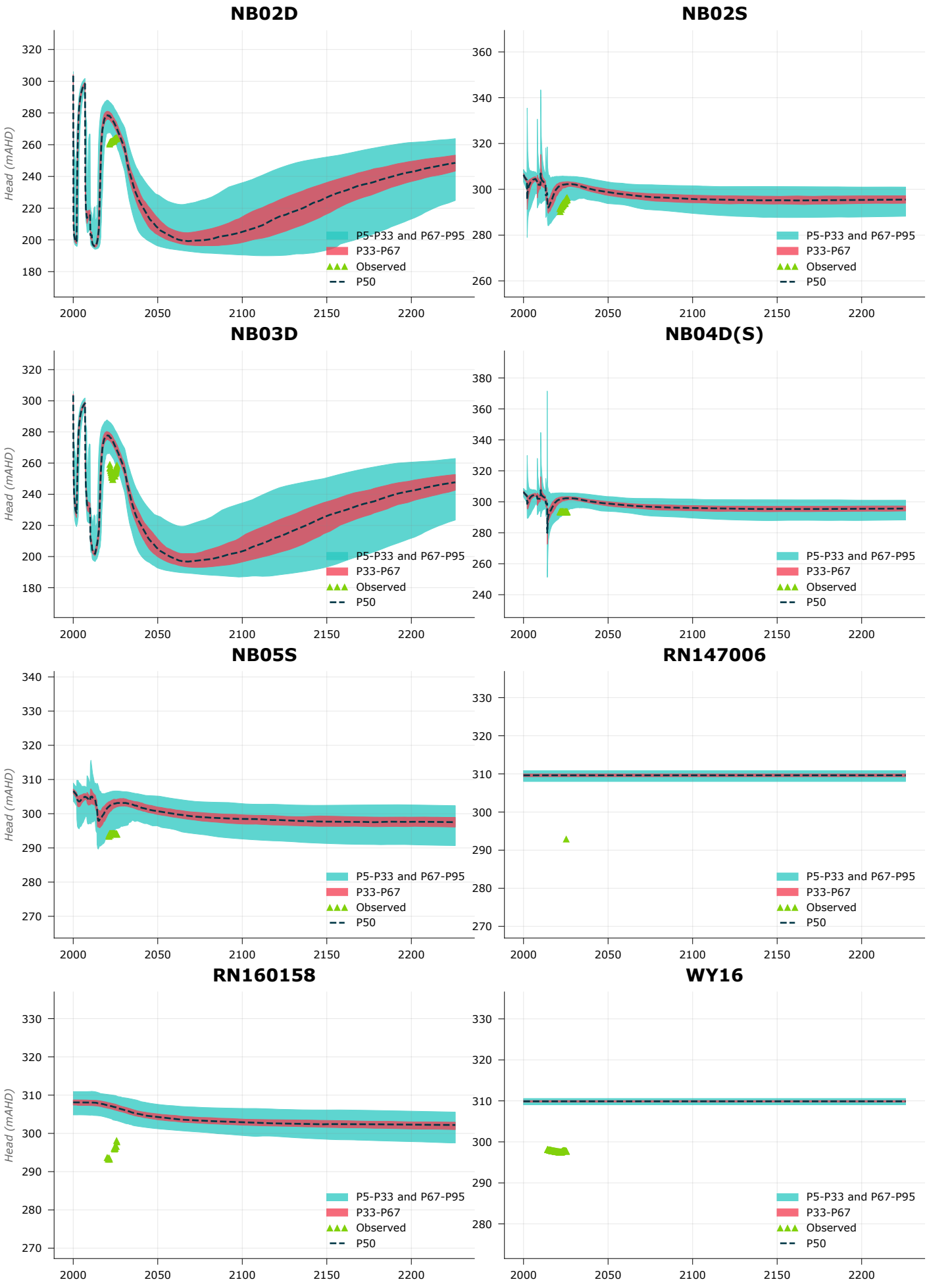

KN56
Head (mAHD)
340
330
320
310
300
290
280
270
2000
2050
2100
2150
2200
P5-P33 and P67-P95
P33-P67
Observed
P50

KN79A
Head (mAHD)
320
300
280
260
240
220
200
2000
2050
2100
2150
2200
P5-P33 and P67-P95
P33-P67
Observed
P50

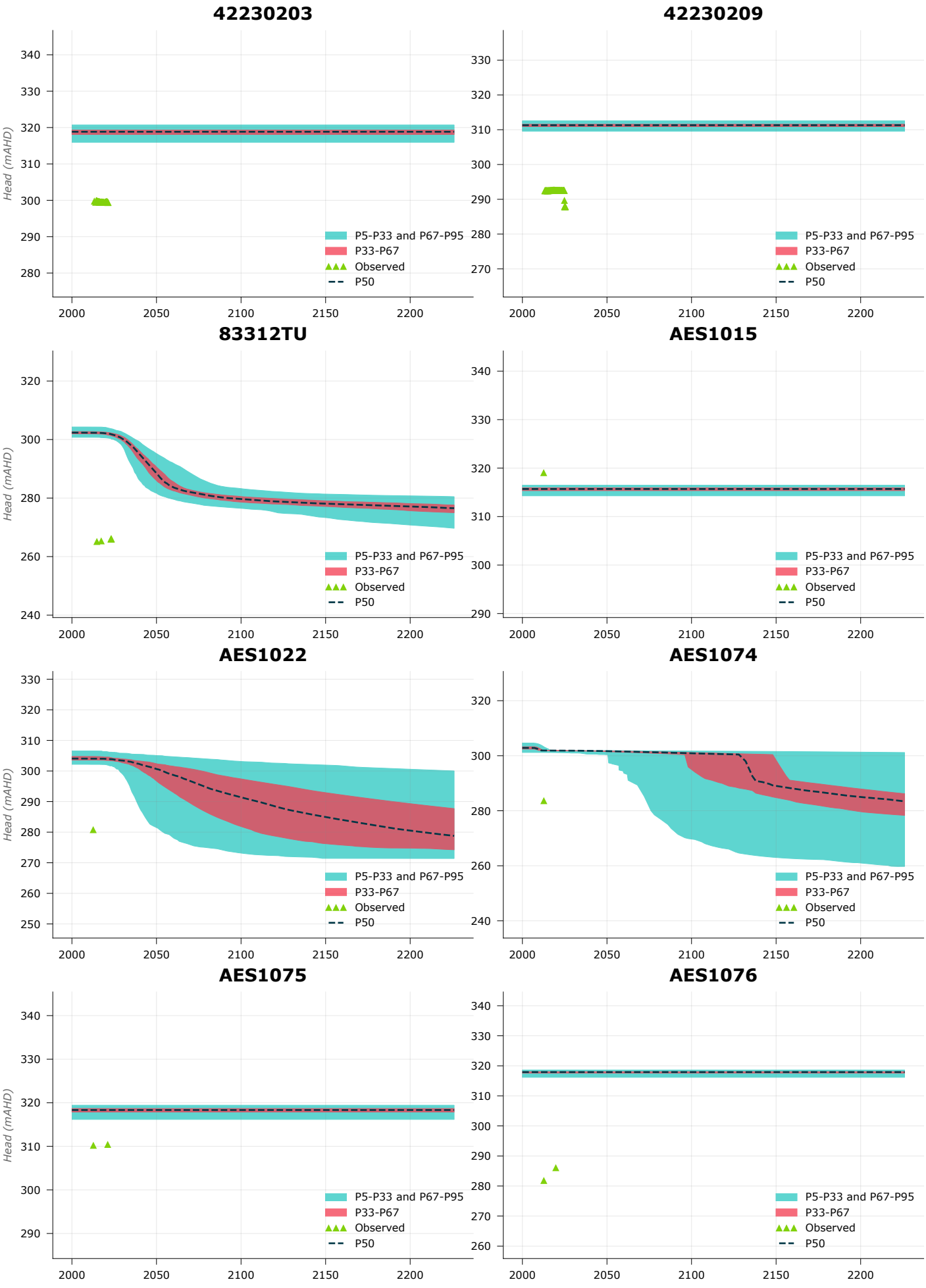

KN79C
Head (mAHD)
320
300
280
260
240
220
200
180
160
2000
2050
2100
2150
2200
P5-P33 and P67-P95
P33-P67
Observed
P50

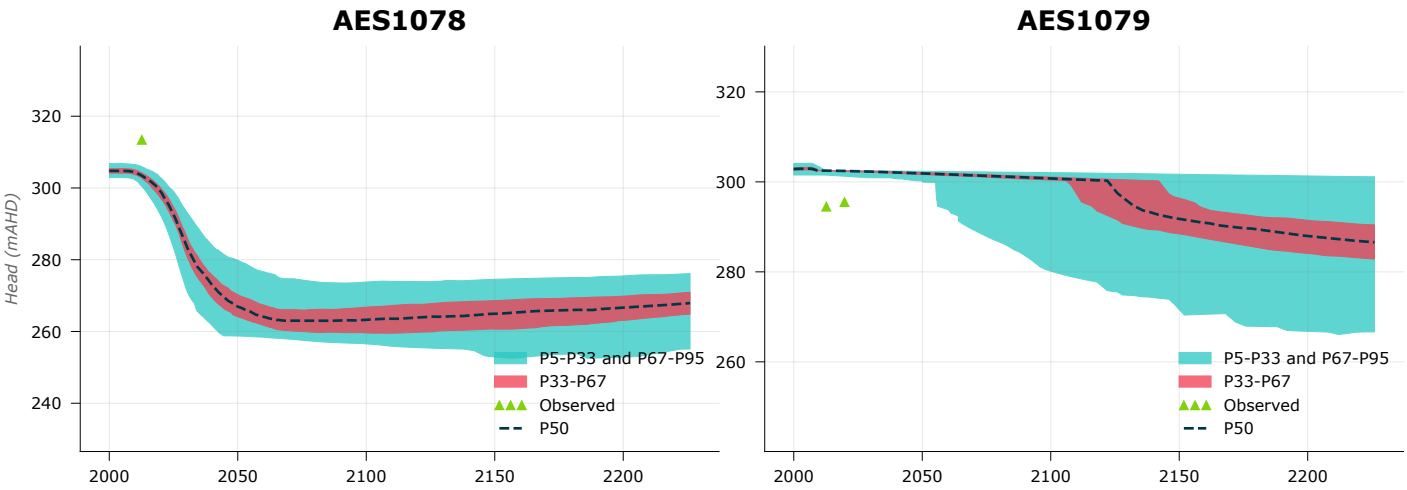
KN79M
Head (mAHD)
340
330
320
310
300
290
280
270
2000
2050
2100
2150
2200
P5-P33 and P67-P95
P33-P67
Observed
P50


L22
M10
M10R
M15
MA5
MA8UT
NB01D
NB01S
Head (mAHD)
P5-P33 and P67-P95
P33-P67
Observed
P50

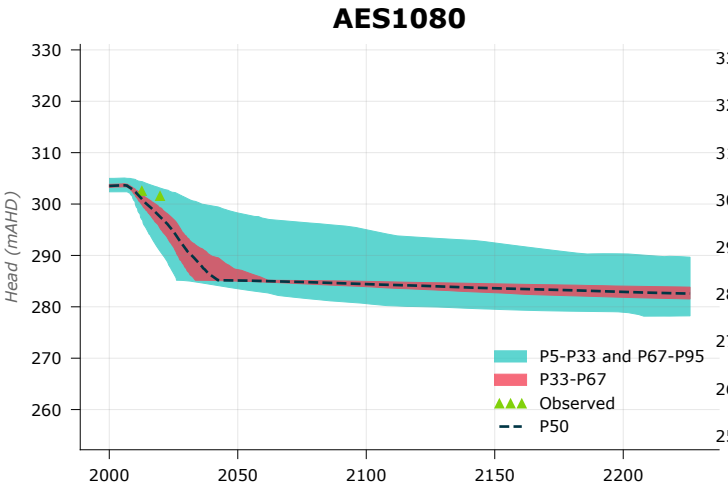

NB02D
NB02S
NB03D
NB04D(S)
NB05S
RN147006
RN160158
WY16
Head (mAHD)
P5-P33 and P67-P95
P33-P67
Observed
P50

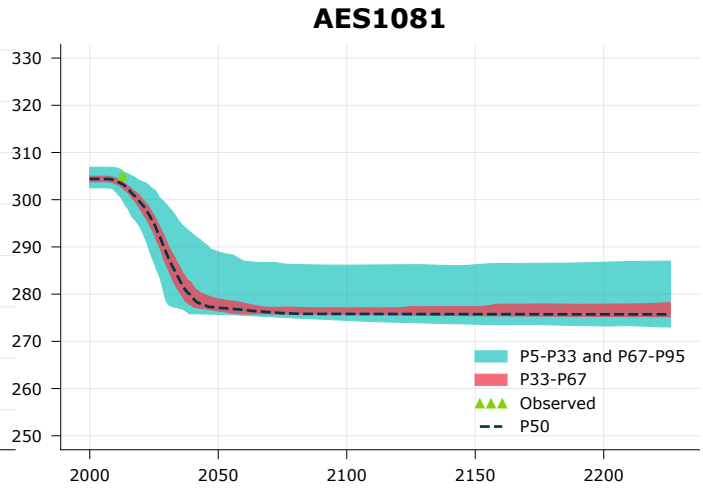

107857_S
10790W
119075
119076
147717
15080M
192511
33553_S
Head (mAHD)
P5-P33 and P67-P95
P33-P67
Observed
P50

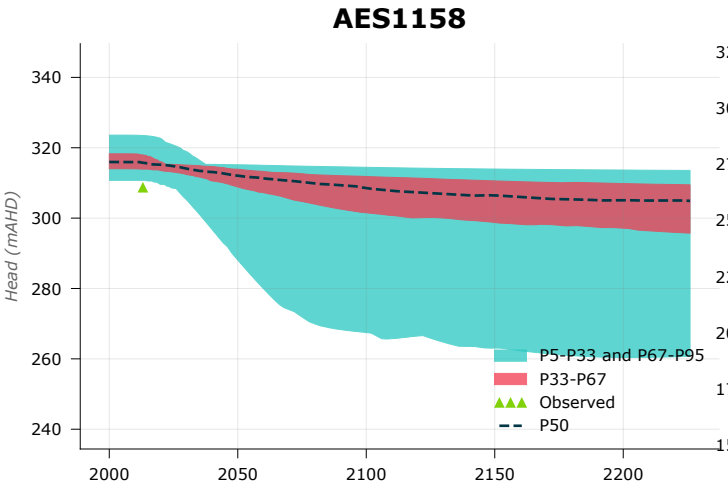

42230203
42230209
83312TU
AES1015
AES1022
AES1074
AES1075
AES1076
Head (mAHD)
P5-P33 and P67-P95
P33-P67
Observed
P50

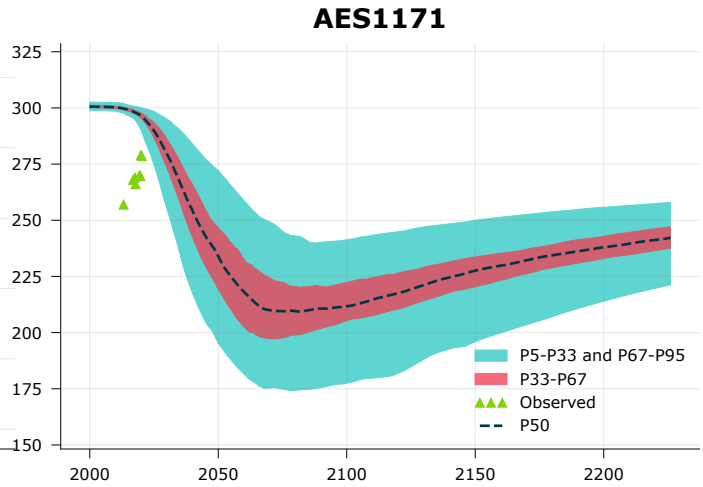

AES1078
Head (mAHD)
320
300
280
260
240
2000
2050
2100
2150
2200
P5-P33 and P67-P95
P33-P67
Observed
P50

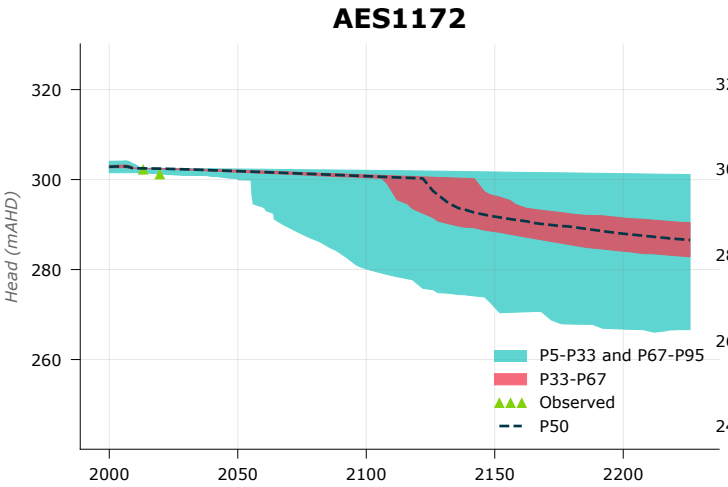
AES1079
320
300
280
260
2000
2050
2100
2150
2200
P5-P33 and P67-P95
P33-P67
Observed
P50

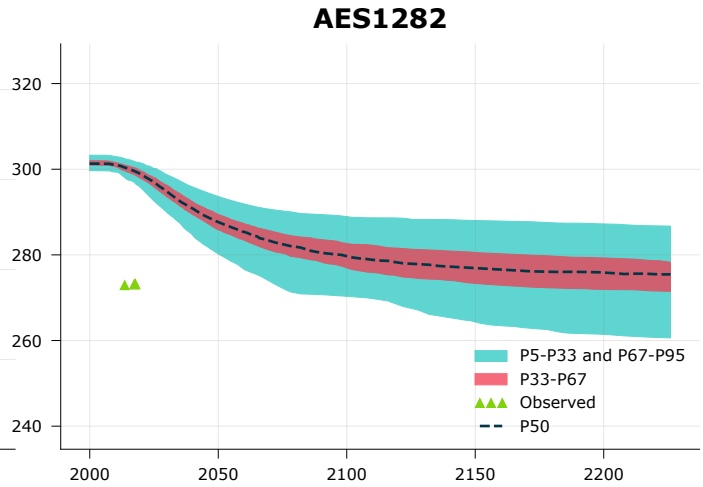

AES1080
Head (mAHD)
330
320
310
300
290
280
270
260
2000
2050
2100
2150
2200
P5-P33 and P67-P95
P33-P67
Observed
P50

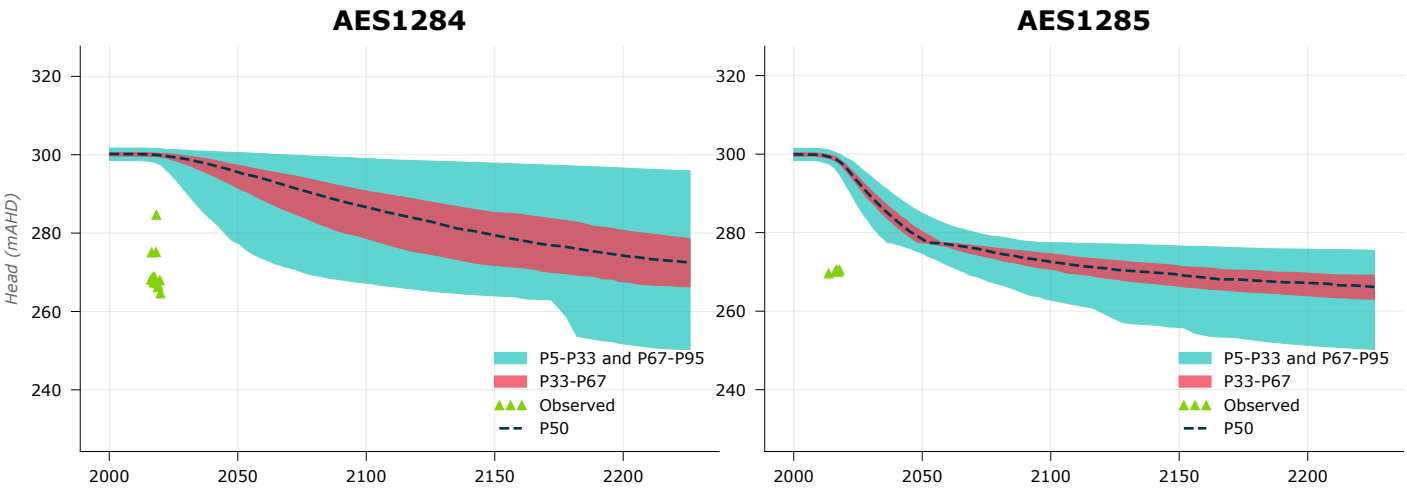

AES1081
330
320
310
300
290
280
270
260
250
2000
2050
2100
2150
2200
P5-P33 and P67-P95
P33-P67
Observed
P50


AES1158
Head (mAHD)
340
320
300
280
260
240
2000
2050
2100
2150
2200
P5-P33 and P67-P95
P33-P67
Observed
P50

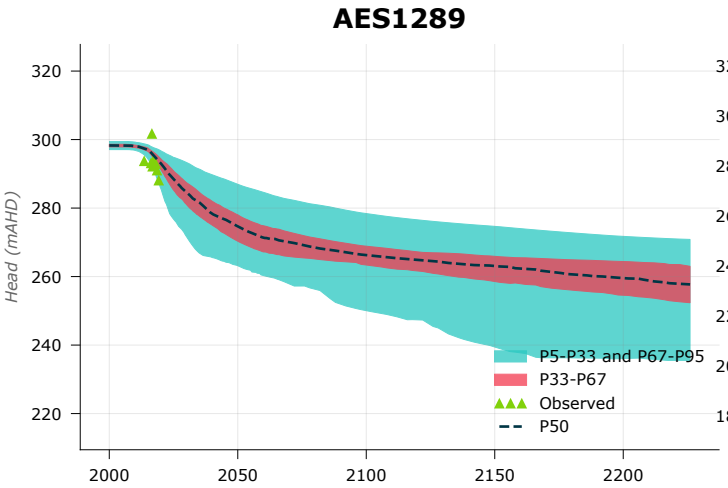

AES1171
325
300
275
250
225
200
175
150
2000
2050
2100
2150
2200
P5-P33 and P67-P95
P33-P67
Observed
P50

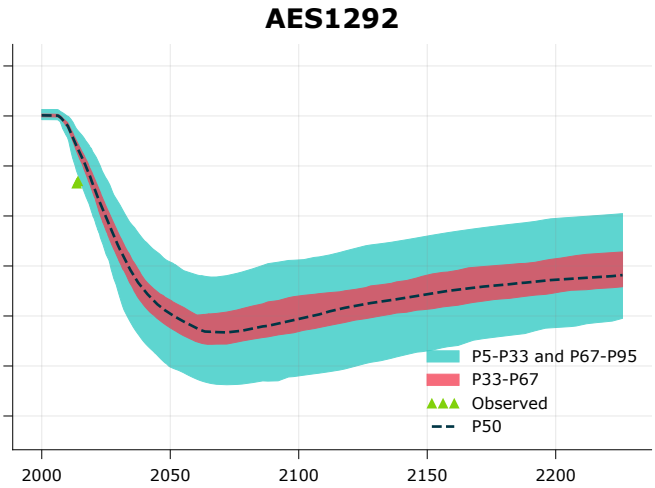

AES1172
Head (mAHD)
320
300
280
260
2000
2050
2100
2150
2200
P5-P33 and P67-P95
P33-P67
Observed
P50

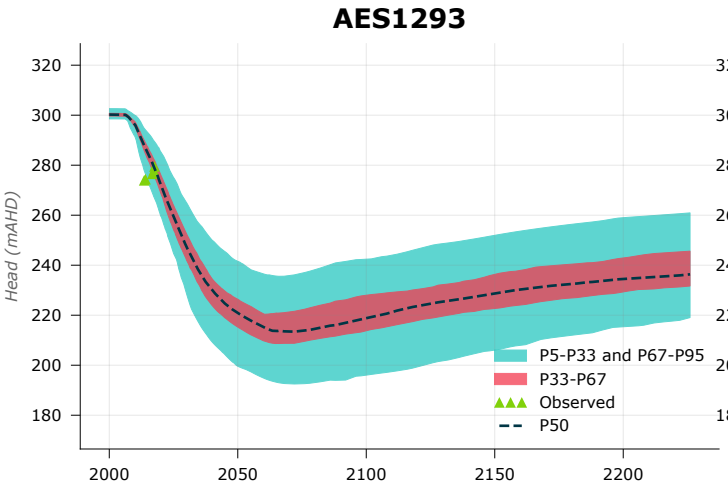

AES1282
320
300
280
260
240
2000
2050
2100
2150
2200
P5-P33 and P67-P95
P33-P67
Observed
P50

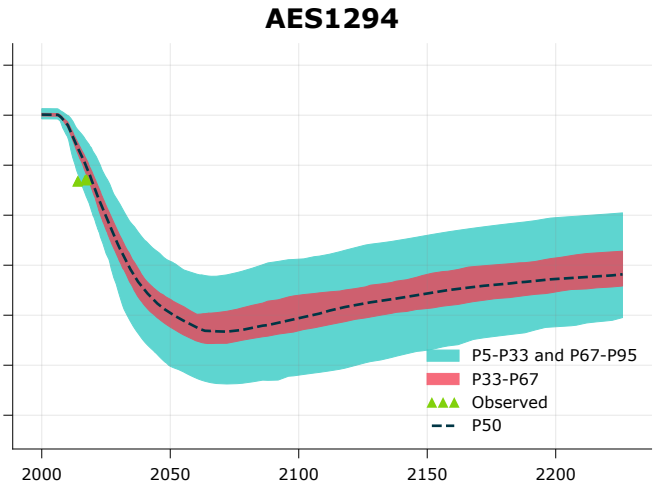

AES1284
Head (mAHD)
320
300
280
260
240
2000
2050
2100
2150
2200
P5-P33 and P67-P95
P33-P67
Observed
P50

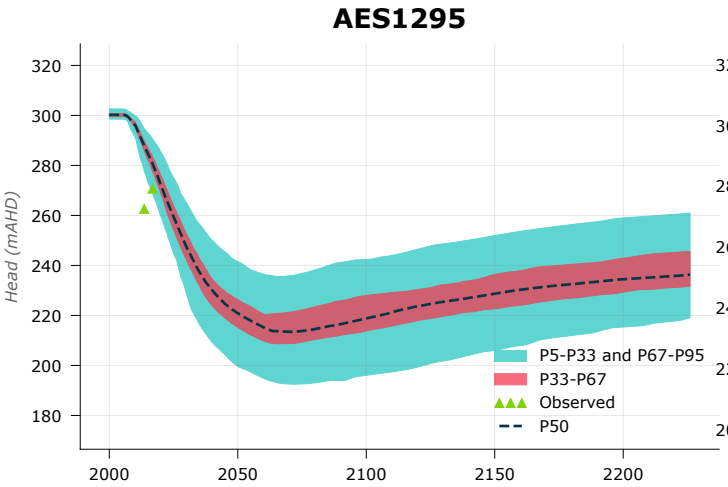
AES1285
320
300
280
260
240
2000
2050
2100
2150
2200
P5-P33 and P67-P95
P33-P67
Observed
P50

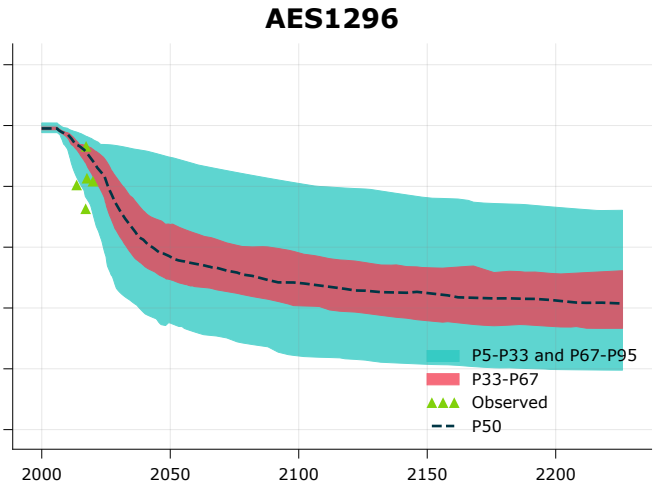

AES1289
Head (mAHD)
320
300
280
260
240
220
2000
2050
2100
2150
2200
P5-P33 and P67-P95
P33-P67
Observed
P50

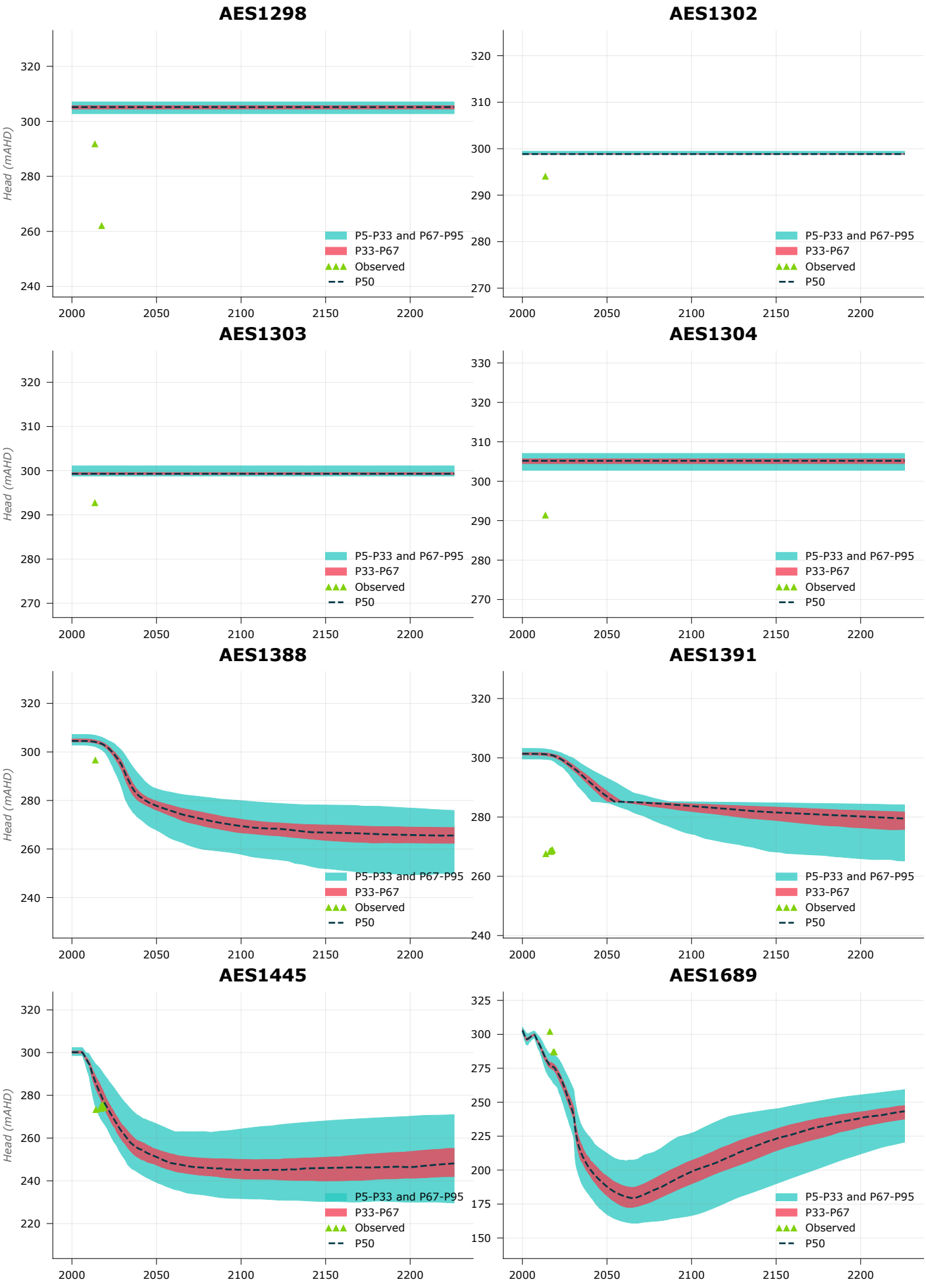

AES1292
320
300
280
260
240
220
200
180
2000
2050
2100
2150
2200
P5-P33 and P67-P95
P33-P67
Observed
P50

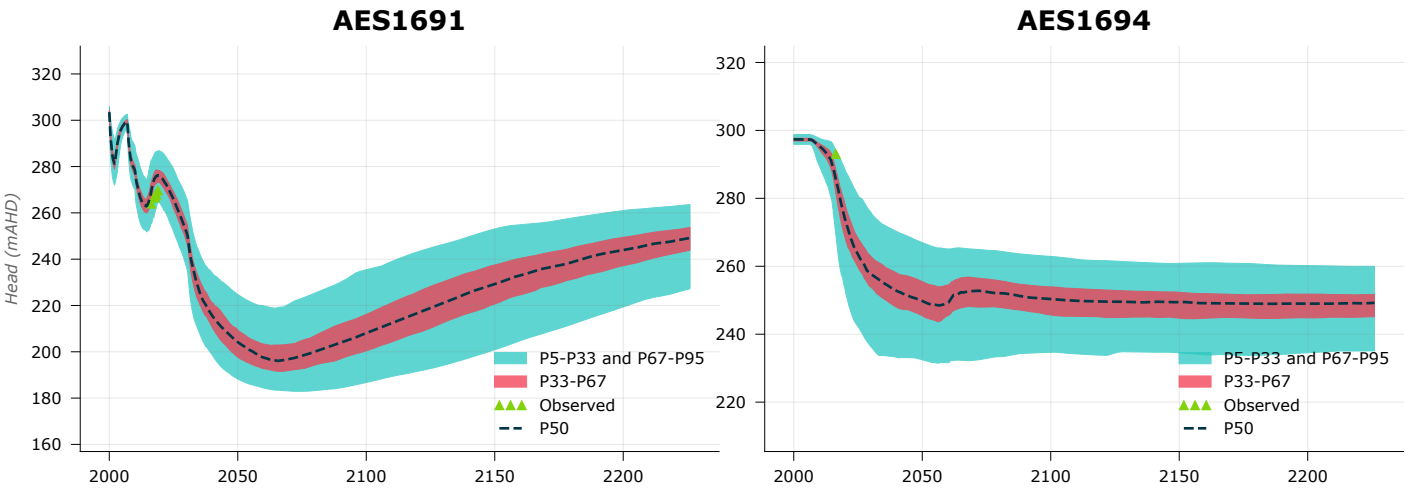

AES1293
Head (mAHD)
320
300
280
260
240
220
200
180
2000
2050
2100
2150
2200
P5-P33 and P67-P95
P33-P67
Observed
P50


AES1294
320
300
280
260
240
220
200
180
2000
2050
2100
2150
2200
P5-P33 and P67-P95
P33-P67
Observed
P50

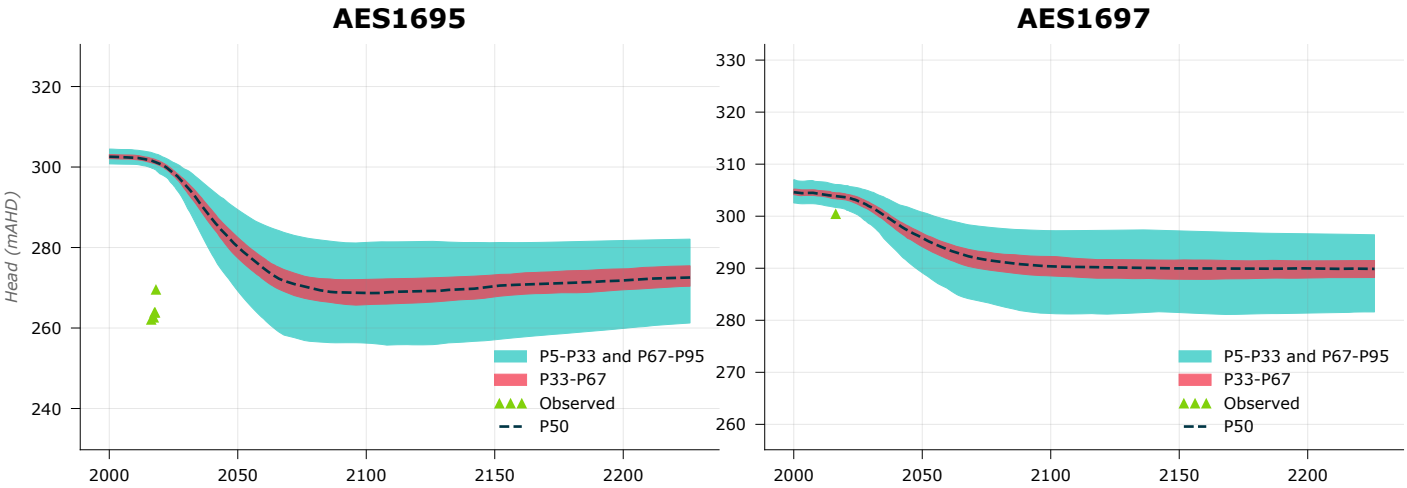

AES1295
Head (mAHD)
320
300
280
260
240
220
200
180
2000
2050
2100
2150
2200
P5-P33 and P67-P95
P33-P67
Observed
P50


AES1296
320
300
280
260
240
220
200
2000
2050
2100
2150
2200
P5-P33 and P67-P95
P33-P67
Observed
P50

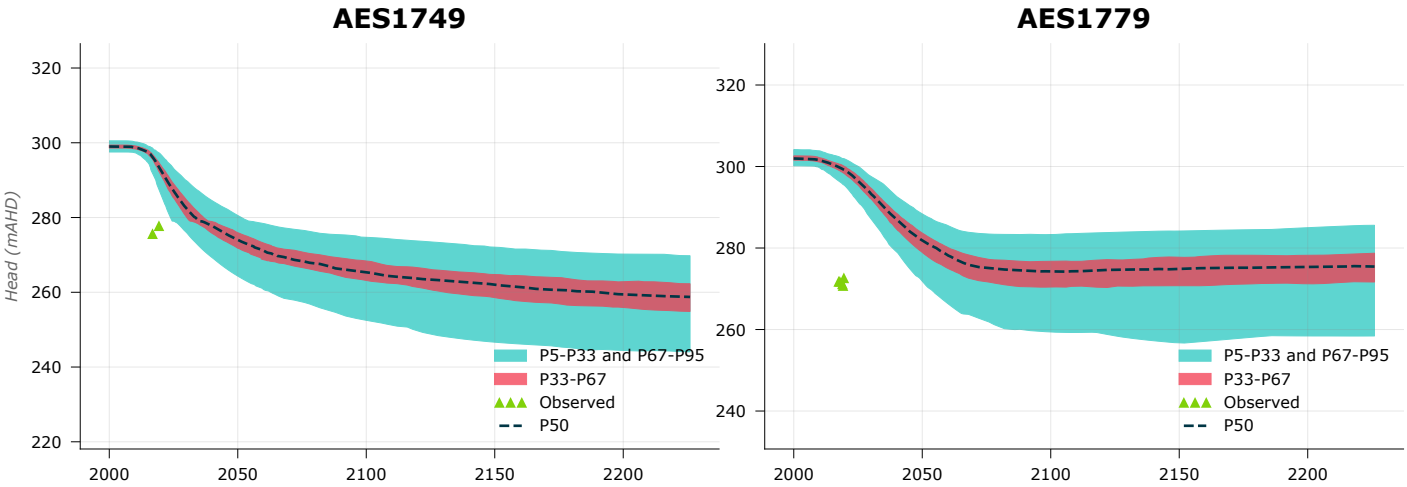

AES1298
AES1302
AES1303
AES1304
AES1388
AES1391
AES1445
AES1689
Head (mAHD)
P5-P33 and P67-P95
P33-P67
Observed
P50
2000
2050
2100
2150
2200


AES1691
Head (mAHD)
320
300
280
260
240
220
200
180
160
2000
2050
2100
2150
2200
P5-P33 and P67-P95
P33-P67
Observed
P50

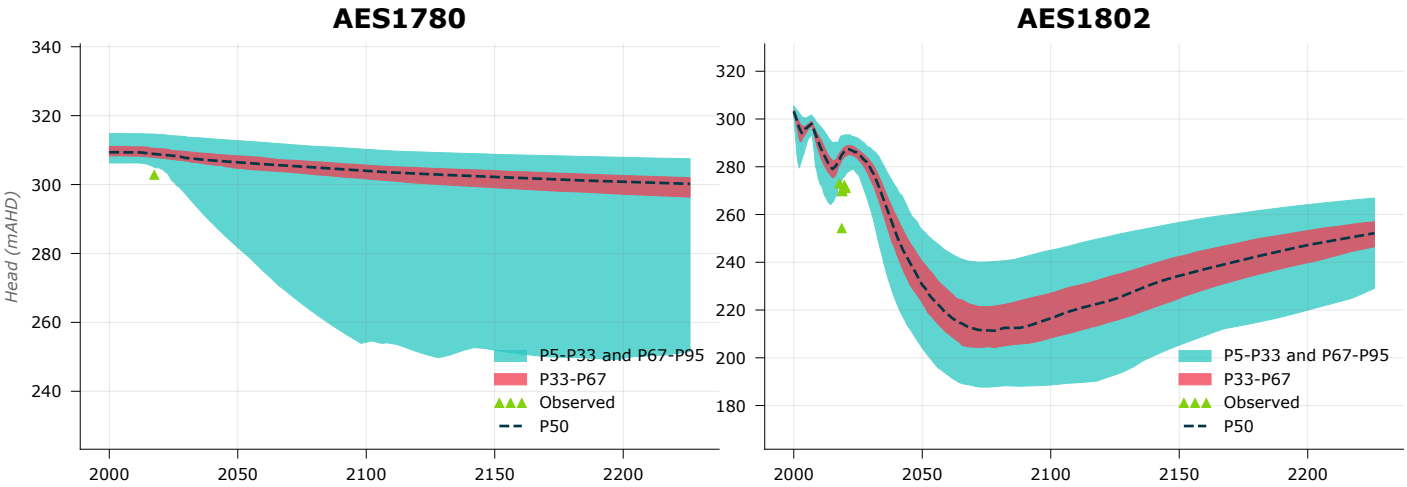
AES1694
320
300
280
260
240
220
2000
2050
2100
2150
2200
P5-P33 and P67-P95
P33-P67
Observed
P50


AES1695
Head (mAHD)
320
300
280
260
240
2000
2050
2100
2150
2200
P5-P33 and P67-P95
P33-P67
Observed
P50

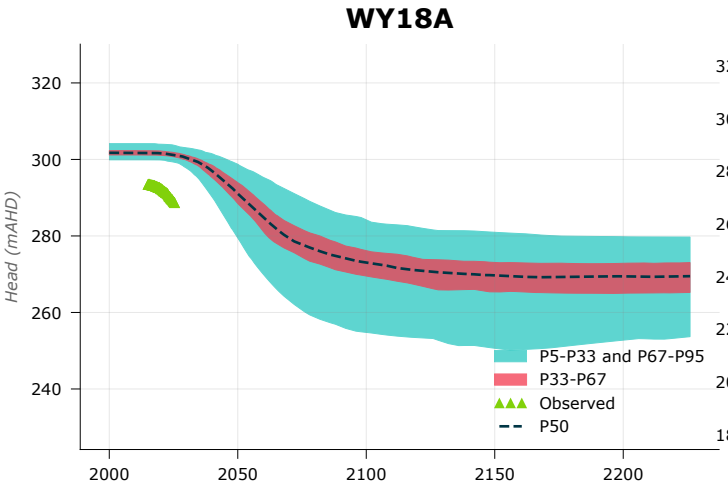
AES1697
330
320
310
300
290
280
270
260
2000
2050
2100
2150
2200
P5-P33 and P67-P95
P33-P67
Observed
P50

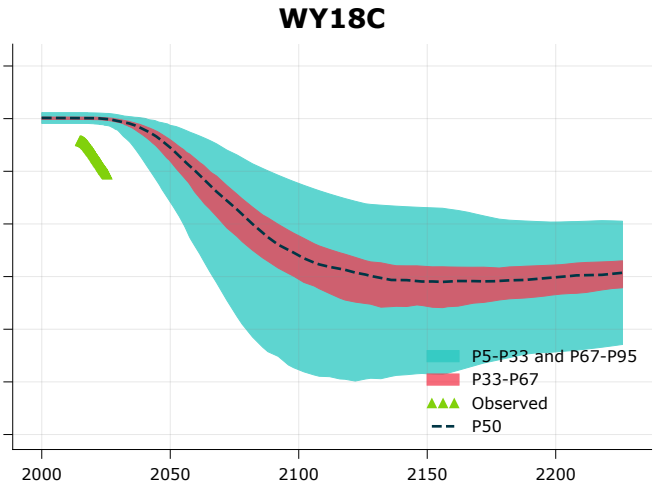

AES1749
Head (mAHD)
320
300
280
260
240
220
2000
2050
2100
2150
2200
P5-P33 and P67-P95
P33-P67
Observed
P50

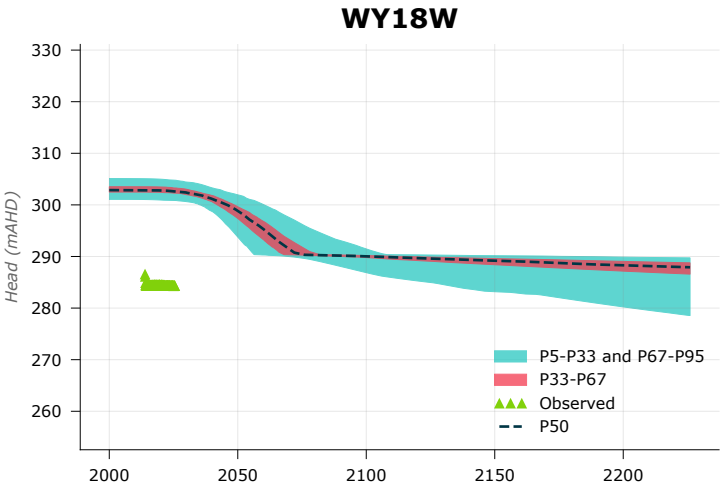
AES1779
320
300
280
260
240
2000
2050
2100
2150
2200
P5-P33 and P67-P95
P33-P67
Observed
P50


AES1780
Head (mAHD)
340
320
300
280
260
240
2000
2050
2100
2150
2200
P5-P33 and P67-P95
P33-P67
Observed
P50

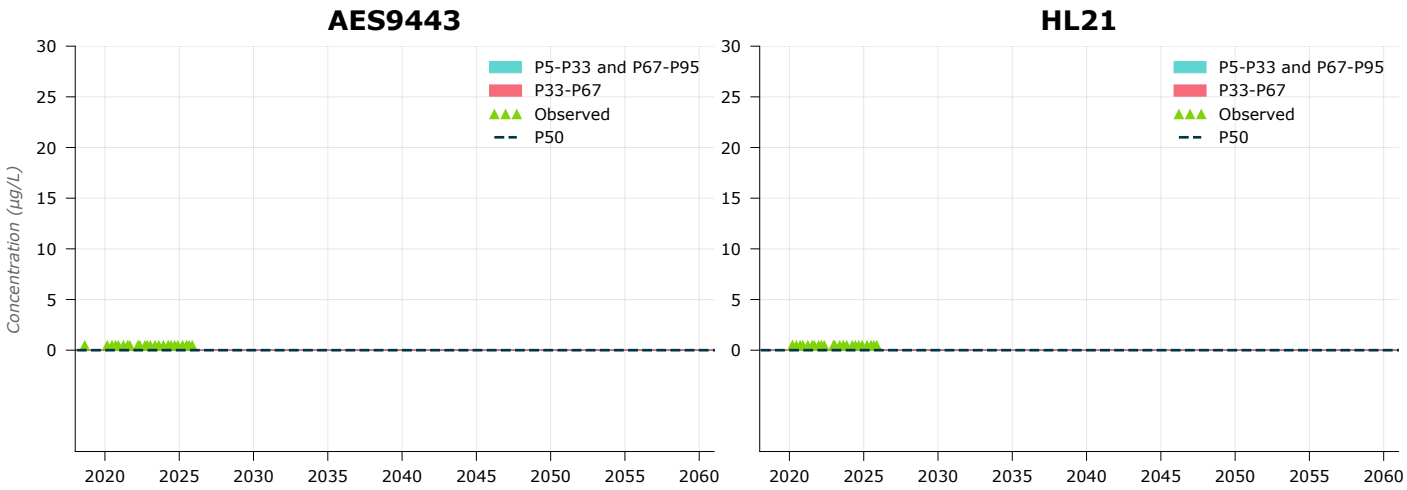
AES1802
320
300
280
260
240
220
200
180
2000
2050
2100
2150
2200
P5-P33 and P67-P95
P33-P67
Observed
P50

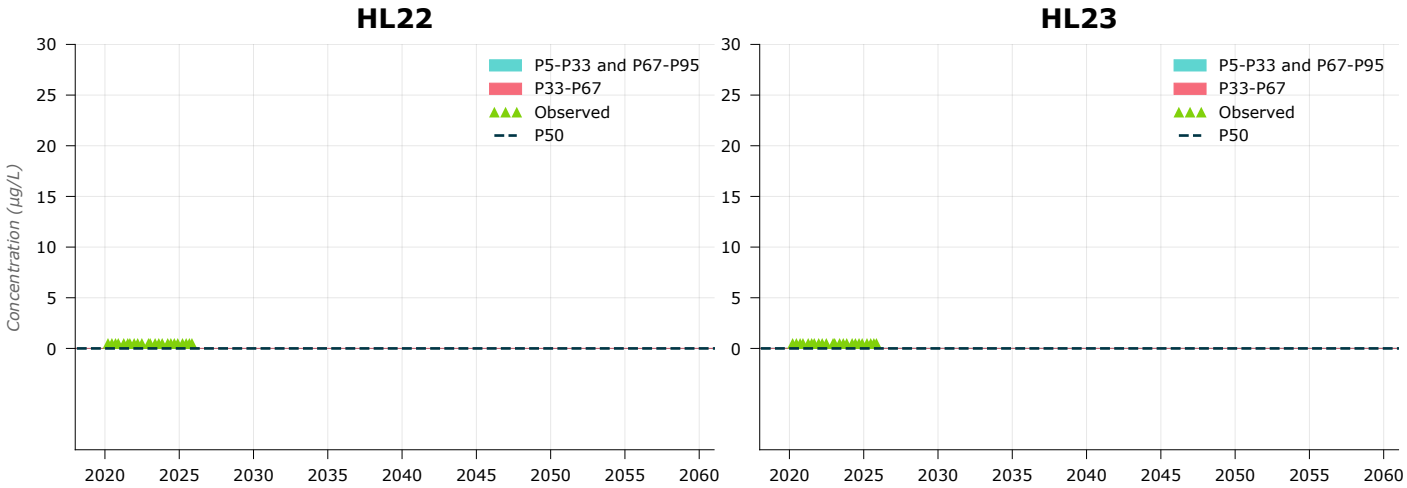

WY18A
Head (mAHD)
320
300
280
260
240
2000
2050
2100
2150
2200
P5-P33 and P67-P95
P33-P67
Observed
P50

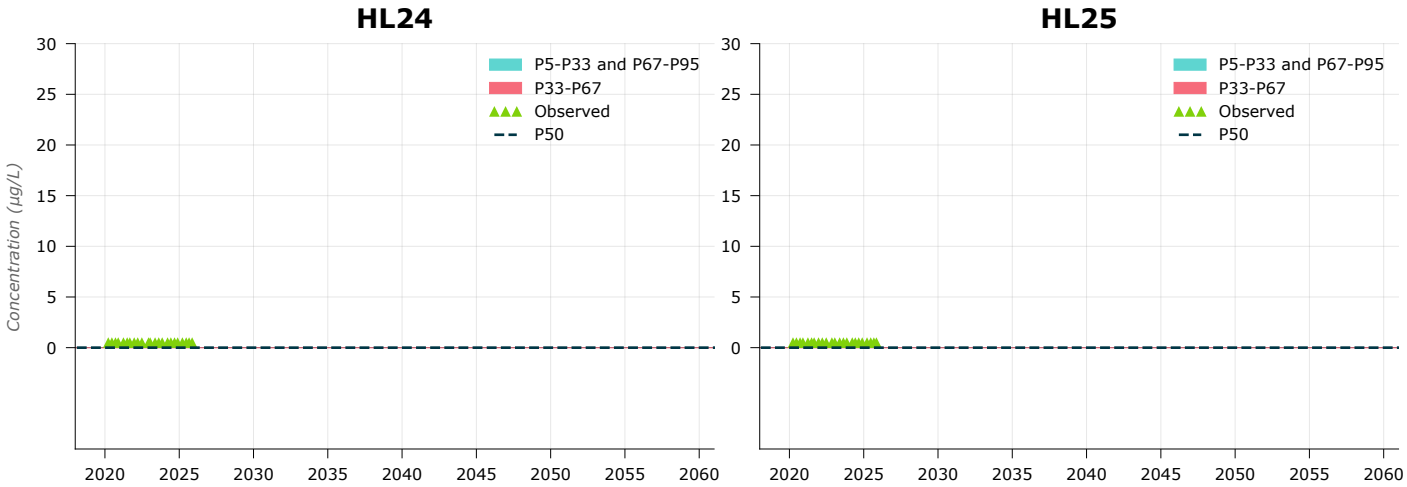

WY18C
320
300
280
260
240
220
200
180
2000
2050
2100
2150
2200
P5-P33 and P67-P95
P33-P67
Observed
P50

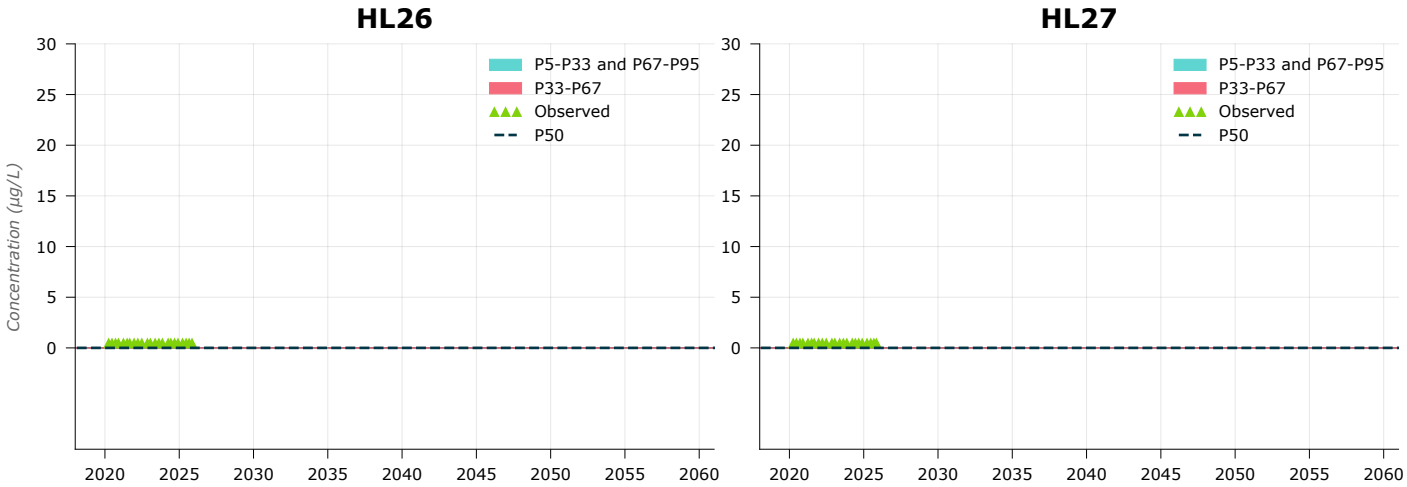

WY18W
Head (mAHD)
330
320
310
300
290
280
270
260
2000
2050
2100
2150
2200
P5-P33 and P67-P95
P33-P67
Observed
P50

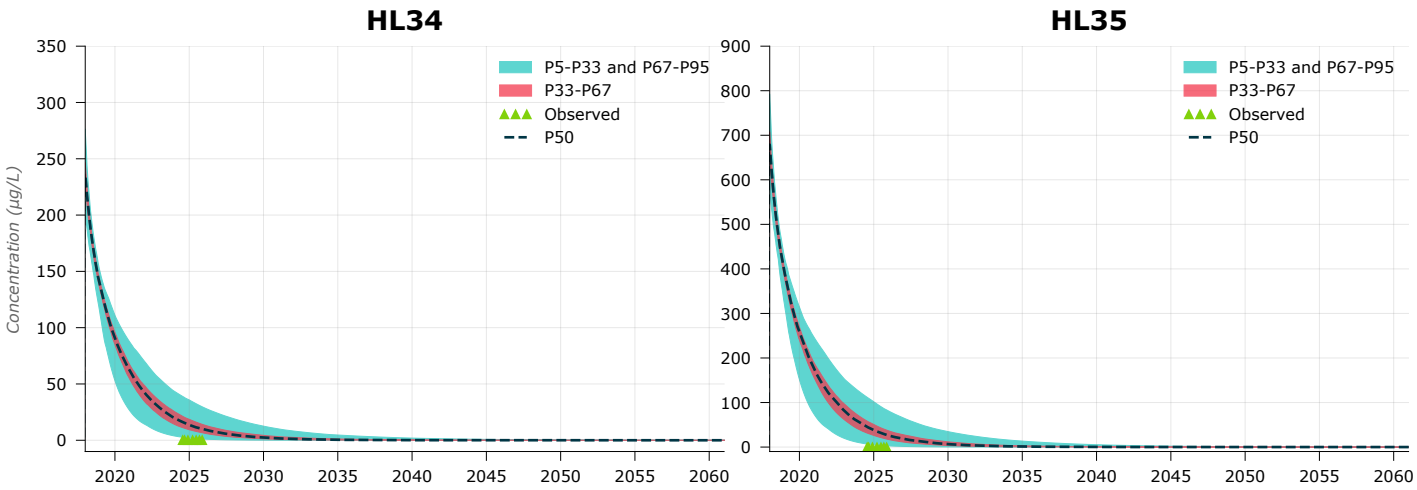
Appendix F. Predictive uncertainty – Benzene concentrations


AES9443
HL21
P5-P33 and P67-P95
P33-P67
Observed
P50
Concentration (µg/L)
0
5
10
15
20
25
30
2020
2025
2030
2035
2040
2045
2050
2055
2060

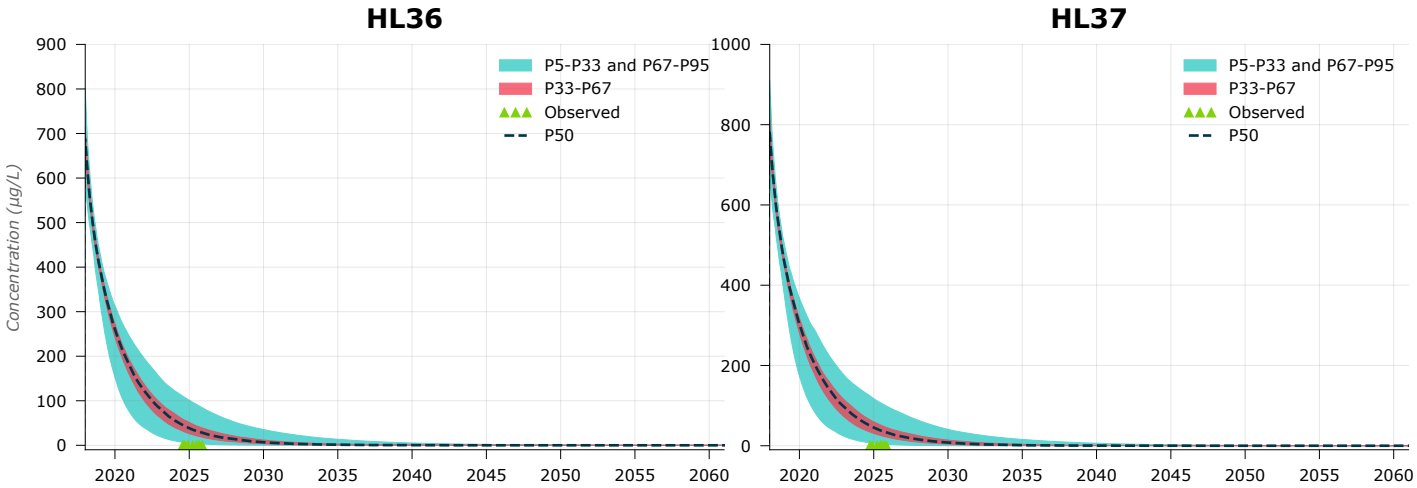

HL22
HL23
P5-P33 and P67-P95
P33-P67
Observed
P50
Concentration (µg/L)
0
5
10
15
20
25
30
2020
2025
2030
2035
2040
2045
2050
2055
2060


HL24
HL25
P5-P33 and P67-P95
P33-P67
Observed
P50
Concentration (µg/L)
0
5
10
15
20
25
30
2020
2025
2030
2035
2040
2045
2050
2055
2060

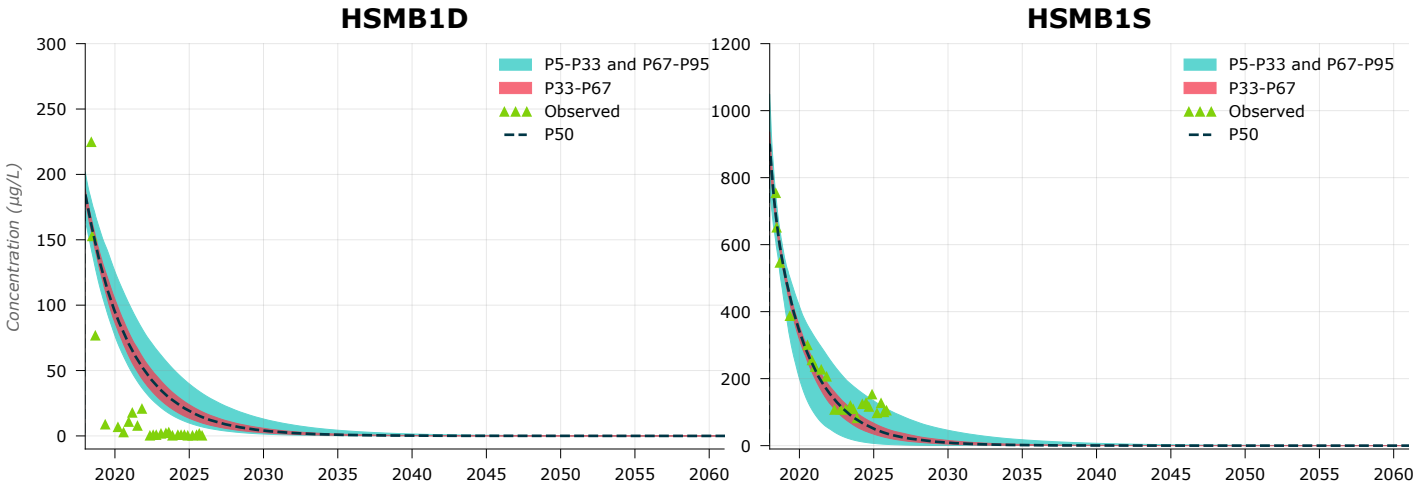

HL26
HL27
P5-P33 and P67-P95
P33-P67
Observed
P50
Concentration (µg/L)
0
5
10
15
20
25
30
2020
2025
2030
2035
2040
2045
2050
2055
2060


HL34
Concentration (µg/L)
P5-P33 and P67-P95
P33-P67
Observed
P50
0
50
100
150
200
250
300
350
2020
2025
2030
2035
2040
2045
2050
2055
2060

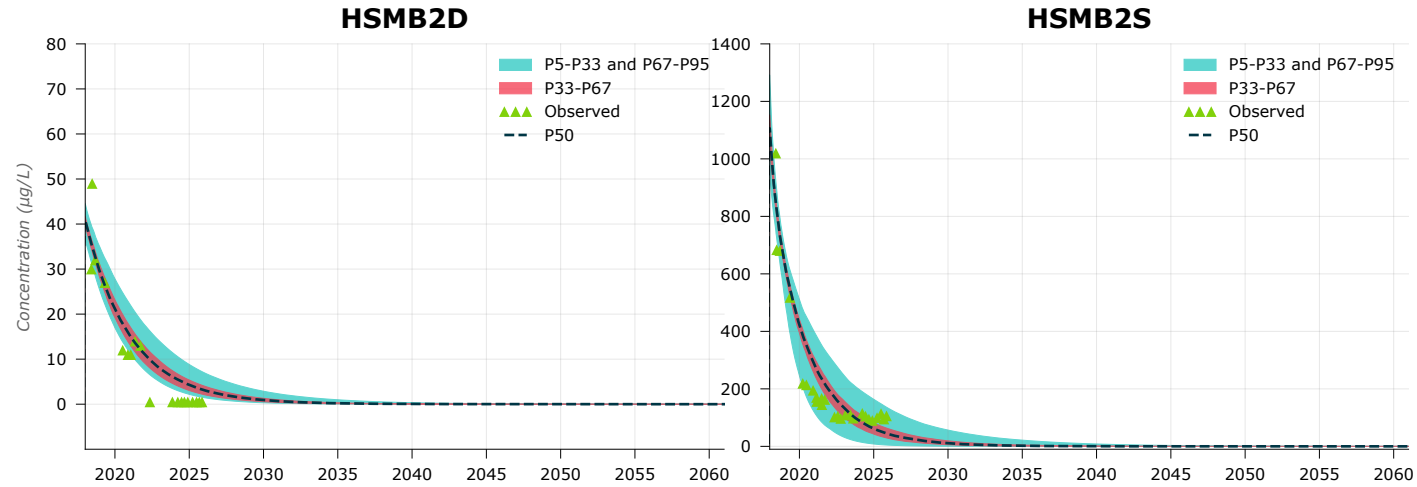
HL35
P5-P33 and P67-P95
P33-P67
Observed
P50
0
100
200
300
400
500
600
700
800
900
2020
2025
2030
2035
2040
2045
2050
2055
2060


HL36
Concentration (µg/L)
P5-P33 and P67-P95
P33-P67
Observed
P50
0
100
200
300
400
500
600
700
800
900
2020
2025
2030
2035
2040
2045
2050
2055
2060

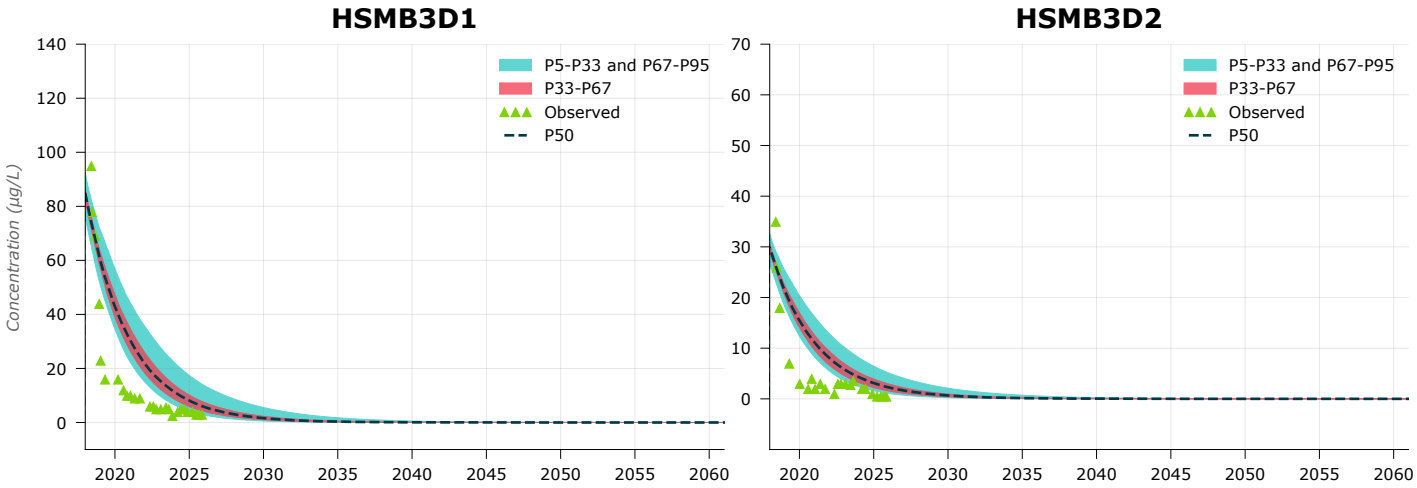
HL37
P5-P33 and P67-P95
P33-P67
Observed
P50
0
200
400
600
800
1000
2020
2025
2030
2035
2040
2045
2050
2055
2060


HSMB1D
Concentration (µg/L)
P5-P33 and P67-P95
P33-P67
Observed
P50
0
50
100
150
200
250
300
2020
2025
2030
2035
2040
2045
2050
2055
2060

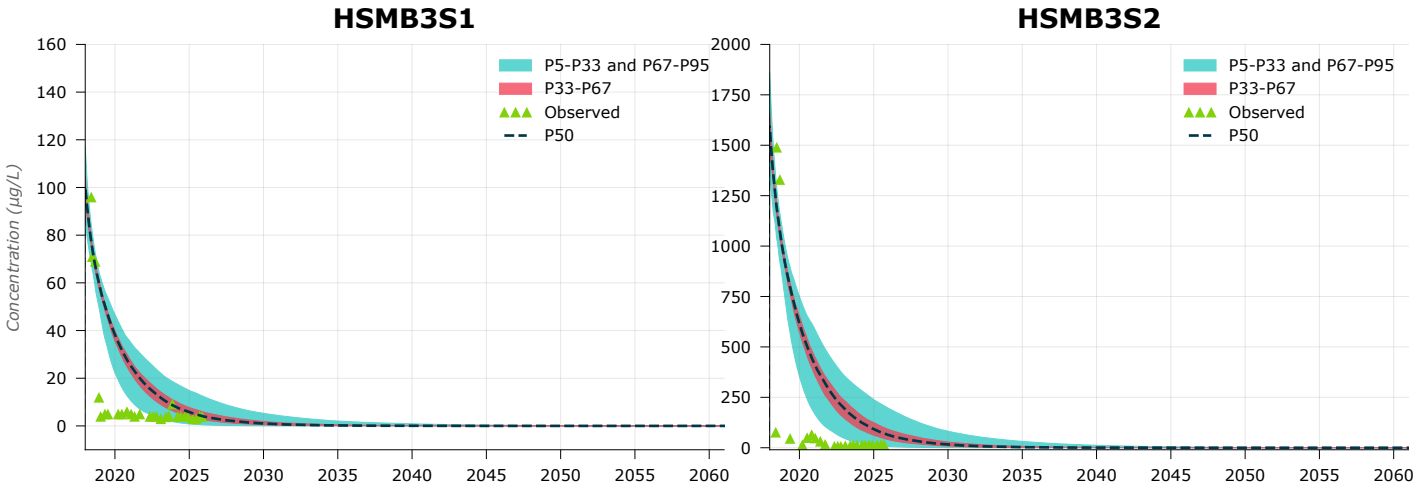
HSMB1S
P5-P33 and P67-P95
P33-P67
Observed
P50
0
200
400
600
800
1000
1200
2020
2025
2030
2035
2040
2045
2050
2055
2060


HSMB2D
Concentration (µg/L)
P5-P33 and P67-P95
P33-P67
Observed
P50
0
10
20
30
40
50
60
70
80
2020
2025
2030
2035
2040
2045
2050
2055
2060

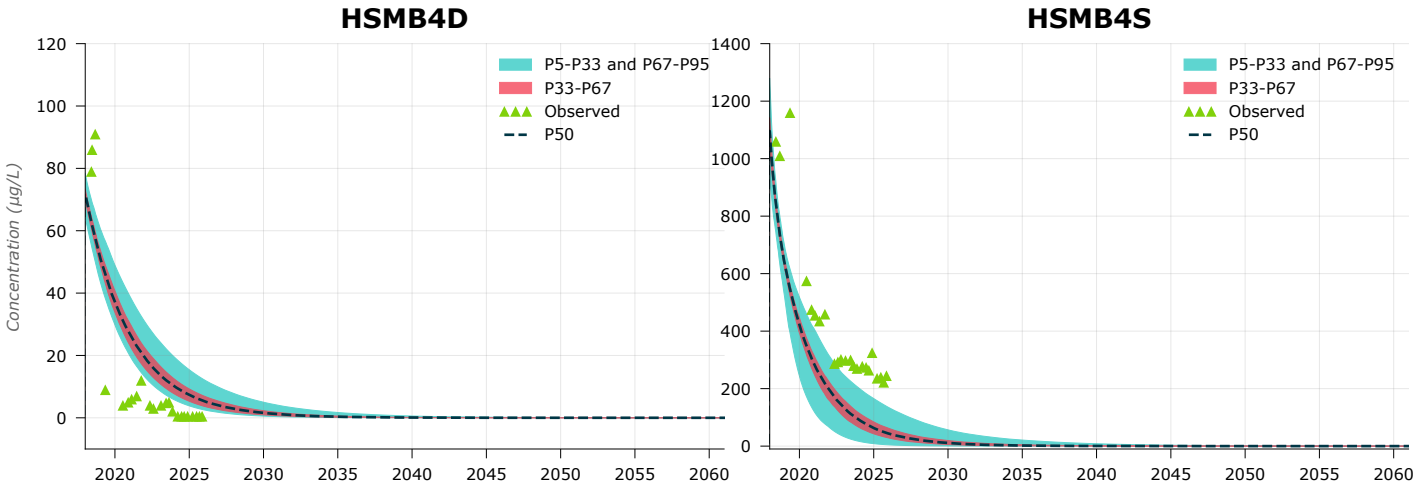
HSMB2S
P5-P33 and P67-P95
P33-P67
Observed
P50
0
200
400
600
800
1000
1200
1400
2020
2025
2030
2035
2040
2045
2050
2055
2060


HSMB3D1
Concentration (µg/L)
P5-P33 and P67-P95
P33-P67
Observed
P50
0
20
40
60
80
100
120
140
2020
2025
2030
2035
2040
2045
2050
2055
2060

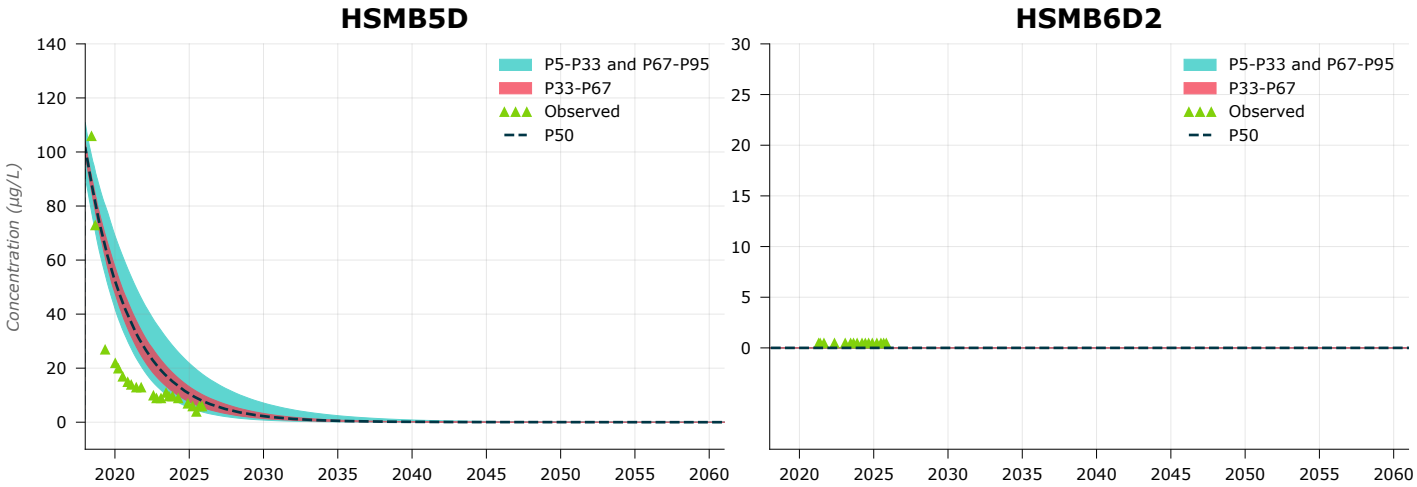
HSMB3D2
P5-P33 and P67-P95
P33-P67
Observed
P50
0
10
20
30
40
50
60
70
2020
2025
2030
2035
2040
2045
2050
2055
2060


HSMB3S1
Concentration (µg/L)
P5-P33 and P67-P95
P33-P67
Observed
P50
0
20
40
60
80
100
120
140
160
2020
2025
2030
2035
2040
2045
2050
2055
2060

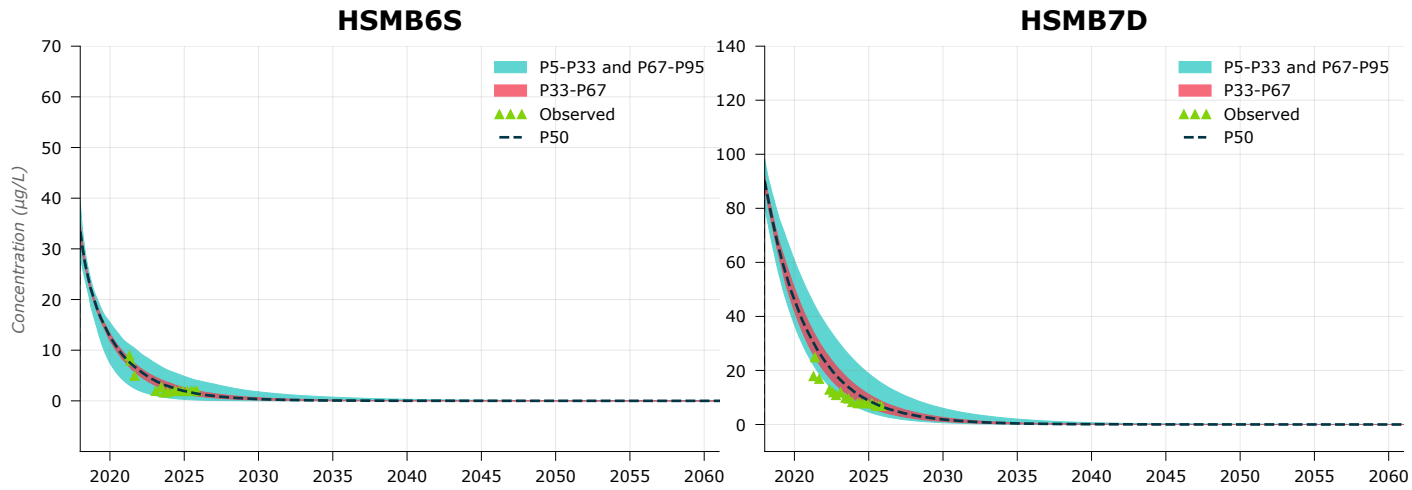
HSMB3S2
P5-P33 and P67-P95
P33-P67
Observed
P50
0
250
500
750
1000
1250
1500
1750
2000
2020
2025
2030
2035
2040
2045
2050
2055
2060

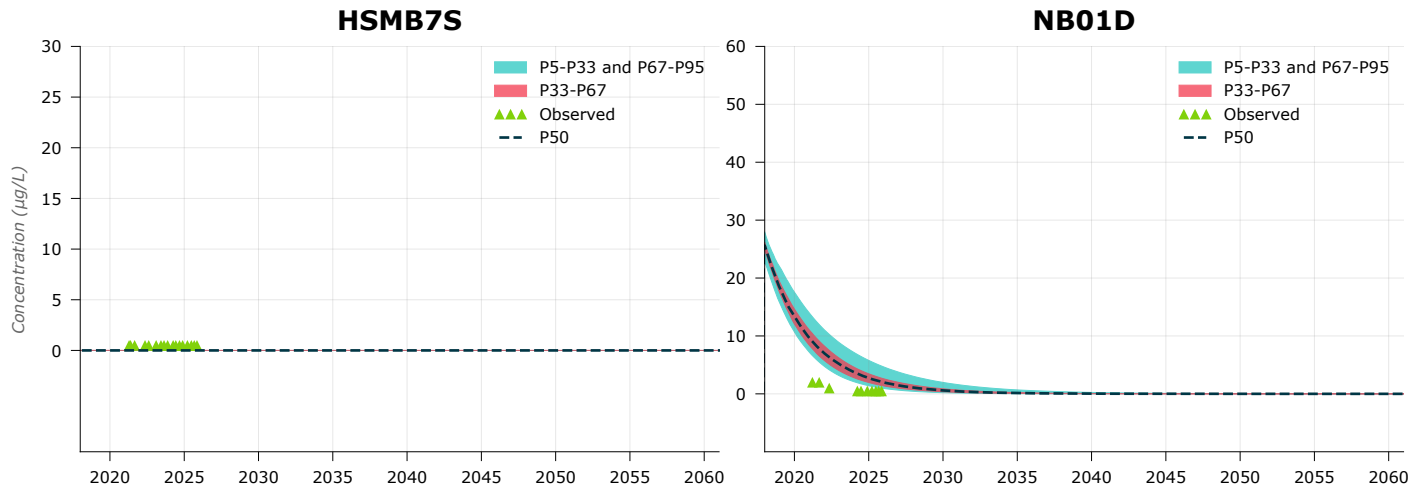

HSMB4D
Concentration (µg/L)
P5-P33 and P67-P95
P33-P67
Observed
P50
0
20
40
60
80
100
120
2020
2025
2030
2035
2040
2045
2050
2055
2060

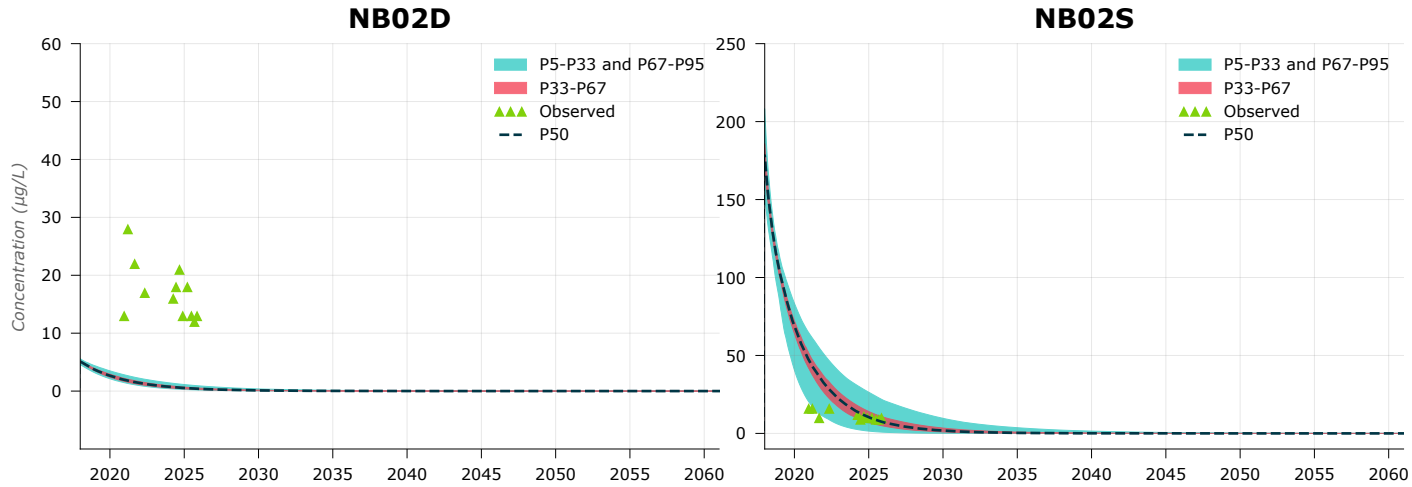
HSMB4S
P5-P33 and P67-P95
P33-P67
Observed
P50
0
200
400
600
800
1000
1200
1400
2020
2025
2030
2035
2040
2045
2050
2055
2060

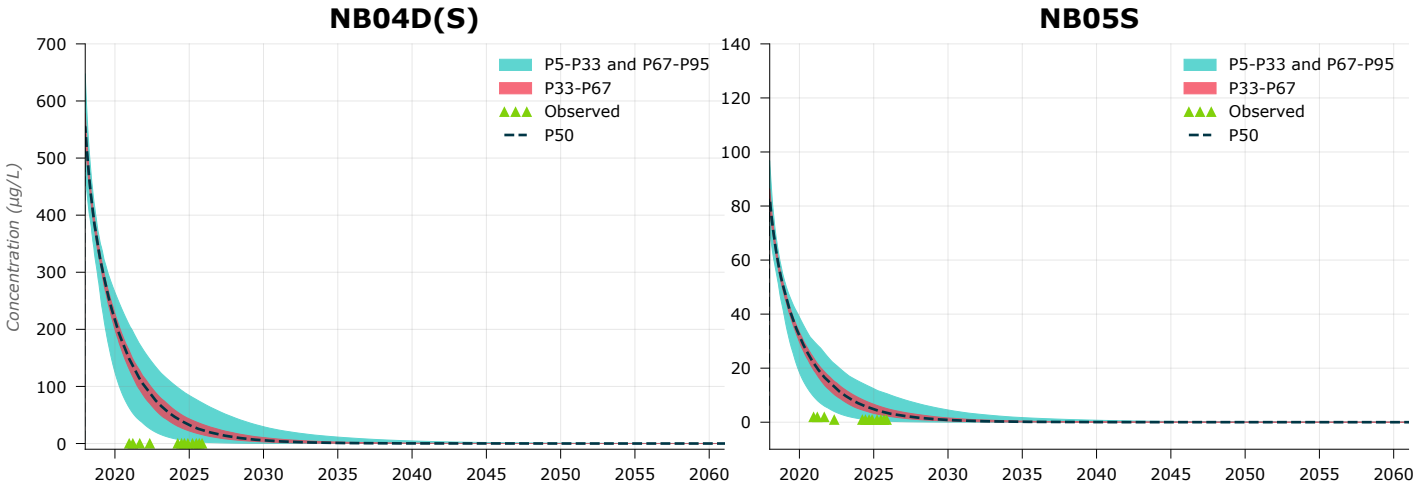

HSMB5D
Concentration (µg/L)
P5-P33 and P67-P95
P33-P67
Observed
P50
0
20
40
60
80
100
120
140
2020
2025
2030
2035
2040
2045
2050
2055
2060

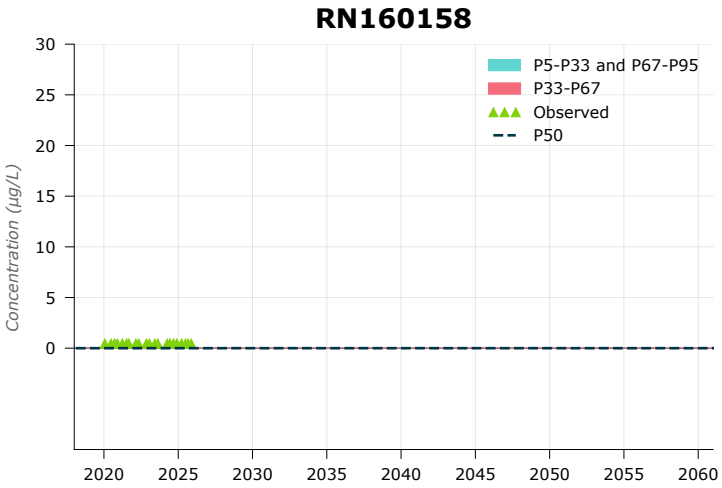
HSMB6D2
P5-P33 and P67-P95
P33-P67
Observed
P50
0
5
10
15
20
25
30
2020
2025
2030
2035
2040
2045
2050
2055
2060


HSMB6S
HSMB7D
P5-P33 and P67-P95
P33-P67
Observed
P50
Concentration (µg/L)

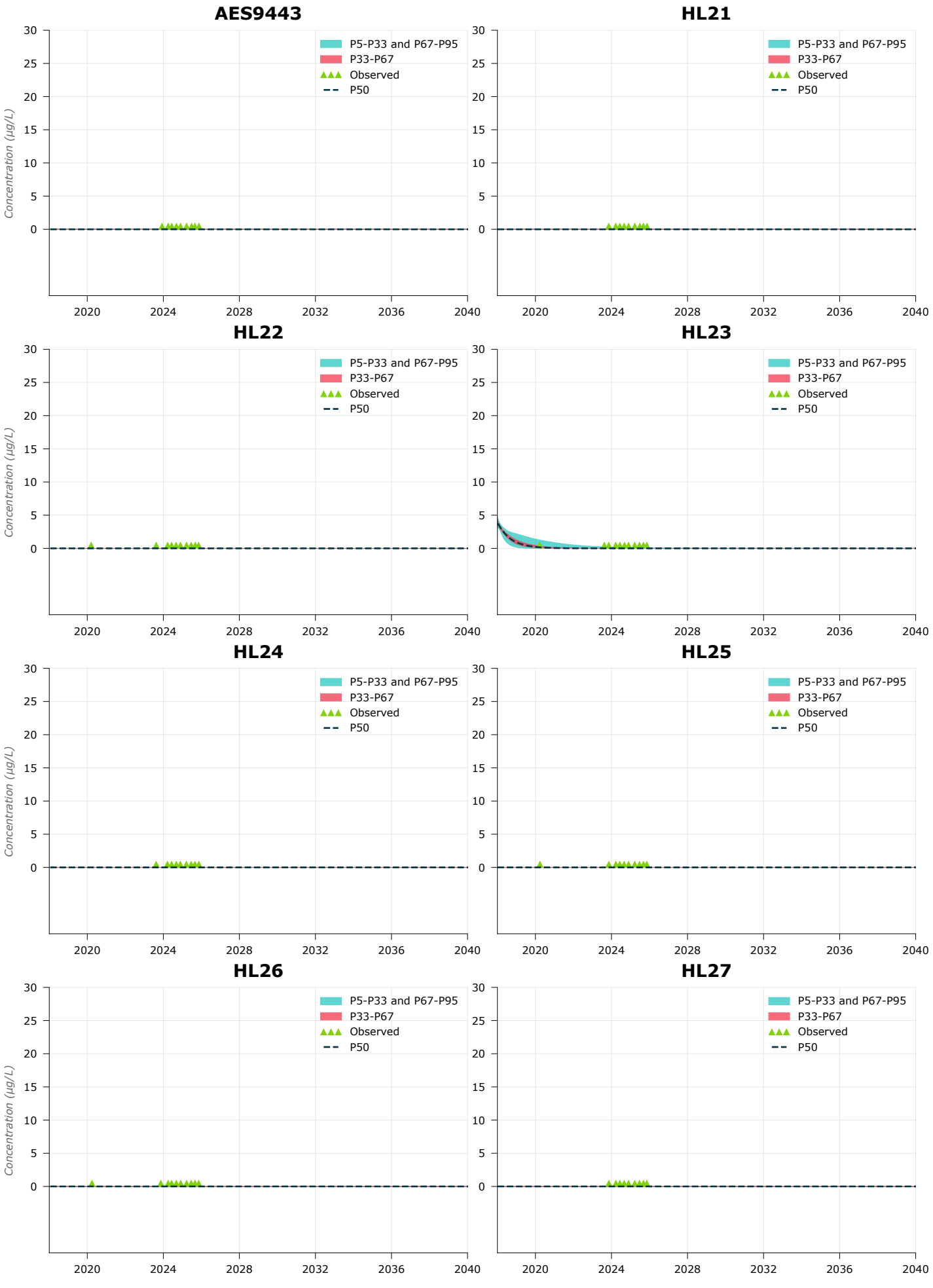

HSMB7S
NB01D
P5-P33 and P67-P95
P33-P67
Observed
P50
Concentration (µg/L)

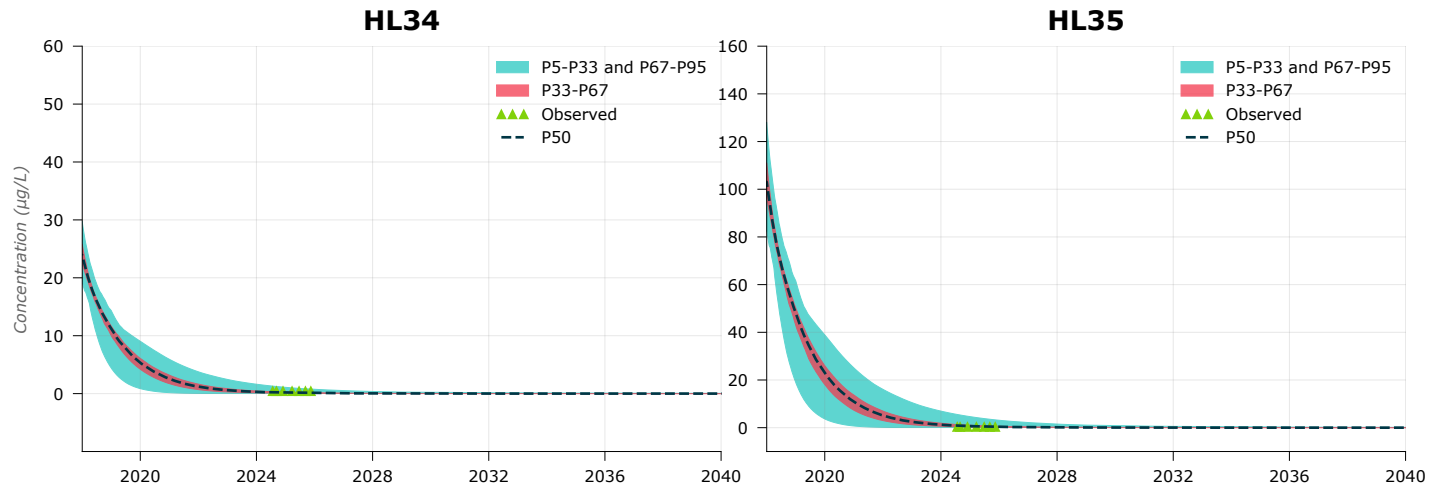

NB02D
NB02S
P5-P33 and P67-P95
P33-P67
Observed
P50
Concentration (µg/L)


NB04D(S)
NB05S
P5-P33 and P67-P95
P33-P67
Observed
P50
Concentration (µg/L)

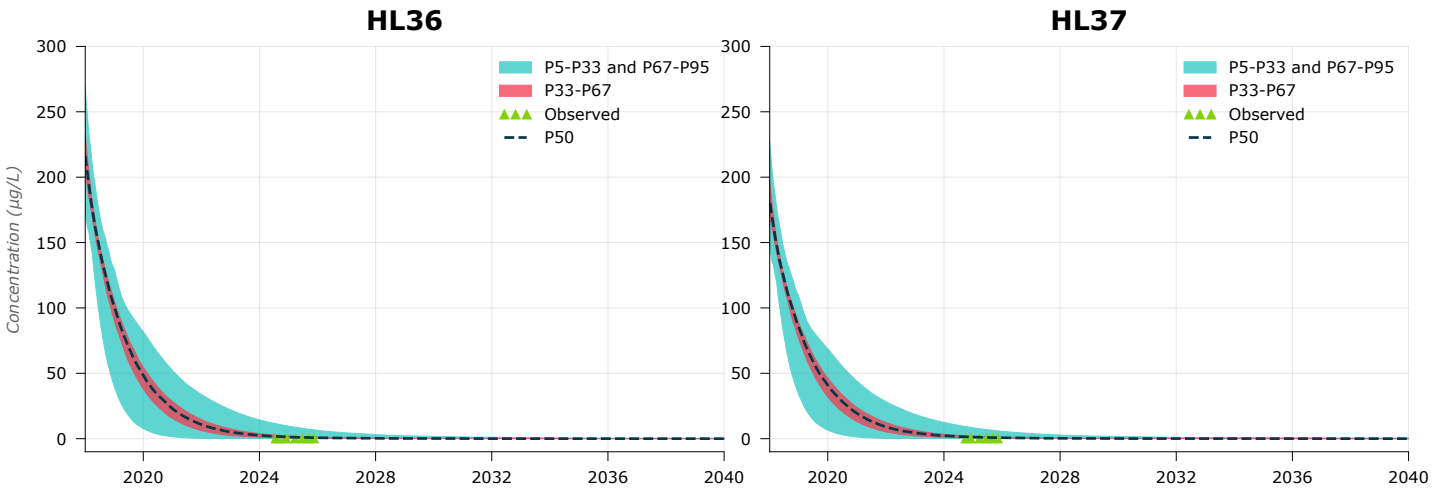

RN160158
P5-P33 and P67-P95
P33-P67
Observed
P50
Concentration (µg/L)
30
25
20
15
10
5
0
2020
2025
2030
2035
2040
2045
2050
2055
2060

Appendix G. Predictive uncertainty – Naphthalene concentrations

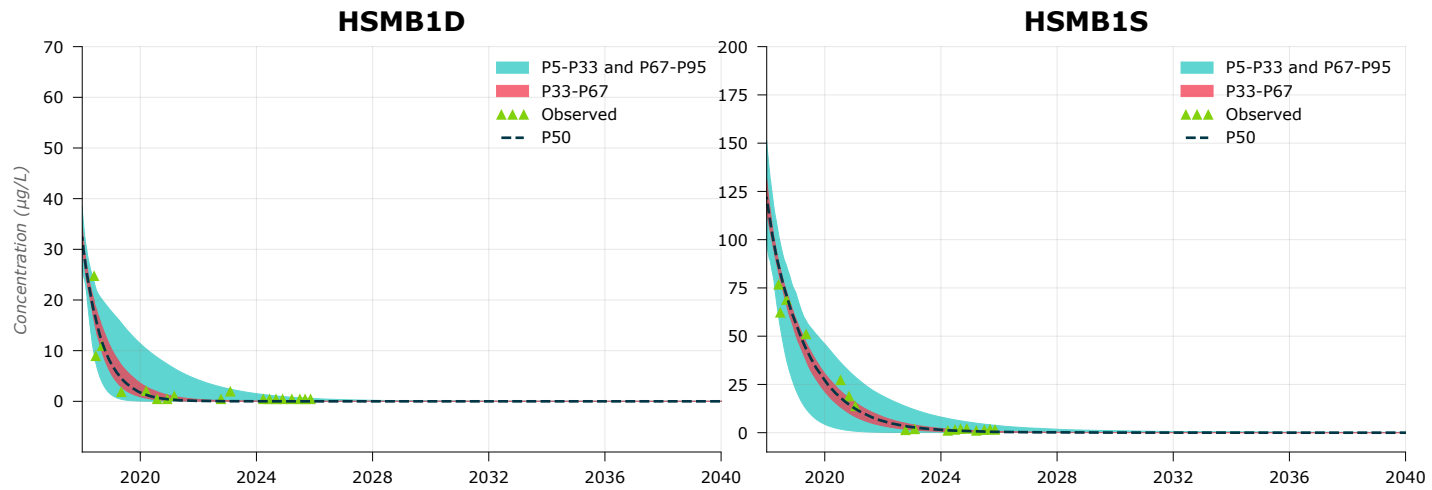

AES9443
HL21
HL22
HL23
HL24
HL25
HL26
HL27
P5-P33 and P67-P95
P33-P67
Observed
P50
Concentration (µg/L)
0
5
10
15
20
25
30
2020
2024
2028
2032
2036
2040


HL34
Concentration (µg/L)
P5-P33 and P67-P95
P33-P67
Observed
P50
0
10
20
30
40
50
60
2020
2024
2028
2032
2036
2040

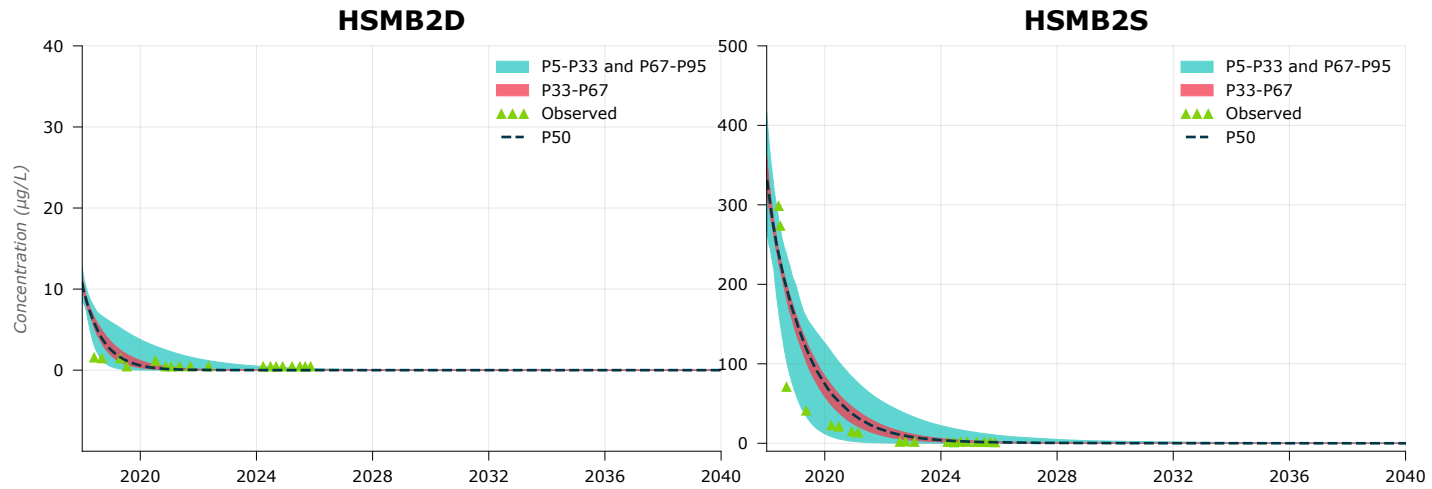
HL35
P5-P33 and P67-P95
P33-P67
Observed
P50
0
20
40
60
80
100
120
140
160
2020
2024
2028
2032
2036
2040


HL36
Concentration (µg/L)
P5-P33 and P67-P95
P33-P67
Observed
P50
0
50
100
150
200
250
300
2020
2024
2028
2032
2036
2040

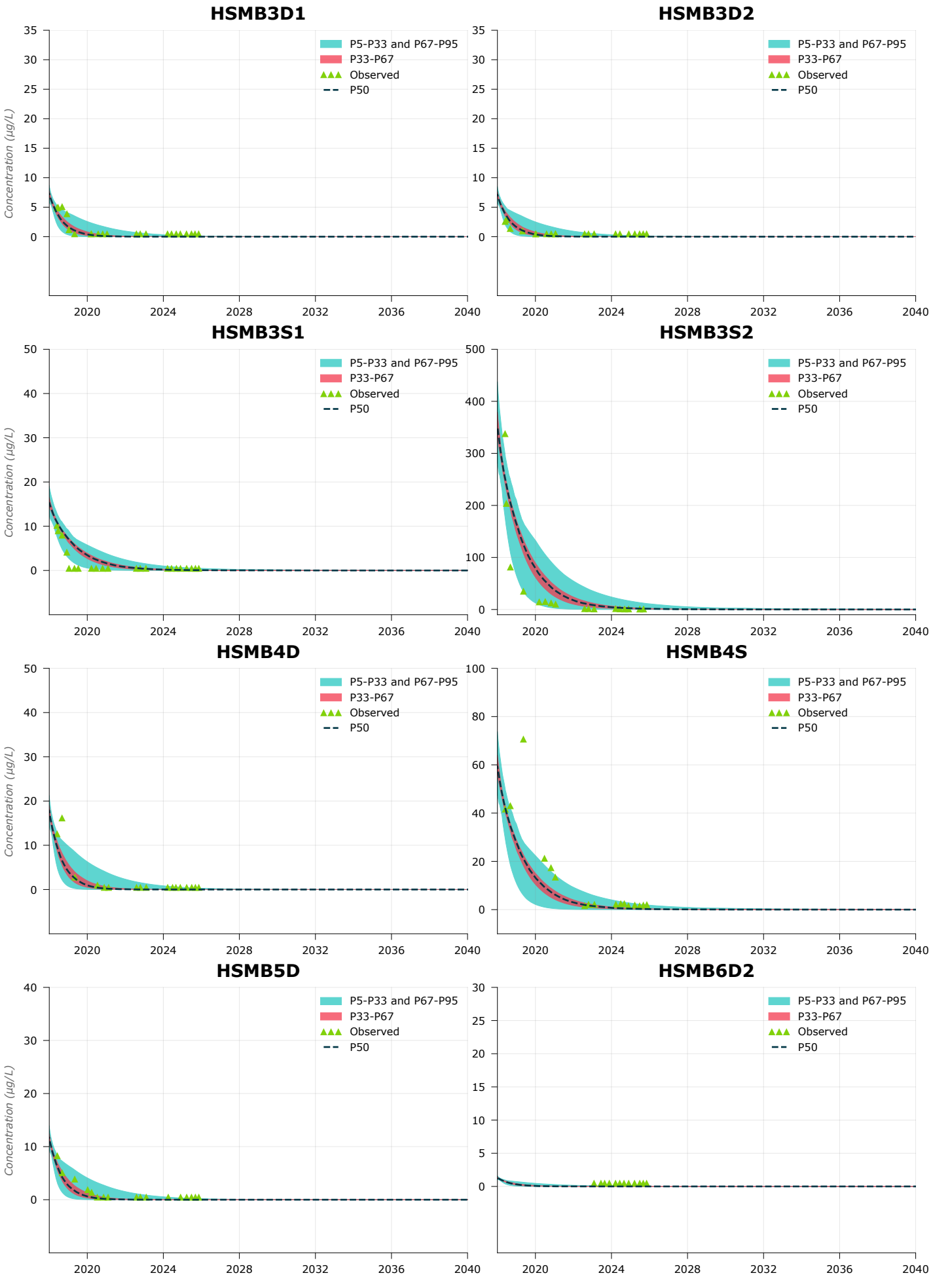
HL37
P5-P33 and P67-P95
P33-P67
Observed
P50
0
50
100
150
200
250
300
2020
2024
2028
2032
2036
2040

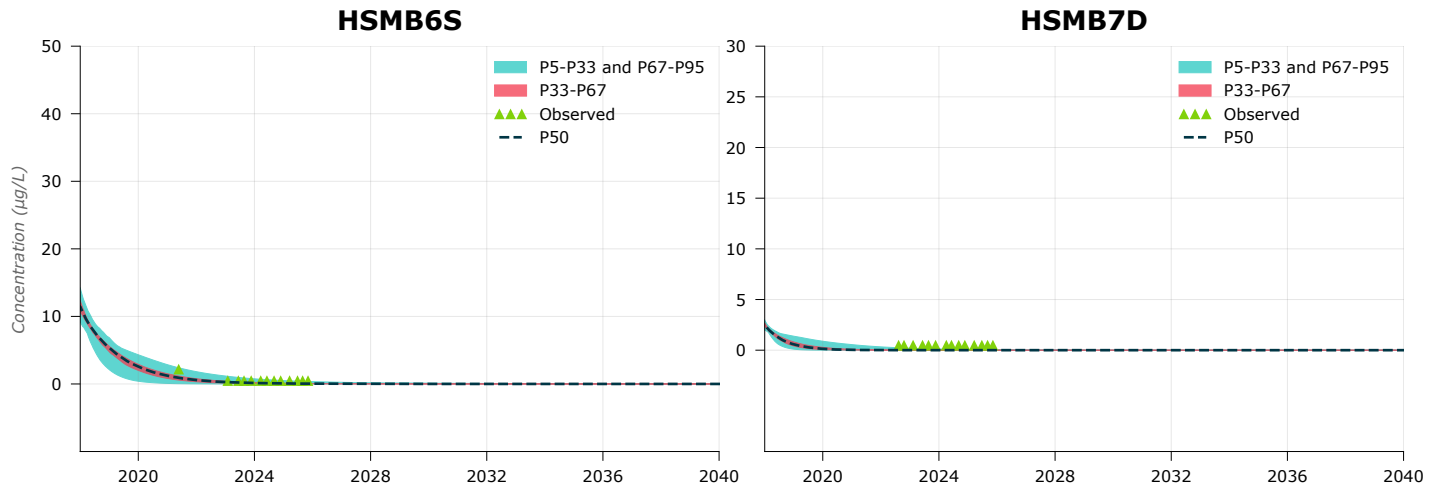

HSMB1D
Concentration (µg/L)
P5-P33 and P67-P95
P33-P67
Observed
P50
0
10
20
30
40
50
60
70
2020
2024
2028
2032
2036
2040

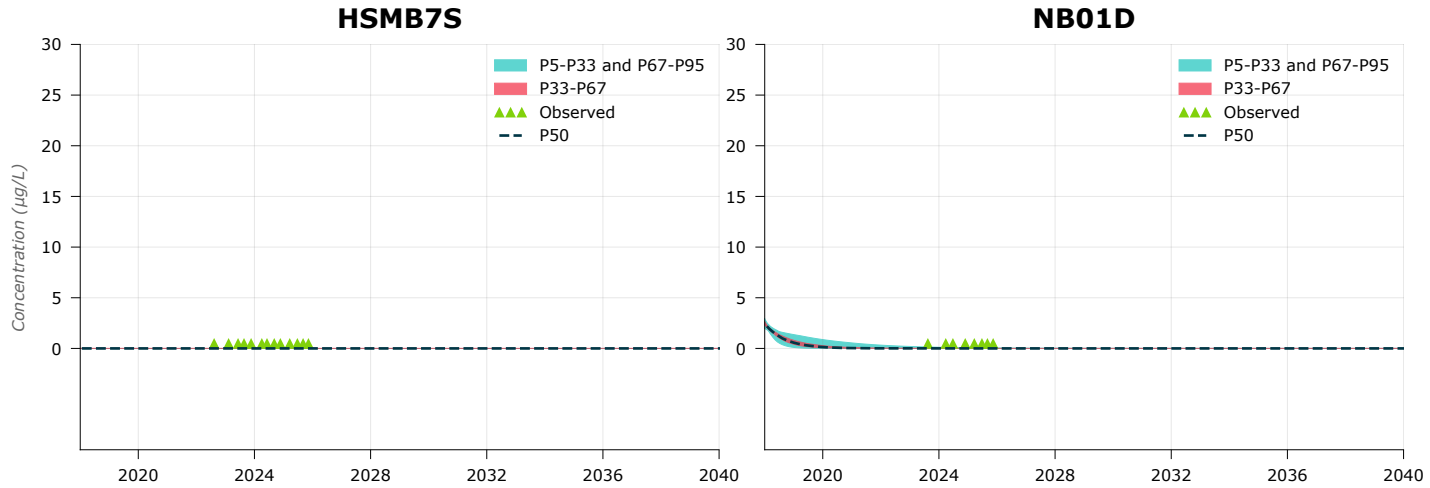
HSMB1S
P5-P33 and P67-P95
P33-P67
Observed
P50
0
25
50
75
100
125
150
175
200
2020
2024
2028
2032
2036
2040

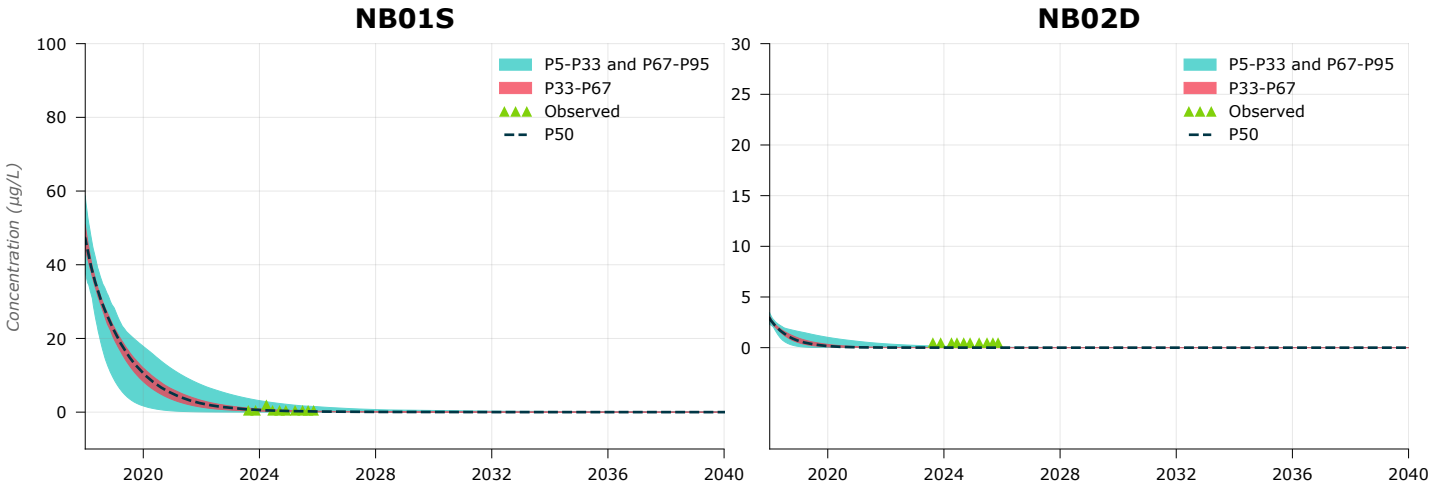

HSMB2D
Concentration (µg/L)
P5-P33 and P67-P95
P33-P67
Observed
P50
0
10
20
30
40
2020
2024
2028
2032
2036
2040

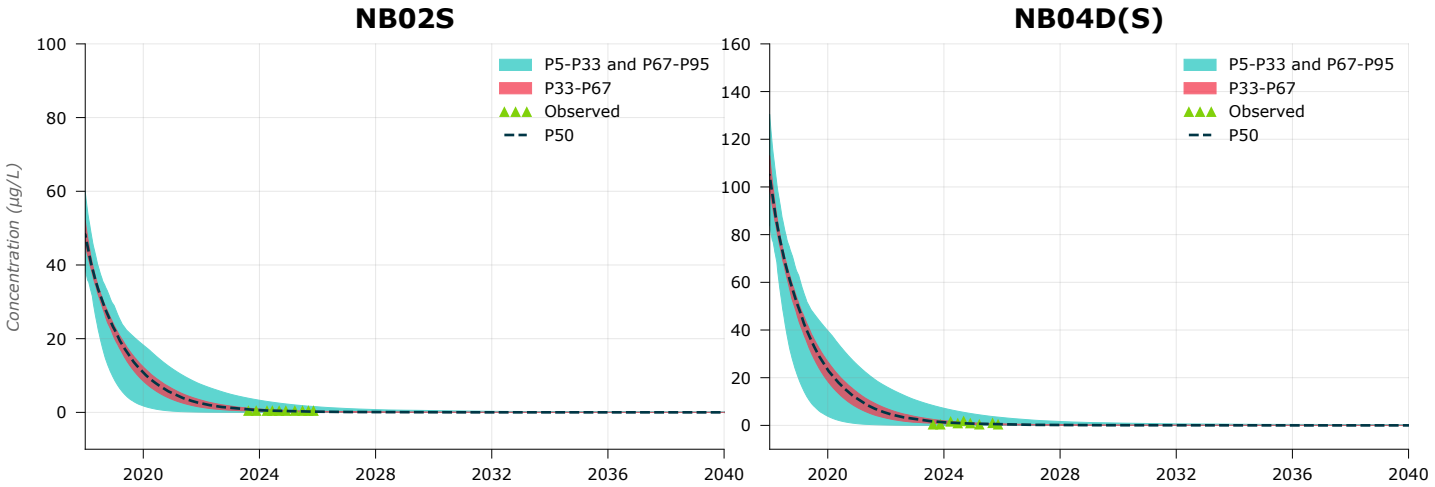
HSMB2S
P5-P33 and P67-P95
P33-P67
Observed
P50
0
100
200
300
400
500
2020
2024
2028
2032
2036
2040

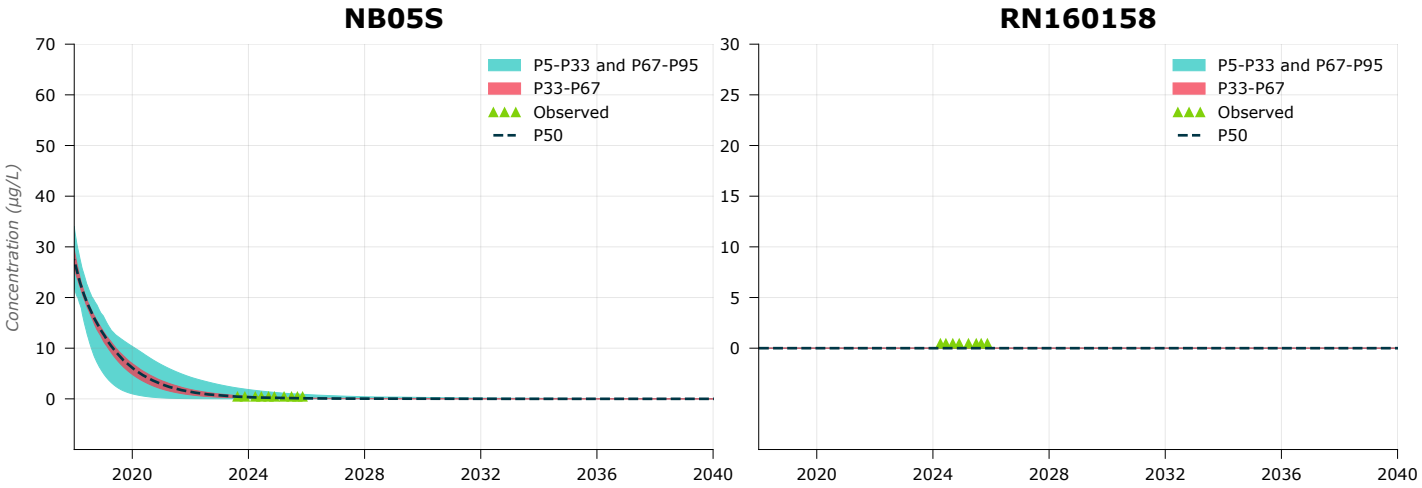

HSMB3D1
HSMB3D2
HSMB3S1
HSMB3S2
HSMB4D
HSMB4S
HSMB5D
HSMB6D2
P5-P33 and P67-P95
P33-P67
Observed
P50
Concentration (µg/L)
2020
2024
2028
2032
2036
2040


HSMB6S
HSMB7D
P5-P33 and P67-P95
P33-P67
Observed
P50
Concentration (µg/L)
2020
2024
2028
2032
2036
2040


HSMB7S
NB01D
P5-P33 and P67-P95
P33-P67
Observed
P50
Concentration (µg/L)
2020
2024
2028
2032
2036
2040


NB01S
NB02D
P5-P33 and P67-P95
P33-P67
Observed
P50
Concentration (µg/L)
2020
2024
2028
2032
2036
2040


NB02S
NB04D(S)
P5-P33 and P67-P95
P33-P67
Observed
P50
Concentration (µg/L)
2020
2024
2028
2032
2036
2040


NB05S
RN160158
P5-P33 and P67-P95
P33-P67
Observed
P50
Concentration (µg/L)
70
60
50
40
30
20
10
0
30
25
20
15
10
5
0
2020
2024
2028
2032
2036
2040